



Martínez Rabert, Eloy (2024) *A mathematical study of the ecology that shapes microbial communities of nitrifiers*. PhD thesis.

<https://theses.gla.ac.uk/84125/>

Copyright and moral rights for this work are retained by the author

A copy can be downloaded for personal non-commercial research or study, without prior permission or charge

This work cannot be reproduced or quoted extensively from without first obtaining permission from the author

The content must not be changed in any way or sold commercially in any format or medium without the formal permission of the author

When referring to this work, full bibliographic details including the author, title, awarding institution and date of the thesis must be given

Enlighten: Theses

<https://theses.gla.ac.uk/>
research-enlighten@glasgow.ac.uk

A mathematical study of the ecology that shapes microbial communities of nitrifiers

Eloy Martínez Rabert

BSc Chemical Engineering, Autonomous University of Barcelona

MSc Biological and Environmental Engineering, Autonomous University of Barcelona

SUBMITTED IN FULFILMENT OF THE REQUIREMENTS FOR THE DEGREE OF
Doctor of Philosophy

**James Watt School of Engineering
College of Science and Engineering
University of Glasgow**

SUBMITTED: September 2023

Nothing is less real than realism.

Details are confusing.

*It is only by selection, by elimination, by emphasis,
that we get at the real meaning of things.*

– Georgia O’Keeffe

Abstract

Nitrification, the biotic transformation of ammonia to nitrate via nitrite, plays a fundamental role in natural and engineered systems. In the last decades, our understanding of nitrification has changed significantly – from the collaboration between two aerobic microbial cohorts, ammonia-oxidizing bacteria (AOB) and nitrite-oxidizing bacteria (NOB), to the complex ecological network involving five microbial cohorts from both bacterial and archaeal domains and including anaerobic microbes: AOB, NOB, ammonia-oxidizing archaea (AOA), comammox bacteria (CMX) and anammox bacteria (AMX). Although this complexity has hindered the full comprehension of nitrification, new opportunities could arise for novel biotechnology designs to remove nitrogen compounds from sewage in a more efficient and sustainable way. The comprehension of the complex ecological network of nitrifiers is the first step to achieve this goal. In order to elucidate the ecological mechanisms that shape the nitrifying community, statistical methods (meta-analysis and nonparametric statistics) and multiscale modelling (Individual-based Model framework) were combined.

The meta-analysis, reviewing approximately 100 references in literature and more than 300 data points, found that AOA and CMX have higher growth yield, higher ammonia affinity and lower maximum specific growth rate than AOB, in accordance with the conventional life strategy theory (r-strategy, K-strategy and Y-strategy). This would explain their dominance in oligotrophic environments. However, CMX, with the maximum energy harvest per mole of ammonia, and some AOB (especially from *Nitrosospira* genus) have higher ammonia affinity than some AOA species. Moreover, similar oxygen affinity between AOB and AOA was found, and the presumed dominance of AOB over NOB in oxygen-limiting environments was discussed. Although *Nitrobacter* have the lowest oxygen affinity, *Nitrospira* have a similar affinity than AOB and AOA. Moreover, lower statistical variance of oxygen affinity than ammonia and nitrite affinities was observed, suggesting that nitrogen availability (ammonia and nitrite) is stronger selective pressure than oxygen. This meta-analysis also showed that the measured kinetic parameters (and potential niche specializations) are mainly defined by the fundamental differences in the biochemistry of nitrifying populations.

Hypothesis and theory-based studies in microbial ecology have been neglected in favour of those that are descriptive and aim for data-gathering of uncultured microbial species. This tendency limits our capacity to create new mechanistic explanations of microbial community dynamics. The modelling studies presented in this thesis were designed following the guidelines of *in-silico* bottom-up methodology, in which the simulated domain is piecing together sub-systems (*i.e.*, key elements and processes) to give rise to more complex systems. Ruling out the belief that experimentation before modelling is indispensable, this thesis shows that mathematical modelling can be used as a

tool to direct experimentation by validating theoretical principles and generating new hypotheses on microbial ecology. Two modelling studies is presented in this work. The first *in-silico study* aimed to explore the underlying mechanism that control the microbial community assembly in aggregates. For this, an artificial microbial community noninteracting (neutralism), collaborating (commensalism) and/or competing was simulated under different environmental conditions. This study identified specific spatial distributions of populations in function of the ecological interaction considered. When multiple ecological interactions were considered, the resultant spatial distribution was the one controlled by the most limiting substrate. Based on this, a theoretical modulus was defined, called *eco-interaction modulus*. With this, we are able to quantify the effect of environmental conditions and ecological interactions on the resultant microbial community. Although competition for space is generally overlooked, the *in-silico* results show its role on the assembly of microbial communities in aggregates. The second modelling study aimed to investigate the resilience of CMX under different nitrogen and/or oxygen limited environments considering all their reported catabolic activities. The *in-silico* results from this study suggest that even extremely low oxygen concentrations ($\sim 1.0 \mu\text{M}$) allow for a proportional growth of AMX and CMX similar to the one experimentally observed. Additionally, a diversity of metabolic activities for CMX was observed in all tested conditions (*i.e.*, metabolic heterogeneity), being essential for the survival of comammox *Nitrospira* under hypoxic conditions together with AMX. Moreover, metabolic heterogeneity would also explain the transient accumulation of nitrite experimentally observed in aerobic environments with higher ammonia availability.

Overall, the meta-analysis presented in this thesis highlights the importance of considering the microbial taxonomy, the biochemistry of populations, and the metabolic versatility of microbes for the definition of ecological niches of nitrifying populations. Additionally, the lack of defined ecological niches in nitrification might not be only because we are not considering key environmental variables that establish the ecological niches, but we are observing niche overlapping, that is, distinct nitrifying cohorts co-dominate in the same ecological niche. On the other hand, the *in-silico* studies reveal that (i) although ecological relationships between different species dictates the distribution of microbes in aggregates, the environment controls the final spatial distribution of the community, (ii) the specific microbial patterns observed are, in turn, the optimal spatial organization for microbes to thrive in aggregates and how *columned stratification* allows the co-existence of populations at different growth rates, and (iii) metabolic heterogeneity mechanistically explains the early findings on comammox *Nitrospira* – the coexistence with anammox bacteria under hypoxic conditions, the dominance of complete nitrification activity in nitrogen limiting environments and the transient accumulation of nitrite under aerobic conditions. Finally, this thesis shows that the systematic attribute of the *in-silico* bottom-up methodology, together with the gradual increasing in complexity of the simulated system, allows to draw stronger hypothesis on mechanisms, which accelerates the research task.

Table of Contents

Abstract.....	3
Table of Contents.....	5
List of Tables.....	9
List of Figures.....	12
List of Accompanying Material.....	24
Acknowledgments.....	25
Declaration of Originality.....	26
Abbreviations and Special Symbols.....	27
1. Introduction.....	29
1.1. Background.....	30
1.2. Research Aims and Objectives.....	31
1.3. Thesis outline.....	32
2. Literature review.....	33
2.1. Nitrogen cycle and human impact.....	34
2.2. Nitrification and anammox.....	36
2.2.1. Ammonia oxidizers (AOM).....	37
2.2.1.1. Ammonia-oxidizing bacteria (AOB).....	37
2.2.1.2. Ammonia-oxidizing archaea (AOA).....	38
2.2.2. Nitrite oxidizers (NOB).....	41
2.2.3. Complete ammonia oxidizers, comammox bacteria (CMX).....	44
2.2.4. Anaerobic ammonia oxidizers, anammox bacteria (AMX).....	45
2.3. Contribution of nitrification to N ₂ O emissions.....	46
2.4. The ecology of nitrifiers.....	48
2.5. Conclusions.....	50

3. Biochemistry shapes growth kinetics of nitrifiers and defines their activity under specific environmental conditions.	51
3.1. Introduction	52
3.2. Materials and Methods	54
3.2.1. Maximum specific growth rate (μ_{\max})	54
3.2.2. Specific affinities for substrates ($a^0_{\text{NH}_3}$, $a^0_{\text{NO}_2}$, $a^0_{\text{O}_2}$)	55
3.2.3. Growth yield (Y_{XS})	55
3.2.4. Statistical analyses	56
3.3. Results and Discussion	56
3.3.1. Ammonia oxidizers	58
3.3.2. Nitrite oxidizers	61
3.3.3. Oxygen competition among nitrifiers	63
3.4. Conclusions	65
4. Multiscale models driving hypothesis and theory-based research in microbial ecology ...	67
4.1. Introduction	68
4.2. Experimental and theoretical models	68
4.3. <i>In-silico</i> bottom-up methodology	69
4.4. Scales of modelling for microbial communities	73
4.4.1. Individual scale. Models that describe individual microbial activity	73
4.4.2. Micro-scale. Prediction of emerging properties of communities	74
4.4.3. Macro-scale. Scaling up and down key process	75
4.5. Outlook	75
5. Methods – Individual-based Model for microbial aggregates.	76
5.1. Applications and alternative methods	77
5.2. Description of the mathematical model	79
5.2.1. Biological model. Individual-based Model	80
5.2.1.1. Shoving algorithm	82
5.2.2. Physical model. Diffusive transport	83
5.2.2.1. Discretization of diffusion-reaction equation	83

5.2.2.2.	Reaction term	86
5.2.3.	Integration.....	87
5.2.3.1.	Adaptative integration steps.....	88
6.	Environmental and ecological controls of the spatial distribution of microbial populations in aggregates.....	89
6.1.	Introduction	90
6.2.	Methods.....	92
6.2.1.	Set of simulations	93
6.2.2.	Calculation of colony size	93
6.2.3.	Definition of eco-interaction modulus (ϕ_{EI}).....	94
6.2.4.	Statistical analyses	95
6.3.	Results and Discussion.....	95
6.3.1.	Influence of single eco-interaction on microbial communities	95
6.3.1.1.	Neutral environment and the inevitable competition for space	96
6.3.1.2.	Competition for substrate.....	99
6.3.1.3.	Substrate-related commensalism: division of labour	100
6.3.2.	Concurrence of multiple eco-interactions.....	103
6.3.2.1.	Eco-interaction modulus (ϕ_{EI})	105
6.3.3.	Shear forces (detachment) controlling the spatial distribution of populations .	107
6.4.	Conclusions	109
7.	Competitive and substrate limited environments drive metabolic heterogeneity for comammox <i>Nitrospira</i>	110
7.1.	Introduction	111
7.2.	Methods.....	113
7.2.1.	Growth yield estimation of comammox <i>Nitrospira</i>	113
7.2.2.	Multiscale model to describe the community assembly of comammox <i>Nitrospira</i> and anammox bacteria	115
7.2.3.	Simulation experiments	116
7.2.4.	Ecological analysis at floc level	117

7.2.5.	Parameters for the quantification of nitrogen removal	118
7.2.6.	Statistical analyses	118
7.3.	Results	118
7.4.	Discussion	121
7.4.1.	Metabolic heterogeneity for comammox <i>Nitrospira</i>	122
7.4.2.	Optimization of anaerobic oxidation performance	125
7.4.3.	Metabolic heterogeneity explains transient nitrite accumulation	126
7.4.4.	(Eco)physiological analysis of comammox <i>Nitrospira</i>	126
7.5.	Conclusions	130
8.	Conclusions and Recommendations.	131
8.1.	Restatement of Research Objectives	132
8.2.	Main Findings	132
8.2.1.	Biochemistry defines ecological niches of aerobic nitrifiers.....	133
8.2.2.	Ecological, environmental and spatial controls of microbial community assembly in aggregates	134
8.2.3.	Metabolic heterogeneity explains the early discoveries of comammox <i>Nitrospira</i> 135	
8.2.4.	Theoretical and quantitative research in microbial ecology using mathematical modelling	135
8.3.	Proposed Future Research and Current Limitations.....	137
	Appendix A – Chapter 3.....	139
	Appendix B – Chapter 5	157
	Appendix C – Chapter 6	165
	Appendix D – Chapter 7.....	182
	Appendix E – Multivariate Kendall’s Tau (Tau-N)	207
	References	221

List of Tables

Table 2.1. Summary of main physiological features of NOB genera (Nitrobacter: Nb; Nitrospira: Ns; Nitrospina: Nn; Nitrotoga: Ng; Nitrococcus: Nc). Nitrolancaea and Candidatus Nitromaritima genera were not included.	43
Table 3.1. Summary of the kinetic parameters of nitrifiers (AOM, CMX, NOB) used in this study.	57
Table 4.1. Example of statement of model components D, Q, I, A, F.	72
Table 5.1. Comparison between existing Individual-based Models for microbial populations	78
Table 6.1. Definition of eco-interactions. Summary of ecological net effect on bacteria and their respective metabolic stoichiometries. Full stoichiometric matrix in Table C.2.	92
Table 7.1. Comparison between experimental and estimated growth yield values (in mol_{CX}/mol_N) of comammox Nitrospira's activities with current methodology in this study and TEEM2. The growth yield of anammox bacteria (AMX) is also included in the table (average of experimental data from literature).	115
Table A.1. Arrhenius coefficient (θ) of nitrifying bacteria and archaea. Effect of temperature on maximum growth rate.	140
Table A.2. Maximum specific growth rate (μ_{max}) values at 20°C of nitrifying bacteria and archaea.	141
Table A.3. Specific affinity for oxygen ($a^0_{O_2}$) of nitrifying bacteria and archaea.	142
Table A.4. Specific affinity for ammonia ($a^0_{NH_3}$) of ammonia oxidizing bacteria and archaea. 142	
Table A.5. Specific affinity for nitrite ($a^0_{NO_2}$) of nitrite oxidizing bacteria.	143
Table A.6. Biomass growth yield (Y_{XS}) of ammonia oxidizing bacteria and archaea.	143
Table A.7. Biomass growth yield (Y_{XS}) of nitrite oxidizing bacteria.	144
Table A.8. Inventory of the terminal oxidases of ammonia and nitrite oxidisers. The presence of terminal oxidase in each nitrifier groups is indicated with their references.	144
Table A.9. Intrinsic half-saturation constant for oxygen (K_{O_2}) of terminal oxidases isolated in nitrifiers.	144
Table A.10. References of apparent substrate affinity ($K_{m(app)}$) for O₂ of nitrite-oxidizing bacteria (NOB).	145
Table A.11. Summary and description of the data collected from literature of considered ammonia oxidizers. References are provided in Supplementary Tables.	146
Table A.12. Summary and description of the data collected from literature of considered nitrite oxidizers. References are provided in Supplementary Tables.	147

Table C.1. Summary of kinetic parameters of microbial populations (B1, B2, B3) for all simulation setups.	167
Table C.2. Stoichiometric matrix of microbial populations (B1, B2, B3) for all simulation setups.	168
Table C.3. Details of simulation experiments. For each setup, eco-interactions between microbial species, environment of the reactor, and substrate concentrations on bulk liquid ([A], [B], [C] and [D]) are specified. Also, it includes in which Figures the results are shown.....	169
Table D.1. Key parameter values to calculate ΔG_{Cat01} of Nitrospira metabolic activities. Values of standard reduction potential at pH 7 (Ψ_i) are from eQuilibrator 3.0 (Beber et al., 2022). γA^* is the number of electrons “accepted” per mole of electron acceptor.	187
Table D.2. List of general parameters used in all simulation experiments.	188
Table D.3. Summary of growth kinetics of comammox Nitrospira and anammox bacteria. Specific maintenance rate (a) was assumed to be 10% of the maximum growth rate (μ_{max}) (Bodegom, 2007). $K_{S,N}$ – half saturation constant for substrate N; K_{I,O_2} – inhibition constant for O_2 . Growth kinetic parameters are established assuming non-kinetic competition between metabolic activities of comammox Nitrospira and anammox bacteria, consistent with the values reported for anammox bacteria (Straka, 2019; van der Star et al., 2008).	189
Table D.4. Summary of oxygen tolerance of anammox bacteria from literature.	190
Table D.5. Metabolic stoichiometries of Nitrospira metabolisms and anammox bacteria.	191
Table D.6. Evaluation of ϵ value for aerobic nitrifiers (AOB, NOB, and comammox Nitrospira).	192
Table D.7. Statistical significance (p-value) from comparison of relative abundances of comammox Nitrospira metabolisms and anammox across the different oxygen concentration. A) Ammonia feeding ($NH_3:NO_2:NO_3 = 500:0:0 \mu M$). B) Equimolar feeding ($NH_3:NO_2:NO_3 = 500:500:500 \mu M$). C) Non-equimolar feeding ($NH_3:NO_2:NO_3 = 500:375:500 \mu M$). Symbol legend: ns – not significant; * – $p < 0.05$; ** – $p < 0.01$; *** – $p < 0.001$	193
Table D.8. Statistical significance (p-value) from comparison of relative abundances of comammox Nitrospira metabolisms and anammox across the different N feeding regimes. A) Hypoxic environment with $1.0 \mu M O_2$. B) Hypoxic environment with $1.5 \mu M O_2$. C) Hypoxic environment with $3.0 \mu M O_2$. D) Aerobic environment with $93.8 \mu M O_2$. Symbol legend: ns – not significant; * – $p < 0.05$; ** – $p < 0.01$; *** – $p < 0.001$. Feeding regimes ($NH_3:NO_2:NO_3$): ammonia feeding – $500:0:0 \mu M$; equimolar feeding – $500:500:500 \mu M$; non-equimolar feeding – $500:375:500 \mu M$	194
Table D.9. Statistical significance (p-value) from comparison of Nitrospira’s metabolism ratio represented as $\ln(A/B)$ at different nitrogen feeding regimes ($NH_3:NO_2:NO_3$) and oxygen concentrations. A) Metabolic ratios between CMX and division of labour (AO+NO). B) Metabolic	

ratios between CMX and AO. Symbol legend: ns – not significant; * – $p < 0.05$; ** – $p < 0.01$.
 Feeding regimes ($\text{NH}_3:\text{NO}_2:\text{NO}_3$): ammonia feeding – 500:0:0 μM ; equimolar feeding – 500:500:500 μM ; non-equimolar feeding – 500:375:500 μM194

Table D.10. Summary of higher-order interactions (HOI) that influenced the community assembly of comammox *Nitrospira* and anammox bacteria. Continuation of Table D.10 on the next page.
195

Table D.11. Statistical significance (p-value) from comparison of relative abundances of comammox *Nitrospira* metabolisms and AMX across the different oxygen concentration. Assuming nitrite affinity of comammox *Nitrospira* equal to A) 1.0 μM of NO_2^- , B) 12.5 μM of NO_2^- and C) 449.2 μM of NO_2^- . Symbol legend: ns – not significant; * – $p < 0.05$; ** – $p < 0.01$; * – $p < 0.001$.**.....197

Table D.12. Statistical significance (p-value) from comparison of relative abundances of comammox *Nitrospira* metabolisms and AMX across the different nitrite affinities of comammox *Nitrospira*. A) Hypoxic environment with 1.0 μM O_2 . B) Hypoxic environment with 1.5 μM O_2 . C) Hypoxic environment with 3.0 μM O_2 . Symbol legend: ns – not significant; * – $p < 0.05$; ** – $p < 0.01$; * – $p < 0.001$.**.....197

Table E.1. Examples of data trend measurement (τN) for $H(S1, S2) \in \mathbb{R}^2$ and $H(S1, S2, S3) \in \mathbb{R}^3$217

Table E.2. Examples of data trend measurement (τN) for $H(S1, S2, S3, S4) \in \mathbb{R}^4$218

Table E.3. Examples of data trend measurement (τN) for $H(S1, S2, S3, S4, S5) \in \mathbb{R}^5$219

Table E.4. Examples of data trend measurement (τN) for $H(S1, S2, S3, S4, S5, S6) \in \mathbb{R}^6$220

List of Figures

Figure 1.1. Evolution of our understanding of nitrification from A) pre-1995 to B) today.....	30
Figure 2.1. Major processes of nitrogen cycle according to the redox state. Nitrogen inventory for organic nitrogen, ammonia, nitrate, nitrous oxide gas and dinitrogen gas (grey squares), and estimated conversions (green, blue and salmon squares) are included. The interconversion of ammonia and organic nitrogen (organic-N) does not involve a change in the redox state of the nitrogen atom. The ammonia inventory is found mainly in rocks and sediments. This ammonia becomes available with the erosion. Whereas the terrestrial inventory of ammonia is known, the marine inventory is estimated to be between 340 and 3600 Tg-N. DNRA refers to dissimilatory nitrate reduction to ammonia. Anthropogenic flux from (Battye et al., 2017; Tian et al., 2020). The anthropogenic nitrogen fixation includes N-fixing crops and the synthesis of NH₃ by Haber-Bosch process. Figure adapted from (Kuypers et al., 2018).	34
Figure 2.2. Schematic illustration of electron transport and generation of proton motive force (energy metabolism) in ammonia-oxidizing bacteria (AOB). CBB represents the Calvin-Bassam-Benson cycle. Complex I is the NADH ubiquinone oxidoreductase. Complex II is the succinate dehydrogenase. Complex III (ubiquinol-cytochrome c reductase) and complex IV (cytochrome aa₃) are the sites where electron transport is coupled to proton pump. Complex V is the ATP synthase, the site of oxidative phosphorylation to generate ATP. Black arrows with H⁺ labels represent the proton flux through the periplasmic membrane. Double thick lines represent the cell wall.	38
Figure 2.3. Reconstruction of the proposed pathways of ammonia oxidation, electron transfer and generation of proton motive force (energy metabolism) in ammonia-oxidizing archaea (AOA). A) Hypothetical two-step model (proposed by Kozłowski et al. (2016)). B) Hypothetical three-step model (proposed by Lehtovirta-Morley (2018)). Complex I is the NADH ubiquinone oxidoreductase. QRED is the quinone reductase. HURM represents the hydroxylamine ubiquinone redox module. Cup represents the cupredoxin-like proteins. Complex II is the succinate dehydrogenase. Complex III (ubiquinol-cytochrome bc₁ reductase) and complex IV (cytochrome aa₃) are the sites where electron transport is coupled to proton pump. Complex V is the ATP synthase, the site of oxidative phosphorylation to generate ATP. Black arrows with H⁺ labels represent the proton flux through the periplasmic membrane. Double dashed lines represent the S-layer.	40
Figure 2.4. Proposed NO dismutation of <i>N. maritimus</i>. Coupling of ammonia oxidation and NO dismutation under anoxic conditions (presence of nitrite). The dismutation of NO to O₂(aq.) and N₂O (aq.) is thermodynamically favourable ($\Delta G^0 = -165$ kJ/mol O₂). Figure adapted from Kraft et al. (2022).	41

Figure 2.5. Schematic illustration of electron transport and generation of proton motive force (energy metabolism) in nitrite-oxidizing bacteria (NOB). **A)** All NOB genera. **B)** Specific of NOB genera. Complex I is NADH ubiquinone oxidoreductase. Complex II is the succinate dehydrogenase. Complex III (ubiquinol-cytochrome c reductase) and complex IV (terminal oxidase, cyt. aa₃, cyt. bd-like or cyt. cbb₃) are the sites where electron transport is coupled to proton pump. Complex V is the ATP synthase, the site of oxidative phosphorylation to generate ATP. Complex I, II, III and V are found in all NOB genera. The enzymatic differences of ETC between NOB genera are found on NXR and complex IV. Black arrows with H⁺ labels represent the proton flux through the periplasmic membrane. Double thick lines represent the cell wall.42

Figure 2.6. Schematic illustration of electron transport and generation of proton motive force (energy metabolism) in comammox Nitrospira (CMX). rTCA represents the reductive tricarboxylic acid cycle. Complex I is the NADH ubiquinone oxidoreductase. Complex II is the succinate dehydrogenase. Complex III (ubiquinol-cytochrome c reductase) and complex IV (cytochrome aa₃) are the sites where electron transport is coupled to proton pump. Complex V is the ATP synthase, the site of oxidative phosphorylation to generate ATP. Black arrows with H⁺ labels represent the proton flux through the periplasmic membrane. Double thick lines represent the cell wall. Figure adapted from (Daims et al., 2015).44

Figure 2.7. Current view of anammox process. Electron transport and generation of proton motive force (energy metabolism) in anammox bacteria (AMX). Substrates (NH₄⁺ and NO₂⁻) and product (N₂) in green. Nir is the nitrite reductase. HZS is the hydrazine synthase. HDH is the hydrazine dehydrogenase. HOX is the hydroxylamine oxidase. NXR is the nitrite oxidoreductase. Nrf is the nitrite reductase forming ammonium. R/b are Rieske-heme b complexes (bc1 complexes). ETM is a yet-to-be identified electron transfer module. Black arrows with H⁺ labels represent the proton flux and through the periplasmic membrane and proton generation. Dashed lines depict reactions and processes to be established. Figure adapted from (Kartal & Keltjens, 2016).46

Figure 2.8. Contribution of nitrification to N₂O emissions. **A)** Biotic (black arrows) and abiotic (red arrows) processes leading to N₂O production in nitrifiers. Participating enzymes are noted above or below the arrows. “Edis?” represents the unknown enzyme that would catalyse the NO dismutase to N₂O and O₂ in AOA (Kraft et al., 2022). The key enzymes for each nitrifier are listed below the scheme. Only the hypothetical two-step pathway of AOA is represented in dotted arrow (catalysed by hypothetical HURM enzyme). **B)** Influence of oxygen availability to N₂O yield in AOB (expressed as N₂O/NO₂⁻ ratio). Marine Nitrosomonas – (Goreau et al., 1980); Mixed culture (from soil) – (Khalil et al., 2004; Zhu et al., 2013); Nitrosomonas europaea – (Lipschultz et al., 1981)..47

Figure 2.9. Trophic network of nitrification associated with the exchange of nitrogenous compounds. **A)** Scheme illustration of interactions between ammonia oxidizers (AOB, AOA and CMX), nitrite oxidizers (NOB) and anammox bacteria (AMX) considering the three main substrates of nitrification – NH₃, NO₂⁻ and NO₃⁻. ⁽¹⁾CMX release NO₂⁻ at high concentration of NH₃ (Daims et

- al., 2015). **B**) Nitrification by reciprocal feeding. Colour legend: nitrification – yellow arrows; nitrataion – green arrows; comammox process – blue arrow; anammox process – brown arrows; mineralization – red arrows.....49
- Figure 3.1. Maximum specific growth rate (μ_{max}) with A) specific affinity for ammonia (a^0_{NH3}) and B) growth yield (Y_{XS}) of ammonia-oxidizing microorganisms (AOB, AOA and CMX). The black bars show the range of μ_{max} values; green bars represent the range of a^0_{NH3} value for ammonia (Figure 3.1A); and red bars represent the range of Y_{XS} values (Figure 3.1B). Blue: non-marine nitrifiers; orange: marine nitrifiers. Legend bottom of figures: B – Bacteria; A – Archaea; C – Complete ammonia oxidizer. Dashed lines cross the calculated average value for each parameter function of the range of values reported.....59**
- Figure 3.2. Maximum specific growth rate (μ_{max}) with A) specific affinity for nitrite (a^0_{NO2}) and B) growth yield (Y_{XS}) of nitrite-oxidizing bacteria. The black bars show the range of μ_{max} values; green bars represent the range of a^0_{NO2} values (Figure 3.2A); red bars represent the range of Y_{XS} value (Figure 3.2B). Blue: non-marine nitrite oxidizers; orange: marine nitrite oxidizers. Legend bottom of figures: C – NOB with cytoplasmic NXR; P – NOB with periplasmic NXR. sP – NOB with soluble periplasmic NXR. Dashed lines cross the calculated average value for each parameter function of the range of values reported.62**
- Figure 3.3. Oxygen competition. A) Maximum specific growth rate (μ_{max}) with specific affinity for oxygen (a^0_{O2}) for all the nitrifiers' populations considered. The black bars show the range of μ_{max} values; dark green bars represent the range of a^0_{O2} values; and dashed connect the average of each value range. Blue: marine nitrifiers; orange: non-marine nitrifiers. Legends: AOB – Ammonia-oxidizing bacteria; AOA – Ammonia-oxidizing archaea; P-NOB – NOB with periplasmic NXR; C – NOB with cytoplasmic NXR. On the bottom of tags, in parentheses, the terminal oxidase that each group uses to reduce oxygen is shown (Table A.8). Dashed lines cross the calculated average value for each parameter function of the range of values reported. **B**) Apparent substrate affinity ($K_{m(app)}$) for oxygen of NOB. $K_{m(app)}$ values are given for growth measurements (circles) and activity measurements (diamonds). Marker colour legend: Red – NOB with heme-copper oxidase aa_3 -type as terminal oxidase; Green – NOB with putative cytochrome bd -like oxidase as terminal oxidase; Grey – NOB with heme-copper oxidase cbb_3 -type as terminal oxidase. [OMZ]: samples from oxygen minimum zones (OMZ). $K_{m(app)}$ of Nitrospinae is significantly different from that of Nitrospira and Nitrobacter species ($p < 0.0001$) and $K_{m(app)}$ of Nitrospira species are significantly different from that of Nitrobacter species ($p < 0.0001$). References of $K_{m(app)}$ values in Table A.10.64**
- Figure 4.1. Modelling-experimental cycle. Integrated development of experimental and modelling methodologies can lead to higher levels of predictive capacities and operation control. Dotted green arrow depicts the methodology presented here – theoretical model before experimentation.69**
- Figure 4.2. Schematic representation of in-silico bottom-up methodology.70**

- Figure 4.3. Life cycle of a mathematical model (M).** PR represents the peer-review process of the model, in which decides if the model is able to contribute to the current knowledge (K) or not (\emptyset). $M_a(D,Q)$ is the formal representation of a mathematical model based on a specific domain (D), scientific question (Q), and approach ($a = I, A, F$). Abstraction: obtention of information from domain. Formalization: definition of interpretation (I), assumptions (A) and formalism (F).71
- Figure 5.1. Representation of simulation domain.** A) Granular version. B) Suspension version..79
- Figure 5.2. Hypothetical position of microbes in a node.** Only “microbe A” belongs to node I_j because its centre is inside the node.80
- Figure 5.3. Microbial division and inactivation.** α is any stochastic value between 0.45 – 0.55. M_{max} and M_{min} refer to the maximum and minimum mass that microbe can reach, respectively.82
- Figure 6.1. Classification of eco-interactions between species.** Cross-feeding (or syntrophy) and co-protection (or symprostasy) are two specific eco-interactions belonging to mutualism (positive effect for both interacting species).90
- Figure 6.2. Representation of eco-interactions among B1 (purple), B2 (green) and B3 (orange).** A) Neutralism: [0,0,0]; no impact on B1, B2 and B3. B) Competition: [-,-,-]; negative impact on B1, B2 and B3. C) Commensalism: [0,+,+]; no impact on B1, positive impact on B2 and B3. D) Commensalism + competition: [0,+,+] or [-,-,-]; impact on B1, B2 and B3 is defined by the environment.93
- Figure 6.3. Spatial distribution of microbial populations at different substrates concentrations.** A) Aggregate pictures captured after 8 d of simulation considering neutralism, competition and commensalism with $[S]_T = 100$ mM. B) Aggregate pictures captured at 10 d of simulation considering neutralism, competition and commensalism with $[S]_T = 10$ mM. C) Aggregate pictures captured at 15 d of simulation considering neutralism, competition and commensalism with $[S]_T = 1$ mM. None of the simulations are in steady state yet. Black solid line on bottom-right of aggregates represent the scale bar. Substrate profiles on the transverse plane of aggregates have been included on Figure C.2.97
- Figure 6.4. Neutralism [0,0,0].** A) Relative abundances of B1, B2 and B3 populations in the community. Dashed red lines indicate 33.33% and 66.66% relative abundances. B) Microbial fitness (median, F) is calculated in all replicates ($n = 3$ for 1.0 mM and 0.5 mM, $n = 6$ for 0.2 mM). Asterisks indicate the significance level of the difference between B1, B2 and B3 specific growth rate. C) Aggregates captured at steady state (75 d for 1.0 mM and 0.5 mM, 100 d for 0.2 mM). Inactive bacteria are shown in a lighter colour. Black solid lines on bottom represent the scale bars. Significance level legend: ns, not significant; *, $p < 0.05$; **, $p < 0.01$; ***, $p < 0.001$98
- Figure 6.5. Competition [-,-,-].** A) Relative abundances of B1, B2 and B3 populations in the community. Dashed red lines indicate 33.33% and 66.66% relative abundances. B) Microbial fitness (median, F) is calculated in all replicates ($n = 3$ for 1.0 mM and 0.5 mM; $n = 6$ for 0.2 mM and 0.1 mM). Asterisks indicate the significance level of the difference between the specific growth rate

of B1, B2 and B3 populations. **C)** Aggregates captured at steady state (50 d for 1.0 mM and 0.5 mM, 75 d for 0.2 mM and 0.1 mM). Inactive bacteria are shown in a lighter colour. Black solid lines on bottom represent the scale bars. **D)** Average relative size of colonies (with respect to the total perimeter of the aggregate) is calculated in all replicates ($n = 3$ for 1.0 mM and 0.5 mM; $n = 6$ for 0.2 mM and 0.1 mM). Asterisks indicate the significance level of the difference between substrates concentrations. Significance level legend: ns, not significant; *, $p < 0.05$; **, $p < 0.01$; ***, $p < 0.001$100

Figure 6.6. Commensalism [0,+,+]. **A)** Relative abundances of B1, B2 and B3 populations in the community. Dashed red lines indicate 33.33% and 66.66% relative abundances. Square brackets with asterisks indicate the significance level of the difference between relative abundances between populations. Colour of asterisks points out what bacteria it refers to. **B)** Microbial fitness (median, F) is calculated in all replicates ($n = 3$ for 1.0 mM and 0.5 mM; $n = 6$ for 0.2 mM and 0.1 mM). **C)** Aggregates captured at steady state (50 d for 1.0 mM and 0.5 mM, 75 d for 0.2 mM and 0.1 mM). Inactive bacteria are shown in a lighter colour. Black solid lines on bottom represent the scale bars. **D)** Transient change of growth rate ratios of active B2 and B3 over B1 (μ_{B2}/μ_{B1} and μ_{B3}/μ_{B1} , respectively) in all replicates ($n = 3$ for 1.0 mM and 0.5 mM; $n = 6$ for 0.2 mM and 0.1 mM). Growth rate ratios, normalise the comparison and reduce the influence of substrate concentration in the analysis. Dimensionless time was applied to compare simulations with different time length (t_{max}). Asterisks indicate the significance level of difference between 1.0 mM and the other concentrations (1.0 mM vs 0.5 mM; 1.0 mM vs 0.2 mM; 1.0 mM vs 0.1 mM). Colour of asterisks: red – growth rate ratio at $[S]$ is lower than that at 1.0 mM; blue – growth rate ratio at $[S]$ is higher than that at 1.0 mM. Significance level legend: ns, not significant; *, $p < 0.05$; **, $p < 0.01$; ***, $p < 0.001$. Width of the lines indicate the time to which the significance level corresponds. Colour of the lines: green – B2; orange – B3.....102

Figure 6.7. Aggregates captured at steady state considering commensalism and competition for O_2 . Steady state times: 50d for $[S]_T = 1.0$ mM, 0.5 mM, 0.1 mM and $[O_2] = 10$ mg/L, 6 mg/L; 75d for $[S]_T = 1.0$ mM, 0.5 mM, 0.1 mM and $[O_2] = 1$ mg/L; 100d for $[S]_T = 0.05$ mM and $[O_2] = 10$ mg/L, 6 mg/L, 1 mg/L. Inactive bacteria are shown in a lighter colour. Substrate profiles on the transverse plane of aggregates have been included on Figure C.5. Aggregates captured at steady state.....104

Figure 6.8. Eco-interaction modulus diagram for simulations considering commensalism and competition for O_2 with $[A] = 1.0 - 0.1$ mM and $[O_2] = 14 - 1$ mg/L. Aggregates captured at steady state (75 d for $[S]_T = 1.0$ mM and $[O_2] = 1$ mg/L; 50 d for all other conditions). Inactive bacteria are shown in a lighter colour. Eco-interaction modulus calculated by Eq. 6.5 for each replicate. Colour legend: B1 – purple; B2 – green; B3 – orange.....107

Figure 6.9. Influence of shear force (detachment) to spatial distribution of microbial populations. Aggregates captured at 50d when a maximum radius of 30 μm (due to the detachment) was

considered. Aggregates captured at 50 d. Three conditions were evaluated – competition ($[S]_T = 0.2 \text{ mM}$), commensalism ($[S]_T = 0.1 \text{ mM}$), and commensalism + competition ($[S]_T = 0.1 \text{ mM}$ and $[O_2] = 10 \text{ mg/L}$). Inactive bacteria are shown in a lighter colour. Substrate profiles on the transverse plane of aggregates have been included on Figure C.11. The simulation experiments including detachment were started with the same inoculum as those without detachment with the objective to observe the genuine impact of the shear force in the spatial distribution of the microbial populations.....108

Figure 7.1. Influence of nitrogen feeding regime (defined by $NH_3:NO_2:NO_3$ ratio) and oxygen concentration (1.0, 1.5, 3.0 and $93.8 \mu\text{M}$) on comammox Nitrospira and anammox bacteria community. Relative abundances of Nitrospira (AO, NO, CMX, NRMX and An-NRMX) and anammox bacteria (AMX), with each correspondent floc images (bottom panels) under **A**) ammonia feeding ($NH_3:NO_2:NO_3 = 500:0:0 \mu\text{M}$), **B**) equimolar feeding ($NH_3:NO_2:NO_3 = 500:500:500 \mu\text{M}$), and **C**) non-equimolar feeding ($NH_3:NO_2:NO_3 = 500:375:500 \mu\text{M}$). The statistical significance between different oxygen concentrations and nitrogen feeding regimes are shown in Tables D.7 and D.8, respectively. Labels over each bar show Anammox:Nitrospira ratio at steady state. Black circles on floc images represent inactive individuals. Additional floc images of comammox Nitrospira and anammox community are shown in the Figure D.2.120

Figure 7.2. Value of metabolic heterogeneity for comammox Nitrospira. **A**) Impact of metabolic heterogeneity on the survival of comammox Nitrospira under hypoxic conditions (1.0 and $1.5 \mu\text{M}$ of O_2) applying equimolar feeding ($NH_3:NO_2:NO_3 = 500:500:500 \mu\text{M}$) and non-equimolar feeding ($NH_3:NO_2:NO_3 = 500:375:500 \mu\text{M}$). MF – simulation experiments considering metabolic flexibility in Nitrospira; oCMX – simulation experiments considering that Nitrospira only performs CMX activity. Asterisks denote p-value significance where *, $p < 0.05$; **, $p < 0.01$; ***, $p < 0.001$. **B**) Ecological analysis at floc level (pairwise interactions) under conditions where comammox Nitrospira and anammox bacteria remained active (1.0 and $1.5 \mu\text{M}$ of O_2). Ammonia feeding ($NH_3:NO_2:NO_3 = 500:0:0 \mu\text{M}$, left panels); equimolar feeding ($NH_3:NO_2:NO_3 = 500:500:500 \mu\text{M}$, centre panels); non-equimolar feeding ($NH_3:NO_2:NO_3 = 500:500:500 \mu\text{M}$, right panels). Kendall's τ values of metabolisms are presented on a colour scale. Dotted cells indicate p-value significance where \blacksquare , $p < 0.05$; $\blacksquare\blacksquare$, $p < 0.01$; $\blacksquare\blacksquare\blacksquare$, $p < 0.001$. Cross symbol (x) indicates no co-existence of the metabolic pair at the end of the simulation experiments. Bottom-right labels indicate the ecological interaction of metabolic pair: CC – Commensalism+Competition; SC – Syntrophism+Competition; C – Competition. Sample sizes employed for Kendall's τ calculation are shown in Figure D.5....123

Figure 7.3. Influence of nitrogen feeding regime (ammonia, equimolar and non-equimolar feeding) and oxygen concentration (1.0, 1.5, 3.0 and $93.8 \mu\text{M}$) on the anaerobic oxidation performance (ammonia and nitrite oxidation to N_2) expressed as percentage. Data labels depict the relative abundance of anaerobic activities (An-NRMX and AMX). Nitrogen feeding regimes: ammonia feeding – $500:0:0 \mu\text{M}$; equimolar feeding – $500:500:500 \mu\text{M}$; non-equimolar feeding –

500:375:500 μM . Error bars show standard deviation of $n = 3$ simulation replicates. Bars that do not share similar letters denote statistical significance, $p < 0.05$. For more information about the calculus of the anaerobic oxidation performance see Methods – Parameters for the quantification of nitrogen removal.....125

Figure 7.4. Influence of ammonia concentration to the transient accumulation of nitrite at 93.8 μM of O_2 . Three ammonia concentrations were tested. Only 60 – 120 hours are shown (full simulation in Figure D.7): 100 μM of NH_3 (panels **A**), 500 μM of NH_3 (panels **B**), and 1000 μM of NH_3 (panels **C**). Left panels show the dynamics of nitrogen compounds (NH_3 , NO_2^- and NO_3^-) at the early stages of simulation. Right panels show the evolution of relative abundances of comammox *Nitrospira* and anammox bacteria. Error bars show standard deviation of $n = 3$ simulation replicates. If not visible, error bars are smaller than symbols. Gray dashed lines in right panels (dynamics of metabolic activities) depict the time with the maximum concentration of nitrite.127

Figure 7.5. Influence of nitrite affinity ($K_{\text{NO}_2^-}$) of comammox *Nitrospira* on community assembly applying non-equimolar feeding ($\text{NH}_3:\text{NO}_2^-:\text{NO}_3^- = 500:375:500 \mu\text{M}$) and hypoxia conditions (1.0 μM , 1.5 μM and 3.0 μM of O_2). Relative abundances of *Nitrospira* metabolic activities (AO, NO, CMX, NRMX and An-NRMX) and anammox bacteria (AMX), with each correspondent floc images (bottom panels) assuming nitrite affinity ($K_{\text{NO}_2^-}$) equal to **A**) 1.0 μM of NO_2^- ; **B**) 12.5 μM of NO_2^- and **C**) 449.2 μM of NO_2^- . Nitrate affinity of comammox *Nitrospira* was assumed equal to nitrite affinity value. Labels over each bar show Anammox:*Nitrospira* ratio at steady state. The statistical significance between different oxygen concentrations and nitrite affinities are shown in Tables D.11 and D.12, respectively. Black circles on floc images represent inactive individuals.129

Figure 7.6. Influence of nitrite affinity ($K_{\text{NO}_2^-}$) of comammox *Nitrospira* on transient accumulation of nitrite (expressed as percentage) at 93.8 μM O_2 . Only ammonia was fed (1000 μM NH_3). Error bars show standard deviation of $n = 3$ simulation replicates. Bars that do not share similar letters denote statistical significance, $p < 0.05$130

Figure A.1. A) Maximum specific growth rate of (μ_{max}) of AOB and AOA as a function of the pH. Dashed lines represent AOA and solid lines represent AOB. Dotted red line represents the percentage of free ammonia (NH_3) and dotted black line represents the percentage of ammonium (NH_4^+) in function of pH. References: (Anthonisen et al., 1976; Antoniou et al., 1990; French et al., 2012; Jiang, 1999; Jung et al., 2011; Kim et al., 2012; Li et al., 2016; Qin et al., 2014; Tourna et al., 2011). **B)** Maximum specific growth rate of (μ_{max}) of NOB as function of the pH. Dashed lines represent species belonging of genus *Nitrospira* and solid lines represent species belonging of genus *Nitrobacter*. References: (Blackburne et al., 2007a, 2007b; Boon & Laudelout, 1960; Hunik et al., 1993; Keen & Prosser, 1987; Kitzinger et al., 2018; Wegen et al., 2019; Zhang et al., 2018).....148

Figure A.2. Regression fits to different kinetic datasets of nitrifiers and their corresponding Pearson correlation coefficient (r) with significance (p value) and sample size (n). **A)** μ_{max} versus $a^0_{\text{NH}_3}$ of AOB, AOA and CMX **B)** μ_{max} versus $a^0_{\text{NH}_3}$ of AOB only **C)** μ_{max} versus $a^0_{\text{NH}_3}$ of AOA only **D)**

- μ_{max} versus Y_{XS} of AOB, AOA and CMX (excluding acidophilic AOB) **E** μ_{max} versus Y_{XS} of AOA only **F** μ_{max} versus Y_{XS} of AOB only **G** μ_{max} versus a^0_{NO2} of NOB **H** μ_{max} versus Y_{XS} of NOB **I** μ_{max} versus a^0_{NO2} of AOB, AOA and NOB..... 149
- Figure A.3. AOB and AOA maximum growth rates (μ_{max}) from distinct environments.** P-values (One-way ANOVA) between environments on bottom table. Number of bibliographic data is indicated above each boxplot. Boxplots depict the 75-100% quantile range, with the centre line depicting the median (50% quantile) and crosses depicting the average value. Data of each environment are shown as points. Table legend: Sedim – Sediments; WatCol – Water column; HotWat – Hot water; AcidSoil – Acidic soil; WWTP – Wastewater Treatment Plant..... 150
- Figure A.4. AOB and AOA growth yields (Y_{XS}) from distinct environments.** P-values (One-way ANOVA) between environments on bottom table. Number of bibliographic data is indicated above each boxplot. Boxplots depict the 75-100% quantile range, with the centre line depicting the median (50% quantile) and crosses depicting the average value. Data of each environment are shown as points. Table legend: WWTP – Wastewater Treatment Plant..... 151
- Figure A.5. AOB and AOA specific affinity for ammonia (a^0_{NH3}) from distinct environments.** P-values (One-way ANOVA) between environments on bottom table. Number of bibliographic data is indicated above each boxplot. Boxplots depict the 75-100% quantile range, with the centre line depicting the median (50% quantile) and crosses depicting the average value. Data of each environment are shown as points. Values of a^0_{NH3} were \log_{10} transformed before statistical analysis due to the order of magnitude difference in the determined values. 152
- Figure A.6. NOB maximum growth rates (μ_{max}) from distinct environments.** P-values (One-way ANOVA) between environments on bottom table. Number of bibliographic data is indicated above each boxplot. Boxplots depict the 75-100% quantile range, with the centre line depicting the median (50% quantile) and crosses depicting the average value. Data of each environment are shown as points. Table legend: OMZ – Oxygen Minimum Zone; Water col. – Water column; WWTP – Wastewater Treatment Plant..... 153
- Figure A.7. NOB growth yields (Y_{XS}) from distinct environments.** P-values (One-way ANOVA) between environments on bottom table. Number of bibliographic data is indicated above each boxplot. Boxplots depict the 75-100% quantile range, with the centre line depicting the median (50% quantile) and crosses depicting the average value. Data of each environment are shown as points. Table legend: WWTP – Wastewater Treatment Plant. 154
- Figure A.8. NOB specific affinity for nitrite (a^0_{NO2}) from distinct environments.** P-values (One-way ANOVA) between environments on bottom table. Number of bibliographic data is indicated above each boxplot. Boxplots depict the 75-100% quantile range, with the centre line depicting the median (50% quantile) and crosses depicting the average value. Data of each environment are shown as points. Values of a^0_{NO2} were \log_{10} transformed before statistical analysis due to the order of

<i>magnitude difference in the determined values. Table legend: WWTP – Wastewater Treatment Plant.</i>	155
Figure A.9. AOB, AOA and NOB specific affinity for oxygen ($a^0_{O_2}$) from distinct environments. <i>P-values (One-way ANOVA) between environments on bottom table. Number of bibliographic data is indicated above each boxplot. Boxplots depict the 75-100% quantile range, with the centre line depicting the median (50% quantile) and crosses depicting the average value. Data of each environment are shown as points. Values of $a^0_{NO_2}$ were \log_{10} transformed before statistical analysis due to the order of magnitude difference in the determined values. Table legend: WWTP – Wastewater Treatment Plant.</i>	156
Figure B.1. Quadtree representation (capacity = 1). <i>Each circle represents a microbe in the system. Subregions are labelled clockwise (see blue grid on bottom-left of figure).</i>	158
Figure B.2. Selection of neighbours (green circles) of microbe m (blue circle). <i>The centre of circle (black dot) indicates the exact position of microbe. In this example, quadtree capacity is 4 (i.e., maximum 4 microbes per region). Green square represents the neighbourhood zone of microbe m (blue circle), and dashed orange square shows all regions that intersect with the neighbourhood zone of microbe m.</i>	158
Figure B.3. Scheme of shoving algorithm. <i>Legend: $m.shx$ and $m.shy$ – displacement of microbe m due to shoving of the others; $m.NBR$ – neighbours of microbe m.</i>	159
Figure B.4. Detection of diffusion region. <i>A) Representation of preliminary diffusion region (green square). Legend: BL – boundary layer. B) Neighbouring grid cells (green squares, $g_{i,j}$) of a specific boundary grid cell with microbes (blue square) with potential to be included in diffusion region.</i>	160
Figure B.5. Algorithm of diffusion region determination.	161
Figure B.6. Algorithm scheme of the integration process.	162
Figure C.1. Influence of inoculum size and substrate gradients on intermixing of microbial populations considering neutralism, competition and commensalism with $[S]_T = 100$ mM. <i>A) Aggregate pictures captured at 8 d of simulation starting with an inoculum size of 20 μm (diameter) and considering diffusion resistance of substrates. B) Aggregate pictures captured at 4 d of simulation starting with an inoculum size of 160 μm (replicating the starting point of Mitri et al. (2016)) and removing the substrate gradients (no diffusion resistance). None of the simulations are in steady state yet.</i>	170
Figure C.2. Substrate profiles on the transverse plane of aggregates considering neutralism, competition or commensalism. <i>A) Substrate profiles from simulations at $[S]_T = 100$ mM ($t = 8$ d). B) Substrate profiles from simulations at $[S]_T = 10$ mM ($t = 10$ d). C) Substrate profiles from simulations at $[S]_T = 1$ mM ($t = 15$ d). Legend: [A] – purple line; [B] – green line; [C] – orange line.</i>	171

- Figure C.3. Regression fits to different relative abundance/microbial fitness data pairs from simulation experiments with their corresponding Pearson's coefficient (r) with their significance value (p -value) and sample size (n). A) Neutralism simulations. B) Competition simulations. C) Commensalism simulations. Legend: B1– purple circles; B2 – green circles; B3 – orange circles.172**
- Figure C.4. Substrate profiles on the transverse plane of aggregates considering commensalism. Legend: [A] – purple line; [B] – green line; [C] – orange line.173**
- Figure C.5. Substrate profiles on the transverse plane of aggregates considering commensalism and competition. Legend: [A] – purple line; [B] – green line; [C] – orange line; [O₂] – black line.174**
- Figure C.6. Relative abundance of active bacteria from simulation experiments considering commensalism and competition. Dashed red lines indicate 33.33% and 66.66% relative abundances. Colour of asterisks points out what bacteria it refers to. In the table are shown the significant level of the difference between B1, B2 and B3 relative abundances. Significance level legend: ns, not significant; *, $p < 0.05$; **, $p < 0.01$; ***, $p < 0.001$. Colours of y-axis text and table headers indicate the ecological environment (and spatial distribution of microbial populations) of simulation experiments: red – competitive environment (columned stratification); blue – commensal environment (layered stratification).175**
- Figure C.7. Microbial fitness (F) from simulation experiments considering commensalism and competition. Asterisks indicate the significance level of the difference between B1, B2 and B3 specific growth rate. Significance level legend: ns, not significant; *, $p < 0.05$; **, $p < 0.01$; ***, $p < 0.001$176**
- Figure C.8. Regression fits to different relative abundance/microbial fitness data pairs from simulation experiments considering commensalism and competition with their corresponding Pearson's coefficient (r) with their significance value (p -value) and sample size (n). Legend: B1– purple circles; B2 – green circles; B3 – orange circles.177**
- Figure C.9. Ecological environment distribution in a hybrid stratification case considering concurrence of commensalism and competition ($[S]_T = 0.1 \text{ mM}$, $[O_2] = 3.75 \text{ mg/L}$; $\phi EI = 1.07$). Inactive bacteria are shown in a lighter colour. The substrate profiles are from the transverse plane of aggregate.178**
- Figure C.10. Influence of substrate diffusivity on spatial distribution of microbial populations (commensalism + competition; $[S]_T = 1.0 \text{ mM}$, $[O_2] = 10.0 \text{ mg/L}$). Inactive bacteria are shown in a lighter colour. The substrate profiles are from the transverse plane of aggregates.179**
- Figure C.11. Substrate profiles on the transverse plane of aggregates considering or not detachment.180**
- Figure D.1. Apparent substrate affinity ($K_{m(app)}$) for ammonia (panel A) and nitrite (panel B) of comammox *Nitrospira* and anammox bacteria. Colour legend: light blue – comammox *Nitrospira*;**

- orange – anammox bacteria. References of substrate affinities for: comammox *Nitrospira* – (Kits et al., 2017; Sakoula et al., 2021); anammox bacteria – (Ni et al., 2009; Oshiki et al., 2011; Puyol et al., 2013; Straka, 2019; Strous, Kuenen, et al., 1999; van der Star et al., 2008).....198
- Figure D.2. Additional floc images of comammox *Nitrospira* and anammox bacteria community from simulations at different nitrogen feeding regimes and oxygen concentrations (1.0, 1.5, 3.0, 93.8 μM).** Ammonia feeding ($\text{NH}_3:\text{NO}_2:\text{NO}_3 = 500:0:0 \mu\text{M}$). **B)** Equimolar feeding ($\text{NH}_3:\text{NO}_2:\text{NO}_3 = 500:500:500 \mu\text{M}$). **C)** Non-equimolar feeding ($\text{NH}_3:\text{NO}_2:\text{NO}_3 = 500:375:500 \mu\text{M}$). Black circles represent inactive individuals.....199
- Figure D.3. Metabolic ratios of *Nitrospira* (AO, NO and CMX) represented as $\ln(A/B)$ at different nitrogen feeding regimes ($\text{NH}_3:\text{NO}_2:\text{NO}_3$ ratio) and oxygen concentrations.** A) Metabolic ratios between CMX and division of labour (AO+NO). **B)** Metabolic ratios between CMX and AO. Error bars show standard deviation of $n = 3$ simulation replicates. Feeding regimes – ammonia feeding: $500:0:0 \mu\text{M}$; equimolar feeding: $500:500:500 \mu\text{M}$; non-equimolar feeding: $500:375:500 \mu\text{M}$. The statistical significance between the different nitrogen feeding regimes is shown in Table D.9.....200
- Figure D.4. Ecological analysis at floc level under conditions where only comammox *Nitrospira* remained active (3.0 and 93.8 μM of O_2).** Ammonia feeding ($\text{NH}_3:\text{NO}_2:\text{NO}_3 = 500:0:0 \mu\text{M}$, left panels), equimolar feeding ($\text{NH}_3:\text{NO}_2:\text{NO}_3 = 500:500:500 \mu\text{M}$, centre panels), and non-equimolar feeding ($\text{NH}_3:\text{NO}_2:\text{NO}_3 = 500:375:500 \mu\text{M}$, right panels). The correlation coefficients of metabolisms are presented on a colour scale. Dotted cells indicate statistically significant correlation (\blacksquare : $p < 0.05$; $\blacksquare\blacksquare$: $p < 0.01$; $\blacksquare\blacksquare\blacksquare$: $p < 0.001$). Cross symbol (x) indicates no co-existence of the metabolic pair at the end of the simulation experiments. Bottom-right labels indicate the ecological interaction of metabolic pair: CC – Commensalism + Competition; SC – Syntrophism + Competition; C – Competition. Sample sizes employed for Kendall's τ calculation are shown in Figure D.5.....201
- Figure D.5. Sample sizes employed for Kendall's coefficient calculation.** Different nitrogen feeding regime was applied: ammonia feeding (left panels, $\text{NH}_3:\text{NO}_2:\text{NO}_3 = 500:0:0 \mu\text{M}$), equimolar feeding (centre panels, $\text{NH}_3:\text{NO}_2:\text{NO}_3 = 500:500:500 \mu\text{M}$), and non-equimolar feeding (right panels, $\text{NH}_3:\text{NO}_2:\text{NO}_3 = 500:375:500 \mu\text{M}$),). Total replicates: 36 in all conditions.....202
- Figure D.6. Influence of nitrate concentration in influent to anaerobic oxidation performance (ammonia and nitrite oxidation to N_2) expressed as percentage.** Data labels depict the relative abundance of anaerobic activities (An-NRMX and AMX). Feeding regimes: non-equimolar feeding – $500:375:500 \mu\text{M}$; non-equimolar feeding without NO_3 – $500:375:0 \mu\text{M}$. Error bars show standard deviation of $n = 3$ simulation replicates. Asterisks denote p -value significance where *, $p < 0.05$. For more information about the calculus of the anaerobic oxidation performance (see Methods of Chapter 7 – Parameters for the quantification of nitrogen removal).203
- Figure D.7. Influence of ammonia concentration to the transient accumulation of nitrite at 93.8 μM of O_2 .** Three ammonia concentrations were tested. Full simulation (5.0 years): 100 μM of

NH_3 (panels **A**), 500 μM of NH_3 (panels **B**), and 1000 μM of NH_3 (panels **C**). Left panels show the dynamics of nitrogen compounds (NH_3 , NO_2 and NO_3) at the early stages of simulation. Right panels show the evolution of relative abundances of comammox *Nitrospira* and anammox. Error bars show standard deviation of $n = 3$ simulation replicates. If not visible, error bars are smaller than symbols.

.....204

Figure D.8. Analysis of ecological environment and dominant substrates (global eco-interaction modulus, ϕEI^*). First 50 weeks are shown (full simulation in Fig. D.9). Feeding regimes: only ammonia feeding ($\text{NH}_3:\text{NO}_2:\text{NO}_3 = 500:0:0 \mu\text{M}$, left panels), equimolar feeding ($\text{NH}_3:\text{NO}_2:\text{NO}_3 = 500:500:500 \mu\text{M}$, centre panels), and non-equimolar feeding ($\text{NH}_3:\text{NO}_2:\text{NO}_3 = 500:375:500 \mu\text{M}$, right panels). Error bars show standard deviation of $n = 3$ simulation replicates. If not visible, error bars are smaller than line weight.205

Figure D.9. Analysis of ecological environment and dominant substrates (global eco-interaction modulus, ϕEI^*). Full simulation (5.0 years). Feeding regimes: only ammonia feeding ($\text{NH}_3:\text{NO}_2:\text{NO}_3 = 500:0:0 \mu\text{M}$, left panels), equimolar feeding ($\text{NH}_3:\text{NO}_2:\text{NO}_3 = 500:500:500 \mu\text{M}$, centre panels), and non-equimolar feeding ($\text{NH}_3:\text{NO}_2:\text{NO}_3 = 500:375:500 \mu\text{M}$, right panels). Error bars show standard deviation of $n = 3$ simulation replicates. If not visible, error bars are smaller than line weight.....206

Figure E.1. Visual representation of concordance and discordance for two joint variables (X and Y). All points in the grey area are concordant, and all points in the white area are discordant with respect to (x_i^*, y_i^*)208

Figure E.2. Representation of concordance and discordance for three joint variables (X, Y, Z). All points in grey region are concordant, and all points in white region are discordant with respect to (x_i^*, y_i^*, z_i^*)210

List of Accompanying Material

Code 1. Individual-based Model framework for microbial aggregates (granule and suspension version) [v2.4.3]. Available on <https://github.com/Computational-Platform-IbM/IbM>.

Code 2. Ecological analysis of pairwise and higher-order interactions: nOEN platform (n-Order Ecological Network) [v1.0.0]. Available on <https://github.com/soundslikealloy/nOEN>.

Code 3. Multivariate Kendall's Tau (Tau-N) using paired orthants [v1.0.0]. Available on <https://github.com/soundslikealloy/multivarcorr>.

Video C.1. Development of aggregates and substrate profiles from simulations considering neutralism, competition and commensalism with $[S]_T = 10$ mM (from 0 d to 10 d).

Video C.2. Development of aggregates and substrate profiles from simulations considering neutralism, competition and commensalism with $[S]_T = 1$ mM (from 0 d to 15 d).

Video C.3. Development of aggregates and substrate profiles from simulations considering or not the influence of shear forces (detachment) (from 0 d to 50 d). The simulation experiments including detachment were started with the same inoculum as those without detachment with the objective to observe the genuine impact of the shear force in the spatial distribution of the microbial populations.

Supplementary Videos (Videos C.1 – C.3) are available on PLOS Computational Biology Journal (Martinez-Rabert et al., 2022). Link: <https://doi.org/10.1371/journal.pcbi.1010807>

Acknowledgments

First, I would like to express my gratitude to Professor Cindy Smith and Professor Will Sloan for all your help and supervision over the years. Last but not least, thanks to my supervisor, and now my colleague and friend Dr. Rebeca Gonzalez-Cabaleiro for all the encouragement, supervision and the myriad of fantastic scientific discussions over the past few years. I would also like to thank Dr. Umer Ijaz for your assistance in using Orion Cluster, and Dr. Marta Vignola for all your comments and recommendations improving the quality of my research.

I gratefully acknowledge the EPSRC for funding this project, allowing me the opportunity to conduct this research and meet incredible people, and also the Soehngen Institute of Anaerobic Microbiology (SIAM) for funding my research visits to TU Delft.

To my fellow PhD students and postdocs, William Barr, Tymon Herzyk, Dr. Vironika Bahat and Dr. Fabien Cholet, thanks for your coffee-hour chats and laughs. Sincerest thanks to Valentine Okonkwo for his continuous support and encouragement during the long nights at ARC, and the celebrations at Paesano and Inn Deep. To those I have not named individually, please know I am extremely grateful for your contributions to this PhD.

Finally, I thank you to my parents Valentí and Esther, and my brothers Sergi and Claudia for their belief and support throughout the course of this PhD. To my close friends, Alex, Claudia, David and Raul, thanks for the fabulous moments together and unforgettable trips. Thanks to Carles, Paqui, Scott, Sam and Milan for the incredible MTB riding moments. Cristina and Archie, although unfortunately our paths went in different directions, I sincerely thank you for your love, support, encouragement and patience in my most difficult times. I hope everything goes well both. Without my family and friends, I would not have been able to finish this journey, if it were not for your constant support and encouragement.

Declaration of Originality

I certify that the thesis presented here for examination for a PhD degree of the University of Glasgow is solely my own work other than where I have clearly indicated that it is the work of others (in which case the extent of any work carried out jointly by me and any other person is clearly identified in it) and that the thesis has not been edited by a third party beyond what is permitted by the University's PGR Code of Practice.

The copyright of this thesis rests with the author. No quotation from it is permitted without full acknowledgement.

I declare that this thesis does not include work forming part of a these presented successfully for another degree.

I declare that this thesis has been produced in accordance with the University of Glasgow's Code of Good Practice in Research.

I acknowledge that if any issues are raised regarding good research practice based on review of this thesis, the examination may be postponed pending the outcome of any investigation of the issues.

Name: Eloy Martínez Rabert

Registration Number: XXXXXXXX

Abbreviations and Special Symbols

Abbreviations

(d)FBA	(Dynamic) Flux Balance Analysis
3HP/4HB	3-hydroxypropionate/4-hydroxybutyrate cycle
AMO	Ammonia monooxygenase
AMX	Anaerobic ammonia oxidation (Anammox) or Anammox bacteria
An-NRMX	Anaerobic nitrite-reducing ammonia oxidation
AO	Ammonia oxidation (catabolic activity)
AOA	Ammonia-oxidizing archaea
AOA-FW	Non-marine ammonia-oxidizing archaea
AOA-SW	Marine ammonia-oxidizing archaea
AOB	Ammonia-oxidizing bacteria
AOB-FW	Non-marine ammonia-oxidizing bacteria
AOB-SW	Marine ammonia-oxidizing bacteria
AOM	Ammonia-oxidizing microbes (including bacteria and archaea)
CBB	Calvin-Bassam-Benson cycle
CMX	Complete ammonia oxidation (comammox) or comammox bacteria
CO ₂ -e	Global Warming Potential (GWP) value relative to CO ₂
CSTR	Continuous Stirred Tank Reactor
C-type NOB	Nitrite-oxidizing bacteria with cytoplasmic nitrite oxidoreductase
CytL	Cytochrome P460
DNRA	Dissimilatory nitrite reduction to ammonium
ETC	Electron transport chain
ETM	Electron transfer module
HAO	Hydroxylamine oxidoreductase
HDH	Hydrazine dehydrogenase
HOX	Hydroxylamine oxidase
HURM	Hydroxylamine Ubiquinone Redox Module
HZS	Hydrazine synthase
IbM	Individual-based Model
<i>Nb</i>	<i>Nitrobacter</i> genus (nitrite-oxidizing bacteria)

<i>Nc</i>	<i>Nitrococcus</i> genus (nitrite-oxidizing bacteria)
<i>Ng</i>	<i>Nitrotoga</i> genus (nitrite-oxidizing bacteria)
NirK _(rev)	(Reverse) nitrite reductase
<i>Nn</i>	<i>Nitrospina</i> genus (nitrite-oxidizing bacteria)
NO	Nitrite oxidation (catabolic activity)
NOB	Nitrite-oxidizing bacteria
NOB-FW	Non-marine nitrite-oxidizing bacteria
NOB-SW	Marine nitrite-oxidizing bacteria
NOO	Nitric oxide oxidoreductase
NOR	Nitric oxide reductase
NRMX	Nitrate-reducing ammonia oxidation (catabolic activity)
<i>Ns</i>	<i>Nitrospira</i> genus (nitrite-oxidizing bacteria)
NXR	Nitrite oxidoreductase
OMZ	Oxygen minimum zones
PbM	Population-based Model
P-type NOB	Nitrite-oxidizing bacteria with periplasmic nitrite oxidoreductase
rTCA	Reductive tricarboxylic acid cycle
sP-type NOB	Nitrite-oxidizing bacteria with soluble periplasmic nitrite oxidoreductase
WWTP	Wastewater treatment plant

Special Symbols

Pr{ }	Probability
:	Such that (<i>e.g.</i> , { $x : x > 0$ } means “set of numbers x such that $x > 0$ ”)
⊙	Paired
∈	Belongs to, is an element of
∧	Logical conjunction (AND)
∨	Logical (inclusive) disjunction (OR)
≡	Equivalence (the same as)
⇒	Implies
→	Follows a specific data trend
¬	Negation or inverse (in this case, positive/negative)

1.

Introduction.

1.1. Background

Advances in metagenomics and culture-independent studies have greatly increased our knowledge of microbial communities revealing, in part, that microbial ecology is not as simple as once thought (Hugenholtz et al., 1998; Marco, 2011). Nitrification process is a direct example of this (Figure 1.1). In 1891, Winogradsky and Warington established that nitrification was an aerobic two-step process where ammonia is first oxidized to nitrite by ammonia-oxidizing bacteria (AOB) and then, nitrite oxidized to nitrate by nitrite-oxidizing bacteria (NOB) (Dworkin & Gutnick, 2012) (Figure 1.1A). In the following decades, nitrification research made great progress by revealing new nitrifying cohorts and clarifying their biochemistry (Figure 1.1B).

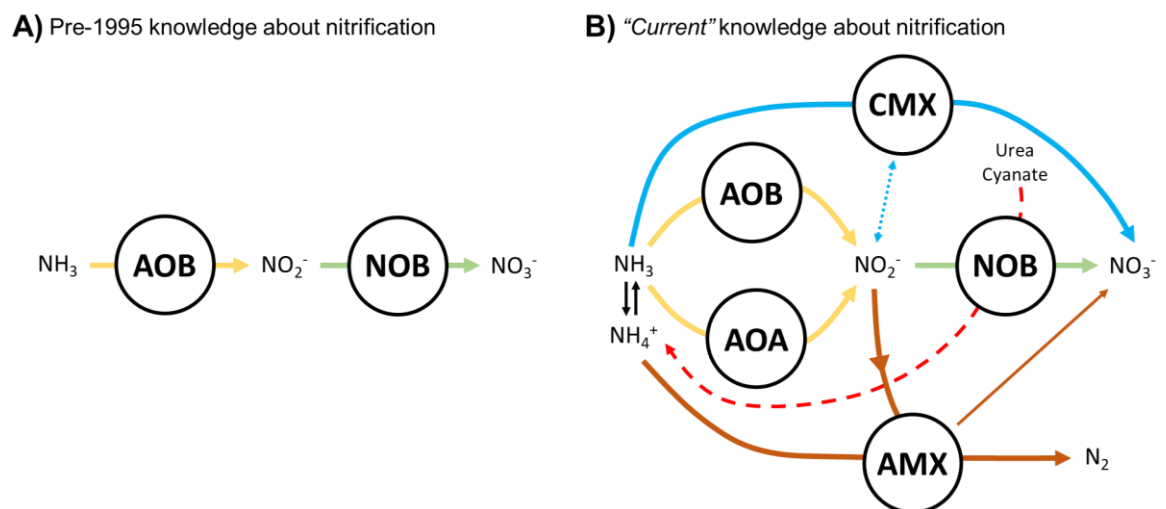


Figure 1.1. Evolution of our understanding of nitrification from A) pre-1995 to B) today.

The conception that biological ammonia oxidation was only possible under aerobic conditions was refuted when anaerobic ammonia oxidation (anammox process) was discovered in a denitrifying reactor (Mulder et al., 1995). In 2005, the first archaeal ammonia oxidizers (ammonia-oxidizing archaea, AOA) was isolated from terrestrial and marine habitats (Könneke et al., 2005; Treusch et al., 2005). Then, in 2015, some NOB species (belonging to *Nitrospira* sublineage II) were proven to fully catalyse the complete ammonia oxidation process to nitrate (named comammox bacteria, CMX) (Daims et al., 2015; van Kessel et al., 2015). Together, with further observations of diverse NOB metabolic activity and new NOB isolates, the previously underestimated NOB group revealed wide metabolic and physiological diversity (Daims et al., 2016). Considering this new information, the full understanding of nitrification in both natural and engineered systems is challenged. Understanding the relationship between nitrifying populations, new opportunities for novel

designs of biotechnologies might arise, enabling the control of nitrogen concentration in water in a more sustainable way.

Any research question can be addressed in different ways: top-down approach, bottom-up approach or a combination of both (outside-in approach). A top-down approach attempts to first recognise the patterns in the data and then find the mechanisms that generate those patterns. Examples of this approach are meta-studies (*e.g.*, meta-analysis, metagenomics, meta-transcriptomics or meta-proteomics) and data-driven modelling such as the application of machine learning. On the other hand, bottom-up approaches apply the well-known and hypothetical mechanisms to fit their predictions with the observed data, assembling new theories. The identification and comprehension of the subsystems that are part of complex systems is essential. Examples of bottom-up approach are *in-vitro* systems of simple communities (from monoculture to few species) and first-principles models. Note that modelling exercises are perfectly suited to bottom-up approaches because the full control of the studied system, as long as the model is free of bugs and misconceptions.

No approach is perfect. A disadvantage of top-down approaches is the consideration of the system as a black box, hampering the fully comprehension of fundamental mechanisms when multiple variables are at play. Bottom-up approach is problematic when the system is especially complex and fundamental mechanisms are unknown. Therefore, an outside-in approach can help to overcome the flaws of both approaches.

1.2. Research Aims and Objectives

The aim of this research is to elucidate the ecological mechanisms that shape the microbial communities of nitrifiers incorporating the latest discoveries on this topic. To achieve this aim, the following objectives were identified:

- To identify the ecological niches in which a specific population of aerobic nitrifiers will dominate based on the kinetic parameters that define the microbial growth and the known biochemical information.
- To develop an *in-silico* methodology in order to study the influence of the ecological interactions and the environment on the microbial community assembly.
- To evaluate the influence of cell-cell, cell-environment and cell-space interactions on the community of nitrifiers in aggregates.

- To investigate the survival capacity of comammox bacteria under nitrogen and oxygen limiting conditions considering their potential metabolic heterogeneity.

1.3. Thesis outline

This thesis details the combination of top-down and bottom-down approaches (outside-in approach) for the quantitative analysis of the ecology of nitrifiers.

Chapter 2 presents a detailed review of literature about nitrifying and anammox bacteria, the role of nitrification on nitrogen cycle and the contribution of nitrification on nitrous oxide emissions (one of the most important greenhouse gasses).

Chapter 3 presents the meta-analysis of the kinetic parameters of aerobic nitrifiers and the influence of the environment on nitrifying activity. This meta-analysis reviews about 100 references in literature and includes more than 300 data points.

The current situation of research in microbial ecology is the topic of Chapter 4. This section describes the tendency to top-down approaches on ecological studies, bringing the absence of new hypotheses and theories. In order to deal with this, a modelling methodology based on bottom-up approach is proposed to generate new hypotheses and theories on microbial ecology (*in-silico* bottom-up methodology).

Chapter 5 details the multi-scale model utilised in this thesis. The integration of biological model (Individual-based Model) and physical model (diffusive transport) together with their respective formulations are described here.

Chapter 6 presents the *in-silico* study of the main ecological interactions between nitrifiers, environmental impacts on the community, and the space competition inherent in microbial aggregates. Additionally, a theoretical modulus is defined, being able to quantify the effect of environmental conditions and ecological interactions on microbial community assembly.

Chapter 7 presents the *in-silico* study of the resilience of comammox bacteria under nitrogen and oxygen limited environments (applying the conditions of the early discoveries of comammox) and considering their metabolic heterogeneity. A novel statistical method to evaluate the ecological interactions is detailed and evaluated. The theoretical modulus defined in Chapter 6 is applied to determine which substrate rules the community assembly.

Finally, Chapter 8 summarizes the main finding of this research and also includes recommendations for future research.

2.

Literature review.

2.1. Nitrogen cycle and human impact

Nitrogen is an essential element in cellular biomass, being present in building components such as amino acids (building blocks of proteins) and nucleic acids (building blocks of DNA). In some cases, nitrogen compounds are also utilized as energy source (as electron donors or acceptors) by microorganisms, such as nitrifiers, denitrifiers or anammox bacteria (Stein & Klotz, 2016). The Earth's atmosphere is composed of 78% dinitrogen gas (N_2) (Haynes, 2016), but this cannot be assimilated by all life forms. Thanks to biological nitrogen cycle, atmospheric N_2 is balanced in all available forms of nitrogen (organic and inorganic), that is, ammonia/ammonium (NH_3/NH_4^+), nitrite (NO_2^-), nitrate (NO_3^-) and organic nitrogen (C-N) (Figure 2.1).

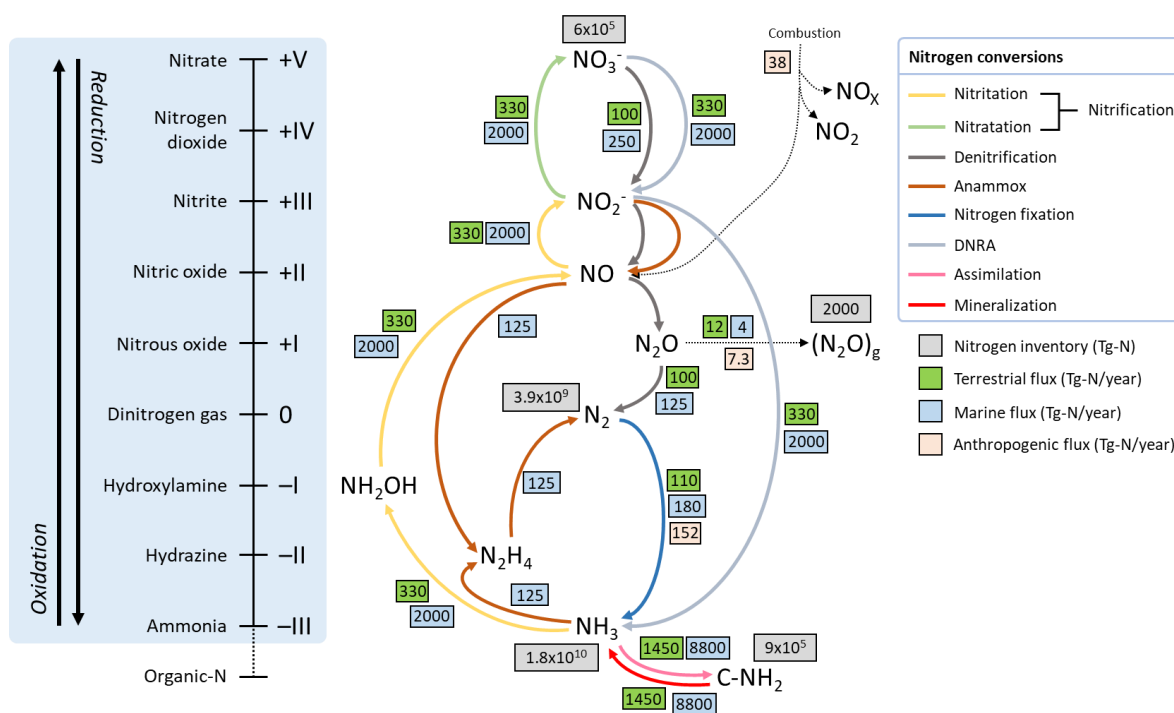


Figure 2.1. Major processes of nitrogen cycle according to the redox state. Nitrogen inventory for organic nitrogen, ammonia, nitrate, nitrous oxide gas and dinitrogen gas (grey squares), and estimated conversions (green, blue and salmon squares) are included. The interconversion of ammonia and organic nitrogen (organic-N) does not involve a change in the redox state of the nitrogen atom. The ammonia inventory is found mainly in rocks and sediments. This ammonia becomes available with the erosion. Whereas the terrestrial inventory of ammonia is known, the marine inventory is estimated to be between 340 and 3600 Tg-N. DNRA refers to dissimilatory nitrate reduction to ammonia. Anthropogenic flux from (Battye et al., 2017; Tian et al., 2020). The anthropogenic nitrogen fixation includes N-fixing crops and the synthesis of NH_3 by Haber-Bosch process. Figure adapted from (Kuypers et al., 2018).

The nitrogen cycle is a coordinated network of reactions where distinct biogeochemical processes are interconnected. The microbial nitrogen cycle consists of seven major processes, combining oxidation and reduction reactions of several nitrogen forms (Figure 2.1): (i) nitrification, including nitritation (oxidation of NH_3 to NO_2^-), nitrataion (oxidation of NO_2^- to NO_3^-), and complete ammonia oxidation (comammox, oxidation of NH_3 to NO_3^-); (ii) denitrification (reduction of NO_3^- to N_2 , with NO_2^- , NO and N_2O as intermediates); (iii) anaerobic ammonia oxidation (anammox); (iv) nitrogen fixation; (v) dissimilatory nitrite reduction to ammonium (DNRA); (vi) assimilation (transformation of mineral ammonia (NH_3) to organic nitrogen (*e.g.*, urea, cyanate, amino acids or nucleic acids); and (vii) mineralization (transformation of organic nitrogen to mineral ammonia).

However, humankind have modified this natural cycle by introducing anthropogenic sources and conversions. Prior to the discovery and exploitation of Haber-Bosch process in 1909 (the industrial fixation of N_2 to NH_3), nearly all of the reactive nitrogen in the biosphere was generated and recycled through biogeochemical process. The latest studies about the humankind contributions to nitrogen cycle estimated that around 190 Tg-N/year of reactive nitrogen proceed from anthropogenic activities (110 Tg-N/year from fertilizers, 42 Tg-N/year from N-fixing crops and 38 Tg-N/year from combustion) (Battye et al., 2017). These contributions do not only lead to an environmental degradation and loss of diversity due to the accumulation of N-forms in soil and water (soil acidification and eutrophication), but also to the increase of greenhouse gases emissions, such as N_2O (298 $\text{CO}_2\text{-e}$). The estimated global N_2O budget from anthropogenic sources for the period 2007 to 2016 was 4.2–11.4 Tn-N/year (mean 7.3 Tn-N/year). The main anthropogenic contribution of N_2O emissions comes from agricultural activity (2.5–5.8 Tn-N/year; mean 3.8 Tn-N/year), followed by the combustion of fossil fuels and biomass (1.3–1.9 Tn-N/year; mean 1.6 Tn-N/year), sewage depositions (0.7–2.2 Tn-N/year; mean 1.3 Tn-N/year), and wastewater treatment (0.2–0.5 Tn-N/year; mean 0.3 Tn-N/year) (Tian et al., 2020).

Today, discharge limits for nitrogen are in place (<10 mg-N/L according to the European Council Directive 91/271/ECC; <0.08 mg-N/L according to EPA). Generally, wastewater treatment plant (WWTP) exploits the natural capacity of some microbial cohorts to transform the different forms of soluble nitrogen (organic nitrogen, NH_3 , NO_2^- and NO_3^-) to N_2 , reducing their accumulation in the aquatic environment (Chen et al., 2020). Conventional wastewater treatment systems rely on the combination of nitrification (aerobic oxidation of NH_3 to NO_3^-) and denitrification (anaerobic reduction of NO_3^- to N_2). However, the use of

these conventional processes significantly increases the energetic demands of WWTP (Drewnowski et al., 2019). This is because nitrification requires extensive aeration to create suitable conditions for nitrification (from 50% to 90% of the total electricity consumption), and external organic carbon is sometimes needed to induce heterotrophic denitrification. Additionally, ~4.1% of the treated nitrogen is emitted to the atmosphere in form of N₂O (Tian et al., 2020), contributing to an increase in the global greenhouse emissions.

Different reactor configurations have been implemented to minimize the external addition of oxygen and carbon source (*e.g.*, modified Ludzack-Ettinger configuration or 4-stage Bardenpho configuration (Chen et al., 2020)). However, more sustainable nitrogen removal processes have emerged in recent decades. The most relevant example of this is the combination of nitrification and anammox processes (Lackner et al., 2014) that are able to convert NH₃ to N₂ gas reducing up to 60% of oxygen requirements (van Dongen et al., 2001). In compact bioreactors, aerobic ammonia oxidizers convert half of the available ammonia to nitrite under oxygen limitation. This is followed by the conversion of the remaining NH₃ and NO₂⁻ to N₂ by anammox process. In addition to the lower aeration requirements, this system do not need the addition of organic carbon, and the production of N₂O from denitrification is avoided. Nevertheless, the application of anammox-based processes is limited to treat ammonia-rich wastewaters, such as effluents from anaerobic sludge digesters (Pedrouso et al., 2021).

2.2. Nitrification and anammox

The ecological roles of nitrification can be summarized in (i) transformation of NH₃ to NO₃⁻ reducing the availability of nitrogen source for plants and algae (*i.e.*, NH₄⁺/NH₃), although it is worth noticing that plants can also absorb NO₃⁻ adapting their root morphology (Giehl & von Wirén, 2014) and some algae (such as *Chlamydomonas acidophila*) preferred NO₃⁻ as nitrogen source for photosynthesis and growth under phosphorous-limiting environments (Lachmann et al., 2019); (ii) production of substrate for denitrification (NO₂⁻ and NO₃⁻), closing the nitrogen cycle; (iii) production of N₂O in aquatic and terrestrial ecosystems; (iv) consumption of oxygen in sediments and water columns, generating anoxic and anaerobic environments; and (v) acidification of the environment.

Nitrification involves three main cohorts of aerobic microbes: ammonia oxidizers (bacteria and archaea (Könneke et al., 2005; Treusch et al., 2005)); nitrite oxidizers (bacteria); and complete ammonia oxidizers (comammox bacteria) (Costa et al., 2006; Daims et al., 2015;

van Kessel et al., 2015). Ammonia can also be oxidised under anaerobic conditions by anaerobic ammonia oxidizers (anammox bacteria) (Mulder et al., 1995; Strous, Fuerst, et al., 1999). Anammox bacteria are not strictly nitrifiers, but they have also been considered in this thesis due to their ubiquity (Wang et al., 2019), application in wastewater treatment (Lackner et al., 2014) and their ecological implications on nitrification (Section 2.4).

2.2.1. Ammonia oxidizers (AOM)

Ammonia oxidizers (AOM) are a vast community of nitrifiers belonging to the two prokaryotic domains, bacteria and archaea. Phylogenetically, ammonia-oxidizing bacteria (AOB) belong to Pseudomonadota phylum (formerly Proteobacteria (Oren & Garrity, 2021)) and include species of *Nitrosomonas*, *Nitrosococcus*, and *Nitrospira* genera (Aakra et al., 2001). Ammonia-oxidizing archaea (AOA) belong to Thaumarchaeota phylum and include species of *Nitrosopumilus*, *Nitrosoarchaeum*, *Nitrososphaera*, *Nitrosotalea*, *Nitrosotenuis*, *Nitrosocosmicus* and *Nitrosocaldus* genera (Alves et al., 2018). In most WWTPs, the dominant ammonia oxidizers belong to *Nitrosomonas* genus (Dueholm et al., 2022).

2.2.1.1. Ammonia-oxidizing bacteria (AOB)

AOB are chemolithoautotrophs and aerobes. The main source of energy of AOB is through the oxidation of NH_3 to NO_2^- , and this energy is employed for maintenance and growth. These autotrophic bacteria fix atmospheric CO_2 by the Calvin-Bassam-Benson cycle (CBB cycle) (Chain et al., 2003). In ammonia oxidation, NH_3 is first oxidized to hydroxylamine (NH_2OH) by a membrane-bound enzyme ammonia monooxygenase (AMO). Then, NH_2OH is oxidized to nitric oxide (NO) by hydroxylamine oxidoreductase (HAO) and, finally, NO is oxidized to NO_2^- by a yet-to-be-determined NO oxidoreductase (NOO) (Caranto & Lancaster, 2017). Reverse nitrite reductase (NirK_{rev}) was proposed as the candidate enzyme for the bacterial NOO (Lancaster et al., 2018). Currently it is assumed that the only energy-generating steps are the two-step oxidation of NH_2OH to NO_2^- (González-Cabaleiro et al., 2019; Yuan & Vanbriesen, 2002). When NH_2OH is oxidized to NO, three electrons are released – two of these electrons are transferred to AMO, and the last electron is transferred to the electron transport chain (ETC). The oxidation of NO to NO_2^- contributes with an additional electron to ETC (Figure 2.2). The main terminal oxidase (enzyme responsible to catalyse the reduction of oxygen to water using the electrons from electron donor) is the heme-copper oxygen reductase aa₃-type, but some *Nitrosomonas* species (such as *Nitrosomonas eutropha* and *Nitrosomonas* sp. strain GH22) also encode for cbb₃-type

oxidase and quinol oxidase bo_3 (Sedlacek et al., 2019; Thandar et al., 2016; Whittaker et al., 2000).

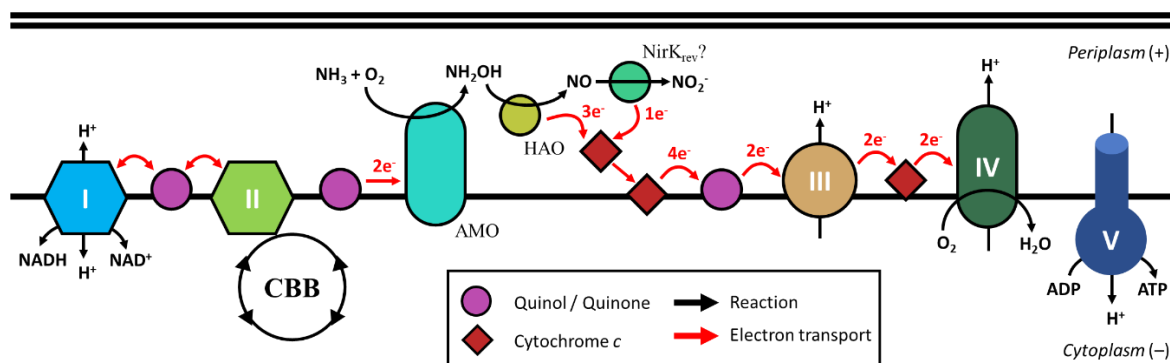


Figure 2.2. Schematic illustration of electron transport and generation of proton motive force (energy metabolism) in ammonia-oxidizing bacteria (AOB). CBB represents the Calvin-Bassam-Benson cycle. Complex I is the NADH ubiquinone oxidoreductase. Complex II is the succinate dehydrogenase. Complex III (ubiquinol-cytochrome c reductase) and complex IV (cytochrome aa₃) are the sites where electron transport is coupled to proton pump. Complex V is the ATP synthase, the site of oxidative phosphorylation to generate ATP. Black arrows with H⁺ labels represent the proton flux through the periplasmic membrane. Double thick lines represent the cell wall.

Generally, AOB are considered obligate aerobes, but it has been observed that some *Nitrosomonas* species (such as *N. europaea* or *N. eutropha*) can generate ATP and grow slowly under anaerobic conditions via nitrifier-denitrification (partial or complete), where NH₃ is oxidized to NO₂⁻ and then, NO₂⁻ is reduced to NO, N₂O and N₂ (Schmidt & Bock, 1997). Also they can use hydrogen or pyruvate as electron donor and NO₂⁻ as electron acceptor (Abeliovich & Vonshak, 1992; Bock et al., 1995), or oxidize NH₃ to NO₂⁻ using nitrogen dioxide (NO₂) as electron acceptor (Schmidt & Bock, 1998).

2.2.1.2. Ammonia-oxidizing archaea (AOA)

AOA are chemolithoautotrophs and aerobes. Like AOB, they obtain energy for maintenance and growth through the oxidation of NH₃ to NO₂⁻ (being NH₂OH and NO also intermediates of archaeal nitrification (Kozlowski et al., 2016)) and use inorganic carbon as sole carbon source. However, the biochemistry of both NH₃ oxidation and inorganic carbon fixation differs from AOB.

In particular, archaeal AMO seems to be more diverse and complex than bacterial AMO (Hodgskiss et al., 2023), explaining the wider range of ammonia affinities observed in AOA in comparison to the ones reported for AOB (see Chapter 3 and (Jung et al., 2022)). The

structure and charge of the archaeal cell wall (composed by proteinaceous macromolecular assemblies that form a two-dimensional crystal lattice, known as surface layer or S-layer) might also explain the wide range of archaeal affinities (P.-N. Li et al., 2018). Additionally, the homologous archaeal HAO has not been isolated yet (Lehtovirta-Morley, 2018). While AOB have iron-based respiratory chain proteins, AOA lack the cytochrome *c* proteins and, instead, have copper-based electron transport chain (Walker et al., 2010). This would explain why archaeal nitrification (but not bacterial nitrification) is significantly constrained by the presence of organic matter (copper complexation) in municipal WWTP (Gwak et al., 2019). The only ETC enzyme that both ammonia oxidizers share is their terminal oxidase (heme-copper oxygen reductase aa₃-type) (Schäfer & Penefsky, 2008; Walker et al., 2010).

Since the discovery of AOA, several pathways of archaeal nitrification have been proposed. One of the most accepted is the involvement of the oxidation of NH₂OH and NO to NO₂⁻ by a novel copper-containing enzyme (Hydroxylamine Ubiquinone Redox Module, HURM) generating five electrons (Kozłowski et al., 2016; Wan et al., 2023). Two of these electrons are transferred to the AMO enzyme, one electron is employed in the reduction of NO₂⁻ to NO, and the last two electrons are transferred to the ETC (Figure 2.3A). After the re-evaluation of bacterial nitrification, Lehtovirta-Morley (2018) proposed that archaeal and bacterial nitrification might proceed in the same order (*i.e.*, the three-step pathway NH₃ → NH₂OH → NO → NO₂⁻, Figure 2.3B). The last step, the oxidation of NO to NO₂⁻, could be catalysed by NirK_{rev} or cupredoxin-like proteins (isolated in *Nitrosopumilus maritimus* and *Candidatus* Angelarchaeales sp. (Diamond et al., 2022; Hosseinzadeh et al., 2016)). The three-step pathway would explain how it is possible that some AOA species (such as *Nitrosocaldus yellowstoneii*, *Candidatus* Nitrosocaldus islandicus, *Candidatus* Nitrosocaldus cavascurensis or *Cenarchaeum symbiosum*) are able to survive lacking *nirK* genes (Abby et al., 2018; Daebeler et al., 2018; Kerou et al., 2016).

On the other hand, AOA fix bicarbonate (HCO₃⁻) via a modified 3-hydroxypropionate/4-hydroxybutyrate cycle (3HP/4HB cycle), which differs from the 3HP/4HB cycle of other archaeal phyla (such as Crenarchaeota). Thaumarchaeal 3HP/4HB cycle is considered the most energy-efficient aerobic pathway for inorganic carbon fixation (Könneke et al., 2014). Additionally, the 3HP/4HB cycle gives AOA the ability to co-assimilate various organic compounds, explaining why mixotrophy has also been observed in Thaumarchaea (Hatzenpichler, 2012).

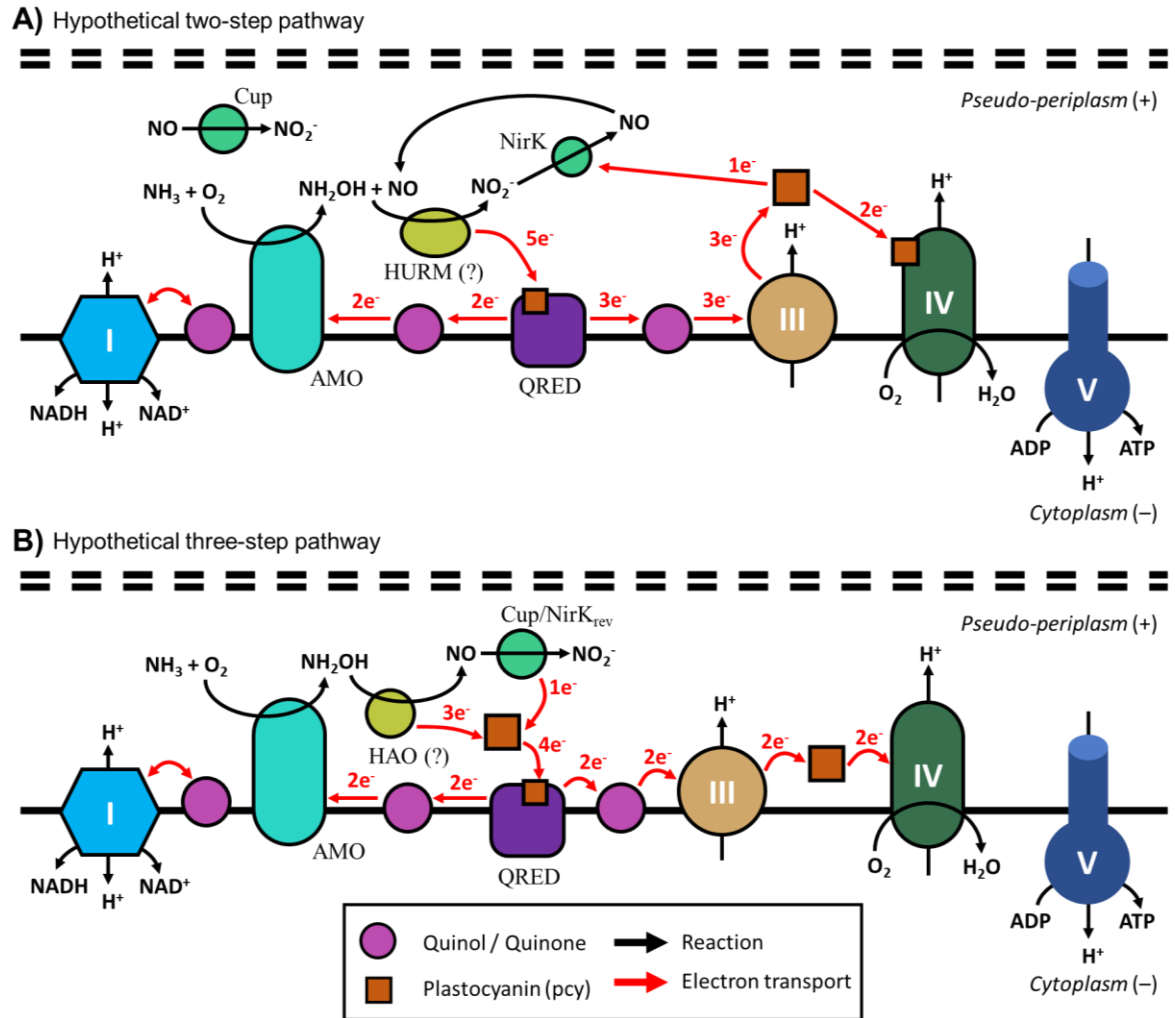


Figure 2.3. Reconstruction of the proposed pathways of ammonia oxidation, electron transfer and generation of proton motive force (energy metabolism) in ammonia-oxidizing archaea (AOA). **A)** Hypothetical two-step model (proposed by Kozłowski *et al.* (2016)). **B)** Hypothetical three-step model (proposed by Lehtovirta-Morley (2018)). Complex I is the NADH ubiquinone oxidoreductase. QRED is the quinone reductase. HURM represents the hydroxylamine ubiquinone redox module. Cup represents the cupredoxin-like proteins. Complex II is the succinate dehydrogenase. Complex III (ubiquinol-cytochrome bc_1 reductase) and complex IV (cytochrome aa_3) are the sites where electron transport is coupled to proton pump. Complex V is the ATP synthase, the site of oxidative phosphorylation to generate ATP. Black arrows with H^+ labels represent the proton flux through the periplasmic membrane. Double dashed lines represent the S-layer.

Recently, it has been found that *N. maritimus* is capable of producing oxygen to sustain the ammonia oxidation in anoxic environments (Kraft *et al.*, 2022). Although the pathway of oxygen production is not fully resolved, Kraft *et al.* (2022) proposed a variation of the already known NO dismutation, found in methane-oxidizing bacteria (Ettwig *et al.*, 2012). In this pathway, NO_2^- is first reduced to NO by NirK. After that, NO is dismutated to N_2O

and oxygen (necessary to activate the ammonia oxidation by AMO). Finally, N_2O is reduced to N_2 (Figure 2.4). This could explain the abundance of AOA in environments with low (and even undetectable) oxygen concentrations, such as marine oxygen-minimum zones (Beman et al., 2012; Berg et al., 2015; Lu et al., 2019; Peng et al., 2013; Qin et al., 2017; Sollai et al., 2019; Stewart et al., 2012).

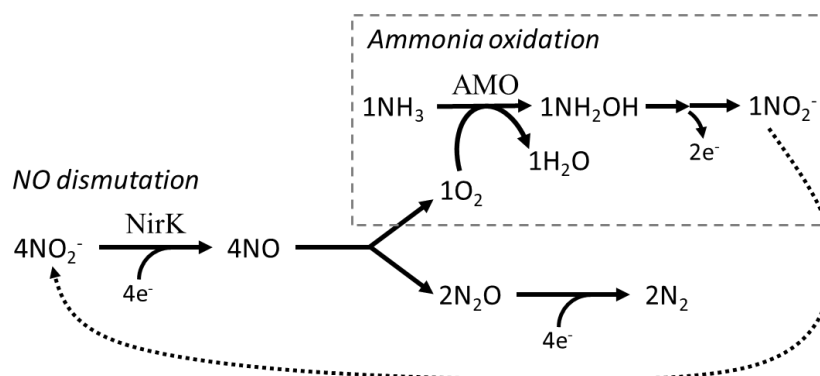


Figure 2.4. Proposed NO dismutation of *N. maritimus*. Coupling of ammonia oxidation and NO dismutation under anoxic conditions (presence of nitrite). The dismutation of NO to $O_2(aq.)$ and $N_2O(aq.)$ is thermodynamically favourable ($\Delta G^0 = -165 \text{ kJ/mol } O_2$). Figure adapted from Kraft et al. (2022).

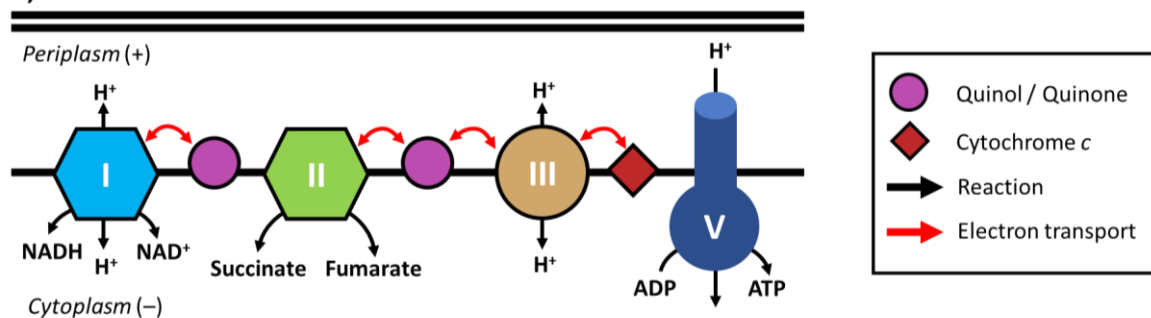
2.2.2. Nitrite oxidizers (NOB)

NOB group belongs to seven genera distributed in four bacterial phyla (in parenthesis) – *Nitrobacter* (Pseudomonadota), *Nitrotoga* (Pseudomonadota), *Nitrococcus* (Pseudomonadota), *Nitrospira* (Nitrospirae), *Nitrospina* (Nitrospinae), *Candidatus Nitromaritima* (Nitrospinae) and *Nitrolancaea* (Chloroflexi) (Daims et al., 2016). In general, all NOB genera are present everywhere and only few of them have been found in particular environments. For example, *Nitrospina* and *Ca. Nitromaritima* have been only identified in marine and hypersaline environments. *Nitrospira* is the most diverse and ubiquitous NOB genus, consisting of at least six phylogenetic sublineages. In fact, *Nitrospira* genus is the only NOB found in geothermal springs (Daims et al., 2016) and is also the dominant NOB in WWTPs (Dueholm et al., 2022).

NOB were formerly identified as obligate chemolithoautotrophs and aerobes, which obtain the energy for maintenance and growth from the oxidation of NO_2^- to NO_3^- shuttling two electrons to the ETC. The key enzyme of nitrite oxidation is the nitrite oxidoreductase (NXR). Different NXR orientation (cytoplasmic or periplasmic orientation) and final terminal oxidases (cyt. aa_3 -type, cyt. *bd*-like or cyt. *cbb_3*-type) have been observed among

the identified NOB genera (Figure 2.5 and Table 2.1). Like AOB, NOB fix atmospheric CO₂ as carbon source, but only some NOB use the CBB cycle (*Nitrobacter*, *Nitrotoga* and *Nitrococcus*), whereas *Nitrospira* and *Nitrospina* use an oxygen tolerant reductive tricarboxylic acid cycle (rTCA) to fix CO₂ (Table 2.1 – Anabolic pathways). The ecological implications of these physiological traits on NOB community are analysed in Chapter 3.

A) All NOB



B) Specific of NOB genera (*Nitrobacter*, *Nitrospira*, *Nitrospina*, *Nitrotoga*, *Nitrococcus*)

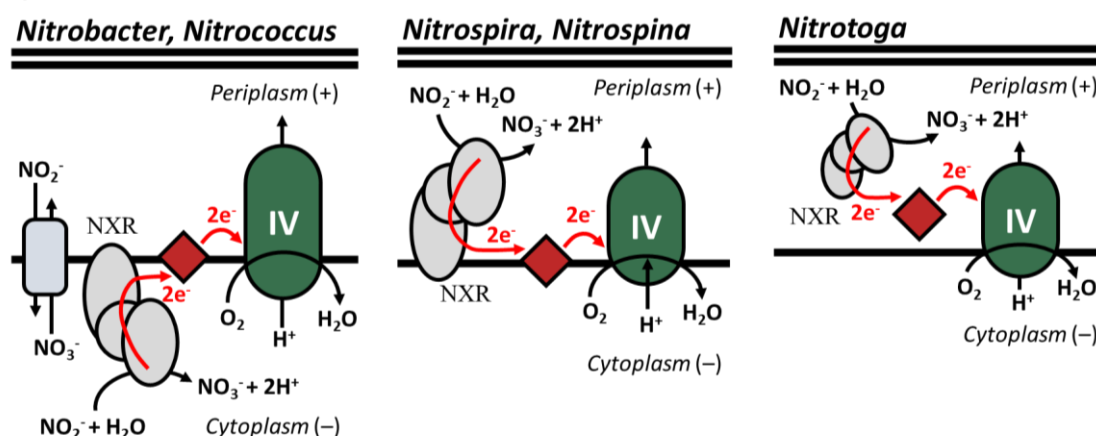


Figure 2.5. Schematic illustration of electron transport and generation of proton motive force (energy metabolism) in nitrite-oxidizing bacteria (NOB). **A)** All NOB genera. **B)** Specific of NOB genera. Complex I is NADH ubiquinone oxidoreductase. Complex II is the succinate dehydrogenase. Complex III (ubiquinol-cytochrome *c* reductase) and complex IV (terminal oxidase, *cyt. aa₃*, *cyt. bd*-like or *cyt. cbb₃*) are the sites where electron transport is coupled to proton pump. Complex V is the ATP synthase, the site of oxidative phosphorylation to generate ATP. Complex I, II, III and V are found in all NOB genera. The enzymatic differences of ETC between NOB genera are found on NXR and complex IV. Black arrows with H⁺ labels represent the proton flux through the periplasmic membrane. Double thick lines represent the cell wall.

The ubiquity and complexity of NOB cannot be explained if its catabolic activity is strictly restricted to nitrite oxidation ($\Delta G^0 = -74.1$ kJ/mole NO₂⁻). Indeed, the capacity of NOB to adapt to several environments is reflected on their wide metabolic diversity (Table 2.1 – Alternative metabolisms). Even now, one of the questions regarding the lifestyle of NOB is

whether nitrite oxidation is the primary catabolic activity of these organisms (Daims et al., 2016). Additionally, the metabolic diversity expands the potential ecological interactions with their nitrifying counterparts (see Section 2.4) and other microbial cohorts, increasing their survivability in harsh environments.

Table 2.1. Summary of main physiological features of NOB genera (Nitrobacter: Nb; Nitrospira: Ns; Nitrospina: Nn; Nitrotoga: Ng; Nitrococcus: Nc). Nitrolanacea and Candidatus Nitromaritima genera were not included.

	<i>Nb</i>	<i>Ns</i>	<i>Nn</i> ⁽²⁾	<i>Ng</i>	<i>Nc</i>
NXR orientation (Ref. 1)⁽¹⁾					
Cytoplasmic NXR	X				X
Periplasmic NXR		X	X		
Soluble periplasmic NXR				X	
Terminal oxidase (Ref. 2)⁽¹⁾					
Cytochrome aa ₃ -type oxidase	X				X
Cytochrome <i>bd</i> -like oxidase		X			
Cytochrome <i>cbb</i> ₃ -type oxidase			X	X	
Anabolic pathway (Ref. 3)⁽¹⁾					
Calvin-Benson-Bassham cycle (CBB)	X			X	X
Reductive tricarboxylic acid cycle (rTCA)		X	X		
Alternative metabolisms (Ref. 4)⁽¹⁾					
Urea degradation		X	X ^(*)		
Cyanate degradation		X			
Anoxic respiration (NO ₃ ⁻ or others)	X	X			
Heterotrophic growth	X	X ⁽³⁾		X ^(*)	X ^(*)
PHA/PHB storage	X	X			X
Glycogen storage		X	X ⁽⁴⁾	X	X
Polyphosphate storage	X			X	
Complete ammonia oxidation		X			
Substance tolerance (Ref. 5)⁽¹⁾					
Ammonia inhibition threshold (mg NH ₃ -N L ⁻¹)	10-50	4.3	ND ⁽⁵⁾	15-20	ND
Nitrous acid inhibition threshold (mg HNO ₂ -N L ⁻¹)	1.0	0.2	ND	1.8	ND

(*) Presence of responsible genes only.

⁽¹⁾ Reference list.

- **Ref. 1:** *Nb* – (Spieck et al., 1996; Starkenburg et al., 2006); *Ns* – (Koch et al., 2015; Lücker et al., 2010; Spieck et al., 1996; Spieck et al., 1998); *Nn* – c; *Ng* – (Boddicker & Mosier, 2018; Kitzinger et al., 2018); *Nc* – (Füßel et al., 2017).
- **Ref. 2:** *Nb* – (Nomoto et al., 1993; Starkenburg, Larimer, et al., 2008; Tanaka et al., 1983); *Ns* – (Lücker et al., 2010); *Nn* – (Lücker et al., 2013); *Ng* – (Boddicker & Mosier, 2018; Kitzinger et al., 2018); *Nc* – (Füßel et al., 2017).
- **Ref. 3:** *Nb* – (Starkenburg et al., 2006); *Ns* – (Lücker et al., 2010); *Nn* – (Lücker et al., 2013); *Ng* – (Boddicker & Mosier, 2018; Kitzinger et al., 2018); *Nc* – (Füßel et al., 2017).
- **Ref. 4:** *Nb* – (Bock, 1976; Starkenburg et al., 2006); *Ns* – (Lücker et al., 2010); *Nn* – (Lücker et al., 2013); *Ng* – (Boddicker & Mosier, 2018; Kitzinger et al., 2018); *Nc* – (Füßel et al., 2017).
- **Ref. 5:** *Nb* – (Blackburne et al., 2007b); *Ns* – (Blackburne et al., 2007b; Ushiki et al., 2017); *Ng* – (Li et al., 2020; Ma et al., 2017).

⁽²⁾ From uncultured marine *Nitrospina*.

⁽³⁾ Purely heterotrophic growth has not been yet observed (mixotrophic growth).

⁽⁴⁾ Glycogen deposits were found in *Nitrospina gracilis*, but heterotrophic growth of *Nitrospina* was not observed.

⁽⁵⁾ ND – Not determined

2.2.3. Complete ammonia oxidizers, comammox bacteria (CMX)

Although *Nitrospira* is identified as a NOB genus, some *Nitrospira* species belonging to sublineage II are able to perform complete ammonia oxidation (from NH_3 to NO_3^- , comammox process). This is the case for *Nitrospira inopinata* (Kits et al., 2017) and *Candidatus Nitrospira kreffii* (Sakoula et al., 2021). This group of *Nitrospira* is referred as comammox *Nitrospira*. The theoretical conception (Costa et al., 2006) and further discovery of comammox *Nitrospira* (Daims et al., 2015; van Kessel et al., 2015) refuted the conception that nitrification is an obligated two-step process where NH_3 is oxidized to NO_2^- by ammonia oxidizers (AOB and AOA) and then NO_2^- is oxidized to NO_3^- by NOB.

Comammox *Nitrospira* have the same core metabolism (*i.e.*, nitrite oxidation to obtain energy and rTCA to fix CO_2) and metabolic flexibility of canonical NOB *Nitrospira* (Table 2.1. – Alternative metabolisms) (Daims et al., 2015; Palomo et al., 2018; van Kessel et al., 2015; Yang et al., 2020). The distinctive metabolism of comammox *Nitrospira* is the capacity to perform the first step of nitrification (*i.e.*, the oxidation of NH_3 to NO_2^-), complementing the energy generation from nitrite oxidation (Figure 2.6).

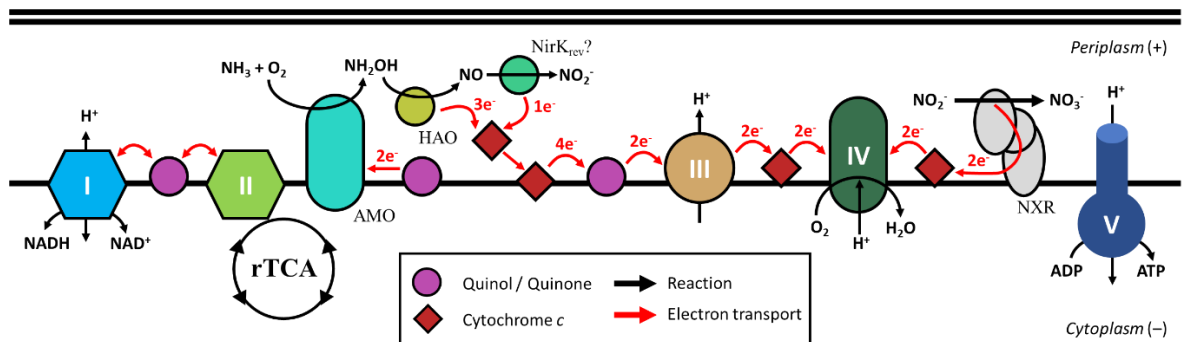


Figure 2.6. Schematic illustration of electron transport and generation of proton motive force (energy metabolism) in comammox *Nitrospira* (CMX). rTCA represents the reductive tricarboxylic acid cycle. Complex I is the NADH ubiquinone oxidoreductase. Complex II is the succinate dehydrogenase. Complex III (ubiquinol-cytochrome c reductase) and complex IV (cytochrome aa_3) are the sites where electron transport is coupled to proton pump. Complex V is the ATP synthase, the site of oxidative phosphorylation to generate ATP. Black arrows with H^+ labels represent the proton flux through the periplasmic membrane. Double thick lines represent the cell wall. Figure adapted from (Daims et al., 2015).

The oligotrophic lifestyle of comammox *Nitrospira* (high affinity for ammonia and high biomass growth yield) was already predicted in the theoretical conceptualization (Costa et al., 2006), and subsequently demonstrated by physiological studies (Kits et al., 2017;

Sakoula et al., 2021). However, there is still an open debate about the oxygen requirements for the chemoautotrophic growth of comammox *Nitrospira* (addressed in Chapter 7).

2.2.4. Anaerobic ammonia oxidizers, anammox bacteria (AMX)

The group of AMX belongs to six genera within the phylum Planctomycetes, including *Candidatus* Kuenenia, *Candidatus* Brocadia, *Candidatus* Anammoxoglobus, *Candidatus* Anammoximicrobium, *Candidatus* Jettenia and *Candidatus* Scalindua. The first five genera are commonly found in WWTP, whereas the last one is commonly found in saline environments (Wu et al., 2020).

AMX are chemolithoautotrophs and anaerobes with a biochemistry that is not fully elucidated yet. This is because of the lack of a pure culture, standard cultivation techniques, and genetic tools (Peeters & van Niftrik, 2019). AMX catabolism supposes the anaerobic oxidation of NH_4^+ coupled to the reduction of NO_2^- , leading to N_2 through the synthesis of the intermediate hydrazine (N_2H_4). First, NO_2^- is reduced to NO by a nitrite reductase (Nir) using one electron. Next, NO is combined with NH_4^+ to form N_2H_4 by hydrazine synthase (HZS) using three electrons. Finally, N_2H_4 is oxidized to N_2 by hydrazine dehydrogenase (HDH) releasing the four electrons harvested in the previous two reductions (Figure 2.7).

Although NH_2OH is not considered an intermediate of anammox process, it is postulated that the highly abundant hydroxylamine oxidase (HOX) found in AMX might oxidize NH_2OH to NO, releasing three electrons that could be employed in synthesis of N_2H_4 combining NH_4^+ and NO (Kuenen, 2020). In this case, the role of HOX would be recycling the by-product NH_2OH formed by HZS, although some AMX might generate N_2H_4 with the combination of NH_4^+ and NH_2OH (Oshiki, Ali, et al., 2016; Schalk et al., 2000).

AMX grow by fixating atmospheric CO_2 by the Wood-Ljungdahl pathway (also known as reductive acetyl-CoA pathway) (Schouten et al., 2004). The slight generation of NO_3^- by AMX (Strous, Kuenen, et al., 1999) is from the oxidation of NO_2^- to NO_3^- by NXR complex, supplying the reductive power required to fix CO_2 and generate new biomass (Kuenen, 2020). Recently, it has been demonstrated that some AMX species (such as *Ca. Kuenenia stuttgartiensis*) can also grow assimilating formate (Lawson et al., 2021).

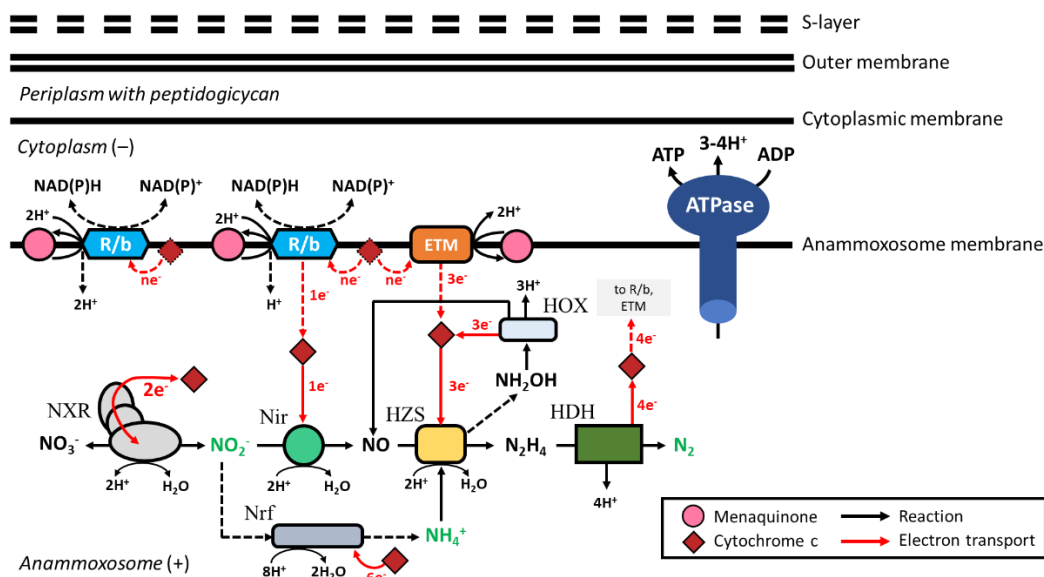


Figure 2.7. Current view of anammox process. Electron transport and generation of proton motive force (energy metabolism) in anammox bacteria (AMX). Substrates (NH_4^+ and NO_2^-) and product (N_2) in green. Nir is the nitrite reductase. HZS is the hydrazine synthase. HDH is the hydrazine dehydrogenase. HOX is the hydroxylamine oxidase. NXR is the nitrite oxidoreductase. Nrf is the nitrite reductase forming ammonium. R/b are Rieske-heme b complexes (bc1 complexes). ETM is a yet-to-be identified electron transfer module. Black arrows with H^+ labels represent the proton flux and through the periplasmic membrane and proton generation. Dashed lines depict reactions and processes to be established. Figure adapted from (Kartal & Keltjens, 2016).

2.3. Contribution of nitrification to N_2O emissions

Nitrification contributes to N_2O emissions directly, but also indirectly by fuelling denitrification with NO_2^- and NO_3^- (being N_2O an obligate intermediate of denitrification). Nitrification (specially nitritation) is considered the major contributor of N_2O emissions in most WWTP, oceans, and agricultural soils (Freing et al., 2012; Law et al., 2012; R. Liu et al., 2016).

N_2O is generated by AOB through different metabolic pathways (Figure 2.8A). In anaerobic conditions, AOB are able to perform the nitrifier-denitrification, using NO_2^- as electron acceptor and generating N_2O (Wrage et al., 2001). Recently, it has been found that AOB also produce N_2O via nitrifier-denitrification under aerobic conditions (Wrage-Mönnig et al., 2018). Another source of N_2O emissions by AOB is from the anaerobic oxidation of NH_2OH to N_2O by the constitutive and periplasmic cytochrome P460 (CytL) (Caranto et al., 2016). Additionally, CytL can bind NO and synthesize N_2O in presence of NH_2OH . Caranto et al. (2016) proposed that CytL can be used for NH_2OH and NO detoxification in anaerobic and

microaerobic conditions through the synthesis and subsequent emission of N_2O . Conditions of hypoxia can lead to a significant increase of N_2O generation in AOB (Figure 2.8B), especially in marine AOB (Goreau et al., 1980). AOB might also contribute to the abiotic generation of N_2O (red arrows; Figure 2.8A) with the accumulation of their intermediates (NH_2OH and NO) and product (NO_2^-) (Harper et al., 2015; Heil et al., 2016).

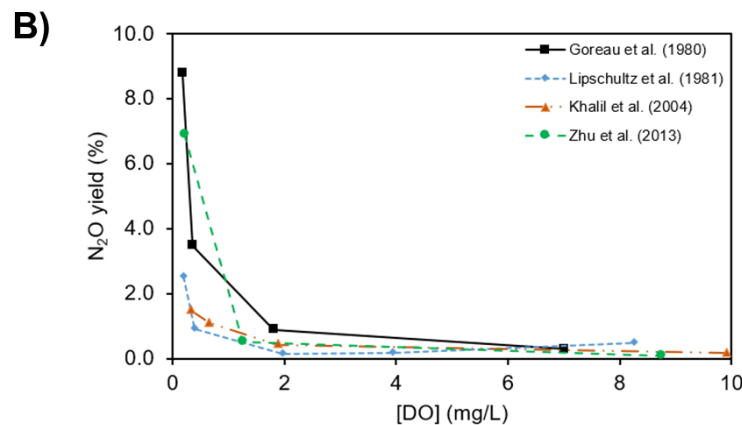
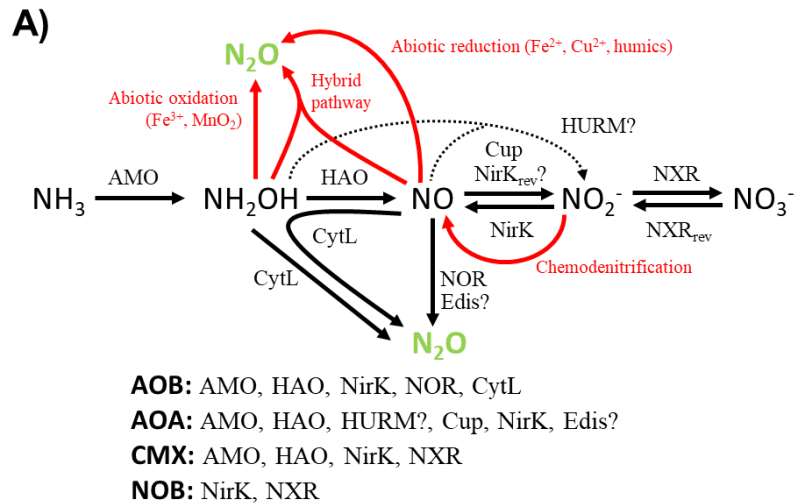


Figure 2.8. Contribution of nitrification to N_2O emissions. **A)** Biotic (black arrows) and abiotic (red arrows) processes leading to N_2O production in nitrifiers. Participating enzymes are noted above or below the arrows. “Edis?” represents the unknown enzyme that would catalyse the NO dismutase to N_2O and O_2 in AOA (Kraft et al., 2022). The key enzymes for each nitrifier are listed below the scheme. Only the hypothetical two-step pathway of AOA is represented in dotted arrow (catalysed by hypothetical HURM enzyme). **B)** Influence of oxygen availability to N_2O yield in AOB (expressed as N_2O/NO_2^- ratio). Marine *Nitrosomonas* – (Goreau et al., 1980); Mixed culture (from soil) – (Khalil et al., 2004; Zhu et al., 2013); *Nitrosomonas europaea* – (Lipschultz et al., 1981).

Like AOB, AOA and CMX also contribute to N_2O emissions. However, their contributions are significantly lower than AOB (0.08% to 0.47% for AOB, 0.04% to 0.07% for AOA; 0.07% for CMX; expressed as N_2O yield, N_2O/NO_2^- ratio) (Hink et al., 2017; Kits et al.,

2019). In contrast to AOB, hypoxia conditions did not boost the generation of N₂O on AOA and CMX (Kits et al., 2019; Stieglmeier et al., 2014). Noteworthy, AOA and CMX do not possess genes which encode any potential NO reductase (NOR) or CytL (Figure 2.8A). Therefore, these communities are not able to catalyse the biotic oxidation of NH₂OH via nitrifier-denitrification like AOB (Kits et al., 2019; Tourna et al., 2011; Walker et al., 2010). Kits et al. (2019) and Wan et al. (2023) studies indicate that NH₂OH is the main contributor of abiotic N₂O production in AOA and CMX via hybrid pathway (abiotic reaction between NH₂OH and NO) or abiotic NH₂OH oxidation. Both AOA and CMX encode NirK, responsible for the reduction of NO₂⁻ to NO (Figure 2.8A). AOA might biotically contribute to N₂O emissions under anoxic conditions (presence of NO₂⁻) via the novel NO dismutase pathway proposed by Kraft et al. (2022).

There is no evidence that NOB contribute to N₂O emissions, at least by biotic production. It is important to keep in mind that the uncoupling of nitrification steps (nitritation and nitratation) would contribute to the N₂O emissions, accumulating NO₂⁻ in the environment and favouring the production of N₂O from denitrification by heterotrophic bacteria, nitrifier-denitrification by AOB or hybrid formation and abiotic reaction with chemical oxidants or reductants (Gruber et al., 2021).

2.4. The ecology of nitrifiers

Microorganisms do not live isolated from the surrounding environment and their community partners. The interactions between microorganism (known as ecological interactions) are classified according to the net effect on each of the interacting species – positive effect for both (mutualism), negative effect for both (competition), combination of positive/negative effect (parasitism or predation), no effect (neutralism) and combination of positive/effect and no effect (commensalism and amensalism) (Arthur & Mitchell, 1989; Bronstein, 1994). Inevitably, the participation of several microbial cohorts in nitrification establishes a complex ecological network in which survival of some species depend on others (*e.g.*, AOB feed NOB), competition for the same substrate (*e.g.*, AOB and AOA compete for NH₃) or even co-concurrence of dependency and competition (AOB and AMX compete for NH₃, but simultaneously AOB feed AMX with NO₂⁻ and protect them against O₂). With this ecological complexity, higher-order interactions (*i.e.*, interactions between more than two species/cohorts) emerge. Higher-order interactions control the community assembly (Bailey et al., 2016; Morin et al., 2022), which explains the existence of large and stable microbial

communities (Grilli et al., 2017; Shen et al., 2023) and challenges May's criteria of stability (Allesina & Tang, 2012), which is based on pairwise interactions.

The trophic network of nitrification associated with exchange of nitrogenous compounds is shown in Figure 2.9A, considering the main three substrates of nitrification (NH_3 , NO_2^- and NO_3^-), and the nitrifying cohorts (AOB, AOA, NOB, CMX) and AMX. Because biotic nitrification is an aerobic process, all nitrifying cohorts (AOB, AOA, NOB and CMX) compete for oxygen. At the same time, ammonia oxidizers (AOB, AOA, CMX) and AMX compete for $\text{NH}_3/\text{NH}_4^+$. AMX also compete with NOB for NO_2^- . The positive synergies between nitrifiers comprise (i) coupling of nitrification (AOB and AOA) and nitrification (NOB), (ii) partial nitrification (AOB) and anammox process by AMX, (iii) co-protection between AOB and NOB (NH_3 inhibits NOB (Blackburne et al., 2007b; Kim et al., 2008; Li et al., 2020; Ushiki et al., 2017) and HNO_2 inhibits AOB (Claros et al., 2013; Hellinga et al., 1999; Jubany et al., 2008; Wett & Rauch, 2003; Wyffels et al., 2004)) and (iv) the protection of AMX against oxygen by nitrifiers (AOB, AOA, NOB and CMX).

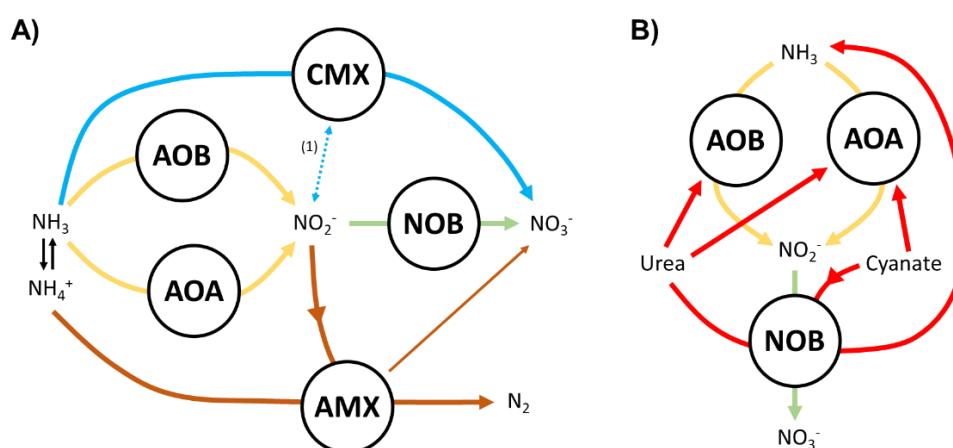


Figure 2.9. Trophic network of nitrification associated with the exchange of nitrogenous compounds. A) Scheme illustration of interactions between ammonia oxidizers (AOB, AOA and CMX), nitrite oxidizers (NOB) and anammox bacteria (AMX) considering the three main substrates of nitrification – NH_3 , NO_2^- and NO_3^- . ⁽¹⁾CMX release NO_2^- at high concentration of NH_3 (Daims et al., 2015). B) Nitrification by reciprocal feeding. Colour legend: nitritation – yellow arrows; nitrification – green arrows; comammox process – blue arrow; anammox process – brown arrows; mineralization – red arrows.

Some NOB species (mainly belonging to genus *Nitrospira*) are capable to hydrolyse urea and cyanate to NH_3 and CO_2 (Table 2.1). Because NOB do not use NH_3 as energy source (only part of the generated NH_3 is used as nitrogen source for biomass synthesis), a new interaction emerges between nitrifiers, known as reciprocal feeding. First NOB with urease

and/or cyanase provide NH_3 to AOM. Then, NOB obtain NO_2^- from AOM (Figure 2.9B). Reciprocal feeding between AOB and NOB has already been observed (Koch et al., 2015). Genes involved in urea transport and degradation have been found in certain AOB and AOA species. Therefore, AOM might also degrade urea to obtain NH_3 and CO_2 (Alonso-Sáez et al., 2012; Sedlacek et al., 2019). In addition, some AOA, such as *Nitrososphaera gargensis*, are also able to grow on cyanate as sole energy source (Palatinszky et al., 2015). Nitrification by reciprocal feeding would be crucial in certain ecosystems where urea and cyanate are the key substrate instead of NH_3 , such as acidic soils, oceanic habitats and some estuaries (Daims et al., 2016).

2.5. Conclusions

In this chapter, the biological nitrogen cycle was presented together with the adverse effects of human activity on the stability of this. The discoveries of the last 30 years (especially anammox process in 1995, and comammox *Nitrospira* in 2015) have expanded our understanding of the ecology of nitrifiers allowing the development of more efficient and sustainable bioprocesses for nitrogen remediation, such as the combination of partial nitrification and anammox process.

The biochemistry of nitrifying cohorts (AOB, AOA, NOB, CMX) and AMX was reviewed. Differences in the biochemistry were observed among aerobic ammonia oxidizers (AOB, AOA, CMX) and also among NOB genera. These differences explained the distinctive contributions of N_2O emissions among the ammonia oxidizers and the wide metabolic flexibility and ubiquity of NOB.

Anammox bacteria cocultured with comammox *Nitrospira* (instead of AOB) has the potential to achieve high levels of nitrogen removal with lower energy consumption (van Kessel et al., 2015), limited N_2O emissions (Kits et al., 2019) and sludge production (Luo et al., 2022). However, the survivability of comammox *Nitrospira* in hypoxic conditions and the assembly of a stable community with anammox bacteria remain unexplained. This question is addressed in Chapter 7.

In the following Chapter, a meta-analysis of the kinetic parameters that define the growth of nitrifiers is presented, with the aim of understanding and predicting the ecological niches in which specific populations of nitrifiers will dominate.

3.

Biochemistry shapes growth kinetics of nitrifiers and defines their activity under specific environmental conditions.

3.1. Introduction

Nitrifying community, composed of ammonia-oxidizing bacteria (AOB), ammonia-oxidizing archaea (AOA), nitrite-oxidizing bacteria (NOB) and comammox bacteria (CMX), has a vast microbial diversity. All these microbial cohorts share the same ecological niche (*i.e.*, specific environmental condition(s) in which different species coexist (Pocheville, 2015)) because they are aerobic. Moreover, ammonia oxidizers (AOB, AOA and CMX) compete for the same electron donor and nitrogen source, ammonia. On the other hand, NOB stand out for their incredible physiological and metabolic diversity among the different genera (Daims et al., 2016). Considering this, the following question arises – is it possible to find trends between the parameters that define microbial growth and thus help us to predict the dominance of specific nitrifying cohorts in distinct ecological niches?

Because AOA have an overall higher affinity for ammonia and oxygen than AOB, it is generally considered the dominant population in low ammonia and low pH conditions, and soil and aquatic environments (Baolan et al., 2014; Liu et al., 2017; Yin et al., 2018). On the contrary, AOB grow generally faster than AOA and therefore dominate in environments where substrate limitation is not the main selective pressure (*e.g.*, wastewater treatment plants) (Lehtovirta-Morley, 2018; Li et al., 2016; Park et al., 2006; Yin et al., 2018). These observations, however, have not been fully proven and in many low ammonia environments (<15 μ M), such as estuaries or riverine sediments, AOB outnumber AOA (Lagostina et al., 2015; Mosier & Francis, 2008; Santoro et al., 2008). Therefore, although some general conclusions have been established, the relative abundances of both groups of ammonia oxidizers dominating in specific ecological niches remains unknown along with their relative contribution to the global nitrification process.

The few measurements of ammonia affinity for CMX (from *Nitrospira inopinata* and *Candidatus Nitrospira kreffii*), proved to be one of the highest of all affinities reported for ammonia oxidizers (only AOA species *Nitrosopumilus maritimus* and *Nitrosoarchaeum koreensis* have a higher affinity (Jung et al., 2011; Jung et al., 2022; Kits et al., 2017)). With a higher ammonia affinity than AOB, and a more energetic catabolic process per mole of NH₃, complete nitrification would yield more energy ($\Delta G^{0'} = -349$ kJ per mole of NH₃) than the single steps ($\Delta G^{0'} = -275$ kJ per mole of NH₃ for ammonia oxidation to nitrite and $\Delta G^{0'} = -74$ kJ per mole of NO₂ for nitrite oxidation to nitrate) (Daims et al., 2015), CMX would be expected to dominate in oligotrophic environments where substrate availability is

limited (Costa et al., 2006). However, CMX have been also identified in a range of engineered systems, including aquaculture biofiltration units, drinking water and wastewater treatment plants (Chao et al., 2016; Pjevac et al., 2017; Wang et al., 2017), with the contribution of their activity to nitrification and their distribution in aforementioned systems still not well understood (Yang et al., 2020). Moreover, the niches in which other populations of NOB dominate are not fully identified, with their lineages unequally distributed in both natural and engineered environments (Daims et al., 2016).

The characteristics of specific microbial activities can be associated with identified “*life strategies*”. One such theory is the commonly accepted r/K-strategy. Those microorganisms that grow fast and dominate in nutrient-rich environments (such as wastewater treatment systems or eutrophic environments) are identified as r-strategists, with a higher maximum specific growth rate (μ_{\max}), whereas those microorganisms which grow slowly and dominate in oligotrophic environments are identified as K-strategists, with higher substrate affinity. The trade-off between oligotrophic and copiotrophic activity is considered in the r/K-strategy theory (Andrews & Harris, 1986; Ho et al., 2017).

Thermodynamics and microbial metabolic studies have led us to consider the apparent existence of another trade-off in kinetic parameters between growth rate and growth yield. This trade-off would also define theoretical environment strategists, that is, microorganisms defined by a high growth rate and a low growth yield (r-strategist) versus those with a low growth rate and high growth yield (Y-strategist) (Kreft, 2004b; Pfeiffer et al., 2001). This trade-off is supported by the measurement of a constant rate of metabolic redox activity, which implies that longer metabolic pathways will potentially harvest more energy but require more time to metabolise one mole of substrate (Andersen & Von Meyenburg, 1980; González-Cabaleiro et al., 2015; Hoff et al., 2020). The branched metabolic pathways of *Escherichia coli*, *Holophaga foetida* and *Acetobacter methanolicus* (Carlson & Sreenc, 2004; Kappler et al., 1997; Müller & Babel, 1993); and the competition between fermentative pathways of *Clostridium homopropionicum* (r-strategist) and *Propionibacterium freudenreichii* (Y-strategist) (Seeliger et al., 2002) support the existence of growth rate/yield trade-off.

These theories further identify that no microorganism can be a “*Jack of all trades*”, but it is unknown what defines a microorganism as r- or K- or Y-strategist at the molecular level.

Moreover, the fitness of specific microbial species is not strictly fixed, but they are able to adapt to dynamic environmental conditions (Velicer & Lenski, 1999).

In this study, the kinetic parameters of AOB, AOA, CMX and NOB were analysed, reviewing ~100 references in literature and more than 300 data points, with the objective to better understand the competitive and collaborative relationships established between different functional groups of aerobic nitrifiers. The aim of this study is to predict the ecological niches in which specific populations of nitrifiers will dominate. Values of maximum specific growth rate (μ_{\max}), growth yield (Y_{XS}) and the affinities for oxygen and nitrogen sources ($a_{O_2}^0$, a_N^0) were collected, normalised, and compared for each of the potential groups competing for the same substrate. The analysis of the data highlights the specific metabolic strategies enabling the survival of different populations, and the relationship between biochemical differences and measured kinetic parameters. Moreover, it explains our inability to fully describe ecological niche differentiation between the different populations involved in the aerobic biogeochemical nitrogen cycle.

3.2. Materials and Methods

In this study, the kinetic parameters for nitrifiers reported in literature were collated. Maximum specific growth rate (μ_{\max}), apparent growth yield (Y_{XS}) and specific affinity for ammonia ($a_{NH_3}^0$), oxygen ($a_{O_2}^0$) and nitrite ($a_{NO_2}^0$) have been annotated and compared for different aerobic nitrifying groups. To enable the comparison, the following extrapolations and conversions were done.

3.2.1. Maximum specific growth rate (μ_{\max})

Maximum specific growth rate is presented in units of h^{-1} at a constant temperature of 20°C for all the measurements. To do this, when necessary, the values obtained from literature were extrapolated to 20°C using the Arrhenius function (Eq. 3.1) (Melcer, 2004).

$$\mu_{T_1} = \mu_{T_2} \cdot \theta^{T_1 - T_2} \quad (3.1)$$

Where θ refers to the dimensionless Arrhenius coefficient. Linear regression and least squares method were applied to fit the Arrhenius function to the experimental data for each μ_{\max} value collected from literature. The corresponding values are presented in Appendix A (Tables A.1 and A.2).

To normalise the effect of pH, all values were extrapolated at the pH considered optimum for each specie or genus. All optimum pH values are reported between 7.0 and 8.0 for the nitrifying groups considered (Figure A.1). To extrapolate the μ_{\max} value at its optimum pH, a function with a bell curve shape was used to define the effect of pH over the μ_{\max} values (Eq. 3.2) (Antoniou et al., 1990; Blackburne et al., 2007a, 2007b; Dochain & Vanrolleghem, 2015; French et al., 2012; Jubany et al., 2008; Jung et al., 2011; Kitzinger et al., 2018; Qin et al., 2014; Tourna et al., 2011).

$$\mu_{\max}(pH) = \frac{\mu_{\max}(pH_{op})}{1 + \left(\frac{10^{-pK_1}}{10^{-pH}}\right) + \left(\frac{10^{-pH}}{10^{-pK_2}}\right)} \quad (3.2)$$

Where pK_1 and pK_2 refer to the pH in which μ_{\max} is half of the value at optimal pH (see Appendix A – Supplementary text).

3.2.2. Specific affinities for substrates ($a_{\text{NH}_3}^0$, $a_{\text{NO}_2}^0$, $a_{\text{O}_2}^0$)

Specific affinity (a^0) evaluates the capacity of microorganisms to survive under specific substrate concentrations (Button, 1991). Specific affinities for ammonia, nitrite and oxygen were calculated using the kinetic constants from literature for AOB, AOA, CMX and NOB and applying Eq. 3.3 (Button, 1985).

$$a_S^0 = \frac{V_{\max}}{K_M} \quad (3.3)$$

Here a_S^0 is the specific affinity for S ($\text{L g-Bio}^{-1} \text{h}^{-1}$), V_{\max} is maximum specific uptake rate ($\mu\text{mol-S g-Bio}^{-1} \text{h}^{-1}$) and K_M is half-saturation constant for S (μM). The literature data is included in Appendix A (Tables A.3, A.4 and A.5).

3.2.3. Growth yield (Y_{XS})

Growth yield or apparent growth yield is defined as the amount of biomass produced per unit of substrate consumed, considering that part of the substrate consumed is required for the maintenance processes. The apparent growth yield is presented in units of g-Bio/g-NH_3 for ammonia oxidizers and g-Bio/g-NO_2 for nitrite oxidizers. To transform the reported growth yield to these units when needed, an average formula for biomass was considered ($\text{C}_5\text{H}_7\text{O}_2\text{N}$). Other conversion factors used are included in Appendix A (Tables A.6 and A.7).

3.2.4. Statistical analyses

Statistical significance of the differences between the parameters describing growth (maximum specific growth rate (μ_{\max}), growth yield (Y_{XS}) and specific affinity (a^0) of the nitrifying groups considered (AOB, AOA, CMX and NOB) was assessed using the one-way ANOVA analysis together with REGWQ TEST. To evaluate the correlations between maximum specific growth rate (μ_{\max}), growth yield (Y_{XS}) and specific affinity (a^0), Pearson's correlation (r) and Kendall's rank correlation (τ) were used.

3.3. Results and Discussion

The collected kinetic parameters of ammonia and nitrite oxidizers were organised in groups based on their metabolic activity, domain, origin and available taxonomic information (Table 3.1). Then, the values were classified into seven different ecological groups as a function of the microorganism and its habitat: non-marine ammonia-oxidizing bacteria (AOB-FW), marine ammonia-oxidizing bacteria (AOB-SW), non-marine ammonia-oxidizing archaea (AOA-FW), marine ammonia-oxidizing archaea (AOA-SW), comammox bacteria (CMX), non-marine nitrite-oxidizing bacteria (NOB-FW) and marine nitrite-oxidizing bacteria (NOB-SW). The groups are also distinguished by the ecosystem they were isolated from: wastewater treatment systems, sediments (including oceanic, estuarine and lake sediments), water column, soils, hot water/spring and acidic soils.

The maximum specific growth rate (μ_{\max}) of AOB, AOA and CMX is compared with the specific affinity for ammonia ($a^0_{\text{NH}_3}$) (Figure 3.1A) and with the growth yield (Y_{XS}) (Figure 3.1B). For NOB, the μ_{\max} values are plotted with the specific affinities for nitrite ($a^0_{\text{NO}_2}$) (Figure 3.2A) and growth yield (Y_{XS}) (Figure 3.2B). For all nitrifying groups, the specific affinities for oxygen ($a^0_{\text{O}_2}$) are presented in Figure 3.3A with their μ_{\max} . Data shown on Figures 3.1 and 3.2 have been organised from the highest to the lowest maximum specific growth rate. Otherwise, data shown on Figure 3.3 has been organised from the highest to the lowest affinity for oxygen.

Table 3.1. Summary of the kinetic parameters of nitrifiers (AOM, CMX, NOB) used in this study.

	Abbreviation	Taxonomic level & culture type [¶]	Parameters	Ecosystem [‡]
Non-marine ammonia-oxidizing bacteria (AOB-FW)				
Mixed culture	Mx AOB-FW	Mixed culture	All [§]	WWTP
<i>Nitrosomonas europaea</i>	Europaea	Species, PC	All	Soil
<i>Nitrosomonas oligotropha</i>	Oligotropha	Species, PC and EC	μ_{\max} , $a^0_{\text{NH}_3}$	Sediments
<i>Nitrospira</i> sp. 40K1	Nspira-40K1	Species, PC	μ_{\max} , $a^0_{\text{NH}_3}$, Y_{XS}	Soil
<i>Nitrospira</i> sp. AF	Nspira-AF	Species, PC	μ_{\max} , $a^0_{\text{NH}_3}$, Y_{XS}	Acidic soil
<i>Nitrospira</i> sp. B6	Nspira-B6	Species, PC	μ_{\max} , $a^0_{\text{NH}_3}$, Y_{XS}	WWTP
<i>Nitrospira</i> sp. L115	Nspira-L115	Species, PC	μ_{\max} , $a^0_{\text{NH}_3}$, Y_{XS}	Acidic soil
Marine ammonia-oxidizing bacteria (AOB-SW)				
<i>Nitrosococcus oceani</i>	Oceani	Species, PC	μ_{\max} , $a^0_{\text{NH}_3}$, Y_{XS}	Sediments
Non-marine ammonia-oxidizing archaea (AOA-FW)				
<i>Nitrosoarchaeum koreensis</i>	Koreensis	Species, EC	μ_{\max} , $a^0_{\text{NH}_3}$, $a^0_{\text{O}_2}$	Soil
<i>Nitrososphaera vienennensis</i>	Vienennensis	Species, PC	μ_{\max} , $a^0_{\text{NH}_3}$, Y_{XS}	Soil
<i>Nitrososphaera gargensis</i>	Gargensis	Species, PC	μ_{\max} , $a^0_{\text{NH}_3}$, Y_{XS}	Hot spring
Marine ammonia-oxidizing archaea (AOA-SW)				
Mixed culture	Mx AOA-SW	Mixed culture	μ_{\max} , $a^0_{\text{O}_2}$	Sediments
<i>Nitrosopumilus maritimus</i>	Maritimus	Species, PC	All	Sediments
<i>Nitrosopumilus piranensis</i>	Piranensis	Species, EC	μ_{\max} , Y_{XS}	Water column
<i>Nitrosopumilus adriaticus</i>	Adriaticus	Species, EC	μ_{\max} , Y_{XS}	Water column
Complete ammonia-oxidizing bacteria (CMX)				
<i>Nitrospira inopinata</i>	Inopinata	Species, PC	μ_{\max} , $a^0_{\text{NH}_3}$, Y_{XS}	Hot water
Non-marine nitrite-oxidizing bacteria (NOB-FW)				
<i>Nitrobacter vulgaris</i>	Vulgaris	Species, PC	μ_{\max} , $a^0_{\text{NO}_2}$, Y_{XS}	WWTP
<i>Nitrospira</i> sp. ND1	ND1	Species, PC	All [§]	WWTP
<i>Nitrospira japonica</i>	Japonica	Species, PC	All	WWTP
<i>Nitrobacter agilis</i>	Agilis	Species, PC	μ_{\max} , $a^0_{\text{NO}_2}$, Y_{XS}	WWTP
<i>Nitrobacter winogradskyi</i>	Winogradskyi	Species, PC	All	Soil
<i>Nitrospira defluvii</i>	Defluvii	Species, PC	μ_{\max} , $a^0_{\text{NO}_2}$, Y_{XS}	WWTP
<i>Nitrospira lenta</i>	Lenta	Species, PC	μ_{\max} , $a^0_{\text{NO}_2}$, Y_{XS}	WWTP
<i>Nitrospira moscoviensis</i>	Moscoviensis	Species, PC	μ_{\max} , $a^0_{\text{NO}_2}$, Y_{XS}	Hot water
<i>Nitrobacter hamburgensis</i>	Hamburgensis	Species, PC	All	Soil
<i>Nitrotoga arctica</i>	Arctica	Species, PC	μ_{\max} , $a^0_{\text{NO}_2}$, Y_{XS}	Soil
Marine nitrite-oxidizing bacteria (NOB-SW)				
<i>Nitrococcus mobilis</i>	Mobilis	Species, PC	μ_{\max} , $a^0_{\text{NO}_2}$	Water column
<i>Nitrospira marina</i>	Marina	Species, PC	μ_{\max} , Y_{XS}	Water column
<i>Nitrospina watsonii</i>	Watsonii	Species, EC	μ_{\max} , $a^0_{\text{NO}_2}$, Y_{XS}	Water column
<i>Nitrotoga</i> sp. AM1	AM1	Species, EC	μ_{\max} , $a^0_{\text{NO}_2}$	Sediments
<i>Nitrospira</i> sp. Ecomares	Ecomares	Species, PC	μ_{\max} , $a^0_{\text{NO}_2}$, Y_{XS}	Sediments

[¶]Culture type: PC – pure culture; EC – enriched culture.

[‡] Ecosystem (sample origin): WWTP – Wastewater treatment plants.

[§]All: All microbial growth parameters have been reported – μ_{\max} , $a^0_{\text{NH}_3}$, $a^0_{\text{O}_2}$, and Y_{XS} for AOB, AOA and CMX; μ_{\max} , $a^0_{\text{NO}_2}$, $a^0_{\text{O}_2}$, and Y_{XS} for NOB

3.3.1. Ammonia oxidizers

Collected data of ammonia oxidizers (Figure 3.1A) shows that AOB populations have on average a higher maximum specific growth rate than AOA and CMX (Table A.2). But AOA and CMX have on average a higher specific affinity for ammonia than AOB (Table A.4). The available measurements of the kinetics of complete nitrifiers show that they have the lowest maximum specific growth rate (being close to some μ_{\max} values reported for AOA) and the highest affinity for ammonia of all analysed ammonia oxidizers except *N. maritimus* and *N. koreensis*. This overall tendency would confirm the consideration of AOA and CMX as K-strategists when compared with AOB, with lower μ_{\max} and higher ammonia affinity (Chen et al., 2017; Yin et al., 2018). When analysing the reported values of μ_{\max} and $a^0_{\text{NH}_3}$ in literature for AOB, AOA and CMX groups (Figure 3.1A), a strong negative correlation was identified ($r = -0.717$, $p < 0.006$; $\tau = -0.539$, $p = 0.01$; $n = 13$; Figure A.2A), supporting the aforementioned consideration that AOA and CMX have higher $a^0_{\text{NH}_3}$ and lower μ_{\max} . A negative correlation is also observed between the data collected for AOB populations only ($r = -0.808$, $p = 0.015$; $\tau = -0.786$, $p < 0.006$; $n = 8$; Figure A.2B) but between the μ_{\max} and $a^0_{\text{NH}_3}$ values for populations of AOA a strong positive correlation was found ($r = 0.756$, $p = 0.02$; $\tau = 0.667$, $p = 0.333$; $n = 4$; Figure A.2C). Although it appears that some species of AOB would dominate in oligotrophic environments, supporting the r/K-strategy theory (*Nitrosomonas* have consistently higher μ_{\max} and lower $a^0_{\text{NH}_3}$ than *Nitrosococcus* or *Nitrosospira*), between species of AOA it is not so clear.

It is important to consider that AOA was the only cohort Identified In extreme oligotrophic environments such as the oxygen minimum zones (OMZ) (Bristow et al., 2016). This excellent capacity of AOA to survive in these extreme environments is observed, for example, on the measured $a^0_{\text{NH}_3}$ of *N. maritimus*, which is 22 times higher than the highest measured $a^0_{\text{NH}_3}$ of AOB. However, in some natural environments identified as oligotrophic environments, AOB outcompeted AOA (Lagostina et al., 2015; Mosier & Francis, 2008; Santoro et al., 2008). This correlates with the measured $a^0_{\text{NH}_3}$ shown in Figure 3.1A. *Nitrosospira* species have a similar $a^0_{\text{NH}_3}$ than some AOA species (Figures 3.1A and A.5) being able to compete against some AOA in these oligotrophic environments. Therefore, the presence or absence of particular species in the environment could determine which one will be the larger contributor to ammonia oxidation in natural environments, AOB, AOA or both.

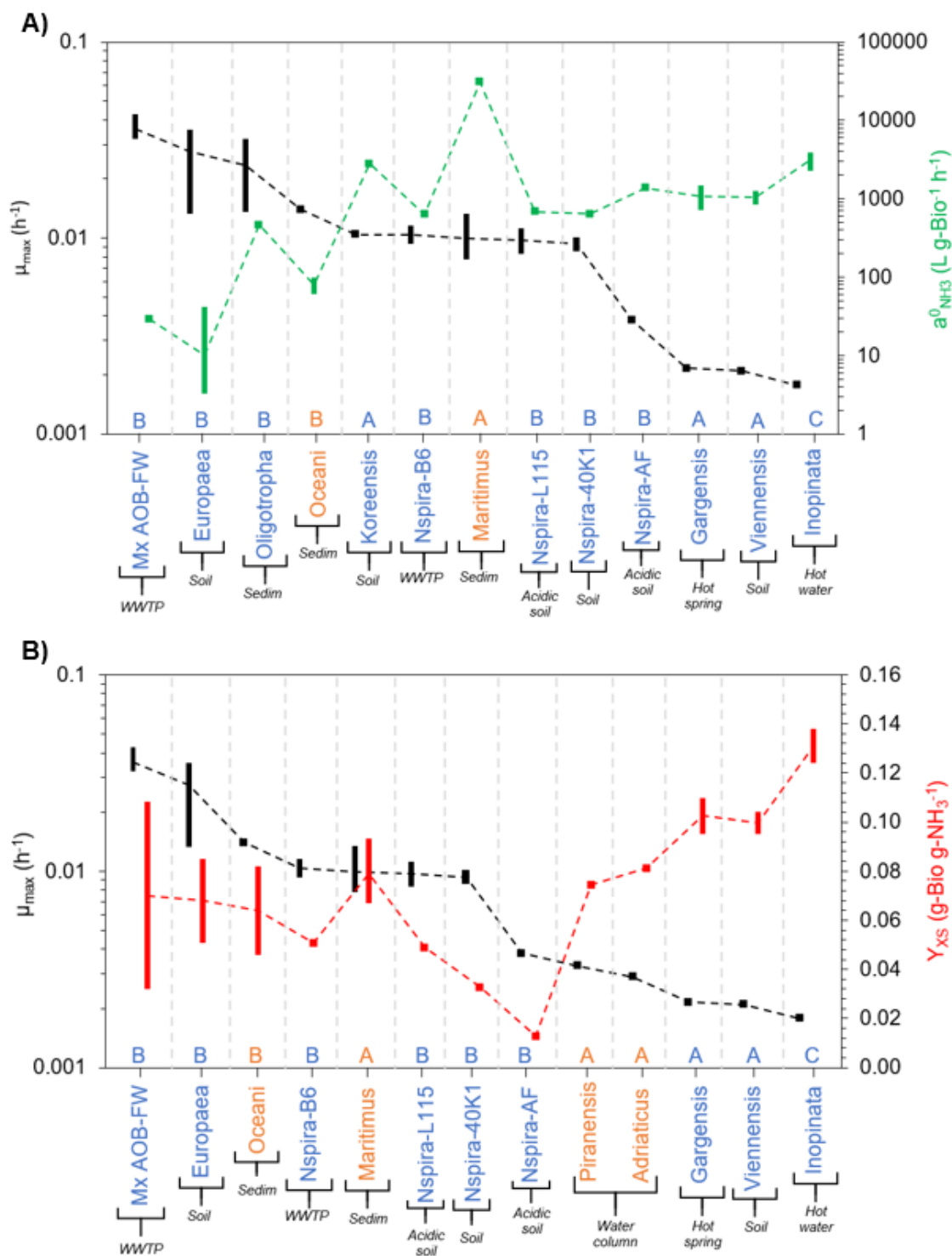


Figure 3.1. Maximum specific growth rate (μ_{max}) with A) specific affinity for ammonia ($a^0_{NH_3}$) and B) growth yield (Y_{XS}) of ammonia-oxidizing microorganisms (AOB, AOA and CMX). The black bars show the range of μ_{max} values; green bars represent the range of $a^0_{NH_3}$ value for ammonia (Figure 3.1A); and red bars represent the range of Y_{XS} values (Figure 3.1B). Blue: non-marine nitrifiers; orange: marine nitrifiers. Legend bottom of figures: B – Bacteria; A – Archaea; C – Complete ammonia oxidizer. Dashed lines cross the calculated average value for each parameter function of the range of values reported.

In Figure 3.1B, μ_{\max} is compared with the growth yield (Y_{XS}) of each considered ammonia oxidizer. As expected, complete nitrifiers show the highest Y_{XS} value (Kits et al., 2017). However, there is a significant difference in the Y_{XS} of AOB and AOA, both groups carrying out partial nitrification ($p = 0.002$; Table A.6). AOA has a consistently higher Y_{XS} than AOB, consequence of a more efficient metabolism. The carbon fixation pathway of AOA has been reported as more efficient (3-hydroxypropionate/4-hydroxybutyrate cycle) than the Calvin-Benson-Bassham cycle of AOB (Könneke et al., 2014).

When analysing the reported values for μ_{\max} and Y_{XS} for AOB (excluding acidophilic AOB *Nitrosospira sp. AF* and *Nitrosospira sp. L115*), AOA and CMX, a negative correlation was identified ($r = -0.404$, $p < 0.1$; $\tau = -0.527$, $p < 0.030$; $n = 11$; Figure A.2D), which supports the hypothesis of an inverse correlation between metabolic efficiency and speed of growth (Kreft, 2004b; Lele & Watve, 2014). A negative correlation is also observed between the parameters reported for AOA ($r = -0.506$, $p = 0.002$; $\tau = -0.60$, $p > 0.1$; $n = 5$; Figure A.2E), but not for AOB ($r = 0.808$, $p = 0.05$; $\tau = 1.000$, $p < 0.003$; $n = 6$; Figure A.2F).

In addition, non-marine AOA have a higher value of Y_{XS} than marine AOA ($p = 0.01$; Figure A.4) (Figure 3.1B). This higher value of Y_{XS} is again associated with lower μ_{\max} values. Contrary, this difference in metabolic efficiency is not observed when non-marine and marine AOB are compared ($p > 0.1$; Figure A.4). Regarding acidophilic AOB, a significantly lower values of Y_{XS} were observed, compared with neutrophilic AOB ($p < 0.01$; Figure A.4). These dissimilarities could be a consequence of the significantly different maintenance requirements of the different environments (Bodegom, 2007). In fact, no trend has been identified between μ_{\max} and Y_{XS} parameters within the same ecological group.

Overall, for ammonia oxidisers, a negative correlation was identified between maximum growth rate and ammonia affinity and growth yield. Therefore, microorganisms that have higher growth yield have higher ammonia affinity meanwhile being slow growers in conditions of non-substrate limitation. In general, lower μ_{\max} , higher $a_{\text{NH}_3}^0$ and higher Y_{XS} were observed for AOA and CMX than for AOB, which implies that these groups have a competitive advantage in substrate limiting conditions. However, there is niche overlapping (*i.e.*, sharing parts of their niche space) with respect to ammonia between AOB and AOA.

3.3.2. Nitrite oxidizers

In addition to the main groups (NOB-FW and NOB-SW), species of NOB are classified based on the localization of the active site of their nitrite oxidoreductase (NXR), the enzyme catalysing nitrite oxidation to nitrate, differentiating between cytoplasmic NXR (C-type NOB), periplasmic NXR (P-type NOB) and soluble periplasmic NXR (sP-type NOB) (see Figure 3.2). In general, *Nitrobacter* and *Nitrococcus* are C-type NOB, *Nitrospira* and *Nitrospina* are P-type NOB and *Nitrotoga* are sP-type NOB (Füssel et al., 2017; Koch et al., 2015; Lücker et al., 2013; Lücker et al., 2010; Spieck et al., 1996; Spieck et al., 1998; Starkenburg et al., 2006).

Figure 3.2A shows that C-type NOB have a significantly lower affinity for nitrite ($a_{\text{NO}_2}^0$) than P-type NOB ($p < 0.0001$) and sP-type NOB ($p < 0.0001$) (Table A.5). However, no correlation has been found with μ_{max} or Y_{XS} parameters (Figure 3.2). Commonly, *Nitrobacter* (C-type NOB) are considered r-strategists and *Nitrospira* (P-type NOB) are considered K-strategists (Nowka et al., 2015; Schramm et al., 1999). However, this is not supported by reported kinetic parameters of NOB. No correlation between μ_{max} and $a_{\text{NO}_2}^0$ is found ($r = 0.062$, $p > 0.1$; $\tau = -0.077$, $p > 0.1$; $n = 14$; Figure A.2G). Analysing the kinetic data shown in Figure 3.2B, a weak negative correlation between μ_{max} and Y_{XS} was observed for NOB ($r = -0.29$, $p > 0.1$; $\tau = -0.308$, $p > 0.1$; $n = 13$; Figure A.2H).

P-type NOB release protons in the periplasmic side of the membrane as nitrite oxidation occurs. This could imply an extra proton motive force generation and therefore, it has been considered that P-type NOB would have a more efficient metabolism than C-type (Lücker et al., 2010). Contrary, no significant difference between reported Y_{XS} values for P-type NOB and C-type NOB has been observed ($p = 0.73$; Table A.7).

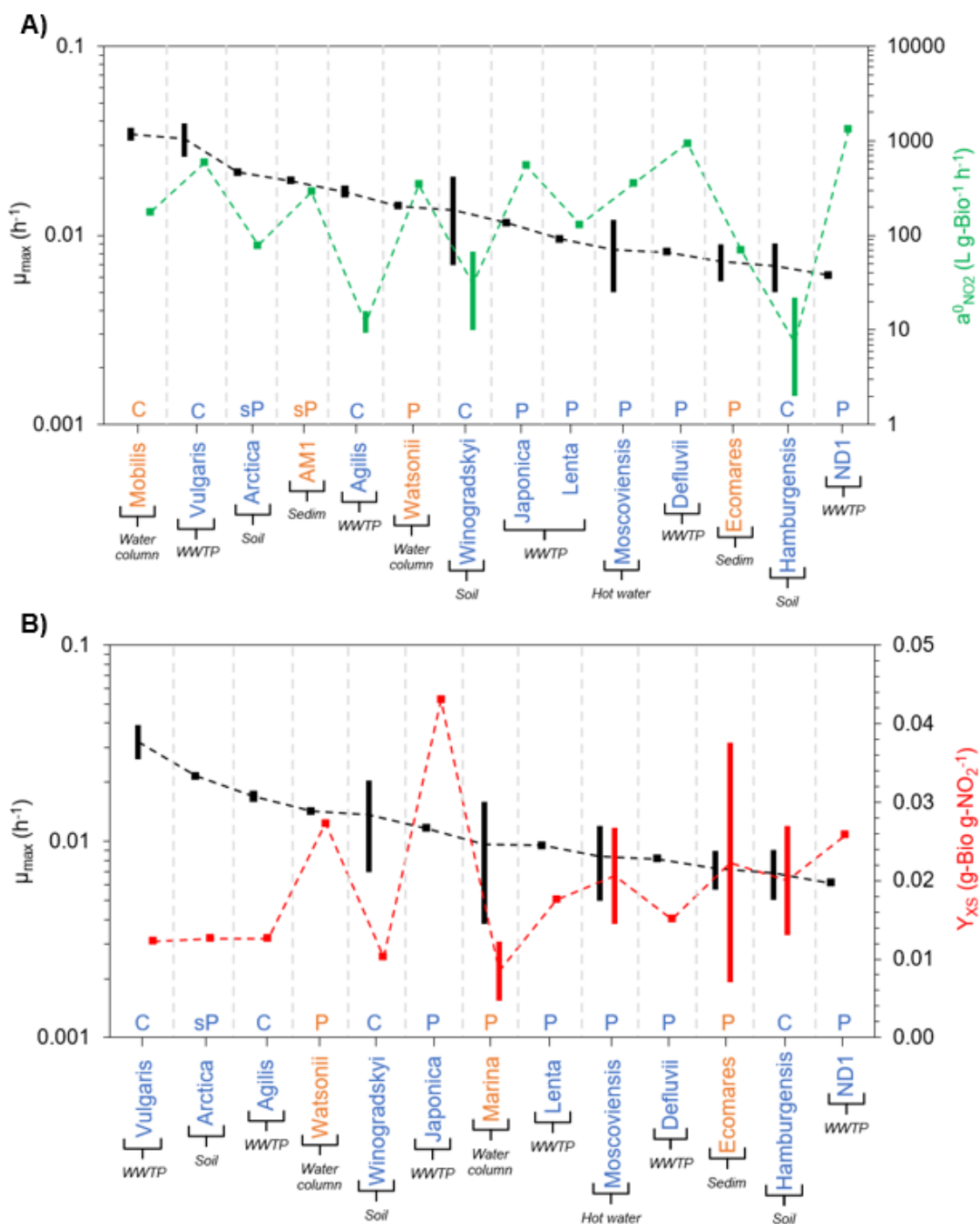


Figure 3.2. Maximum specific growth rate (μ_{max}) with A) specific affinity for nitrite ($a^0_{NO_2}$) and B) growth yield (Y_{XS}) of nitrite-oxidizing bacteria. The black bars show the range of μ_{max} values; green bars represent the range of $a^0_{NO_2}$ values (Figure 3.2A); red bars represent the range of Y_{XS} value (Figure 3.2B). Blue: non-marine nitrite oxidizers; orange: marine nitrite oxidizers. Legend bottom of figures: C – NOB with cytoplasmic NXR; P – NOB with periplasmic NXR. sP – NOB with soluble periplasmic NXR. Dashed lines cross the calculated average value for each parameter function of the range of values reported.

Other morphological differences might be affecting the efficiency of the metabolic process, *e.g.*, the distinct terminal oxidoreductases that they express or the different carbon fixation pathways of *Nitrobacter* (Calvin-Benson-Bassham cycle, CBB) and *Nitrospira* (oxygen tolerant modified *reductive tricarboxylic acid cycle*, rTCA) (Lücker et al., 2013; Lücker et al., 2010; Starkenburg et al., 2006; Starkenburg, Larimer, et al., 2008). Although it is established that rTCA is more efficient than CCB (0.195 moles ATP per g biomass and 0.238 moles ATP per g biomass respectively) (Berg, 2011; Mangiapia & Scott, 2016), this is not reflected in the measured growth yields of NOB (Berg, 2011; Sato et al., 2014). Moreover, *Nitrobacter* encode a heme-copper aa₃-type as terminal oxidase that operates as proton pump, whereas *Nitrospira* encode a putative cytochrome *bd*-like terminal oxidase (Table A.8) that could not be coupled with energy conservation (or can conserve energy via a Q-loop, but less than a proton-pumping mechanism), like the canonical *bd* terminal oxidase (Giuffrè et al., 2014). This might compensate the putative energetic advantage of *Nitrospira* by the orientation of their NXR and carbon fixation pathway.

Like for AOB, no significant differences between Y_{XS} values are observed when marine and non-marine NOB are compared ($p > 0.1$; Figure A.7). Regarding to μ_{\max} and $a^0_{\text{NO}_2}$ values of NOB, a significant variation was observed between *Nitrobacter*, *Nitrococcus* and *Nitrotoga* species from distinct environments ($p < 0.0001$), but less variation between those of *Nitrospira* and *Nitrospina* species (Figures A.6 and A.8).

3.3.3. Oxygen competition among nitrifiers

Oxygen is the main electron acceptor for nitrification, and therefore the seven ecological groups compete for it. Figure 3.3A presents the specific affinity for oxygen ($a^0_{\text{O}_2}$) for all nitrifying groups considered except CMX (their $a^0_{\text{O}_2}$ has not been reported yet). No correlation between the μ_{\max} and $a^0_{\text{O}_2}$ values of considered nitrifying groups was observed ($r = -0.100$, $p > 0.1$; $\tau = -0.111$, $p > 0.1$; $n = 9$; Figure A.2I). In addition, diversity in $a^0_{\text{O}_2}$ values for all species considered is significantly lower than for the values gathered for $a^0_{\text{NH}_3}$, and $a^0_{\text{NO}_2}$ (Figures A.5, A.8 and A.9). Between NOB populations, *Nitrobacter* is identified as the group with the lowest affinity for oxygen and *Nitrospira* with the highest. Considering the $K_{m,(\text{app})}$ values for oxygen of NOB (Figure 3.3B), *Nitrospina* genus might have a higher affinity for oxygen than *Nitrospira*. This correlates with the intrinsic K_{O_2} values of the terminal oxidases of each of the NOB populations (Tables A.8 and A.9).

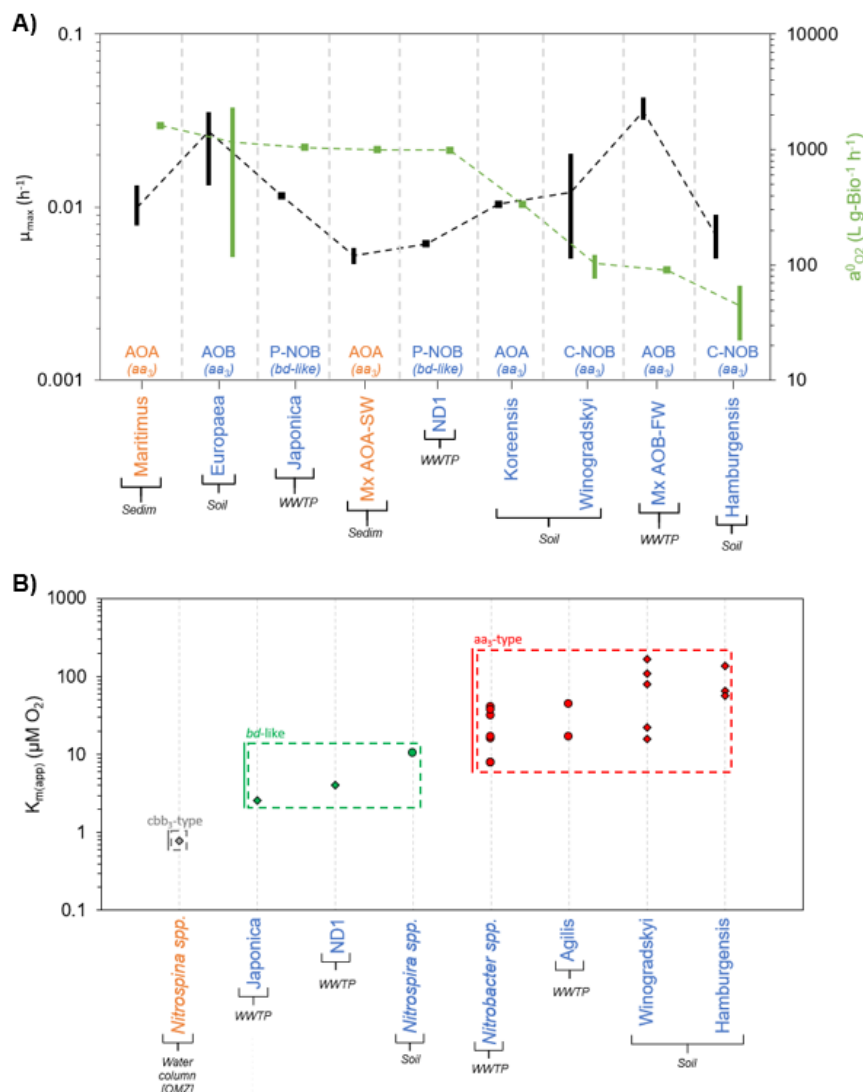


Figure 3.3. Oxygen competition. **A)** Maximum specific growth rate (μ_{max}) with specific affinity for oxygen ($a^0_{O_2}$) for all the nitrifiers' populations considered. The black bars show the range of μ_{max} values; dark green bars represent the range of $a^0_{O_2}$ values; and dashed lines connect the average of each value range. Blue: marine nitrifiers; orange: non-marine nitrifiers. Legends: AOB – Ammonia-oxidizing bacteria; AOA – Ammonia-oxidizing archaea; P-NOB – NOB with periplasmic NXR; C-NOB with cytoplasmic NXR. On the bottom of tags, in parentheses, the terminal oxidase that each group uses to reduce oxygen is shown (Table A.8). Dashed lines cross the calculated average value for each parameter function of the range of values reported. **B)** Apparent substrate affinity ($K_{m(app)}$) for oxygen of NOB. $K_{m(app)}$ values are given for growth measurements (circles) and activity measurements (diamonds). Marker colour legend: Red – NOB with heme-copper oxidase aa₃-type as terminal oxidase; Green – NOB with putative cytochrome bd-like oxidase as terminal oxidase; Grey – NOB with heme-copper oxidase cbb₃-type as terminal oxidase. [OMZ]: samples from oxygen minimum zones (OMZ). $K_{m(app)}$ of Nitrospinae is significantly different from that of Nitrospira and Nitrobacter species ($p < 0.0001$) and $K_{m(app)}$ of Nitrospira species are significantly different from that of Nitrobacter species ($p < 0.0001$). References of $K_{m(app)}$ values in Table A.10.

Considering only NOB, a positive correlation between affinity of the terminal oxidase of the species considered and the specific affinity measured is observed (Figure 3.3). However, no correlation between the terminal oxidase and $a^0_{O_2}$ for AOA and AOB groups is observed (Figure 3.3A). Although, AOA and AOB are reported as carrying an aa₃-type terminal oxidase, which is the oxidase with the lowest affinity for oxygen (Table A.9), Figure 3.3A shows that AOA and AOB, except Mx AOB-FW, have a similar oxygen affinity to *Nitrospira*, which encodes a *bd*-like terminal oxidase (Table A.8). This lack of correlation might be related to the presence of the monooxygenation step in ammonia oxidation (Arp et al., 2002; Vajrala et al., 2013). This additional oxygen consumption could increase the oxygen concentration gradient between cytoplasm and periplasm and, as consequence, intensify the penetration ratio of oxygen into the cell (Harder & Dijkhuizen, 1983; Tempest & Neijssel, 1978).

In general, it is considered that AOA have a higher affinity for oxygen than AOB (Liu et al., 2017; Yin et al., 2018). However, the specific affinity for oxygen of AOA and AOB are not significantly different ($p = 0.72$; Table A.3), suggesting that AOB populations could compete against AOA even in oxygen limiting conditions.

On the other hand, AOB have been considered better competitors for oxygen than NOB (Jubany et al., 2008; Wiesmann, 1994). Figure 3.3A shows that AOB have a significantly higher oxygen affinity than C-type NOB ($p < 0.005$; Table A.3) and similar affinity values to P-type NOB ($p = 0.63$; Table A.3). Therefore, ammonia oxidizers would only dominate the competition for oxygen if *Nitrobacter* (C-type NOB) is the dominant population in the NOB community. Contrary, NOB would compete closely for oxygen with populations of AOB or AOA if *Nitrospira* (P-type NOB) are abundant in the NOB community.

3.4. Conclusions

The meta-analysis presented in this study on the kinetics of different groups of nitrifiers finds specific trends between the parameters of the different populations in the community. High affinity for a substrate does not guarantee the survival of a microorganism in oligotrophic environments if the catabolic activity at low substrate concentrations does not ensure the harvest of enough energy. Likewise, it might not be competitive to carry an efficient but slower metabolism if essential substrates cannot be assimilated in conditions of low concentrations. Those microorganisms which have evolved to thrive in oligotrophic environments, would be metabolically efficient (high Y_{XS}) and show a high substrate affinity

(high a^0). This study shows that high growth yield correlates with high substrate affinity for those populations of nitrifiers that dominate in those environments where substrate limitation is a fundamental selective pressure. Figure 3.1 shows that in general, AOA and CMX present low μ_{\max} , high $a^0_{\text{NH}_3}$ and high Y_{XS} , whereas AOB show higher μ_{\max} , lower $a^0_{\text{NH}_3}$ and lower Y_{XS} .

Nevertheless, Figure 3.1A shows that not all AOA have a significant higher affinity for ammonia than AOB which could explain reported dominance of AOB in some natural oligotrophic environments over AOA (niche overlapping). Also, Figure 3.3A shows the inconsistency of the assumption that AOB have higher affinity for oxygen than NOB (although *Nitrobacter* present a lower affinity for oxygen, *Nitrospira* have a similar affinity than ammonia oxidisers). Notably, it was observed that for all the groups, the range of values found for $a^0_{\text{O}_2}$ is lower than for $a^0_{\text{NH}_3}$ or $a^0_{\text{NO}_2}$, which would reflect that nitrogen availability is stronger selective pressure than oxygen availability.

From this comprehensive analysis of the kinetic parameters of nitrifiers, no specific ecological strategies associated with a specific genus or species within the same ecological groups of nitrifiers were identified. Mainly fundamental differences in the biochemistry of the different populations of nitrifiers (*e.g.*, complete versus partial ammonia oxidation, archaea versus bacteria, different terminal oxidases, different carbon fixation pathways or periplasmic versus cytoplasmic NXR) lead to significant differences in the measured kinetic parameters and potential niche specializations. This suggests that the kinetics associated with any microbial species, might be determined by the specific metabolic traits and activity catalysed, with constrained capacity for adaptation.

4.

**Multiscale models driving
hypothesis and theory-based
research in microbial ecology.**

4.1. Introduction

Hypothesis testing as a scientific approach in environmental microbiology and biotechnology is bounded by the intrinsic complexity of microbial communities. Theory-based studies are relegated by an increasing number of microbial ecology studies that focus on descriptive experiments that aim to collect novel data on uncultured microbial species. Critical testing of ecological hypotheses requires rigorous experimental design while the application of novel molecular technologies for data collection has led to multitude of top-down research approaches where data is just described (Prosser, 2020). Generation of knowledge through induction (*e.g.*, accumulative characterization of uncultured microbial species) does not *per se* translate in new theoretical/mechanistic explanations for community assembly or specific fitness traits.

Here it is proposed the development of research focused on the mechanisms that shape microbial ecology, driving new theoretical hypotheses. These hypotheses are further validated through the interaction between mathematical modelling and laboratory experimentation. In this chapter, a modelling methodology based on bottom-up approaches is described in order to generate, together with experimental validation, new hypotheses and theories. By using theoretical platforms, we can target the minimization of complexity associated to natural communities directing research exploration in a more efficient way. To understand the implications associated with this methodology, first it is discussed the actual position of mathematical models and experimentation in scientific research.

4.2. Experimental and theoretical models

Considering that any mathematical model represents a conceptualization of reality, it is commonly assumed that experiments should precede any modelling exercise. Modelling is then mostly placed as an alternative complement to experimentation because theoretical results must be demonstrated or validated. Nevertheless, in research, experimental outcomes must also be demonstrated by replication and reproducibility as a major principle underpinning the scientific method. The results obtained by an experiment, an observational study, or in a statistical analysis of a dataset, achieve a high degree of reliability when these studies are replicated (Eric & Kwan, 1999).

Experimentation and modelling exercises cannot be seen as exclusive, but interconnected methodologies (Figure 4.1). A modelling exercise can help defining experimental designs

that validate hypotheses theoretically constructed (dotted green arrow, Figure 4.1). This level of definition also aids reproducibility, especially when applied to complex systems. It can be argued that the most useful models are constructed on the basis of the theoretical knowledge one possesses (Kreft, 2004a; Martinez-Rabert et al., 2022), directing experimentation that aims to validate the principles on which they are built, that is, using mathematical models as hypotheses generator.

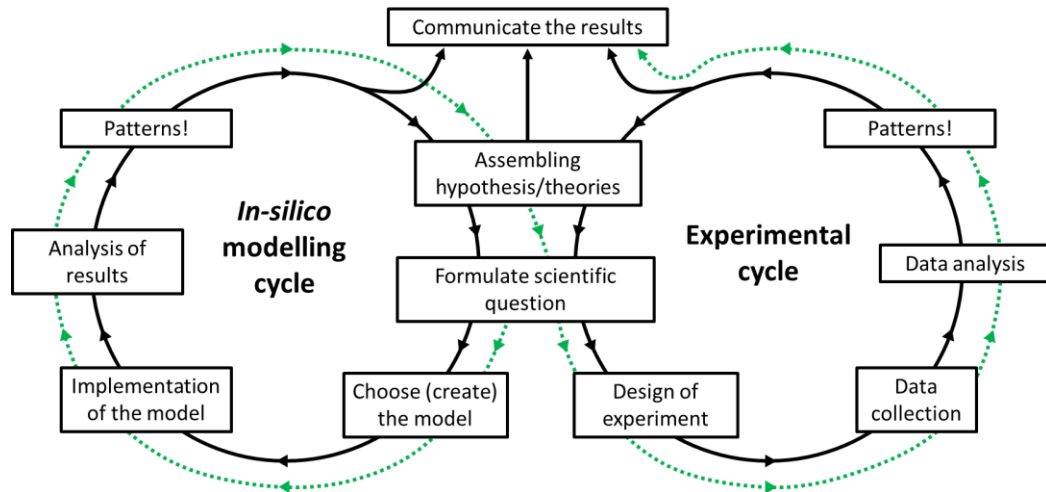


Figure 4.1. Modelling-experimental cycle. Integrated development of experimental and modelling methodologies can lead to higher levels of predictive capacities and operation control. Dotted green arrow depicts the methodology presented here – theoretical model before experimentation.

4.3. *In-silico* bottom-up methodology

When modelling continuous and complex natural processes, they can be treated as a group of discrete and measurable elements interconnected with each other. A bottom-up approach is essentially piecing together sub-systems to give rise to more complex systems. *In-silico* models that follow a bottom-up approach aim to explain how emerging properties of complex communities arise from simpler processes (Rodríguez Amor & Dal Bello, 2019).

The first step to build an *in-silico* bottom-up methodology is the identification of all the elements that describe a particular phenomenon (*i.e.*, the *fragmentation*; Figure 4.2). After that, the elements that will be part of the model are selected. For this step, having enough information is crucial, either with specific experimental data or by means of theories and first principles (generally associated to a set of mathematical equations). Additionally, in the process of selection of elements one must evaluate the model complexity and the possibilities for experimental validation (Bellocchi et al., 2010).

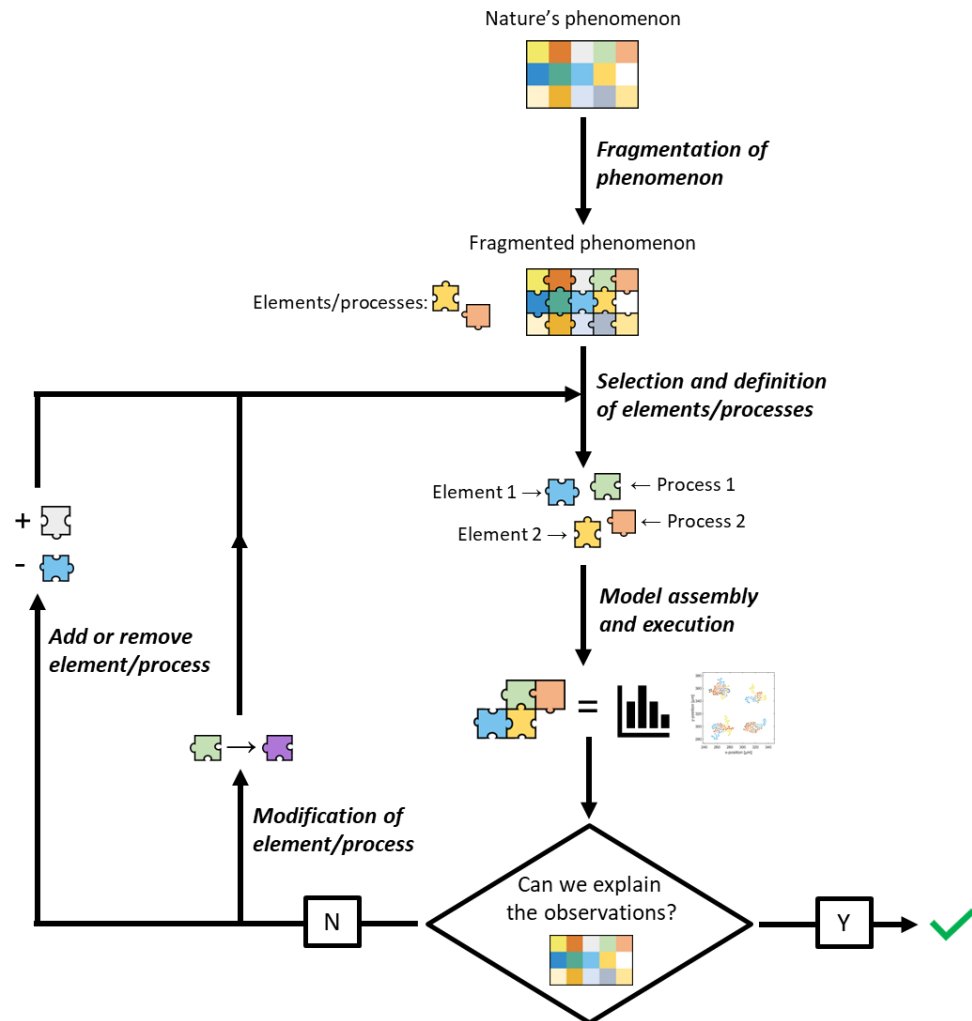


Figure 4.2. Schematic representation of in-silico bottom-up methodology.

Subsequently, the mathematical model is assembled. A mathematical model is a conceptual representation of a mechanism (or a collection of them) limited by our knowledge about reality. All models are constituted by the quintuple:

- *Domain (D)*: set of factual items (elements and processes) that constitute the studied system.
- *Scientific question (Q)*: question(s) that states the reason for modelling and the construction of the model.
- *Interpretation (I)*: validated explanations of each item of the *domain*. Definition of spatial scale(s) and temporal extent is included here.
- *Assumptions (A)*: set of explicitly stated (or implicit premised) conventions and choices that fulfils the holes in our *interpretation* of reality. These establish the limits of our model and simplify the problem (*e.g.*, by ignoring some processes or elements that cannot be well-described).

- *Formalism (F)*: set of mathematical expressions that represents the items of the domain.

The definition of each of the components $\langle D, Q, I, A, F \rangle$ is fundamental for the success of the modelling process. The construction of the mathematical model starts with the abstraction of the current knowledge about the domain (D). Based on our understanding, the scientific question (Q) is stated. Then, the formalization of our knowledge about the domain is addressed, defining interpretation, assumptions and formalism (i.e., the modelling approach, $\langle I, A, F \rangle$) (Figure 4.3). Table 4.1 shows an example of the statement of $\langle D, Q, I, A, F \rangle$.

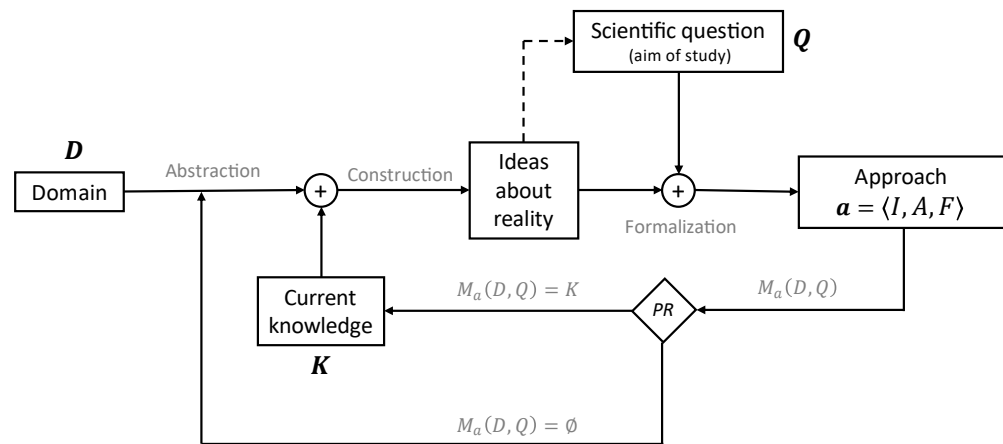


Figure 4.3. Life cycle of a mathematical model (M). PR represents the peer-review process of the model, in which decides if the model is able to contribute to the current knowledge (K) or not (\emptyset). $M_a(D, Q)$ is the formal representation of a mathematical model based on a specific domain (D), scientific question (Q), and approach ($a = \langle I, A, F \rangle$). Abstraction: obtention of information from domain. Formalization: definition of interpretation (I), assumptions (A) and formalism (F).

The limits of the modelling approach $\langle I, A, F \rangle$ are established by the scope of the fundamental processes and the selected elements. The overlook of a key element or process can make our model inaccurate. An example of this is the omission of the diffusion in an aggregated system like presented in *Model 1* in Table 4.1. Although a NH_3 -limiting environment was considered, (being this one of the main pressure factors for the selection of comammox process (Costa et al., 2006)), the enrichment observed in Daims et al. (2015) was not predicted with *Model 1*, but it was with *Model 2* (considering diffusion of compounds). Therefore, a model will be *useful* (i.e., generates reliable knowledge) if and only if there is no discrepancy between the modelling approach $\langle I, A, F \rangle$ and the real domain (D).

Table 4.1. Example of statement of model components (D, Q, I, A, F).

Model 1 (ODE system) ⁽¹⁾	Model 2 (Individual-based Model) ⁽²⁾
Domain (D)	
Suspended microbial community growing under a dynamic ammonia environment simulated as a continuous stirred tank reactor (CSTR) until it reaches the steady state (1825 days). Dense population of cells was generated (simulated as small aggregates).	
Scientific question/aim of modelling (Q)	
<i>In-silico</i> prediction of the selection of comammox (from NH ₃ to NO ₃) over canonical ammonia oxidation (from NH ₃ to NO ₂ ⁻) under NH ₃ -limiting environment. Simulations based on metabolic efficiency of comammox and ammonia oxidation.	
Interpretation (I)	
Aggregates are too small and diffusion gradients for chemical components are neglected	Diffusion gradients for chemical components are computed
Spatial scales	
Individual scale: biomass concentration of reactor Micro-scale: <i>not considered</i> Macro-scale: bulk liquid	Individual scale: independent entities Micro-scale: aggregate region + boundary layer Macro-scale: bulk liquid
Assumptions (A)	
No kinetic competition – same growth kinetics both metabolic activities considered ($\mu_{max}, K_{NH_3}, K_{O_2}, a_m$) Different growth yield ($Y_{X/S}$) – estimated according to bioenergetic analysis. Ideal behaviour of the CSTR operation	
Formalism (F)	
Microbial growth: $\mu_{max} = 0.01 h^{-1}$; $K_{NH_3} = 1.0 \mu M$; $K_{O_2} = 3.13 \mu M$; $a_m = 0.001 h^{-1}$ Growth yield ($Y_{X/S}$): ammonia oxidation – $4.09 \times 10^{-2} mol_X/mol_N$; comammox – $6.51 \times 10^{-2} mol_X/mol_N$	
Bacteria growth rate (Monod): $\mu = \mu_{max} \cdot \frac{[NH_3]}{K_{NH_3} + [NH_3]} \cdot \frac{[O_2]}{K_{O_2} + [O_2]} - a_m$	
Micro-scale: <i>not considered</i>	Micro-scale: 2 nd Fick's law + reaction $\frac{\partial}{\partial t} [S](x, y) = \mathbb{D} \cdot \nabla_{xy}^2 [S](x, y) + R_{xy}$
Macro-scale (mass balance of CSTR): $\frac{d}{dt} [S] = \frac{1}{HRT} \cdot ([S]_{infuent} - [S]) + R_{BL}$; $R_{BL} = \left(\frac{1}{Y_{X/S}}\right) \cdot \mu([S]) \cdot X$	
Results from modelling (with triplicate)	
Ammonia oxidation: 50.0 wt. % comammox: 50.0 wt. %	Ammonia oxidation: 14.0 wt. % comammox: 86.0 wt. %
Experimental results from Daims et al. (2015)	
After a series of sub-cultivation steps, an enrichment culture of comammox bacteria (60 to 80% of the community) was obtained without known ammonia oxidizers (bacteria or archaea) in it.	

⁽¹⁾ Model performed with MATLAB (R2020b) via the built-in function 'ode45()'.⁽²⁾ Information about the Individual-based Model framework for microbial aggregates in Chapter 5 and Appendix B. Legend – μ_{max} : Maximum specific growth rate; K_{NH_3} : half-saturation constant for NH₃; K_{O_2} : half-saturation constant for O₂; a_m : specific maintenance rate; $[NH_3]$, $[O_2]$: substrate concentration; \mathbb{D} – diffusion coefficient; R_{xy} – reaction term in each discretized space; R_{BL} – reaction term in bulk liquid; HRT – hydraulic retention time; X – bacteria concentration.

The outcome from the computational model is validated using the available experimental data. If the model is accurate enough to represent the system of interest, it can be used for prediction and generation of new knowledge ($M_a(D, Q) = K$, Figure 4.3). New theoretical knowledge can be generated by the validation of the discrete elements and processes employed. To increase the accuracy of a mathematical model, one could (i) add (or remove) elements and/or processes that were previously overlooked or (ii) modify those previously selected (iterative procedure, Figure 4.2).

4.4. Scales of modelling for microbial communities

For the modelling of microbial communities, three fundamental scales are defined: individual scale (main elements of the model), micro-scale (processes simulated at the same resolution than individual scale) and macro-scale (elements and processes described from a larger perspective, generally embedded in the bulk liquid region). Table 4.1 presents an example of these scales for the modelling of microbial aggregates (*Interpretation (I) – Spatial scales*).

The different scales of the model are interconnected, and they influence each other. For example, the microbial activity is influenced by the local conditions stated by the micro-scale and, simultaneously, the microbial cells shape the local environment. The integration of multiple scales with different characteristic times (*e.g.*, cell division: ~ 1 hour; diffusion-reaction process: $\sim 10^{-8}$ hours) is possible thanks to the use of proper time discretization and systematic resolution – a *pseudo-steady state* for processes with lower characteristic time is considered a good approximation for most applications when solving those with higher characteristic time (Kissel et al., 1984). Multiscale modelling also covers processes with the gap between characteristic space scales, such as diffusion-reaction process ($\sim 10^{-6}$ m) and the bulk processes ($\sim 10^{-3} - 1$ m). Because the characteristic time and space are positively correlated, ensuring the numerical condition stability (Charney et al., 1950), the systematic resolution presented above also deals with the gap between space scales.

4.4.1. Individual scale. Models that describe individual microbial activity

In microbial ecology, the Monod equation has been widely used to describe microbial dynamics (Henze et al., 2006; Otuzalti & Perendeci, 2018). Growth is defined by empirical parameters measured for specific populations and conditions without considering the

ecological interactions or microbial evolution that would explain the specific dominant activities observed in bioprocesses.

Aware of the limitations imposed by the use of Monod equation (Hellweger, 2017), molecular systems biology attempts to comprehend cell growth through mechanistic descriptions of intracellular processes. With different levels of metabolic and physiological details, these descriptions are able to identify some fitness trade-offs in microbial activity arising from a common set of physicochemical and intracellular constraints. Resource allocation theory defines that microorganisms optimize the use of limited intracellular resources towards expressing the most efficient strategy for growth, allowing the description of their dynamic adaptations to the environment (Karimian & Motamedian, 2020).

An approach like this requires in many cases detailed physiologic and metabolic information, generating mathematical models with a high number of parameters. This limits their application to few model organisms (Cusick et al., 2021). A validation of a first-principles approach can overcome the reduced empirical information by attempting the prediction of kinetic parameters for growth through mathematical equations. For example, bioenergetics analyses provide a tool for quantifying growth yields (González-Cabaleiro et al., 2021; Kleerebezem & Van Loosdrecht, 2010). Efforts towards estimating the trends of other kinetic parameters for description of microbial activity and growth can also be considered on a framework of resource allocation (Sharma & Steuer, 2019).

4.4.2. Micro-scale. Prediction of emerging properties of communities

The integration of models that describe microbial growth with the definition of the local conditions dynamically affected by the microbial activity enables the description of interactions between the media, individuals and community. This allows the prediction of emergent properties that arise from the definition of individual activity (N. I. van den Berg et al., 2022), and possible estimation of ecological trends in communities that can be compared to experimental observations.

Depending on the scientific question asked, abiotic physicochemical processes should be considered. Examples of this are kinetic models of acid-base reactions, chemical speciation or precipitation. The consideration of spatial competition might also be crucial to describe ecological interactions in specific communities (see Chapter 6).

4.4.3. Macro-scale. Scaling up and down key process

Modelling large-scales systems with micro-scale resolution ($\sim 10^{-6}$ m) is highly demanding computationally. To overcome this limitation, micro- and macro-scales processes are independently resolved following the systematic procedure through the establishment of *pseudo-steady states* (Kissel et al., 1984). The full integration of both spatial scales can be achieved if the micro-scale processes are scaled up, and the macro-scale processes are scaled down. The scaling-up is based on the consideration of a statistically representative volume of the larger system in full detail. It is assumed that the representative volume yields a representative influence on the whole system (*i.e.*, the macro-scale). On the other hand, the scaling-down of macro-scale processes needs the definition of boundary conditions for the simulated system. Based on the goal that the model has (or the *scientific question (Q)*), the boundary conditions can be set as (i) unidirectional (only macro-scale influence micro-scale, that is, fixed boundary conditions) or (ii) bidirectional (macro-scale influence micro-scale and vice versa, that is, dynamic boundary conditions).

4.5. Outlook

An alternative avenue to advance the understanding of microbial ecology, community assembly and biological activity would aim at the deconstruction of complexity by means of a bottom-up approach, where multiscale models, robust experimental data collection, and method development are integrated. In essence, it is proposed that the design of cultivation-based experiments would help the validation of hypotheses constructed by mathematical modelling. Although hypothesis-based cultivation experiments can be seen as too idealistic when compared to the intrinsic complexity of microbial ecology, well-designed experiments with targeted scientific questions can lead to the discovery of new metabolic characteristics or relationships between species. In this context, the integration of molecular technologies would aid the validation of theoretical hypotheses. The rationalisation of ecological interactions in a community, and their relation to the environment, breaks down complexity, reduces the necessity of data and accelerates its understanding (Kreft et al., 2020). This promises a higher level of prediction capacity which can directly impact on the development of novel bioprocesses. In this effort, commonalities between communities will be found, which implies that knowledge construction in one field will benefit others (*e.g.*, research on the understanding of gut microbiome or marine microbial communities and anaerobic digestion processes).

5.

**Methods - Individual-based Model
for microbial aggregates.**

The following *in-silico* studies included in this thesis (Chapters 6 and 7) were performed using the same multiscale modelling framework – Individual-based Model (IbM). This chapter provides a detailed description of this model. The source code to reproduce the results and analyses presented in Chapters 6 and 7 is available on a public GitHub repository at <https://github.com/Computational-Platform-IbM/IbM> (including previous versions). For this thesis, the release **v2.4.3** was employed.

5.1. Applications and alternative methods

The most distinguished properties of microbial aggregates are the presence of local gradients and the close localization of distinct microbial species, stimulating the ecological interactions between microbes (Flemming et al., 2016). Individual-based Models aim to describe the heterogeneity of the aggregate and study the influence of ecological interactions to the microbial community assembly. This model framework is characterized by simulating each microbe as a discrete entity with unique traits, and as a reaction point in the spatial domain. Its activity and growth are shaped based on the local environment. Diffusion of the substrates across the simulation domain is modelled together with the biotic reactions. These dynamics are resolved based on the boundary conditions imposed over the limits of the domain. Microbial growth and decay are simulated assuming that cellular dynamics occur at certain cell age, cycle stage or size. Therefore, division and death/inactivation occur independently for each of the cells. With that, the heterogeneity of the aggregate is captured, supporting the non-linear growth of microbes (Hellweger et al., 2016). Additionally, this model does not only include deterministic dynamics (such as diffusion of substrates and products, detachment and cellular growth/decay), but also stochastic dynamics: (i) initial distribution of inoculum (although this can be set if needed), (ii) the initial mass of a new cell, and (iii) when a cell divides, the new individual is positioned in a random place in the neighbourhood of its parent cell.

Other IbM frameworks have also been developed, often simulating different aggregated systems (microbes attached onto a solid surface (biofilms) or self-immobilized microbes (flocs/granules)), different mechanisms (*e.g.*, detachment, extracellular polymeric substance (EPS) generation or spatially varying diffusion), or assuming different community resolution (populations or individuals) (Table 5.1). All these different approaches are tailored to different research questions and applications.

Table 5.1. Comparison between existing Individual-based Models for microbial populations

	This work	NUFEB	iDynoMiCS	BSim	CellModeller
Microbial community structure					
Biofilm		✓	✓		
Granule	✓				✓
Suspension	✓			✓	
Cell motility				✓	
Spatially varying diffusion	✓ ^(NA)				
Population or Individual ⁽¹⁾	IbM	IbM	IbM	IbM	IbM
Dimensions					
2D	✓		✓	✓	✓
3D		✓	✓	✓	
Physical interactions					
Shoving	✓	✓	✓	✓	✓
EPS		✓	✓		
Detachment	✓	✓	✓		
Chemical environment					
pH	✓ ^(NA)	✓			
Cell growth and metabolic description					
Monod based	✓	✓	✓		
Resource allocation				✓	✓
dFBA					
Numerical method(s) for solving differential equations					
Method ⁽²⁾	FDM	FDM, FVM	FDM	FDM	FDM
Reference ⁽³⁾	[1]	[2]	[3]	[4]	[5]
	COMETS	BacArena	IndiMeSH	ACBM	Simbiotics
Microbial community structure					
Biofilm	✓	✓			✓
Granule	✓	✓			
Suspension					
Cell motility	✓		✓	✓	✓
Spatially varying diffusion	✓	✓			
Population or Individual	PbM	IbM	IbM	IbM	IbM
Dimensions					
2D	✓	✓	✓	✓	✓
3D					✓
Physical interactions					
Shoving	✓	✓		✓	✓
EPS	✓				✓
Detachment			✓		
Chemical environment					
pH					✓
Cell growth and metabolic description					
Monod based growth	✓				✓
Resource allocation					✓
dFBA	✓	✓	✓	✓	
Numerical method(s) for solving differential equation					
Method ⁽²⁾	FDM	BP	LBM	FVM	FVM
Reference	[6]	[7]	[8]	[9]	[10]

^(NA) Available in the model but not applied in this thesis. ⁽¹⁾ Population-based Model – (PbM); Individual-based Model – (IbM).

⁽²⁾ Finite-Difference Method – (FDM); Finite-Volume Method – (FVM); Finite-Element Method – (FEM); Build Package (several methods included) – (BP); Lattice Boltzmann Methods – (LBM). ⁽³⁾ References: [1] – (Martinez-Rabert et al., 2022); [2] – (Li et al., 2019); [3] – (Lardon et al., 2011); [4] – (Gorochowski et al., 2012); [5] – (Rudge et al., 2012); [6] – (Dukovski et al., 2021); [7] – (Bauer et al., 2017); [8] – (Borer et al., 2019); [9] – (Karimian & Motamedian, 2020); [10] – (Naylor et al., 2017).

5.2. Description of the mathematical model

The simulation domain is a two-dimensional and micro-scale space. In it, the diffusion of soluble components is resolved. These soluble components are the substrates and products of the microbial activity. The domain is divided in three different zones: the aggregate, the boundary layer and the bulk liquid (Figure 5.1). For this thesis, two versions of the IBM framework have been developed – the granular version (Figure 5.1A) and the suspension version (Figure 5.1B). The only difference between these versions is the starting point of simulation. In the granular version, only one inoculum is placed on the simulation domain, and it is assumed that this is the representative reaction point of the whole reactor. On the other hand, in the suspension version several inoculums are placed on the simulation, and all of them are considered the representative reaction point of the whole reactor.

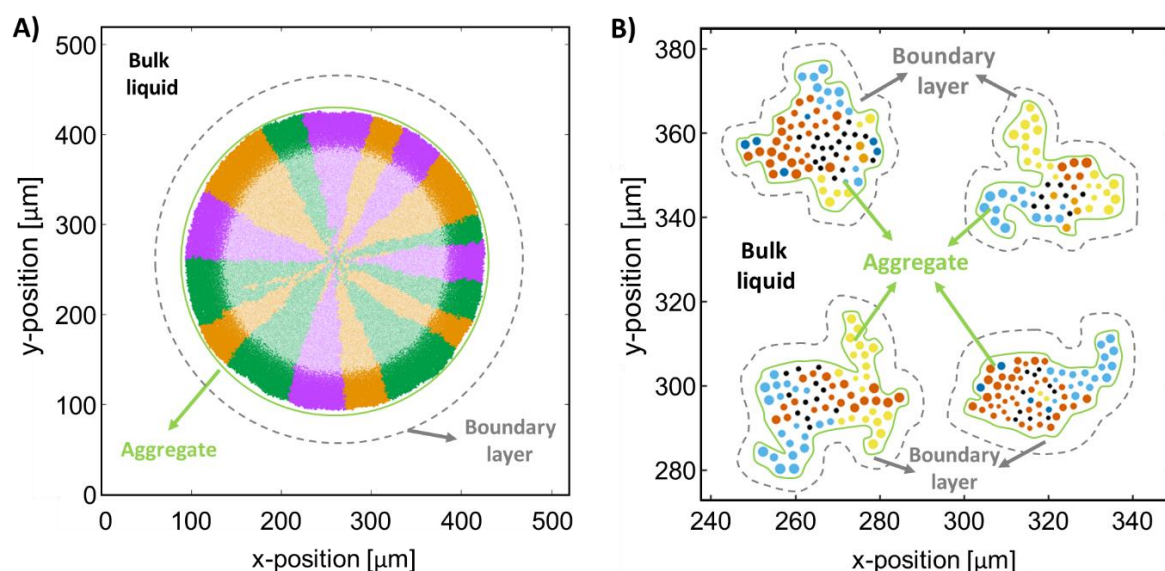


Figure 5.1. Representation of simulation domain. **A)** Granular version. **B)** Suspension version.

When microbes grow and divide, they push each other, thereby increasing the size of the overall aggregate. Diffusion of soluble components occurs throughout the aggregate where they are consumed or produced by the microbes. The boundary layer is the surrounding space of the aggregate defined to simulate the gradient of concentrations between the bulk liquid and the surface of the microbial aggregate. Only diffusion of the soluble components is resolved in this space. At the outside of the boundary layer (considered bulk liquid) the gradient of concentration of all soluble components is considered negligible, assuming a well-mixed homogenous reactor.

The space is discretized in two coordinates (x and y). This discretization is needed to solve the diffusion-reaction equation in the aggregate and boundary layer, and also to set the

position of each individual. The position of a microbe, and subsequent assignment of its local conditions, is set by the location of its centre to the grid (Figure 5.2).

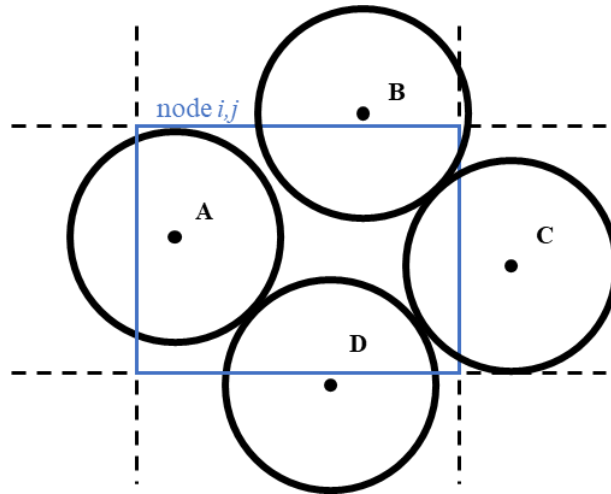


Figure 5.2. *Hypothetical position of microbes in a node. Only “microbe A” belongs to node I,j because its centre is inside the node.*

The model is constituted by two interconnected sub-models – (i) a *biological model* that considers heterogeneity of the system and the intrinsic ecological interactions between microbial species, (ii) a *physical model* that simulates the diffusive transport of the dissolved substrates.

5.2.1. Biological model. Individual-based Model

The growth of each individual is only affected by its local conditions, which in turn are influenced by the activity of surrounding microbes. Like this, the model captures the intrinsic interactions among microbes in the aggregate. Cellular division or death is assumed to occur at a certain microbe’s size independently of the state of other cells, thus capturing the heterogeneity of the aggregate and supporting non-linear growth solutions (Hellweger et al., 2016). In this thesis, cell lysis and release of inter-cellular material have not been considered, but these can be included in the model with the stoichiometry of decay (see Section 5.2.2.2). To describe the actual growth for each individual (μ_m , Eq. 5.1), a specific stoichiometry and Monod kinetics parameters are employed – maximum specific growth rate (μ^{max}), half-saturation constant (K_S), inhibition constant (K_I) and specific maintenance rate (a_m) (Han & Levenspiel, 1988). The change of the mass of each individual is calculated by the differential (Eq. 5.2).

$$\mu_m^n = \mu_m^{max} \cdot \Pi \left(\frac{\phi_{i,j}^n}{K_{S,m} + \phi_{i,j}^n} \right) \cdot \Pi \left(\frac{K_{I,m}}{K_{I,m} + \phi_{i,j}^n} \right) - a_m \quad (5.1)$$

$$\frac{dX_m}{dt} = \mu_m^n \cdot X_m^n \quad (5.2)$$

Where $\phi_{i,j}^n$ refers to the concentration of substrate in node I,j of the simulation domain in a time step n , and X_m refers to the mass in moles of the cell m . The mass of each individual is integrated in time using the forward Euler scheme on Eq. 5.2. Once the mass of each cell is known, its volume and radius (r_m) can be calculated defining a specific cell density (ρ_m) and assuming perfect spherical shape (Eq. 5.3) (Kreft et al., 2001).

$$r_m = \left(\frac{X_m}{\rho_m} \cdot \frac{3}{4\pi} \right)^{1/3} \quad (5.3)$$

The value of μ_m^n that Eq. 5.1 returns, indicates if microbe m is growing ($\mu_m > 0$) or dying ($\mu_m < 0$). The model assumes that once cells achieve a maximum mass (M_{max}), they divide (Figure 5.3). In this case, a new cell is formed (cell $m+1$, Eq. 5.4) with an initial mass that is a random percentage of the total mass of the parent cell (α is a stochastic parameter with a value between 0.45 and 0.55). The mass of the parent cell is updated with the mass remaining after the division (Eq. 5.5).

$$X_{m+1} = \alpha \cdot X_m \quad (5.4)$$

$$X_m = (1 - \alpha) \cdot X_m \quad (5.5)$$

When a cell divides, a random position for the new individual ($m+1$) is assigned in the neighbourhood of its parent (m). When microbes grow or divide, the *shoving algorithm* checks the overlapping space between individuals. If this is bigger than the maximum overlap accepted, cells shove increasing the size of the aggregate.

When $\mu_m < 0$ the individual shrinks, reducing its mass. When cells reach a minimum mass (M_{min}), or a size considered negligible, they become inactive (*i.e.*, they do not grow nor decay) and only can become active again if they increase their mass under more favourable conditions (Figure 5.3).

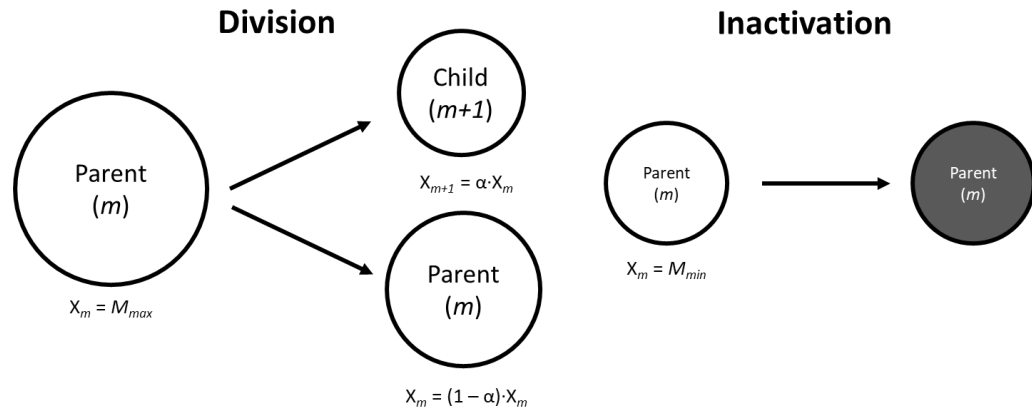


Figure 5.3. Microbial division and inactivation. α is any stochastic value between 0.45 – 0.55. M_{max} and M_{min} refer to the maximum and minimum mass that microbe can reach, respectively.

5.2.1.1. Shoving algorithm

To compute the shoving of the cells after growth or division, first the overlap between microbes is checked by Eqs. 5.6 and 5.7.

$$|\vec{v}| = \sqrt{(x_m - x_{m+1})^2 + (y_m - y_{m+1})^2} \quad (5.6)$$

$$overlap = kDist \cdot (r_m + r_{m+1}) - |\vec{v}| \quad (5.7)$$

Where $|\vec{v}|$ is the norm of the vector that links the centres of both cells m and $m+1$, and $kDist$ is just a multiplier that allows adjustment of the minimal spacing between microbes. If the *overlap* value is bigger than the distance allowed, then microbes are pushing each other function their mass and distance (Eqs. 5.8 – 5.13).

$$\vec{p} = \frac{kDist \cdot (r_m + r_{m+1}) - |\vec{v}|}{|\vec{v}|} \quad (5.8)$$

$$a_m = 1 - \frac{X_m}{X_m + X_{m+1}} ; a_{m+1} = 1 - \frac{X_{m+1}}{X_m + X_{m+1}} \quad (5.9)$$

$$x_{new,m} = x_{old} - (x_{m+1} - x_m) \cdot a_m \cdot \vec{p} \quad (5.10)$$

$$y_{new,m} = y_{old} - (y_{m+1} - y_m) \cdot a_m \cdot \vec{p} \quad (5.11)$$

$$x_{new,m+1} = x_{old} + (x_{m+1} - x_m) \cdot a_{m+1} \cdot \vec{p} \quad (5.12)$$

$$y_{new,m+1} = y_{old} + (y_{m+1} - y_m) \cdot a_{m+1} \cdot \vec{p} \quad (5.13)$$

In this case, the *quadtree algorithm* is applied to detect *overlapping* between microbes and, subsequently, the shoving of these is computed (Samet, 1988) (Appendix B – Quadtree algorithm).

5.2.2. Physical model. Diffusive transport

To describe the diffusion of soluble components, the Fick's second law equation is integrated over time (t) and space (x and y). The consumption and synthesis of the soluble components in this system are evaluated in each node of the simulation domain through the reaction term ($R(x, y, t)$; Eq. 5.14). The reaction term is calculated according to the stoichiometry, the mass and growth rate of microbes present in the specific node. Additionally, steady state for the production/degradation of soluble components was assumed (Kreft et al., 1998).

$$\frac{\partial}{\partial t} \phi(x, y, t) = \mathbb{D} \cdot \nabla_{xy}^2 \phi(x, y, t) + R(x, y, t) \quad (5.14)$$

Where $\phi(x, y, t)$ refers to the concentration of a soluble component in a position of the simulation domain (x, y) and in a time step (t), and \mathbb{D} refers to the effective coefficient of diffusion. To simplify the resolution of Eq. 5.14, a constant \mathbb{D} value is considered for the whole aggregate region (van den Berg et al., 2020).

5.2.2.1. Discretization of diffusion-reaction equation

To solve the diffusion-reaction equation (Eq. 5.14), the implicit Crank-Nicolson method, which is unconditionally stable (Thomas, 1995), is used to discretize in time the diffusion term. For the reaction term, the forward Euler method is used (Eq. 5.15). This can be done because the reaction process has a slower time scale than the diffusion (Kreft et al., 1998).

$$\frac{\phi_{i,j}^{n+1} - \phi_{i,j}^n}{h_t} = \mathbb{D} \cdot \frac{1}{2} [\nabla^2 \phi_{i,j}^{n+1} + \nabla^2 \phi_{i,j}^n] + R(\phi_{i,j}^n) \quad n \in 1:N_t \quad (5.15)$$

Where h_t refers to the time step, N_t to the total number of time steps and $\phi_{i,j}^n$ to substrate concentration in *node* I, j and time n . The Laplacian of Eq. 5.15 (∇^2) is discretised in a two-dimensional space (x, y) using the central finite-difference method (Eq. 5.16), where h is the grid size ($h = \Delta x = \Delta y$).

$$\nabla^2 \phi_{i,j}^n = \frac{\phi_{i-1,j}^n + \phi_{i+1,j}^n + \phi_{i,j-1}^n + \phi_{i,j+1}^n - 4\phi_{i,j}^n}{h^2} \quad (5.16)$$

The Eq. 5.16 (also known as discrete Laplacian) is given as the following kernel (Eq. 5.17). Then, the Laplacian approximation can be re-written in a matrix form (Eq. 5.18), in which the convolution of $[L]$ and $\phi_{i,j}^n$ is denoted using the symbol $*$.

$$[L] = \begin{pmatrix} 0 & 1 & 0 \\ 1 & -4 & 1 \\ 0 & 1 & 0 \end{pmatrix} \quad (5.17)$$

$$\nabla^2 \phi_{i,j}^n = \frac{1}{h^2} ([L] * [\phi^n]) \quad (5.18)$$

Where $[\phi^n]$ is the concentration of soluble compounds ($\phi_{i,j}^n$) defined in matrix form (Eq. 5.19).

$$[\phi^n] = \begin{pmatrix} \phi_{1,1}^n & \phi_{1,2}^n & \dots & \phi_{1,N_y}^n \\ \phi_{2,1}^n & \phi_{2,2}^n & \dots & \vdots \\ \vdots & \vdots & \ddots & \vdots \\ \phi_{N_x,1}^n & \dots & \dots & \phi_{N_x,N_y}^n \end{pmatrix} \in M_{N_x \times N_y} \quad (5.19)$$

Eq. 5.20 defines the convolution of A and B (*i.e.*, $A*B$), being these discrete and 2-dimensional variables. Convolution satisfies the distributive property, multiplicative identity, and associative property with scalar multiplication. These properties are essential to rearrange the diffusion-reaction equation properly (see Appendix B).

$$A[x] * B[x] = \sum_{k=-\infty}^{+\infty} A[x] \cdot B[x - k] \quad (5.20)$$

Then the diffusion-reaction equation (Eq. 5.14) can be re-written as a system of matrixes (Eq. 5.21), where ψ is a constant defined for each soluble component (Eq. 5.22) and $[I_k]$ is the so-called *identity kernel* or *do-nothing convolution kernel* (Eq. 5.23).

$$([I_k] - \psi \cdot [L]) * [\phi^{n+1}] = ([I_k] + \psi \cdot [L]) * [\phi^n] + R([\phi^n]) \cdot h_t \quad (5.21)$$

$$\psi = \frac{\mathbb{D} \cdot h_t}{2 \cdot h^2} \quad (5.22)$$

$$[I_k] = \begin{pmatrix} 0 & 0 & 0 \\ 0 & 1 & 0 \\ 0 & 0 & 0 \end{pmatrix} \quad (5.23)$$

Boundary conditions. To solve Eq. 5.21 in all the simulation domain, the definition of boundary conditions is necessary. In this case, a single boundary condition type is defined – the concentrations at outside of the aggregate (*i.e.*, limits of the boundary layer) are defined

by the conditions of the bulk liquid. This is implemented by the Dirichlet (or first-type) boundary condition (Eq. 5.24).

$$\phi_{-1,j}^n = \phi_{N_x+1,j}^n = \phi_{i,-1}^n = \phi_{i,N_y+1}^n = \gamma \quad (5.24)$$

To implement Dirichlet boundary condition in this system, first the region of the simulation domain is determined. Then, which nodes would belong to the diffusion region (comprising boundary layer and aggregate regions) are determined (see Appendix B – Definition of diffusion and no-diffusion regions). Like this, the concentration matrix $[\phi^n]$ is modified accordingly (Eq. 5.25). Those nodes in which diffusion region is considered have the corresponding concentration value ($[\phi^n]$), and that ones in which no-diffusion region is considered have the boundary value (*i.e.*, concentration of bulk liquid, γ).

$$[\phi^n]^\gamma = \text{diff}R \circ [\phi^n] + \neg\text{diff}R \cdot \gamma \quad (5.25)$$

Where $\text{diff}R$ is a logical matrix with 1 (*true*) in those nodes of diffusion region, and 0 (*false*) in those nodes of no-diffusion region; $\neg\text{diff}R$ is the inverse of $\text{diff}R$. Then, the diffusion-reaction equation including the boundary conditions imposed over the simulation domain is shown in Eq. 5.26. For each soluble component and time iteration, Eq. 5.26 is solved calculating $[\phi^{n+1}]$ using an efficient multigrid method (V-cycle) (Briggs et al., 2000).

$$([I_k] - \psi \cdot [L]) * [\phi^{n+1}] = ([I_k] + \psi \cdot [L]) * [\phi^n]^\gamma + R([\phi^n]) \cdot h_t \quad (5.26)$$

Bulk liquid concentrations. The following *in-silico* studies (Chapters 6 and 7) consider that the simulated aggregate grows in a continuous stirred tank reactor (CSTR), where substrate concentrations in the bulk liquid are dynamic. The average microbial activity of the aggregate (as a representation of the activity of the whole reactor) is used to integrate the concentration of the soluble components in the bulk liquid of the reactor (S) through the mass balance shown in Eq. 5.27.

$$\frac{dS}{dt} = \frac{1}{HRT} \cdot (S_{inf} - S) + R \quad (5.27)$$

Where HRT refers to the hydraulic time of the reactor, S_{inf} to the concentration in the influent, and R to the reaction term considered in reactor. As mentioned, the reaction term R is calculated assuming the average of all the nodes (Eq. 5.28).

$$R = \frac{\sum_{i=1, j=1}^{i=N_x, j=N_y} R_{i,j}^n}{N_x \cdot N_y} \quad (5.28)$$

The substrate concentrations in the influent can be prefixed. For that, a dynamic *HRT* (Eq. 5.29) is applied on the model to maintain the concentration of substrates constant.

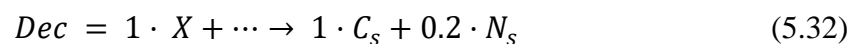
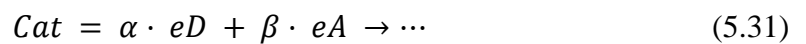
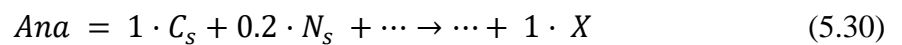
$$HRT = \frac{(S_{inf}-S)}{R_{r,S}} \quad (5.29)$$

The new concentration *S* calculated with the integration of Eq. 5.27 (using the build-in ode45 solver in MATLAB) updates the Dirichlet value (γ) included in Eq. 5.26.

5.2.2.2. Reaction term

The matrix of reaction components $R([\phi^n])$ must be calculated and added to Eq. 5.26. The synthesis and consumption of soluble components are assumed to be the result of microbial activity in the aggregate.

Microbial activity. The kinetics of the microbial activity are calculated function of the local conditions of the node where the cell is located. The stoichiometry of microbial species is also necessary to compute the synthesis and consumption of soluble components. Eqs. 5.30 – 5.32 show examples of stoichiometries for anabolism (*Ana*), catabolism (*Cat*) and decay (*Dec*), where C_s and N_s refer to carbon and nitrogen sources, eD and eA to electron donor and acceptor, and X to biomass considering an average formula of $CH_{1.8}O_{0.5}N_{0.2}$ (Heijnen & van Dijken, 1992; Kleerebezem & Van Loosdrecht, 2010).



The stoichiometry of the overall metabolism (*Met*) is calculated function of the catabolic and anabolic stoichiometries, and the growth yield (Y_{XS} , Eq. 5.33). This expression can only be used if catabolic substrates are different from anabolic ones.

$$Met = \frac{1}{Y_{XS}} \cdot Cat + Ana \quad (5.33)$$

With the metabolic stoichiometry and the kinetic parameters (μ_{max} , K_S , K_I and b^{max}) for each of the microbial species present in the reactor, the growth rate is calculated (μ_m , Eq. 5.1). Then, through the stoichiometry and the bacterial mass, the growth/decay of the cell, substrate uptakes and product generations are calculated (Eqs. 5.34 and 5.35). Eq. 5.34 is the derivative of the mass of a microbe which is integrated in time using a forward Euler scheme;

and Eq. 5.35 computes the reaction term for a specific soluble component s due to the activity of the microbe m .

$$\frac{dX_m}{dt} = \mu_m^n \cdot X_m^n \quad (5.34)$$

$$R_m^n = \frac{\mu_m^n \cdot \delta_{s,m}}{V_{xy}} \quad (5.35)$$

Where X_m refers to the mass in moles of the cell m , $\delta_{s,m}$ to the stoichiometric coefficient of the substrate S for the cell m , and V_{xy} to the volume of one node of the simulation domain.

The calculation of the reaction term for the soluble components is function of the position in the simulation domain (one reaction term per node for each soluble component). Eq. 5.36 is evaluated considering all the microbes that are contributing to the reaction term of a specific soluble component in the *node* I,j .

$$R_{i,j}^n = \sum_{m=1}^{M_{i,j}} R_m^n \quad (5.36)$$

Where $M_{i,j}$ refers to all microbes that are in the *node* I,j . The reaction terms $R_{i,j}^n$ calculated by Eq. 5.36 for all nodes of the simulation domain ($R([\phi^n])$) are then used in the Eq. 5.26 to calculate the concentration of each of the soluble components in the simulation domain.

5.2.3. Integration

Cells divide in a time scale much slower than the diffusion-reaction process (~ 1 hour versus $\sim 10^{-8}$ hours). To solve the system, the model takes advantage of this time scale differentiation to separate the resolution of the diffusion-reaction equation, and the simulation of cell dynamics and its shoving (Kreft et al., 2001).

First, the diffusion-reaction equation is integrated (with a time step dt) until it reaches a pseudo-steady state, allowing a deviation of up to 1% from the actual steady state (Eqs. 5.37 and 5.38). To check whether pseudo-steady state is reached or not, only diffusion region is considered, as the Dirichlet boundary condition and the bulk liquid concentrations are constants in this specific time span. Bulk liquid concentrations only change when the microbial community change significantly, due to a cell division, cell inactivation or a substantial variation in microbial mass.

$$[RES] = [L] * [\phi]^Y + (h^2/\mathbb{D}) \cdot R([\phi]) \quad (5.37)$$

$$Tol := \max \left| \frac{RES_{i,j}}{1 \cdot 10^{-4} + \phi_{i,j}} \right| \leq 1\%, \quad Tol := \begin{cases} \max |RES_{i,j}| \leq 1\% \cdot \phi_{i,j}, & \text{if } \phi_{i,j} \gg 1 \cdot 10^{-6} \\ \max |RES_{i,j}| \leq 1 \cdot 10^{-6}, & \text{if } \phi_{i,j} \ll 1 \cdot 10^{-6} \end{cases} \quad (5.38)$$

When the pseudo-steady state is reached, the biomass growth is integrated in a bigger time step (dt_{bac}). Once the mass of all individuals is updated, the mass balances of the overall reactor are integrated with the the time step dt_{bac} considering the average microbial activity of the aggregate. After that, the Dirichlet boundary condition and the reaction term are updated. At the end of this bigger step, the diffusion-reaction equation needs to be integrated again to reach a new pseudo-steady state. Each n times that the diffusion-reaction equation reaches a pseudo-steady state (dt_{div}), the cell division is checked and if it happens, the *shoving algorithm* is launched (Appendix B – Integration algorithm).

5.2.3.1. Adaptative integration steps

In modelling, there is always a trade-off between accuracy and performance. In order to speed up the model, maintaining accuracy, an adaptative time step is used both for reaching pseudo-steady state and for the main iterations. The main concept is to integrate with larger steps when changes are small and integrate with shorter steps if there are large changes.

Pseudo-steady state steps. The initial step for reaching pseudo-steady state (dt) is based on the Von Neumann stability coefficient (Charney et al., 1950). Clamped between a minimum and maximum value (0.01 and 0.5, respectively), dt is reduced under three conditions:

- At any point if there is an increase in $\max |RES_{i,j}|$ values detected.
- The solution is not converging any more. Empirically this means that the solution is stuck in an oscillation, where it breaks when dt is reduced.
- When any solute concentration in bulk liquid or aggregate region becomes negative.

The dt is only increased if multiple pseudo-steady states have been reached with more diffusion iteration than a threshold, while there has not been any change to the dt .

Microbial activity steps. The time step for microbial activity (dt_{bac}) is dependent on the bulk concentrations. Also clamped between a minimum and maximum (0.05 h and 0.5 h, respectively), dt_{bac} is decreased to ensure a maximum relative difference for any bulk concentration of 2%. If multiple iterations have been performed without decreasing dt_{bac} , this is incrementally increased over multiple iterations until the relative difference in any bulk concentration or maximum threshold is reached.

6.

**Environmental and ecological
controls of the spatial
distribution of microbial
populations in aggregates.**

6.1. Introduction

Microorganisms are the most diverse and widespread forms of life on Earth (Larsen et al., 2017; Lennon & Locey, 2020; Whitman et al., 1998) and key players of global biogeochemical cycles (Falkowski et al., 2008). Any microorganism that is part of a community is influenced by their neighbouring cells, either from the same species (intra-species interactions) or different (inter-species interactions). Ecological interactions (eco-interactions) among microorganisms are classified according to the net effect on each of the two interacting species: positive impact (+), negative impact (–) or no impact (0) (Figure 6.1) (Arthur & Mitchell, 1989; Bronstein, 1994).

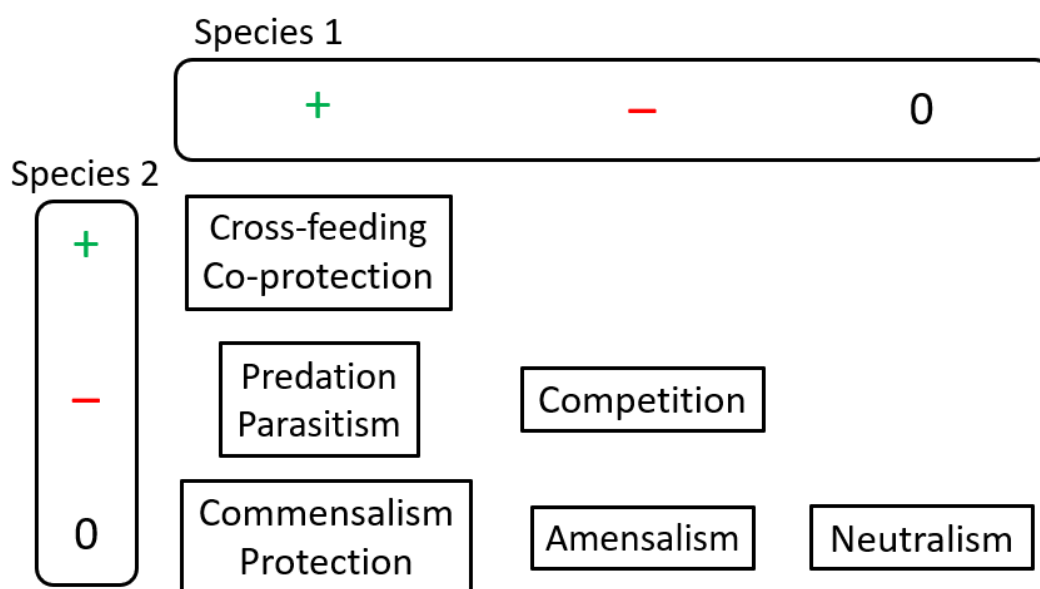


Figure 6.1. Classification of eco-interactions between species. Cross-feeding (or syntrophy) and co-protection (or symprostasy) are two specific eco-interactions belonging to mutualism (positive effect for both interacting species).

In ecosystems, multiple eco-interactions between microorganisms are found, combining both positive and negative interactions. For example, ammonia-oxidizing microorganisms (AOM) and nitrite-oxidizing bacteria (NOB) collaborate on the oxidation of ammonia to nitrate (substrate-related commensalism) while simultaneously competing for oxygen (Stein & Klotz, 2016).

In some cases, microorganisms generate aggregates either by attachment onto a solid surface (biofilm) or self-immobilization of microbes (floc/granule) (Cai, 2020; Costerton et al., 1978; Flemming et al., 2016). The formation of microbial aggregates can be regarded as a multiple-step process, to which physiochemical forces and biological properties play a

crucial role (Liu & Tay, 2002; O'Toole et al., 2000): (1) cell-to-cell contact, (2) attractive forces between cells causing them to aggregate, (3) microbial colonies formation and maturation of microbial aggregate, (4) establishment of the final three-dimensional structure of microbes shaped by shear forces and dispersion/invasion of planktonic microbes.

Biological systems are shaped by a reciprocal organism–environment influence called the “*dynamic fitness landscape*” (Nowak & Sigmund, 2004; Pfeiffer & Schuster, 2005). However, ecological interactions (organism–organism influence) also play a fundamental role in microbial community assembly (Barber et al., 2022; Embree et al., 2015; Zelezniak et al., 2015). In this study, the *dynamic fitness landscape* concept has been adopted but considering organism–organism influence, defining different *ecological environments* for specific eco-interactions between populations in community.

The mechanisms that control spatial distributions of microbial populations, the influence of the environmental factors to microbial community assembly (cell–environment interactions), and the ecological impact of the most relevant spatial distributions to microbial community (cell–space interactions) are still poorly understood. Visual analysis of spatial distribution of microbial populations helps us to comprehend the function and the dynamics in aggregated systems (W. Liu et al., 2016). The link between species interactions (cell–cell interactions) and spatial organization of species has been already established for biofilm systems (W. Liu et al., 2016; Momeni, Brileya, et al., 2013). Among all possible eco-interactions, mutualism between bacterial species (or phenotypes) and the competition with cheaters are the most studied systems in this topic (Dal Co et al., 2020; Mitri et al., 2011; Momeni, Brileya, et al., 2013; Momeni, Waite, et al., 2013; Nadell et al., 2010). However neutralism, competition or commensalism are more common than cooperation/mutualism among cultivable bacteria (Palmer & Foster, 2022). Here, a mechanistic model has been used to simulate the maturation process of microbial aggregates considering neutralism, competition and commensalism to expand our comprehension of how cell–cell, cell–environment and cell–space interactions affect microbial community assembly in aggregates (relative abundances, microbial fitness, microbial colony formation and spatial distribution of microbial populations). Besides, the presence of multiple eco-interactions was also evaluated (competition plus commensalism). In addition to the fact that competition and commensalism are the ecological interactions that govern canonical nitrification (AOM and NOB), the reasons why the other ecological interactions have not been included in this study are indicated in Appendix C (Supplementary Text). This study reveals how the *ecological environment* (established by

the existing interactions among microbial communities and local conditions) controls the spatial organization of individuals and the overall community assembly in aggregates.

6.2. Methods

Briefly, the model considers a two-dimensional space in which self-attached microbes of three different populations grow and divide (identified as B1, B2 and B3). The three populations considered have the same characteristics and growth kinetics (Table C.1). Therefore, the community maintains a theoretical equal-fitness. The theoretical equal-fitness assumption allowed us to elude the influence of growth kinetics upon the microbial community assembly and also to observe the genuine impact of the eco-interaction/s over the microbial fitness. The three populations have different metabolic stoichiometries which, in turn, define the eco-interaction/s between them. The net effects of eco-interactions among the partners are presented here as symbols in a square bracket (Momeni, Brileya, et al., 2013). Following the series [B1,B2,B3] – neutralism [0,0,0]; competition [-,-,-]; and commensalism [0,+,+] (Table 6.1).

Table 6.1. Definition of eco-interactions. Summary of ecological net effect on bacteria and their respective metabolic stoichiometries. Full stoichiometric matrix in Table C.2.

		Ecological net effect (0, – or +) ^a	Metabolic stoichiometries ^b			
			A	B	C	D
Neutralism [0,0,0]	B1	0	-1/Y _{XS}	0	0	1/Y _{XS}
	B2	0	0	-1/Y _{XS}	0	1/Y _{XS}
	B3	0	0	0	-1/Y _{XS}	1/Y _{XS}
Competition [-,-,-]	B1	-	-1/Y _{XS}	1/Y _{XS}	0	0
	B2	-	-1/Y _{XS}	1/Y _{XS}	0	0
	B3	-	-1/Y _{XS}	1/Y _{XS}	0	0
Commensalism [0,+,+]	B1	0	-1/Y _{XS}	1/Y _{XS}	0	0
	B2	+	0	-1/Y _{XS}	1/Y _{XS}	0
	B3	+	0	0	-1/Y _{XS}	1/Y _{XS}

^a Label legend: no effect (0), negative effect (-), positive effect (+).

^b Units: (mol S)·(mol X)⁻¹. Negative value: consumption. Positive value: production.

A constant concentration of substrates was fixed at the limits of the simulation domain (Dirichlet boundary conditions) which diffuse throughout the aggregate, generating local gradients in substrate concentrations. In all experiments, the aggregates grow until the relative abundance of the microbial populations, substrate/product concentrations in the bulk liquid, and actual growth rate (μ) remain unchanged therefore reaching steady state (unless otherwise indicated in the caption of the figure). In these conditions microbial fitness (F) can be calculated as the actual microbial growth rate (μ), because a single environment was

imposed in the simulation experiments (Bruggeman et al., 2020). Although active movement nor dispersion/invasion was considered, microbes could move passively due to shoving forces exerted by neighbouring individuals as they grow and divide. For more information about the model, see Chapter 5.

6.2.1. Set of simulations

The starting point is a premature aggregate of 20 μm in which microbial species are randomly distributed. In all simulations, three different microbial populations have been considered named B1, B2 and B3. For each type of simulation experiment, the eco-interaction/s among microbial species is defined by their metabolic stoichiometries (neutralism, competition, commensalism or commensalism + competition; Figure 6.2) and substrate concentrations in the bulk liquid (range of concentrations).

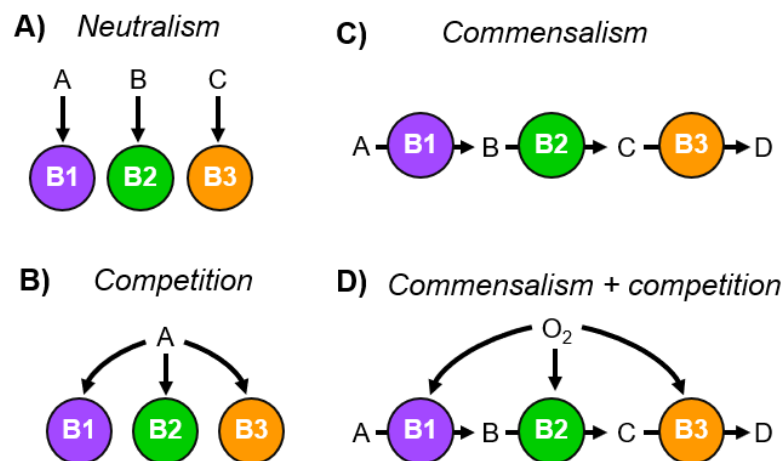


Figure 6.2. Representation of eco-interactions among B1 (purple), B2 (green) and B3 (orange). A) Neutralism: $[0,0,0]$; no impact on B1, B2 and B3. B) Competition: $[-,-,-]$; negative impact on B1, B2 and B3. C) Commensalism: $[0,+,+]$; no impact on B1, positive impact on B2 and B3. D) Commensalism + competition: $[0,+,+]$ or $[-,-,-]$; impact on B1, B2 and B3 is defined by the environment.

The simulations are run in triplicates or sextuplicate, using different random distribution of microbial species as starting point. The details of simulation setups are given in Table C.3.

6.2.2. Calculation of colony size

Colony size (P_c) is the perimeter of circular section in which colony occupies, calculated by Eq. 6.1.

$$P_c = 2\pi\langle r \rangle \left(\frac{\theta}{360} \right) \quad (6.1)$$

Where $\langle r \rangle$ is the average radius of colony section and θ is the angle of colony section. In this case, relative size of colonies was employed to neglect the influence of aggregate radius in the analysis (standardization of results). The relative colony size is defined as (P_c/P_T) , where P_T is the total perimeter of the aggregate.

6.2.3. Definition of eco-interaction modulus (ϕ_{EI})

The Thiele modulus describes the relationship between the characteristic time for diffusion rate over the characteristic time for reaction rate, that is, between the surface reaction rate over the diffusion rate through the aggregate. Although Thiele modulus (ϕ) was originally developed for immobilized catalysts (Thiele, 1939), it has already been applied in microbial aggregates (Chen et al., 2010; Liu et al., 2005) to evaluate the influence of diffusional resistance in biological systems. The modified Thiele modulus for biological systems (ϕ_{Bio} , Eq. 6.2) was obtained by the ratio between characteristic time for diffusion (τ_{diff} ; Eq. 6.3) and characteristic time for Monod-type reaction rate ($\tau_{r,Monod}$; Eq. 6.4):

$$\phi_{Bio} = R \cdot \sqrt{\frac{q_S \cdot X}{D_S \cdot C_S}} \quad (6.2)$$

$$\tau_{diff} = \frac{R^2}{D_S} \quad (6.3)$$

$$\tau_{r,Monod} = \frac{Y_{XS}}{\mu_{max}} \cdot \frac{K_S + C_S}{X} \quad (6.4)$$

Where R is the radius of aggregate (characteristic distance), q_S is the specific uptake rate of substrate S , X is the biomass concentration, D_S is the diffusion coefficient of substrate S , C_S is the concentration of substrate in bulk liquid, and Y_{XS} is the growth yield coefficient. When ϕ_{Bio} value is large, internal diffusion of substrate limits the overall microbial activity. In contrast, when ϕ_{Bio} value is small, the biological reaction (uptake of substrates) is usually rate-limiting. The next step is to correlate the eco-interactions that might influence the spatial distribution of microbial populations. In this case, a ϕ_{Bio} for substrate A (related to commensalism) and another for O_2 (related to competition) (ϕ_A and ϕ_{O_2} , respectively) were defined. Then, the ratio of ϕ_A over ϕ_{O_2} was performed obtaining the eco-interaction modulus (ϕ_{EI} , Eq. 6.5).

$$\phi_{EI} = \frac{\phi_A}{\phi_{O_2}} = \frac{\sqrt{(n_A \cdot q_A)/(D_A \cdot C_A)}}{\sqrt{(n_{O_2} \cdot q_{O_2})/(D_{O_2} \cdot C_{O_2})}} \quad (6.5)$$

Where n_A is the relative abundance of microorganisms that consume A and n_{O_2} is the relative abundance of microorganisms that consume O_2 . Where q_i is the specific substrate uptake rate, D_i is the diffusion coefficient, C_i is the concentration of substrate I in bulk liquid, and n_i is the relative abundance of the microbial population that consume the substrate i .

6.2.4. Statistical analyses

Statistical significance of the differences of relative abundances of B1, B2 and B3, and relative colony size among the tested substrate concentrations was assessed using the Welch's test. One population cannot be considered independent from the others in the same simulation, therefore, statistical significance between the microbial fitness of B1, B2 and B3 was assessed using the paired t -test. To evaluate the correlation between relative abundances of bacteria and microbial fitness (F), Person's correlation was used.

6.3. Results and Discussion

To explore the intrinsic influence of eco-interactions on the development of microbial communities growing in aggregates, a multispecies system was simulated using Individual-based Modelling (IbM). Examples in literature of empirical tests have demonstrated the ability of IbM to make accurate predictions for real biological systems that can offer mechanistic explanations of underlying biological processes (Borer et al., 2020; Ciccarese et al., 2022; Dal Co et al., 2020; Mitri et al., 2016; Momeni, Brileya, et al., 2013; Momeni, Waite, et al., 2013; Schluter et al., 2015; Weber et al., 2014; Xavier et al., 2007; Xavier et al., 2004).

6.3.1. Influence of single eco-interaction on microbial communities

Three single eco-interactions were defined: neutralism (no interaction between populations), competition (all microbial populations consume the same resource), and substrate-related commensalism (some microbial populations consume the metabolic product yielded by others). In a first step, independent simulations were designed with the objective to identify the patterns of spatial structures that are associated to each ecological interaction under different total substrate concentrations ($[S]_T$, see Table C.3).

6.3.1.1. Neutral environment and the inevitable competition for space

Mitri et al. (2016) concluded that spatial organization of microbial communities was only observed when resources were limited. Under conditions of excess of substrates, the microbial colonies remained well-mixed (*i.e.*, high colony heterogeneity). From an ecological perspective, resource availability has a direct impact on interactions among species. For example, a limited resource environment intensifies the competition for the substrate. Then, the influence of the eco-interactions on community assembly could be modified by changing the resource availability up to a hypothetical null effect (neutral environment). A set of simulations was performed considering the three eco-interactions defined (neutralism, competition, and commensalism) under different substrate concentrations (100 mM, 10 mM, 1.0 mM).

Figure 6.3 corroborates that substrate limitation is the cause for the generation of spatial patterns of microbial communities. When substrate is not limiting inside the aggregate (simulations with $[S]_T = 100$ mM), no particular spatial arrangement of microbial populations was observed in any of the considered eco-interaction (Figure 6.3A). Inoculum size and diffusion through the aggregate influence the observed level of colony heterogeneity (Figure C.1) (Mitri et al., 2016). When the substrate concentration in the bulk liquid was reduced from 100 mM to 10 and 1 mM (Figures 6.3B and 6.3C, respectively), distinctive spatial distributions of microbial populations emerged. Radial expansion of populations is associated to the presence of gradients of substrate concentrations (see Videos C.1 and C.2).

The well-mixed structures observed in this study and in Mitri et al. (2016) are associated with environments in which substrates are not limiting (*i.e.*, neutral environment), regardless the eco-interaction between microbial populations. However, there will always be a gradient of substrate concentrations in matured aggregates of a given size (Alphenaar et al., 1993; Tay et al., 2002).

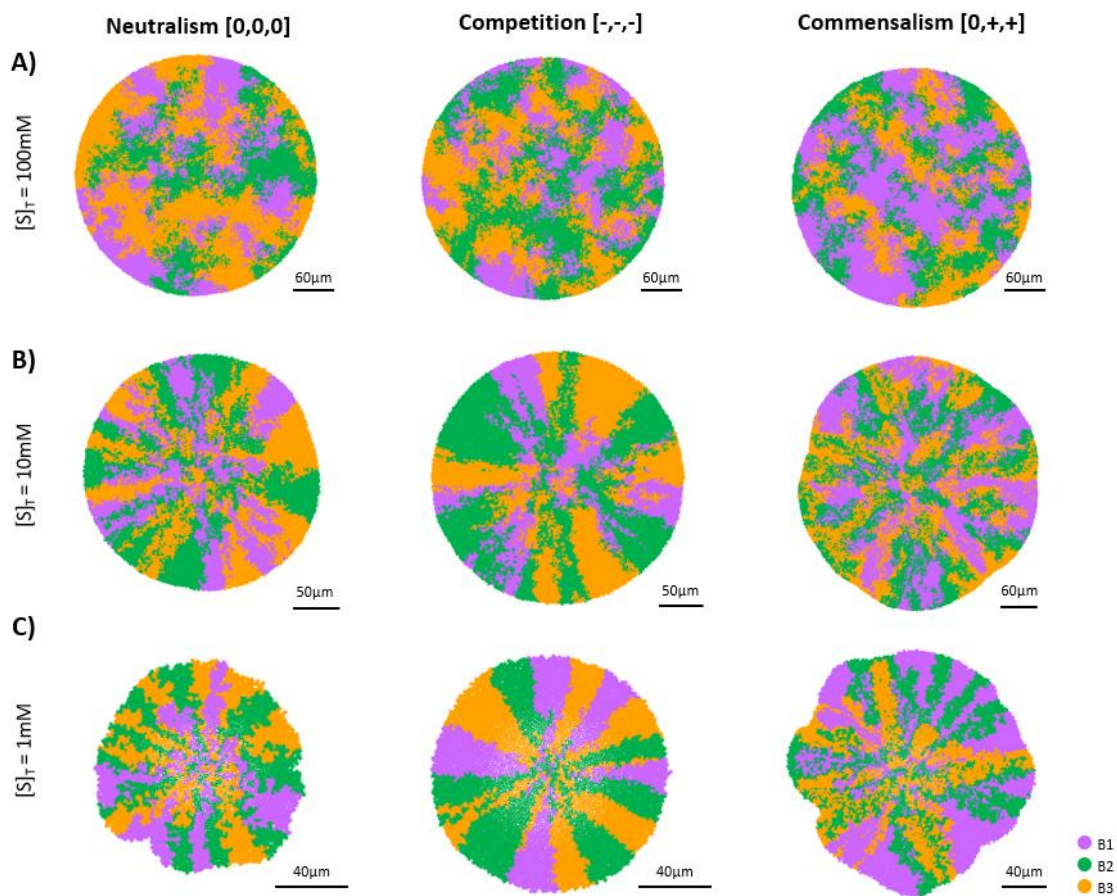


Figure 6.3. Spatial distribution of microbial populations at different substrate concentrations. **A)** Aggregate pictures captured after 8 d of simulation considering neutralism, competition and commensalism with $[S]_T = 100 \text{ mM}$. **B)** Aggregate pictures captured at 10 d of simulation considering neutralism, competition and commensalism with $[S]_T = 10 \text{ mM}$. **C)** Aggregate pictures captured at 15 d of simulation considering neutralism, competition and commensalism with $[S]_T = 1 \text{ mM}$. None of the simulations are in steady state yet. Black solid line on bottom-right of aggregates represent the scale bar. Substrate profiles on the transverse plane of aggregates have been included on Figure C.2. In these simulations, all bacteria are active.

In Figure 6.4, neutralism (null ecological interactions between populations) is analysed with more detail and under conditions of substrate limitation ($[S]_T \leq 1.0 \text{ mM}$). In this situation, microbial populations consume different substrates, but the limitation of substrate availability increases the pressure for space competition between different populations. No significant differences between relative abundances of active bacteria were observed among populations (all around 33%, Figure 6.4), but there was a significant difference between microbial fitness of populations at 1.0 mM (Figure 6.4B). This was the result of stochastic dynamics, such as the initial distribution of inocula or the position of new cells. In addition,

a strong positive correlation between relative abundances and microbial fitness was observed at limiting substrate concentrations ($r = 0.760 - 0.947$, $p < 0.003$; Figure C.3A).

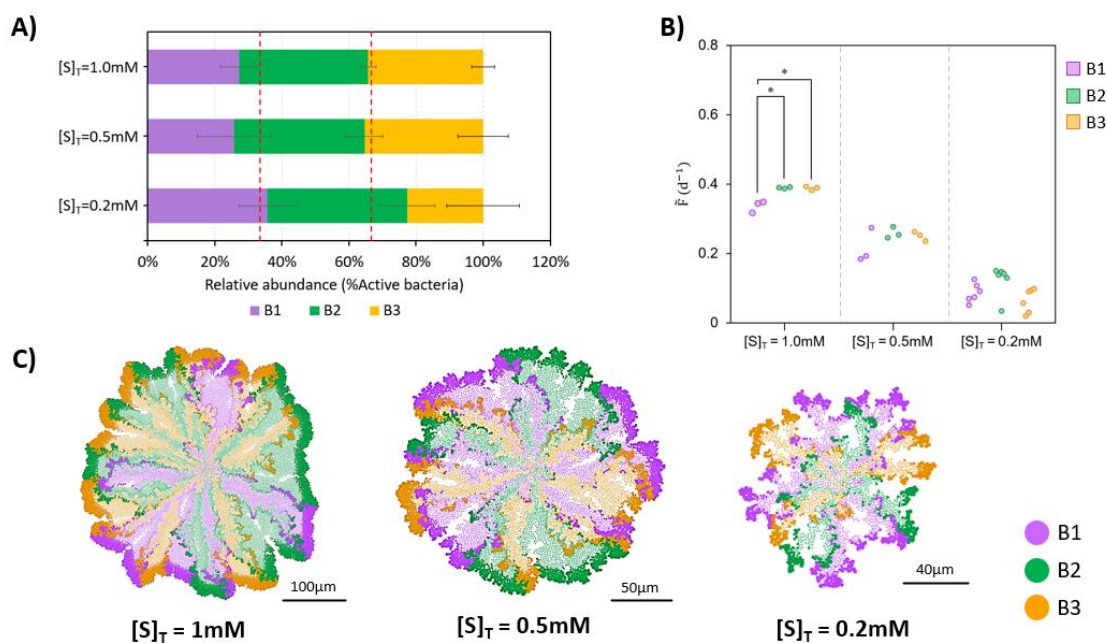


Figure 6.4. Neutralism [0,0,0]. **A)** Relative abundances of B1, B2 and B3 populations in the community. Dashed red lines indicate 33.33% and 66.66% relative abundances. **B)** Microbial fitness (median, \tilde{F}) is calculated in all replicates ($n = 3$ for 1.0 mM and 0.5 mM, $n = 6$ for 0.2 mM). Asterisks indicate the significance level of the difference between B1, B2 and B3 specific growth rate. **C)** Aggregates captured at steady state (75 d for 1.0 mM and 0.5 mM, 100 d for 0.2 mM). Inactive bacteria are shown in a lighter colour. Black solid lines on bottom represent the scale bars. Significance level legend: ns, not significant; *, $p < 0.05$; **, $p < 0.01$; ***, $p < 0.001$.

In neutralism, some bacteria were able to remain active although they were farther from the source of nutrients (*i.e.*, the bulk liquid) than other species (Figure 6.4C). If the substrate is not consumed by the corresponding microbial population, mass transfer resistance (*i.e.*, the resistance to the net movement of substrates through the aggregate) is the only reason for substrate gradients, which explains the aforementioned positive correlation between relative abundances of active bacteria and microbial fitness. If more bacteria of certain species are on the external part of the aggregate, they would grow faster (increasing the fitness median) and, as consequence, be relatively more abundant. In contrast, those bacteria which are in a deeper position, have less available substrate due to the gradients generated and, consequently, grow slower. The aforementioned observations highlight the importance of the spatial distributions in aggregates and therefore the inherently present competition for space when substrates are limiting (cell-space interactions).

6.3.1.2. Competition for substrate

In this section, how the presence of competition for the same substrate could influence the spatial structure of the microbial community is analysed (Figure 6.5). The same microbial community of three populations was employed, but now competing for same substrate ($[S]_T \leq 1.0$ mM).

No significant differences on relative abundances or microbial fitness of populations were observed in the community (Figures 6.5A and 6.5B). In addition, no correlation between relative abundances and microbial fitness was found ($r = -0.040 - 0.290$, $p > 0.240$; Figure C.3B). Figure 6.5C shows radial distribution of microbial populations at already early stages of the maturation of the microbial aggregate. In this thesis, the term '*columned stratification*' will be used to refer the particular spatial distribution observed in competitive case. Patterns of *columned stratification* on microbial populations in competitive environments is consistent with previous findings (Hallatschek et al., 2007; Mitri et al., 2016; Momeni, Brileya, et al., 2013). The similarity on microbial fitness observed in Figure 6.5B was maintained thanks to the spatial distribution, that enabled all bacteria, whatever their relative abundances were, to get access to substrate. This differs with the previous results obtained simulating neutralism, in which a positive correlation between relative abundances and microbial fitness was observed (Figures 6.4 and C.3A). These differences can be explained due to an increased substrate limitation in the competitive environment, which leads to larger substrate gradients and, therefore, to more defined radial spatial structures (*i.e.*, *columned stratification*).

Additionally, a negative correlation between substrate concentration and the relative colony size for the different populations was observed (computed as the perimeter of a circular section that a population occupies without the interference of other populations in the community over the total perimeter of the aggregate, see Methods) (Figure 6.5D). When substrate availability is reduced, the competition for same resource (and for space) is intensified. The minimum colony size to thrive in a competitive environment will be higher as limitation for substrate increases.

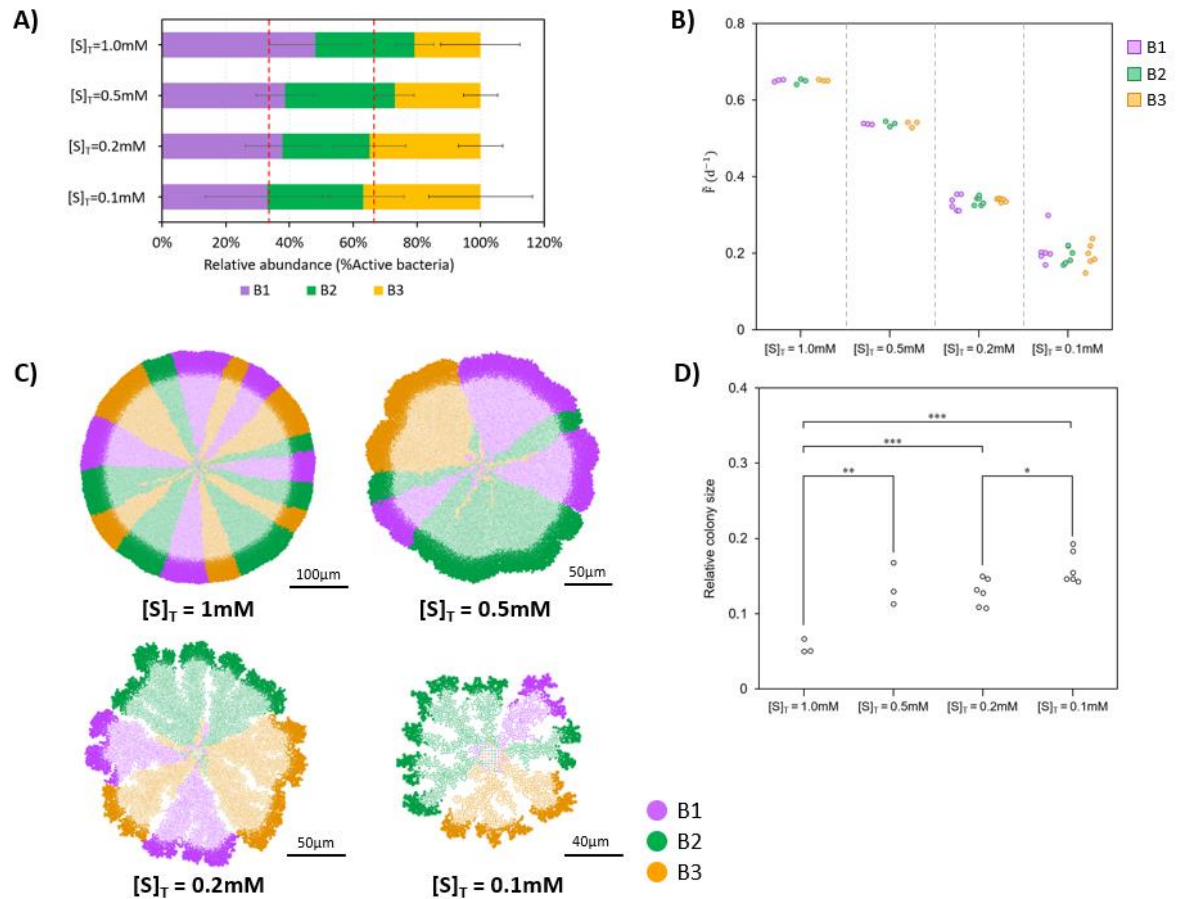


Figure 6.5. Competition [-,-,-]. **A)** Relative abundances of B1, B2 and B3 populations in the community. Dashed red lines indicate 33.33% and 66.66% relative abundances. **B)** Microbial fitness (median, \bar{F}) is calculated in all replicates ($n = 3$ for 1.0 mM and 0.5 mM; $n = 6$ for 0.2 mM and 0.1 mM). Asterisks indicate the significance level of the difference between the specific growth rate of B1, B2 and B3 populations. **C)** Aggregates captured at steady state (50 d for 1.0 mM and 0.5 mM, 75 d for 0.2 mM and 0.1 mM). Inactive bacteria are shown in a lighter colour. Black solid lines on bottom represent the scale bars. **D)** Average relative size of colonies (with respect to the total perimeter of the aggregate) is calculated in all replicates ($n = 3$ for 1.0 mM and 0.5 mM; $n = 6$ for 0.2 mM and 0.1 mM). Asterisks indicate the significance level of the difference between substrates concentrations. Significance level legend: ns, not significant; *, $p < 0.05$; **, $p < 0.01$; ***, $p < 0.001$.

6.3.1.3. Substrate-related commensalism: division of labour

A new set of simulations was performed considering substrate-related commensalism, in which population B1 feeds B2 and then, B2 feeds B3. From this interaction, populations B2 and B3 benefit from the community, while B1 is not benefited or harmed: $[0,+,+]$. As in previous simulations, substrate limitation inside the aggregate was forced ($[S]_T \leq 1.0\text{mM}$)

to study the influence of the commensal environment on the microbial community assembly (Figure 6.6).

No significant differences in the relative abundance of bacteria between the simulations at different substrate concentrations were observed, except at 0.5 and 0.1 mM (Figure 6.6A). Although the same growth kinetics are considered for all populations (μ_{max} , K_s , b_{max} and Y_{XS}), microbial fitness of B1, B2 and B3 populations were significantly different at the end of the simulations (Figure 6.6B). In all substrate concentrations, microbial fitness values followed the same pattern – B1 population grew faster than B2, and B2 grew faster than B3. This can be attributed to the commensal interaction and feeding regime. A strong positive correlation between relative abundances and microbial fitness was observed for all the substrate concentrations tested ($r = 0.950 - 0.982$, $p < 0.001$; Figure C.3C).

Distinct spatial distributions emerged on the different limiting substrate concentrations (Figure 6.6C). At substrate concentrations of 1.0 mM, microorganisms which perform the sequential metabolic steps (B2 and B3) were found on the peripheral part together with their metabolic predecessor (B1). In simulations with 0.5 mM, only B1 and B2 were on the peripheral part, and B3 remained always below their metabolic predecessors. Then, under higher substrate limitations (0.2 mM and 0.1 mM) microbial communities generated a concentric disposition of active bacteria from different populations following the metabolic sequence of commensalism. The term '*layered stratification*' will be used when referring to the concentric distribution of active cells observed in commensal case.

The transient change of the growth rate ratios of active B2 and B3 over B1 ($\widetilde{\mu}_{B2}/\widetilde{\mu}_{B1}$ and $\widetilde{\mu}_{B3}/\widetilde{\mu}_{B1}$, respectively) shows the contribution of space competition on microbial community assembly, and also the importance of the early stages of the maturation process (Figure 6.6D). Metabolic successors (B2 and B3) will always be able to stay at the peripheral zone (even if they grow slower than their predecessor B1) as long as they occupied enough circular region at the early stages of maturation process. This happened when the growth rate of all the populations was similar at the beginning of maturation process (Figure 6.6D). *Layered stratification* minimizes mass transfer resistances and favours the growth rate of the metabolic successors (Figure 6.6D), as the populations grow in the positions where higher concentrations of substrates are generated (Figure C.4).

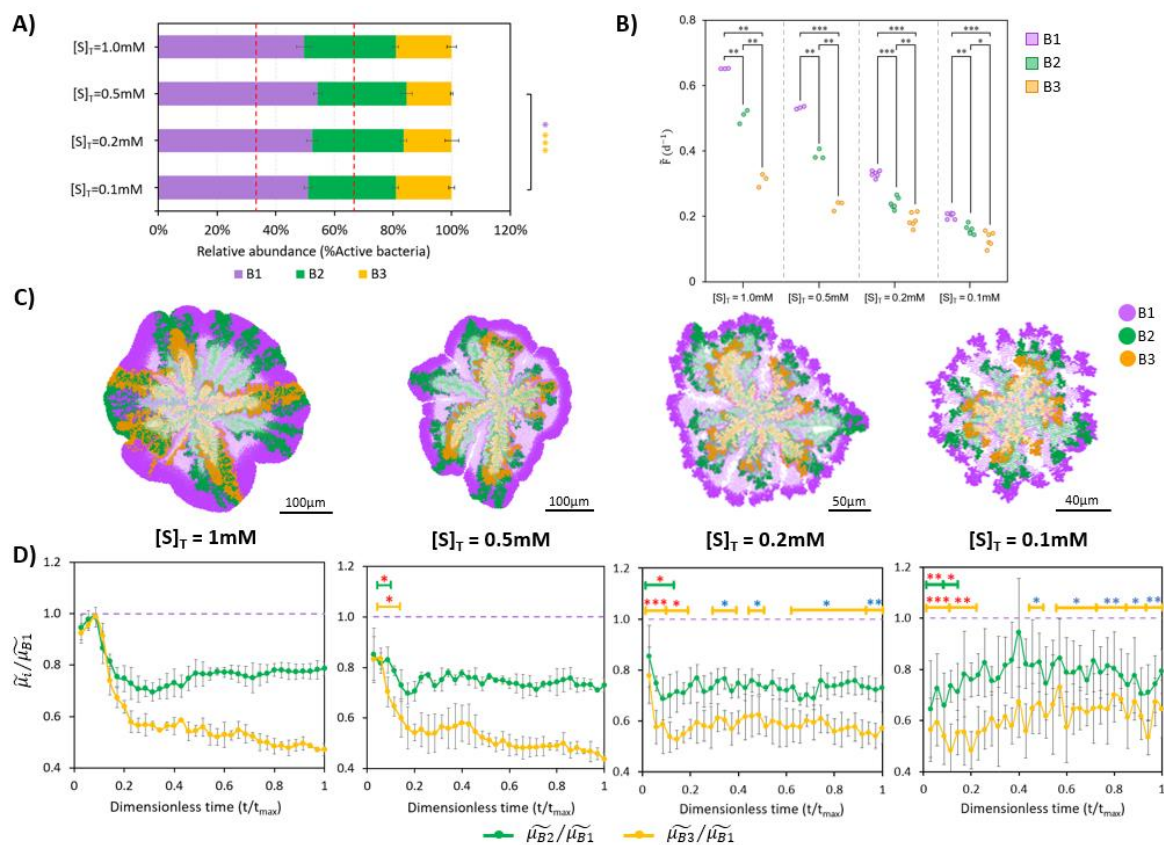


Figure 6.6. Commensalism [0,+,+]. **A)** Relative abundances of B1, B2 and B3 populations in the community. Dashed red lines indicate 33.33% and 66.66% relative abundances. Square brackets with asterisks indicate the significance level of the difference between relative abundances between populations. Colour of asterisks points out what bacteria it refers to. **B)** Microbial fitness (median, \tilde{F}) is calculated in all replicates ($n = 3$ for 1.0 mM and 0.5 mM; $n = 6$ for 0.2 mM and 0.1 mM). **C)** Aggregates captured at steady state (50 d for 1.0 mM and 0.5 mM, 75 d for 0.2 mM and 0.1 mM). Inactive bacteria are shown in a lighter colour. Black solid lines on bottom represent the scale bars. **D)** Transient change of growth rate ratios of active B2 and B3 over B1 ($\tilde{\mu}_{B2}/\tilde{\mu}_{B1}$ and $\tilde{\mu}_{B3}/\tilde{\mu}_{B1}$, respectively) in all replicates ($n = 3$ for 1.0 mM and 0.5 mM; $n = 6$ for 0.2 mM and 0.1 mM). Growth rate ratios, normalise the comparison and reduce the influence of substrate concentration in the analysis. Dimensionless time was applied to compare simulations with different time length (t_{max}). Asterisks indicate the significance level of difference between 1.0 mM and the other concentrations (1.0 mM vs 0.5 mM; 1.0 mM vs 0.2 mM; 1.0 mM vs 0.1 mM). Colour of asterisks: red – growth rate ratio at $[S]$ is lower than that at 1.0 mM; blue – growth rate ratio at $[S]$ is higher than that at 1.0 mM. Significance level legend: ns, not significant; *, $p < 0.05$; **, $p < 0.01$; ***, $p < 0.001$. Width of the lines indicate the time to which the significance level corresponds. Colour of the lines: green – B2; orange – B3.

The association of *layered stratification* with commensalism is observed in many environmentally relevant microbial processes (such as nitrification, organic anaerobic digestion or herbicide degradation) (Breugelmans et al., 2008; Poot et al., 2016; Schramm et al., 1996; Sekiguchi et al., 1999) and *in vitro* communities (Christensen et al., 2002; Momeni, Brileya, et al., 2013; Nielsen et al., 2000). Momeni, Brileya, et al. (2013) cultured two engineered yeast strains in which the metabolic predecessor took lysine from the media and overproduced adenine to feed the metabolic successor observing (and also predicting by modelling) *layered stratification*. The feeding regime in this study was different leading to lysine depletion, therefore populations were organised without following the metabolic sequence. In the study presented here, the substrate of the metabolic predecessor (B1) was constantly fed on the system favouring its dominance, and the *layered stratification* following the metabolic sequence.

6.3.2. Concurrence of multiple eco-interactions

Microbial ecology is more complex than a single eco-interaction system. In the following simulations, the concurrence of two eco-interactions was considered, keeping the same microbial system of three populations: substrate-related commensalism (substrate A) and competition for substrate (O_2).

The results are presented in Figure 6.7 at different concentrations of substrate A (1.0 mM to 0.05 mM) and O_2 (10 mg/L to 1 mg/L). A *layered stratification* of microbial communities (associated with commensalism) was observed when concentration of substrate A was equal or lower than 0.1 mM and concentration of O_2 was equal or higher than 6 mg/L. *Columned stratification* of microbial communities (associated with competition) was observed when the concentration of O_2 was 1 mg/L and/or concentration of substrate A was higher than 0.1 mM. The influence of the environment over the spatial distribution of microbial populations was also indicated by Momeni, Waite, et al. (2013), as the presence or absence of key substrates for cooperation (adenine and lysine) affected spatial distribution of cooperators.

Comparing the substrate profiles on the transverse plane that correspond to the spatial distributions presented in Figure 6.7 (see Figure C.5), a clear relationship between the most limiting substrate and the observed final microbial spatial distribution was found. When substrate A was more limited than O_2 (commensal environment), *layered stratification* of populations was observed. In contrast, a *columned stratification* emerged when O_2 was more

limited than substrate A (competitive environment). The limiting substrate establishes the *ecological environment* of the aggregate and therefore, the spatial distribution of microbial populations.

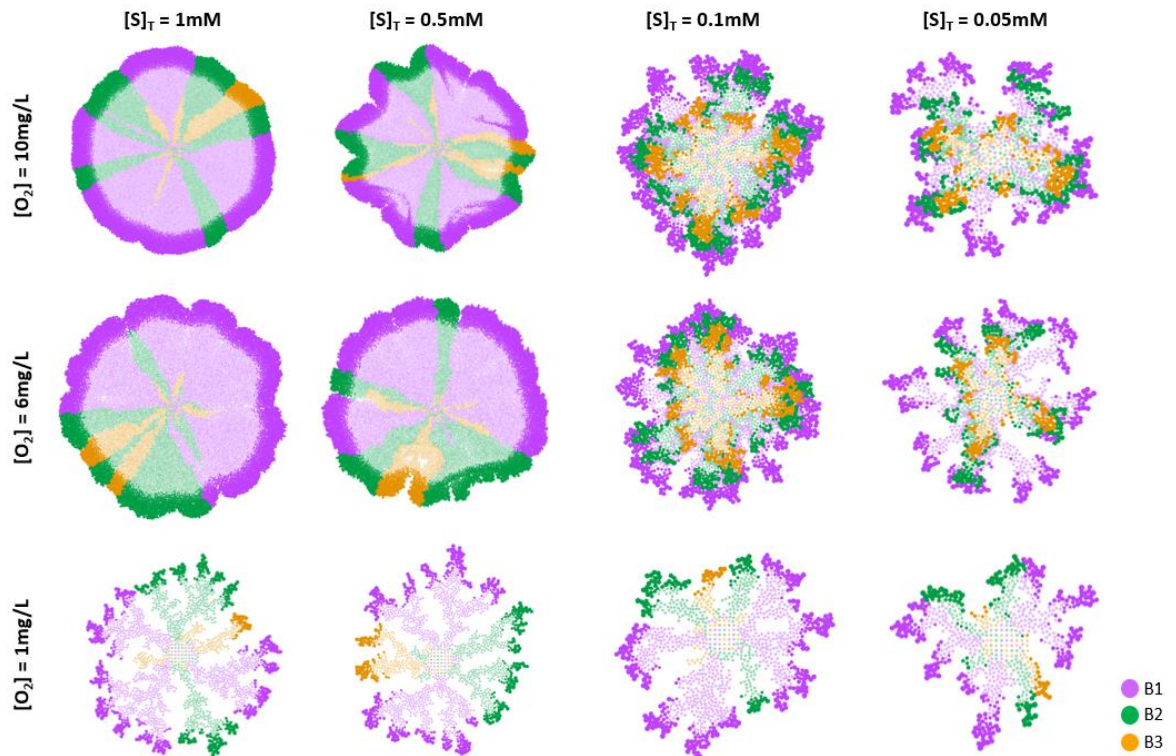


Figure 6.7. Aggregates captured at steady state considering commensalism and competition for O_2 . Steady state times: 50d for $[S]_T = 1.0$ mM, 0.5 mM, 0.1 mM and $[O_2] = 10$ mg/L, 6 mg/L; 75d for $[S]_T = 1.0$ mM, 0.5 mM, 0.1 mM and $[O_2] = 1$ mg/L; 100d for $[S]_T = 0.05$ mM and $[O_2] = 10$ mg/L, 6 mg/L, 1 mg/L. Inactive bacteria are shown in a lighter colour. Substrate profiles on the transverse plane of aggregates have been included on Figure C.5. Aggregates captured at steady state.

The *ecological environment* in the aggregated system (commensal or competitive) not only influenced the spatial distribution of microbial populations, but also the relative abundance of active bacteria (Figure C.6). When a commensal environment was present ($[S]_T \leq 0.1$ mM and $[O_2] \geq 6$ mg/L), a similar proportion of bacteria (B1:B2:B3) to single-interaction commensalism simulations (Figure 6.6A) was observed (1:0.6:0.3 for single-interaction commensalism; 1:0.6:0.4 for commensalism plus competition; $p > 0.05$). In contrast, when a competitive environment was present ($[S]_T > 0.1$ mM and/or $[O_2] = 1$ mg/L), a completely different proportion of bacteria to single-interaction competition (Figure 6.5A) was found (1:1:1 for single-interaction competition; 1:0.4:0.1 for commensalism plus competition; $p < 0.0001$). In a competitive environment, lower proportion of B2 and B3 populations than

in commensal environment was observed. No clear trend of microbial fitness was found as result of the *ecological environment* (Figure C.7). In general, the predominant trend in microbial fitness was the same as in single-interaction commensalism ($F_{B1} > F_{B2} > F_{B3}$, Figure 6.6B), although in some competitive environments (*e.g.*, 1 mM:6 mg/L, 1 mM:1 mg/L or 0.5 mM:1 mg/L; [S]_T:[O₂]) the fitness of the populations was not significantly different (like in single-interaction competition, Figure 6.5B). This can explain why a different proportion of B1, B2 and B3 was found when a competitive environment dominated the community assembly (Figure C.8).

From an ecological perspective, the *columned stratification* found in competitive environments allows populations with lower fitness than their competitors to co-exist. This particular ecological influence of the spatial distribution is fundamental for the dominance of cooperation over cheating (Momeni, Waite, et al., 2013). Therefore, established *columned stratification* might hinder the repression of certain microbial populations living in aggregated systems (*e.g.*, the repression of NOB to achieve partial nitrification and anammox process). However, less competitive species in aggregates must be able to compete for its space and survive at the early stages of maturation when the stratification is not formed. For example, if lone cooperator cells (less competitive due to investment in secretion) meet with the cheater before they have a chance to establish the colony, this cooperation will be inhibited by competition (Mitri et al., 2011).

Layered stratification was identified as the optimal spatial organization of microbial communities in which division of labour occurs (*i.e.*, substrate-related commensalism). This microbial distribution is also observed in protective environments, in which the peripheral population would act as a protector of the others (Almstrand et al., 2014; Cole et al., 2004; Kleerebezem et al., 2021).

6.3.2.1. *Eco-interaction modulus (ϕ_{EI})*

Concentration gradients of substrates in microbial aggregates are the result of mass transfer limitations and biological activity. Inevitably one of them will be the rate-limiting process depending on the conditions and the biological system. Substrate gradients only emerge when mass transfer resistance is sufficient to limit the rate of the reaction. In the presence of multiple substrates, the limiting one can be identified by comparing diffusion and reaction rates. The eco-interaction modulus (Eq. 6.5, ϕ_{EI}) is defined as the ratio between the biological Thiele modulus of involved substrates (see Methods). If ϕ_{EI} is higher than 1.0,

substrate A is the most limiting and therefore, a commensal environment would be present. If ϕ_{EI} is lower than 1.0, O_2 is the most limiting inside the aggregate and a competitive environment would be present.

The eco-interaction modulus (ϕ_{EI}) presented in Eq. 6.5 was computed for all simulation experiments considering commensalism (initiated by consumption of substrate A) and competition for O_2 under different concentrations (Figure 6.8). When ϕ_{EI} was higher than 1.0, microbial communities were distributed following a *layered stratification* (commensal environment), whereas when ϕ_{EI} was lower than 1.0, microbial communities were organized following a *columned stratification* (competitive environment). A particular distribution of microbial species was noticed when $[A]$ and $[O_2]$ was 0.1 mM and 3.75 mg/L, respectively ($\phi_{EI} = 1.07$). In this case, a mixture of *layered* and *columned stratification* was observed, because the substrate limitation in the spatial distribution of populations was not uniform. In certain zones O_2 was the most limiting substrate, in others the substrate A (see Figure C.9).

In addition to the environment (in this case, established by the substrate concentrations), the diffusivity of substrates through the aggregate plays a fundamental role on the control of the spatial distribution of microbial populations, especially for substrates with higher molecular weight (L. van den Berg et al., 2022; van den Berg et al., 2021). Diffusion coefficient (D_i) states the diffusion rate of certain substance into the fluid. Therefore, those substrates with lower diffusion coefficient will tend to be the limiting substrate in the aggregate, establishing the *ecological environment* and, consequently, the spatial distribution of microbial populations. In order to illustrate the influence of diffusion coefficient, one of the cases considering concurrence of commensalism (substrate A) and competition (O_2) was simulated again but now reducing the diffusion coefficient of substrates A, B, C and D (from 3.60×10^{-6} to $0.5 \times 10^{-6} \text{ m}^2/\text{h}$). As example, the environment with 1.0 mM of A and 10.0 mg/L of O_2 (competitive environment, $\phi_{EI} = 0.65$) was applied starting with the same inoculum (Figure C.10). With the new diffusion coefficients, substrate A (instead of O_2) was the most limiting ($\phi_{EI} = 1.51$, commensal environment), obtaining a *layered stratification* of microbial populations.

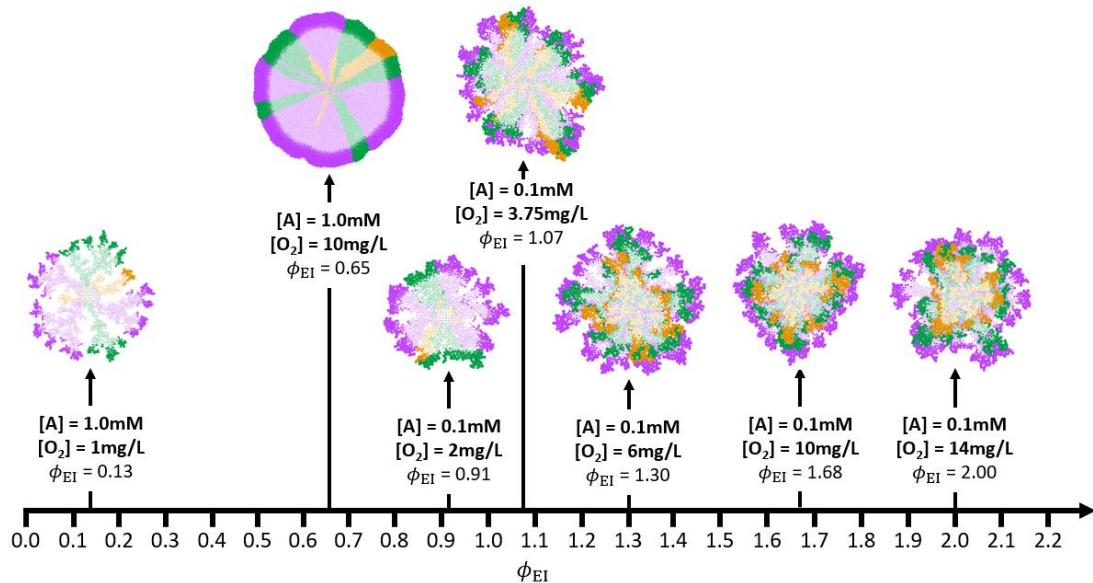


Figure 6.8. Eco-interaction modulus diagram for simulations considering commensalism and competition for O_2 with $[A] = 1.0 - 0.1$ mM and $[O_2] = 14 - 1$ mg/L. Aggregates captured at steady state (75 d for $[S]_T = 1.0$ mM and $[O_2] = 1$ mg/L; 50 d for all other conditions). Inactive bacteria are shown in a lighter colour. Eco-interaction modulus calculated by Eq. 6.5 for each replicate. Colour legend: B1 – purple; B2 – green; B3 – orange.

6.3.3. Shear forces (detachment) controlling the spatial distribution of populations

Formerly, it has been described how the environment (substrate(s) concentration) together with the eco-interactions between species determine the spatial distribution of microbial populations. However, other environmental factors are also participants of the microbial community assembly in aggregates.

Shear forces, responsible for detachment in microbial aggregates, are one of the major factors involved in the formation of biofilms and granules. Steady state structures of aggregates are highly dependent on the shear forces, establishing their thickness and density by microbial detachment (Liu & Tay, 2002). Biofilm thickness has a significant impact on microbial community composition and spatial distribution (Suarez et al., 2019) – a clear stratification of populations was observed in thick biofilms (400 μm), but not in thin ones (50 μm). In order to evaluate the influence of shear forces on the identified spatial distributions (*columned* and *layered stratification*), some of the conditions studied was simulated again but now setting a maximum radius of aggregate of 30 μm . All bacteria that were more than 30 μm away from the centre of the aggregate were removed from the system (detachment) (Figure 6.9).

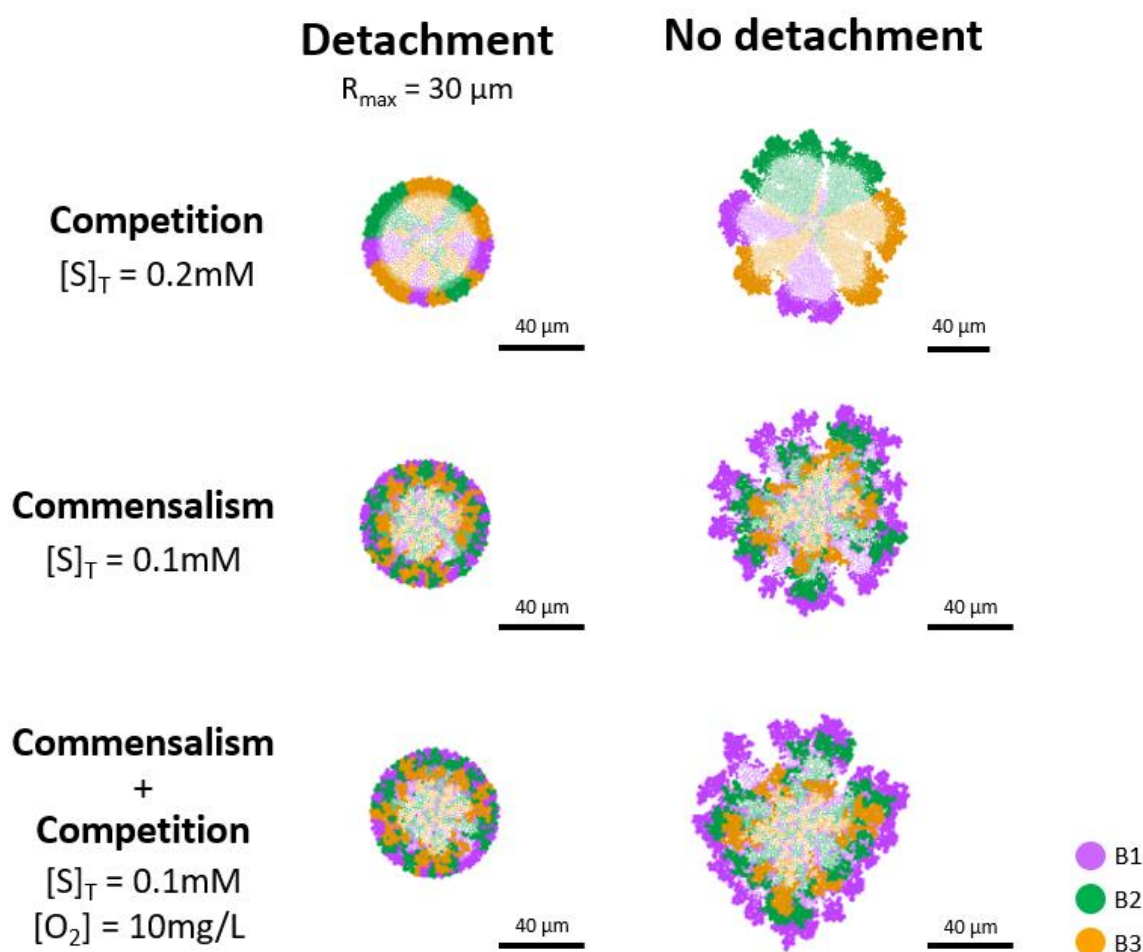


Figure 6.9. Influence of shear force (detachment) to spatial distribution of microbial populations. Aggregates captured at 50d when a maximum radius of 30 μm (due to the detachment) was considered. Aggregates captured at 50 d. Three conditions were evaluated – competition ($[S]_T = 0.2 \text{ mM}$), commensalism ($[S]_T = 0.1 \text{ mM}$), and commensalism + competition ($[S]_T = 0.1 \text{ mM}$ and $[O_2] = 10 \text{ mg/L}$). Inactive bacteria are shown in a lighter colour. Substrate profiles on the transverse plane of aggregates have been included on Figure C.11. The simulation experiments including detachment were started with the same inoculum as those without detachment with the objective to observe the genuine impact of the shear force in the spatial distribution of the microbial populations.

Like in Suarez et al. (2019) study, the spatial distribution of microbial communities was lost when the maximum radius was fixed for simulations involving commensalism or commensalism + competition (*layered stratification*), but not in competition (*columned stratification*) (Figure 6.9). When a maximum size of aggregate was applied, *layered distribution* was not observed because the available region that generated the specific microbial distribution was reduced significantly, and the metabolic successors (B2 and B3)

were able to occupy the outer space of the aggregate that the metabolic predecessors (B1) left free once detached (see Video C.3).

These findings predict that *columned stratification* is more robust than *layered stratification* regarding detachment. The fragility of *layered stratification* might be a challenge for specific bioprocesses in which its efficiency relies on generating this particular spatial distribution of microbial populations. Example of this can be the combination of partial nitrification and anammox process in one stage (Sliemers et al., 2002).

6.4. Conclusions

When analysing microbial growth in communities, the influence of cell-space interaction is generally overlooked. The results presented in this study show how cell-space interaction influences the assembly of microbial communities in aggregates, implying that (i) neutral environment, without any particular distribution of populations, is only a transient state, (ii) in competition, the availability of space controls the colony size of the populations, and (iii) in commensalism their distribution. The spatial structures (defined by ecological interactions) have in turn, implications on microbial growth and survival. The radial distribution of microbial populations (addressed here as *columned stratification*) increases the chance of less competitive individuals to thrive and co-exist with populations that grow faster. On the other hand, the concentric disposition of communities (addressed here as *layered stratification*) would be the optimal distribution for metabolic division of labour (*i.e.*, substrate-related commensalism). In addition, this study shows that although ecological relationships between different populations influence their distribution in aggregates, the environment (as operational conditions related to concentration of substrates or shear forces) is controlling the final observed spatial distribution.

7.

**Competitive and substrate limited
environments drive metabolic
heterogeneity for
comammox *Nitrospira*.**

7.1. Introduction

Nitrification, the biological oxidation of ammonia to nitrate, is a crucial process of the nitrogen cycle in natural and engineered systems. Formerly, nitrification was considered a two-step process where ammonia is first oxidized to nitrite by ammonia-oxidizing microorganisms (bacteria and archaea (Könneke et al., 2005; Treusch et al., 2005)) and then nitrite is oxidized to nitrate by nitrite-oxidizing bacteria. The understanding of nitrification as a process with an obligated division-of-labour was theoretically questioned (Costa et al., 2006), and finally refuted by the discovery of nitrite-oxidizing bacteria belonging to the *Nitrospira* genus capable to catalyse both steps of nitrification on their own (complete ammonia oxidation, comammox) (Daims et al., 2015; van Kessel et al., 2015).

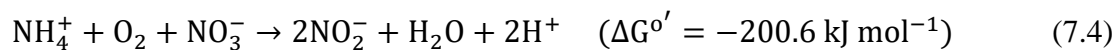
The oligotrophic lifestyle of comammox *Nitrospira* (high affinity for ammonia and high specific growth yield) was already predicted in its theoretical conceptualization (Costa et al., 2006), and subsequently demonstrated by physiological studies (Kits et al., 2017; Sakoula et al., 2021). However, there is still an open debate about the oxygen requirements for the chemoautotrophic growth of comammox *Nitrospira*. Recent studies have found that comammox *Nitrospira* is the dominant ammonia oxidizer in biofilm systems with localized oxygen limitation (Cui et al., 2023; Roots et al., 2019; Shao & Wu, 2021), although others have shown that comammox *Nitrospira* require an adequate oxygen supply to grow (Gottshall et al., 2021; Zhao et al., 2022).

One of the first enrichments of comammox *Nitrospira* was obtained together with anammox bacteria without any oxygen supply (oxygen was not detected by an oxygen sensor with a detection limit of 3.1 μM of O_2) (van Kessel et al., 2015). Given this apparent capacity of comammox *Nitrospira* to survive under so limited oxygen conditions, two novel cyclic ammonia oxidation processes was proposed: (i) ammonia oxidation with combined use of oxygen and nitrate as electron acceptors (nitrate-reducing ammonia oxidation), and (ii) ammonia oxidation with nitrite as electron acceptor via intracellular production of molecular oxygen (anaerobic nitrite-reducing ammonia oxidation) (Kleerebezem & Lückner, 2021).

Although the available energy from the oxidation of nitrite is limited, the members of the *Nitrospira* genus are ubiquitous in natural and engineered systems (Koch et al., 2015). This survival capacity is explained by its physiological versatility and metabolic flexibility (*i.e.*, their ability to obtain energy using alternative electron donor and electron acceptor such as formate and nitrate, respectively) (Koch et al., 2015). Microbial populations commonly

display heterogenous gene expression profiles that result in metabolic differences between individuals of the same population (referred as metabolic or phenotypic heterogeneity) (Ackermann, 2015; Dar et al., 2021; Evans et al., 2020). This diversity can promote the persistence of a microbial population in fluctuating environments and also enable the collaboration between individuals of the same population increasing their ability to survive under nutrient-limiting conditions (*e.g.*, intra-specific commensalism (Zacharia et al., 2021), syntrophism (Mee et al., 2014) or protection (Rosenthal et al., 2018)).

For comammox *Nitrospira*, currently reported catabolic activities include ammonia oxidation (AO), nitrite oxidation (NO) and complete ammonia oxidation (CMX) (Eqs. 7.1 – 7.3). Their capacity to catalyse nitrate-reducing ammonia oxidation (NRMX) and anaerobic nitrite-reducing ammonia oxidation (An-NRMX) have also been hypothesised (Eqs. 7.4 and 7.5).



In this study, using an *in-silico* approach, we have investigated the resilience of comammox *Nitrospira* under different nitrogen and oxygen limited environments (based on early studies (Daims et al., 2015; van Kessel et al., 2015)), and considering its potential metabolic heterogeneity. A population of comammox *Nitrospira* growing together with anammox bacteria under specific environmental conditions was simulated using an Individual-based Model framework. With this framework, we are able to predict the stable activities of comammox *Nitrospira* that are selected under the different oligotrophic environments tested (predicting the potential metabolic niches for comammox *Nitrospira*). These results are compared with reported experimental observations (Daims et al., 2015; Gottshall et al., 2021; van Kessel et al., 2015). We have also evaluated the metabolic activities proposed by Kleerebezem and Lückner (2021) for which no experimental observation has been reported yet.

7.2. Methods

7.2.1. Growth yield estimation of comammox *Nitrospira*

Growth yield for any metabolic activity can be predicted by evaluating the energy harvested per mole of substrate consumed (González-Cabaleiro et al., 2021). Because actual growth yields of hypothetical metabolisms of comammox *Nitrospira* (NRMX and An-NRMX) are unknown, their theoretical values were estimated according to a bioenergetics analysis. To keep the analysis consistent, the methodology was also applied for the growth yield estimation of AO, NO and CMX activities and these values were validated with experimental data (Table 7.1). Only the growth yield value of anammox bacteria was taken as an average from bibliographic values (0.0515 C-mol biomass per mole of N-NH₃ (Ni et al., 2009; Oshiki et al., 2011; Puyol et al., 2014; Straka, 2019)) because the biochemistry of their catabolism is not fully elucidated yet (Kartal & Keltjens, 2016; Ren et al., 2022).

The Gibbs free energy is calculated for each catabolic reaction per mole of electron donor (Eqs. 7.1 – 7.5). In the catabolic activities considered, no ATP is produced via substrate level phosphorylation. Therefore, the energy for growth and maintenance comes solely from the membrane potential. The amount of energy harvested (ΔG_{Cat}^{01}) is calculated according to Eq. 7.6.

$$\Delta G_{Cat}^{01} = v_A^* \cdot \gamma_A^* \cdot F \cdot \Delta\Psi \quad (7.6)$$

Where v_A^* is the amount of electron acceptor used in energy harvesting per mol of electron donor, γ_A^* is the number of electrons in each mole of electron acceptor, F is the Faraday constant, and $\Delta\Psi$ is the potential difference invested in the energy conversion. $\Delta\Psi$ is calculated as the redox potential difference between the electron acceptor and electron donor pairs of the catabolic activity. For AO, NRMX and An-NRMX, $\Delta\Psi$ is calculated as the potential difference between the electron acceptor and the ubiquinone/ubiquinol pair ($\Delta\Psi = \Psi_A - \Psi_U$). Like this it is considering that the energy-conversion steps are the oxidation of hydroxylamine to nitrite, specifically when the electrons are transferred from ubiquinone/ubiquinol pair to complex III (Q cycle) (Berks et al., 1995; González-Cabaleiro et al., 2019; Yuan & Vanbriesen, 2002). For NO activity, $\Delta\Psi$ is calculated as the potential difference between the electron acceptor (O₂) and the electron donor ($\Delta\Psi = \Psi_A - \Psi_D, \text{NO}_2^-$) as the Q cycle does not participate in its catabolic process (Lücker et al., 2010). For CMX activity, $\Delta\Psi$ is calculated as the sum of the potential differences estimated for AO and NO

activities. Like this it is considering that the enzymatic groups for ammonia oxidation and nitrite oxidation of comammox *Nitrospira* are fully compatible and catalyse their respective reactions and transport of electrons to complex IV without limiting the activity of the other enzymatic group. The values of γ_A^* and reduction potentials at pH 7 (Ψ_i) used to calculate the ΔG_{Cat}^{01} values are shown in Table D1. In those catabolic activities where ammonia oxidation takes place (AO, CMX, NRMX and An-NRMX), part of the consumed oxygen is used for ammonia activation in the monooxygenation step (1 mol of O₂) where all the energy is considered dissipated (Yuan & Vanbriesen, 2002).

For all the activities evaluated, the energy required to generate 1 mole of new biomass (CH_{1.8}O_{0.5}N_{0.2}) from inorganic carbon was set as constant of 3500 kJ per C-mole of new biomass formed (ΔG_{Ana}^{01}) considering that the expensive mechanism of reversed electron transfer is necessary in autotrophic growth (Kleerebezem & Van Loosdrecht, 2010). The growth yield values ($Y_{X/D}$, in units of C-mole of biomass formed per mole of electron donor) are calculated according to Eq. 7.7. With the estimated $Y_{X/D}$ value and the stoichiometry of the catabolic activities considered (Eqs. 7.1 – 7.5), the growth yield over electron acceptor and other metabolic compounds is also calculated.

$$Y_{X/D} = \Delta G_{Cat}^{01} / \Delta G_{Ana}^{01} \quad (7.7)$$

The calculated growth yields are compared with the available experimental values when possible (AO, NO and CMX metabolic activities) but also with those obtained applying the Thermodynamic Electron Equivalents revised Model (TEEM2) (McCarty, 2007) (Table 7.1). The detailed description of the TEEM2 methodology is included in Supplementary Methods (Appendix D).

The estimated growth yield values for AO and NO activities agreed with the experimental values reported. The growth yield value reported for CMX was 15% higher than the one predicted with our developed methodology. The highest growth yield values for ammonia (Y_{X/NH_3}), nitrite (Y_{X/NO_2}) and oxygen (Y_{X/O_2}) were found for CMX metabolism, AMX bacteria and NO metabolism respectively, tendencies that were also observed for the calculated theoretical values. Comparing the growth yields predicted by our methodology and the TEEM2, less than 10% of difference was found in the growth yield estimations for AO, NO and CMX (1.0%, 7.7% and 8.2%, respectively). The TEEM2 methodology also predicts the highest Y_{X/NH_3} , Y_{X/NO_2} and Y_{X/O_2} values for CMX, AMX and NO activities, respectively.

Table 7.1. Comparison between experimental and estimated growth yield values (in $\text{mol}_e\text{X}/\text{mol}_\text{N}$) of comammox *Nitrospira*'s activities with current methodology in this study and TEEM2. The growth yield of anammox bacteria (AMX) is also included in the table (average of experimental data from literature).

$x/100$	This study				TEEM2 ($\epsilon = 0.258$)				Literature
	Y_{X/NH_3}	Y_{X/NO_2}	Y_{X/NO_3}	Y_{X/O_2}	Y_{X/NH_3}	Y_{X/NO_2}	Y_{X/NO_3}	Y_{X/O_2}	$Y_{\text{X}/e\text{D}}^{(a)}$
AO	4.09	–	–	2.72	4.13	–	–	2.75	3.91 – 4.27
NO	–	2.42	–	4.84	–	2.61	–	5.23	1.07 – 3.58
CMX	6.51	–	–	3.25	6.00	–	–	3.00	7.53
NRMX	1.67	–	1.67	1.67	2.24	–	2.24	2.24	–
An-NRMX	1.50	1.50	–	–	0.35	0.35	–	–	–
AMX	5.15	5.15	–	–	–	–	–	–	3.40 – 6.60

^(a) eD – electron donor. Y_{X/NH_3} for AO, CMX and AMX; Y_{X/NO_2} for NO. References: (Keen & Prosser, 1987; Martens-Habbena et al., 2009) for AO; (Ehrich et al., 1995; Hunik et al., 1994; Nowka et al., 2015; Watson & Waterbury, 1971) for NO; (Kits et al., 2017) for CMX; (Ni et al., 2009; Oshiki et al., 2011; Puyol et al., 2014; Straka, 2019) for AMX.

7.2.2. Multiscale model to describe the community assembly of comammox *Nitrospira* and anammox bacteria

The Individual-based Model framework detailed in Chapter 5 was employed to simulate the community assembly of comammox *Nitrospira* (considering the aforementioned metabolic activities) and anammox bacteria. These grow in a suspended floc system under a dynamic nitrogen and oxygen limited environment, simulating an ideal continuous stirred tank reactor until it reaches steady state. Reactor parameters were based on the experiment setup of van Kessel et al. (2015) (see Table D.2). The chemical species considered in this study (ammonia, nitrite, nitrate and oxygen) diffuse through the flocs and they are consumed or produced locally by the individuals which function of the local environmental conditions change their growth and decay rates. Model parameters are presented in Table D.2.

In order to evaluate the actual influence of the metabolic heterogeneity on comammox *Nitrospira*, and to be able to extrapolate the outcome of this study, no particularities of specific bacteria species were considered. The kinetic parameters defining the Monod curve for comammox *Nitrospira* and anammox bacteria (μ_{max} , K_{N} , K_{O_2} , a) were assumed equal (non-kinetic competition, Table D.3) and were chosen following the guidelines stated below. Under strongly limited environmental conditions like the ones simulated, the competition for substrate has to be evaluated function of differences in growth yield ($Y_{\text{X}/\text{S}}$), as growth occurs far from its maximum (μ_{max}) (Kreft, 2004b). Although differences in substrate affinity between species can play a role in selection (discussed in Section 7.4.4), the reported range

of affinity values of ammonia and nitrite for comammox *Nitrospira* and anammox bacteria overlaps (Figure D.1). Therefore, ammonia and nitrite affinities (K_{NH_3} and K_{NO_2} , respectively) are considered of 1.0 μM for all the simulations in agreement with the values reported for anammox bacteria (Figure D.1). The presence of certain protection for oxygen of aerobic *Nitrospira* to anammox bacteria was ensured assuming $K_{\text{I},\text{O}_2}^{\text{AMX}}/K_{\text{O}_2}^{\text{NS}} = 1$, which is consistent with reported experimental data regarding the oxygen tolerance of anammox bacteria (Table D.4). Lastly, complete metabolic stoichiometries of *Nitrospira* and anammox populations are detailed in Table D.5. We did not consider active movement, dispersion/invasion nor loss of microorganisms with effluent, but microbes move passively due to the shoving forces exerted by neighbouring individuals as they grow and divide (see Chapter 5).

7.2.3. Simulation experiments

All the simulation experiments started by considering 12 different microbial inocula randomly generated. The time of simulation was 5.0 years based on the early enrichments of comammox *Nitrospira* (Daims et al., 2015; van Kessel et al., 2015), obtaining a stable community of comammox *Nitrospira* and anammox bacteria. The concentration of substrates and products in the liquid bulk were calculated according to the mass balance of a reactor operating in a continuous mode, where the simulated activity was assumed representative of the average activity of the whole reactor (see Chapter 5).

The environmental conditions were selected based on early studies of comammox *Nitrospira* (Daims et al., 2015; van Kessel et al., 2015). Three different nitrogen feeding regimes were applied (defined as $\text{NH}_3:\text{NO}_2:\text{NO}_3$): ammonia feeding – 500:0:0 μM (Daims et al., 2015); equimolar feeding – 500:500:500 μM (van Kessel et al., 2015); non-equimolar feeding – 500:375:500 μM (van Kessel et al., 2015). The influence of oxygen availability was evaluated by establishing a constant bulk liquid oxygen concentration: anaerobic/hypoxic conditions (0.0 μM , 1.0 μM , 1.5 μM and 3.0 μM of O_2) (van Kessel et al., 2015), and aerobic conditions (93.8 μM of O_2) (Daims et al., 2015). For each condition, the simulations were run in triplicates using different inocula (randomly generated).

Two additional sets of simulation experiments were performed to complement the main results of this work. The first one considering a population of comammox *Nitrospira* exclusively performing CMX activity to assess the importance of metabolic heterogeneity in its survival under hypoxic conditions. The second one with lower and higher feedings of

ammonia in aerobic conditions (93.8 μM of O_2) following the experiment presented in Daims et al. (2015).

7.2.4. Ecological analysis at floc level

In order to study the ecological implications of the metabolic heterogeneity of comammox *Nitrospira* in the community assembly with anammox bacteria, an ecological analysis at floc level was performed through a new measure of rank correlation between multiple variables (multivariate Kendall's τ coefficient, see Appendix E), being able to interpretate not only pairwise interactions but also the higher-order interactions (*i.e.*, interactions between more than two individuals). For this, the relative abundances of comammox *Nitrospira* activities (AO, NO, CMX, NRMX and An-NRMX) and anammox bacteria (AMX) at the end of simulations were used. The relative abundances of each metabolic group were collected independently from all aggregates and replicates before using them in the correlation test. Only those aggregates in which all metabolic activities were present in the inoculum were subjected to the multivariate Kendall's rank correlation test. The multivariate Kendall's τ coefficient (τ_N) ranges from -1 to $+1$.

For pairwise interactions (corresponding to the *conventional* Kendall's coefficient, (τ), a value of -1 indicates that one dataset ranking is the reverse of the other (*i.e.*, negative correlation), whereas a value of $+1$ indicates that the two rankings of the datasets are the same (*i.e.*, positive correlation). A value of 0 indicates no correlation between the datasets. The interpretation of Kendall's τ from an ecological perspective depends on the type of ecological interaction:

$$\text{Collaboration} \Rightarrow \begin{cases} \tau > 0 \rightarrow + \text{ influence} \\ \tau = 0 \rightarrow \text{no influence} \end{cases} \quad (7.8)$$

$$\text{Competition} \Rightarrow \begin{cases} \tau = 0 \rightarrow \text{no influence} \\ \tau < 0 \rightarrow - \text{ influence} \end{cases} \quad (7.9)$$

$$\begin{array}{l} \text{Collaboration} \\ + \\ \text{Competition} \end{array} \Rightarrow \begin{cases} \tau > 0 \rightarrow + \text{ influence} \\ \tau = 0 \rightarrow \text{no influence} \\ \tau < 0 \rightarrow - \text{ influence} \end{cases} \quad (7.10)$$

For higher-order interactions (τ_N coefficients), a value of $+1$ indicates that the N ranking of datasets follows the particular tendency (represented with upwards (\uparrow) and downwards (\downarrow) arrows), whereas a value of -1 indicates that the N ranking of datasets follows another tendency entirely. A value of 0 indicates no correlation among the datasets. A unique τ_N

coefficient is associated to a specific data trend (see Appendix E; Tables E.1 – E.4). The source code to perform the ecological analysis at floc level is available on a public GitHub repository at <https://github.com/soundslikealloy/nOEN> (release v1.0.0).

7.2.5. Parameters for the quantification of nitrogen removal

In this study, the amount of ammonia and nitrite oxidized to nitrate is referred as aerobic nitrification performance, calculated by Eq. 7.11.

$$\text{Aerobic nitrification performance (\%)} = \frac{[NO_3]_{net}}{[NH_3]_{inf} + [NO_2]_{inf}} \cdot 100 \quad (7.11)$$

Where $[NO_3]_{net}$ is the net concentration of nitrate in the bulk liquid (difference between concentration in bulk liquid and influent, $[NO_3]_{BL} - [NO_3]_{inf}$), $[NH_3]_{inf}$ is the concentration of ammonia in the influent, and $[NO_2]_{inf}$ is the concentration of nitrite in the influent. The rest of ammonia and nitrite is oxidized to N_2 by anaerobic activities (An-NRMX and AMX), referred as anaerobic oxidation, and its performance is calculated by Eq. 7.12.

$$\text{Anaerobic oxidation performance (\%)} = \left(1 - \frac{[NO_3^-]_{net} - \{[NH_3]_{BL} + [NO_2^-]_{BL}\}}{[NH_3]_{inf} + [NO_2^-]_{inf}} \right) \cdot 100 \quad (7.12)$$

Where $[NH_3]_{BL}$ and $[NO_2^-]_{BL}$ are ammonia and nitrite concentration in bulk liquid, respectively.

7.2.6. Statistical analyses

The statistical significance of the difference between relative abundances (wt. %) and metabolic ratios across the different nitrogen feeding regimes and oxygen concentrations were assessed using Welch's *t*-test (Welch, 1947). To evaluate the correlation among the relative abundances of *Nitrospira*'s metabolic activities and oxygen concentration, Kendall's rank correlation method (τ) was employed (Kendall, 1938).

7.3. Results

Figure 7.1 shows the results from the simulation experiments of comammox *Nitrospira* and anammox bacteria community growing on suspended flocs under nitrogen and oxygen limiting conditions. Three different nitrogen feeding regimes (defined by $NH_3:NO_2:NO_3$ ratio) and five oxygen concentrations were evaluated (Daims et al., 2015; van Kessel et al.,

2015). All simulation experiments started with same proportion of comammox *Nitrospira* performing AO, NO, CMX, NRMX or An-NRMX, and anammox bacteria.

In all tested conditions, the co-existence of different metabolic activities of comammox *Nitrospira* was observed in steady state, predicting metabolic heterogeneity for comammox *Nitrospira* in limiting conditions of nitrogen and oxygen. Only two metabolic activities of comammox *Nitrospira* were totally suppressed under specific conditions: (i) NO activity at 1.0 μM of O_2 and feeding only ammonia or non-equimolar nitrogen regime (Figures 7.1A and 7.1C), and (ii) An-NRMX activity at $\geq 3.0 \mu\text{M}$ of O_2 regardless of the nitrogen feeding regime. Although NRMX activity was not completely suppressed, its presence on the community was always under 2.0 wt. %. In general, no specific distribution of comammox *Nitrospira* or anammox bacteria was observed (Figures 7.1 and D.2). The absence of stratification of aerobic comammox *Nitrospira* (performing AO, NO, CMX or NRMX) and anammox bacteria suggested that anammox did not need to be protected against oxygen at these low oxygen concentrations ($\leq 1.5 \mu\text{M}$ of O_2). Layered stratification of AO and NO activities, an expected distribution in commensalism (W. Liu et al., 2016), was only observed when ammonia feeding and aerobic conditions (93.8 μM of O_2) were applied (Figures 7.1A and D.2A).

In anaerobic conditions, AMX dominated the community in both equimolar and non-equimolar feedings of ammonia and nitrite (~96 wt. % of AMX and ~4 wt. % of An-NRMX). Anaerobic activities (An-NRMX and AMX) only remained active at 1.5 μM of O_2 or below (Figure 7.1). In these hypoxic conditions, aerobic comammox *Nitrospira* (performing AO, NO, CMX or NRMX) were also present. The aerobic activities always outnumbered the anaerobic ones when ammonia feeding was applied (69.1% of aerobes and 30.9% of anaerobes at 1.0 μM of O_2 , $p < 0.003$; 85.3% of aerobes and 14.7% of anaerobes at 1.5 μM of O_2 , $p < 0.001$; Figure 1A). NO activity was significantly benefited by an equimolar feeding of ammonia and nitrite ($p < 0.01$; Figure 7.1B), turning to be the dominant aerobic activity at 1.0 μM of O_2 . A significant reduction of NO abundance (or a total suppression at 1.0 μM of O_2) was obtained with the reduction of nitrite in feeding and the presence of anammox bacteria (Figures 7.1A and 7.1C). At higher concentrations of oxygen ($\geq 3.0 \mu\text{M}$ of O_2), ammonia and nitrite oxidation were mainly carried out by AO, NO and CMX activities (~98 wt. %) in all feeding regimes. Although we did not set any oxygen

inhibition to An-NRMX activity, this metabolic activity was totally suppressed by their competitors.

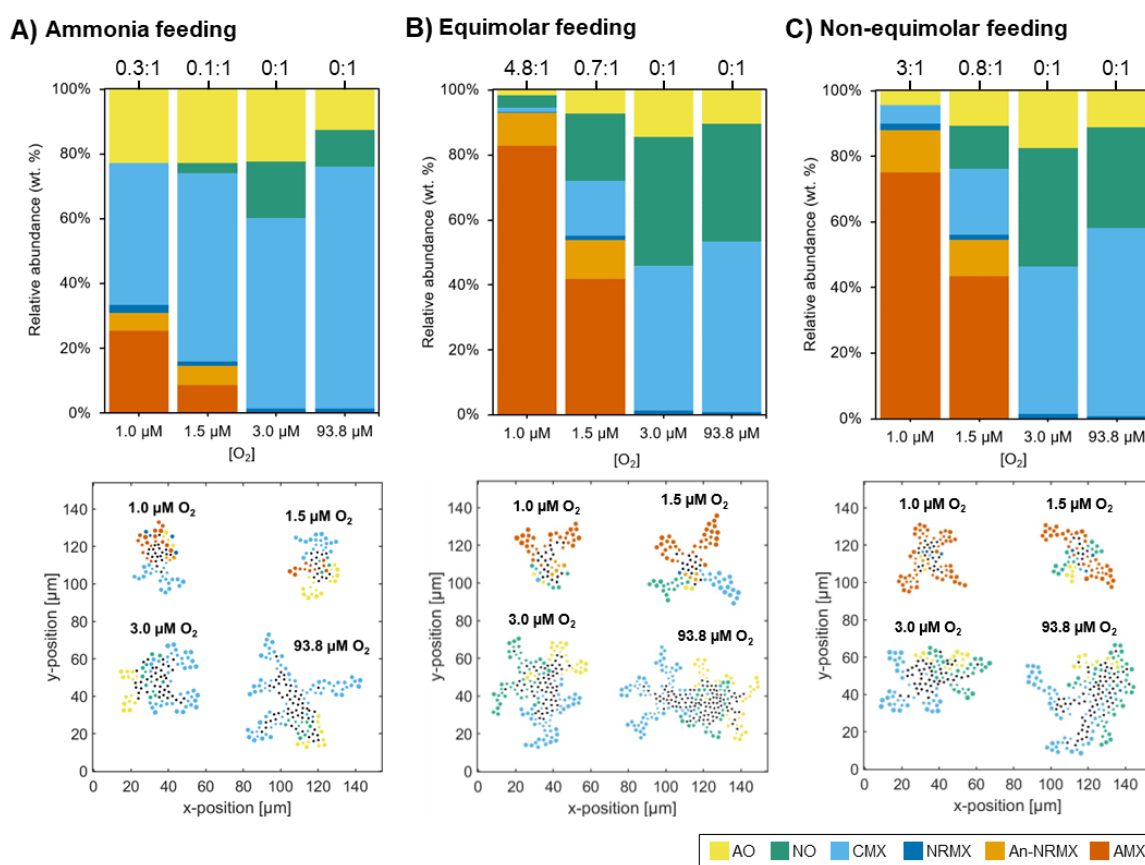


Figure 7.1. Influence of nitrogen feeding regime (defined by $\text{NH}_3:\text{NO}_2:\text{NO}_3$ ratio) and oxygen concentration (1.0, 1.5, 3.0 and 93.8 μM) on comammox *Nitrospira* and anammox bacteria community. Relative abundances of *Nitrospira* (AO, NO, CMX, NRMX and An-NRMX) and anammox bacteria (AMX), with each correspondent floc images (bottom panels) under **A)** ammonia feeding ($\text{NH}_3:\text{NO}_2:\text{NO}_3 = 500:0:0 \mu\text{M}$), **B)** equimolar feeding ($\text{NH}_3:\text{NO}_2:\text{NO}_3 = 500:500:500 \mu\text{M}$), and **C)** non-equimolar feeding ($\text{NH}_3:\text{NO}_2:\text{NO}_3 = 500:375:500 \mu\text{M}$). The statistical significance between different oxygen concentrations and nitrogen feeding regimes are shown in Tables D.7 and D.8, respectively. Labels over each bar show Anammox:*Nitrospira* ratio at steady state. Black circles on floc images represent inactive individuals. Additional floc images of comammox *Nitrospira* and anammox community are shown in the Figure D.2.

The co-existence of division of labour (AO+NO) and complete ammonia oxidation (CMX) was present almost in all cases except in those conditions where NO activity was totally suppressed (Figures 7.1A and 7.1C at 1.0 μM of O_2). Absolute dominance of CMX activity over division of labour was not observed in any case:

- Applying ammonia feeding only (Figure 7.1A), CMX activity significantly outnumbered division of labour, increasing their dominance at higher oxygen concentration ($p < 0.04$ at $1.0 \mu\text{M}$ of O_2 ; $p < 0.009$ at $1.5 \mu\text{M}$ of O_2 ; $p < 0.001$ at $3.0 \mu\text{M}$ of O_2 ; $p < 0.001$ at $93.8 \mu\text{M}$ of O_2 ; Figure D.3A).
- Applying equimolar feeding (Figure 7.1B), division of labour significantly outnumbered CMX activity under hypoxic conditions ($p < 0.03$ at $1.0 \mu\text{M}$ of O_2 ; $p < 0.05$ at $1.5 \mu\text{M}$ of O_2 ; $p < 0.002$ at $3.0 \mu\text{M}$ of O_2 ; $p = 0.238$ at $93.8 \mu\text{M}$ of O_2 ; Figure D.3A).
- Same proportion of division of labour and CMX activity was always observed in non-equimolar feeding ($p > 0.08$; Figure 7.1C).

Although AO activity never outnumbered CMX, a correlation between lower oxygen concentrations and higher relative proportions of AO over CMX was observed ($\tau = 1.00$, $p < 0.02$ for only ammonia feeding; $\tau = 0.80$, $p < 0.05$ for equimolar feeding; $\tau = 0.80$, $p < 0.05$ for non-equimolar feeding; Figure D.3B).

7.4. Discussion

Comammox *Nitrospira* cocultured with anammox bacteria (Cui et al., 2023; Shao & Wu, 2021) has the potential to achieve high levels of nitrogen removal with a reduced energy consumption for aeration, limited N_2O emissions (Kits et al., 2019) and sludge production (Luo et al., 2022). However, its activity remains unexplained, including their capacity to survive in hypoxic conditions and their actual contribution to biological nitrogen removal. Using a multiscale model (Individual-based Model), we have shown that under oxygen and/or nitrogen limiting conditions, selective co-existence of different metabolic activities of comammox *Nitrospira* occurs (metabolic heterogeneity). Our modelling results suggest that even at extremely low oxygen concentrations ($1.0 \mu\text{M}$ of O_2) comammox *Nitrospira* is able to survive in a proportion similar to the experimentally observed in van Kessel et al. (2015) (Anammox:*Nitrospira* \approx 3:1).

Complete dominance of any of the metabolic activities of comammox *Nitrospira* was not observed at steady state for any simulated conditions. The trends observed in the relative abundances of NO and CMX activities can be explained by the metabolic efficiencies associated to these activities (growth yield values of Table 7.1), and the most limiting substrate that controls the microbial community assembly (*i.e.*, the dominant substrate; see Supplementary Discussion – Appendix D). NO activity dominated as aerobic activity under

oxygen limitation when nitrite was available (Figure 7.1B; 1 μM of O_2). This can be explained because it is the activity with the highest growth yield on oxygen (Y_{X/O_2}). CMX activity dominated when ammonia was limited and oxygen not (Figure 1A; 93.8 μM of O_2) due to its higher efficiency on ammonia (Y_{X/NH_3}) over its aerobic competitors.

Under strong limited conditions of substrates and high competition, metabolic efficiency also defines the survival of microbial species. In low oxygen conditions, comammox *Nitrospira* performing NO activity was outcompeted by AMX when nitrite feeding was withdrawn or reduced (Figures 7.1A and 7.1C; 1 μM of O_2), because AMX has a higher growth yield on nitrite (Y_{X/NO_2}) than NO populations (Table 7.1). Repression of NO benefited the other metabolic activities of comammox *Nitrospira* with lower Y_{X/O_2} (AO, CMX and NRMX). Under this competitive environment, the collaboration between comammox *Nitrospira* (performing AO or NRMX) and anammox bacteria emerges (collaborative competition, Figures 7.1A and 7.1C, Table D.10D). In all tested conditions AO, CMX and NRMX activities coexisted. Although the growth yield of CMX on ammonia (Y_{X/NH_3}) and oxygen (Y_{X/O_2}) was higher than AO and NRMX, the difference was not enough for the suppression of the latter activities.

7.4.1. Metabolic heterogeneity for comammox *Nitrospira*

The results presented in Figure 7.2A suggest that comammox *Nitrospira* might only be able to thrive together with anammox bacteria under hypoxic conditions because of its metabolic heterogeneity. This is highlighted in the cases in which anammox bacteria is not dependent of other individuals for nitrite availability (equimolar feeding case; Figure 7.2A). Additionally, metabolic heterogeneity would explain the ubiquity of comammox *Nitrospira* (Xia et al., 2018) and their stable association with anammox bacteria (Gottshall et al., 2021; van Kessel et al., 2015). The considered simple competition among comammox *Nitrospira* and anammox bacteria becomes a more complex ecological network, which combines both collaborative interactions (commensalism and syntrophism) and competition (Figures 7.2B and D.4, Table D.10).

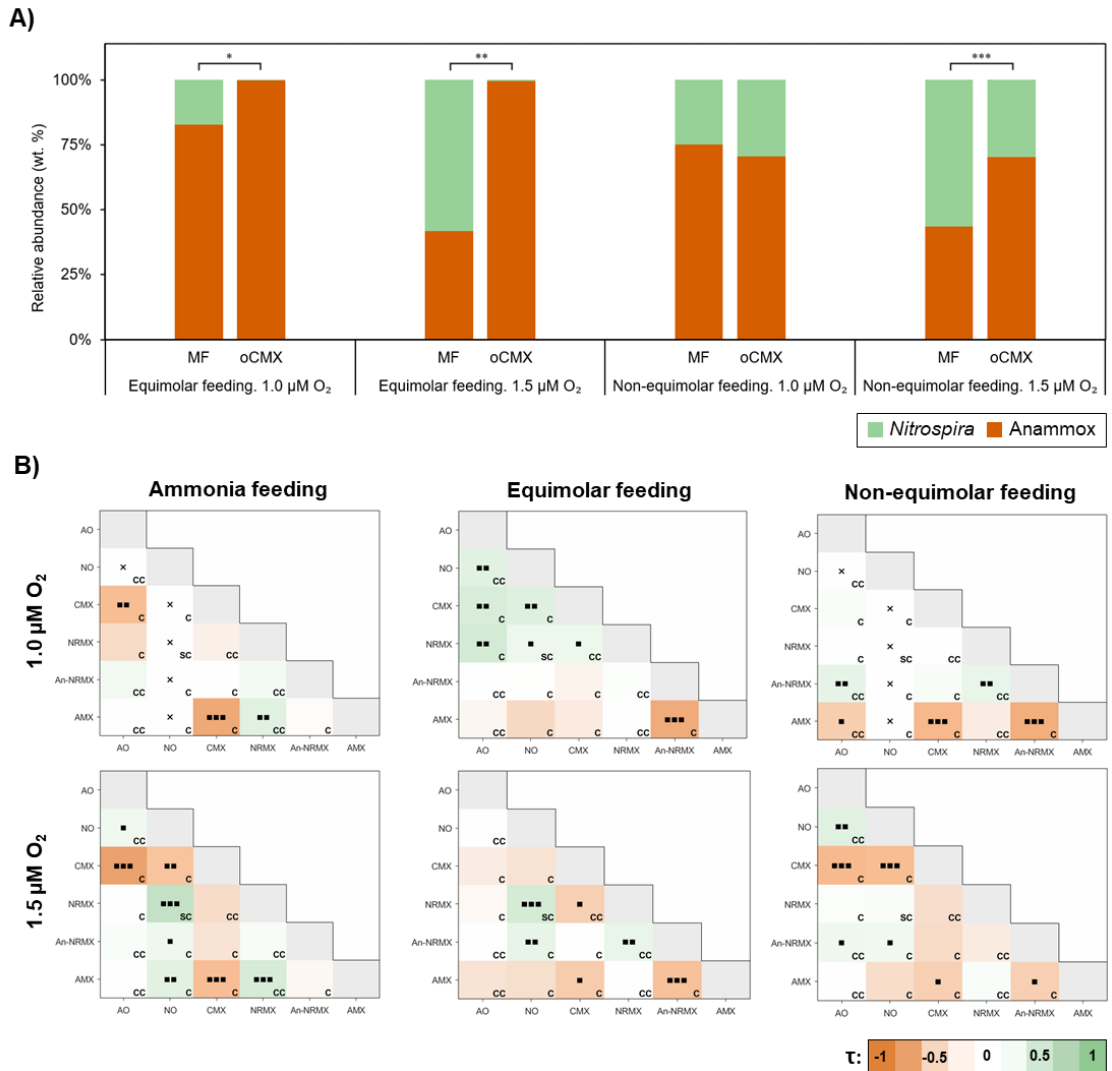


Figure 7.2. Value of metabolic heterogeneity for comammox Nitrospira. **A)** Impact of metabolic heterogeneity on the survival of comammox Nitrospira under hypoxic conditions (1.0 and 1.5 μM of O_2) applying equimolar feeding ($\text{NH}_3:\text{NO}_2:\text{NO}_3 = 500:500:500 \mu\text{M}$) and non-equimolar feeding ($\text{NH}_3:\text{NO}_2:\text{NO}_3 = 500:375:500 \mu\text{M}$). MF – simulation experiments considering metabolic flexibility in Nitrospira; oCMX – simulation experiments considering that Nitrospira only performs CMX activity. Asterisks denote p-value significance where *, $p < 0.05$; **, $p < 0.01$; ***, $p < 0.001$. **B)** Ecological analysis at floccle level (pairwise interactions) under conditions where comammox Nitrospira and anammox bacteria remained active (1.0 and 1.5 μM of O_2). Ammonia feeding ($\text{NH}_3:\text{NO}_2:\text{NO}_3 = 500:0:0 \mu\text{M}$, left panels); equimolar feeding ($\text{NH}_3:\text{NO}_2:\text{NO}_3 = 500:500:500 \mu\text{M}$, centre panels); non-equimolar feeding ($\text{NH}_3:\text{NO}_2:\text{NO}_3 = 500:500:500 \mu\text{M}$, right panels). Kendall's τ values of metabolisms are presented on a colour scale. Dotted cells indicate p-value significance where ■, $p < 0.05$; ■■, $p < 0.01$; ■■■, $p < 0.001$. Cross symbol (x) indicates no co-existence of the metabolic pair at the end of the simulation experiments. Bottom-right labels indicate the ecological interaction of metabolic pair: CC – Commensalism+Competition; SC – Syntrophism+Competition; C – Competition. Sample sizes employed for Kendall's τ calculation are shown in Figure D.5.

The influence of ecological interactions between metabolic pairs (represented with Kendall's τ) was significantly positive (Kendall's $\tau > 0$) or without influence (Figure 7.2B), showing the positive impact of metabolic heterogeneity for comammox *Nitrospira*. Note that positive influence was also observed in the competition cases (C label in Figure 7.2B). This is because a third activity favoured both competitive metabolic activities with a commensal interaction (higher-order interactions; *e.g.*, AO, NO and An-NRMX: AO activity fed nitrite to both NO and An-NRMX activities; Table D.10A). Note that with an equimolar feeding and 1.0 μM of O_2 (1st row and 2nd column; Figure 7.2B), positive interaction among all aerobic activities of comammox *Nitrospira* (AO, NO, CMX, NRMX) was observed. The strong hypoxic conditions and feeding of nitrite give a clear advantage of anaerobic activities (An-NRMX and AMX) over the aerobic ones (AO, NO, CMX, NRMX). However, some individuals performing aerobic activities were able to survive because the difference of Y_{X/O_2} was not enough to suppress any aerobic activity by oxygen competition. Because all aerobic individuals were strongly constrained by low oxygen concentration, the acquisition of space by any aerobic activity gave an opportunity to take the space from the anaerobic individuals (*i.e.*, An-NRMX and AMX). In this case, space competition (instead of competition for substrate) controlled the community assembly (Table D.10B) – less competitive individuals (aerobic activities) versus more competitive individuals (anaerobic activities).

Under hypoxia conditions (1.5 μM of O_2) and ammonia feeding no influence between AO/An-NRMX and AO/AMX pairs were found (Kendall's $\tau \approx 0$, Figure 7.2B). However, a significant synergy between AO, NO, NRMX and An-NRMX/AMX was observed. This ecological network combines a syntrophic loop between NO and NRMX and commensal fed of nitrite to An-NRMX and AMX (commensal-syntrophic pool, Table D.10C). Furthermore, the capacity of NO activity to compete against CMX for oxygen favoured division of labour ($\uparrow\text{AO}$ $\uparrow\text{NO}$ $\downarrow\text{CMX}$: $\tau_N > 0.35$, $p < 0.013$; Table D.10D) and NRMX activity ($(\uparrow\text{AO})$ $\uparrow\text{NO}$ $\downarrow\text{CMX}$ $\uparrow\text{NRMX}$: $\tau_N > 0.31$, $p < 0.05$; Table D.10E).

In those conditions where anammox bacteria were not present (≥ 3.0 μM of O_2 ; Figure D.4) a strong competition for oxygen between CMX and NO activities was still present. The restriction of NRMX by CMX activity (due to the lower metabolic efficiency for ammonia of NRMX, Table 7.1) and the uniform influence of interactions in all feeding regimes were only observed in aerobic conditions (Figure D.4, 93.8 μM of O_2). Throughout the tested

conditions (Figures 7.2B and D.4), a variety of Kendall's τ values was observed indicating the adaptability that metabolic heterogeneity gives to comammox *Nitrospira*.

The collaboration between comammox *Nitrospira* and anammox bacteria is supported by AO and NRMX activities, yielding nitrite for anammox bacteria. Figure 7.2B shows that comammox *Nitrospira* performing NRMX would be a better partner for anammox bacteria than when performing AO activity (Kendall's $\tau \geq 0$ between AMX and NRMX; Kendall's $\tau \leq 0$ between AMX and AO, last row of panels in Figure 7.2B). The theoretically predicted lower growth yield for ammonia of NRMX activity reduces the competitive pressure to anammox bacteria and increases the production of nitrite per biomass generated.

7.4.2. Optimization of anaerobic oxidation performance

The *in-silico* experiments show that NRMX activity has the capacity to positively contribute to the collaboration between comammox *Nitrospira* and anammox bacteria by reducing the nitrate produced by CMX and NO activities to nitrite (always Kendall's $\tau \geq 0$ between NRMX and AMX; Figure 7.2B). Considering this, the collaboration between comammox *Nitrospira* and anammox was *in-silico* maximised by reducing the oxygen concentration to minimize the inhibition of anammox and feeding ammonia and nitrite non-equimolarly ensuring the suppression of NO activity responsible for the drain of nitrite (Figure 7.3).

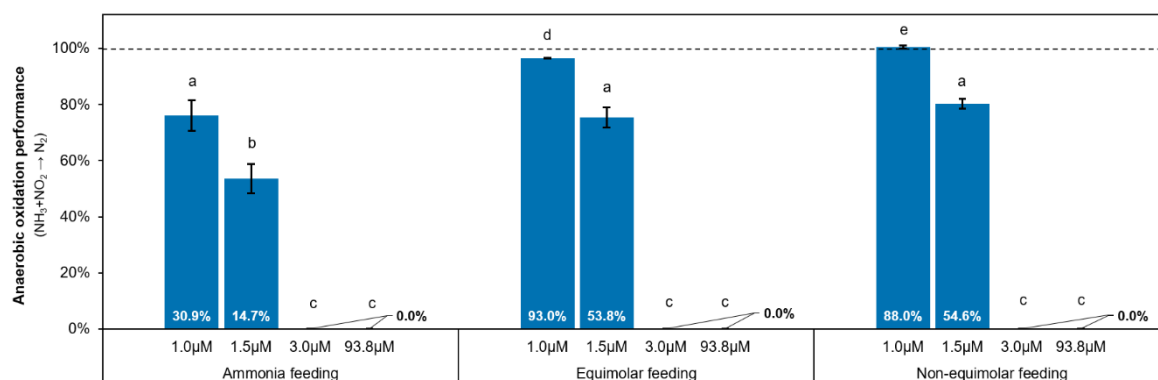


Figure 7.3. Influence of nitrogen feeding regime (ammonia, equimolar and non-equimolar feeding) and oxygen concentration (1.0, 1.5, 3.0 and 93.8 μM) on the anaerobic oxidation performance (ammonia and nitrite oxidation to N_2) expressed as percentage. Data labels depict the relative abundance of anaerobic activities (An-NRMX and AMX). Nitrogen feeding regimes: ammonia feeding – 500:0:0 μM ; equimolar feeding – 500:500:500 μM ; non-equimolar feeding – 500:375:500 μM . Error bars show standard deviation of $n = 3$ simulation replicates. Bars that do not share similar letters denote statistical significance, $p < 0.05$. For more information about the calculus of the anaerobic oxidation performance see Methods – Parameters for the quantification of nitrogen removal.

Furthermore, improvement of anaerobic oxidation performance was predicted, showing similar performance with lower relative abundance of anaerobic activities (see data labels of statistic group *a*, or comparison between group *d* and *e* in Figure 7.3). Due to the low metabolic efficiency of NRMX with respect to ammonia (low Y_{X/NH_3} value, Table 7.1), the collaboration between comammox *Nitrospira* and anammox bacteria was also predicted as dependent on the residual nitrate concentration (lower anaerobic oxidation performance was observed when non-equimolar feeding without nitrate was applied, $p < 0.05$; Figure D.6).

7.4.3. Metabolic heterogeneity explains transient nitrite accumulation

Daims et al. (2015) observed a transient accumulation of nitrite correlating with different ammonia feedings. With the objective to validate the model, and mechanistically explain the transient accumulation of nitrite, two extra simulation experiments were performed with different ammonia concentrations and aerobic conditions (100 μM and 1000 μM of NH_3 at 93.8 μM of O_2 ; Figures 7.4A and 7.4C, respectively).

The same trend as the experimental findings was observed in the *in-silico* experiments: no transient accumulation of nitrite at low ammonia concentration (Figure 7.3A), and a larger peak of nitrite transient accumulation at increasing ammonia concentrations (53.4 \pm 31.5 μM of NO_2 for 500 μM of NH_3 ; 110.9 \pm 33.2 μM of NO_2 for 1000 μM of NH_3 ; $p < 0.05$, $n = 3$; Figures 7.4B and 7.4C, respectively). The co-existence of division of labour (AO+NO) and CMX activity together with the dissociation between AO and NO activities can explain the transient accumulation of nitrite in the bulk liquid (significant lag phase of NO activity was observed at 500 μM and 1000 μM of NH_3 ; Figures 7.4B and 7.4C).

7.4.4. (Eco)physiological analysis of comammox *Nitrospira*

Currently, physiological characterizations of *Nitrospira inopinata* (Kits et al., 2017) and *Candidatus Nitrospira kreffii* (Sakoula et al., 2021) are available. In these studies, it was reported that although both comammox species have similar ammonia affinity (0.063 μM NH_3 for *N. inopinata*, and 0.040 μM NH_3 for *Ca. N. kreffii*), they have different nitrite affinities (449.2 μM NO_2^- for *N. inopinata*, and 12.5 μM NO_2^- for *Ca. N. kreffii*). Nitrite affinity of comammox *Nitrospira* might play a fundamental role in microbial community assembly (especially on competition between NO, An-NRMX and AMX for nitrite) and transient accumulation of nitrite.

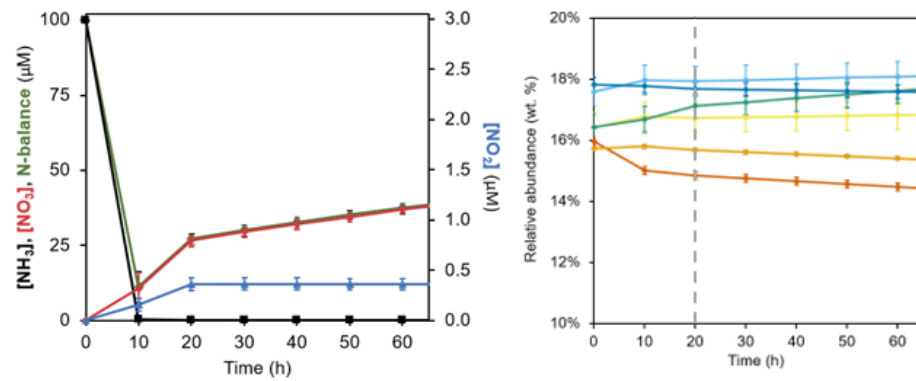
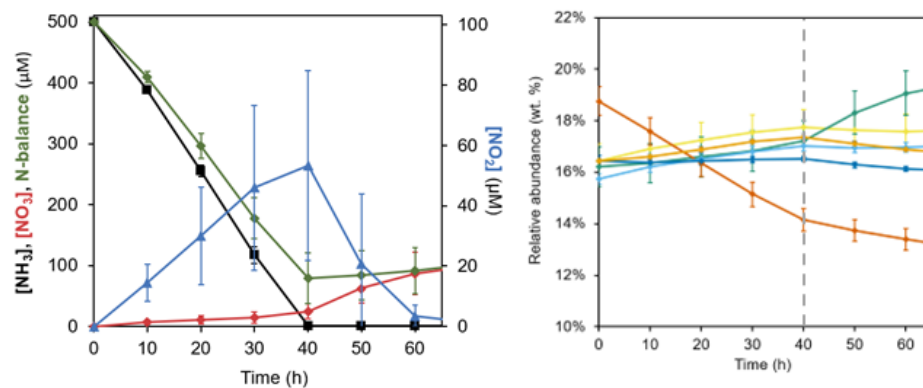
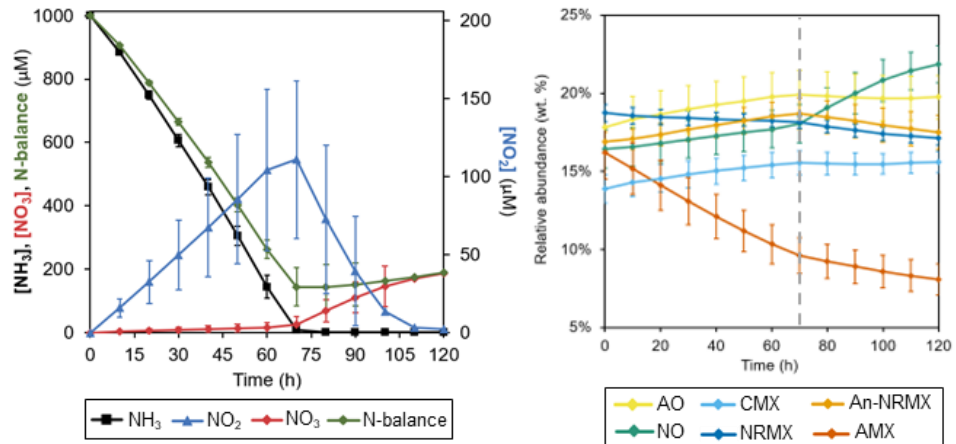
A) Ammonia feeding (100 μM)**B) Ammonia feeding (500 μM)****C) Ammonia feeding (1000 μM)**

Figure 7.4. Influence of ammonia concentration to the transient accumulation of nitrite at 93.8 μM of O_2 . Three ammonia concentrations were tested. Only 60 – 120 hours are shown (full simulation in Figure D.7): 100 μM of NH_3 (panels A), 500 μM of NH_3 (panels B), and 1000 μM of NH_3 (panels C). Left panels show the dynamics of nitrogen compounds (NH_3 , NO_2 and NO_3) at the early stages of simulation. Right panels show the evolution of relative abundances of comammox Nitrospira and anammox bacteria. Error bars show standard deviation of $n = 3$ simulation replicates. If not visible, error bars are smaller than symbols. Gray dashed lines in right panels (dynamics of metabolic activities) depict the time with the maximum concentration of nitrite.

To evaluate the influence of the physiological differences between *N. inopinata* and *Ca. N. kreftii*, the following simulation experiments were carried out: (i) non-equimolar feeding regime ($\text{NH}_3:\text{NO}_2^-:\text{NO}_3^- = 500:375:500 \mu\text{M}$) and hypoxia conditions (1.0 μM , 1.5 μM and 3.0 μM of O_2) assuming nitrite affinity of comammox *Nitrospira* equal to 12.5 μM NO_2^- and 449.2 μM NO_2^- (Figure 7.5); and (ii) only ammonia feeding (1000 μM NH_3) and aerobic conditions (93.8 μM O_2) assuming nitrite affinity of comammox *Nitrospira* equal to 12.5 μM NO_2^- and 449.2 μM NO_2^- (Figure 7.6). For both set of simulations, nitrate affinity of comammox *Nitrospira* was assumed equal to the nitrite affinity value.

The suppression of NO and An-NRMX activities was higher when reducing the nitrite affinity of comammox *Nitrospira* (*i.e.*, increasing the value of K_{NO_2}). NO activity was also fully suppressed at 1.5 μM of O_2 , whereas An-NRMX was no longer active at $\leq 1.5 \mu\text{M}$ of O_2 (Figures 7.5B and 7.5C). When nitrite affinity was assumed equal to 449.2 μM of NO_2^- , NO activity consisted only 2.9 ± 3.5 wt. % of the whole community at 3.0 μM of O_2 (Figure 7.5C). A smaller nitrite affinity (higher K_{NO_2} value) meant a reduction of competitive capacity of both activities (NO and An-NRMX) to survive against the stronger competitor (*i.e.*, AMX). Intriguingly, AMX remained active at 3.0 μM of O_2 after reducing the nitrite affinity of comammox *Nitrospira* to 12.5 μM NO_2^- and 449.2 μM NO_2^- (Figures 7.5B and 7.5C), while AMX was not active at 3.0 μM of O_2 assuming a nitrite affinity of comammox *Nitrospira* equal to 1.0 μM of NO_2^- (Figure 7.5A). Additionally, higher proportion of AMX at 3.0 μM of O_2 was observed as lower nitrite affinity of comammox *Nitrospira* was assumed (see labels over bars of Figure 7.5). This is due to the reduction of competitive capacity of NO activity, suggesting that the suppression of AMX at the main simulation setup (*i.e.*, K_{NO_2} value of comammox *Nitrospira* equal to 1.0 μM of NO_2^- ; Figure 7.5A) was a combination of oxygen inhibition and the presence of a competitive NO activity. Like in the main simulation setup under 1.0 μM and 1.5 μM of O_2 (bottom panel of Figure 7.5A), no stratification of aerobic comammox *Nitrospira* (performing AO, NO, CMX or NRMX) and anammox bacteria was observed (bottom panels of Figures 7.5B and 7.5C). On the other hand, higher proportion of AMX at $\leq 1.5 \mu\text{M}$ of O_2 was observed assuming a nitrite affinity of comammox *Nitrospira* equal to 12.5 μM NO_2^- (Figure 7.5B) than assuming 449.2 μM NO_2^- (Figure 7.5C). This can be associated with the presence/absence of NRMX activity, supporting the importance of NRMX activity to the collaboration between comammox *Nitrospira* and anammox bacteria.

Regarding transient accumulation of nitrite, a significant increase of nitrite accumulation was only observed when nitrite affinity of comammox *Nitrospira* was set to $449.2 \mu\text{M NO}_2^-$ ($p < 0.002$; Figure 7.6), being the peak of nitrite close to the levels observed experimentally by Daims et al. (2015) (30% of the added ammonia).

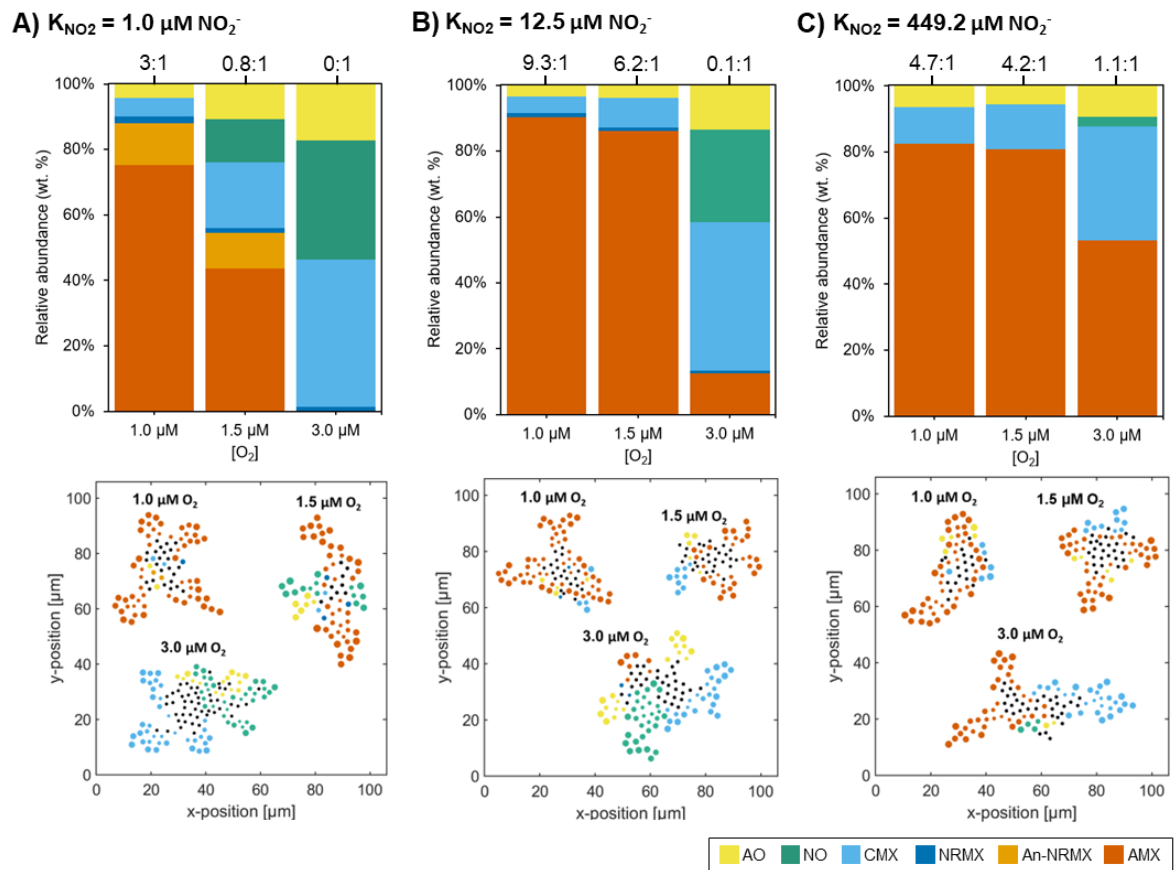


Figure 7.5. Influence of nitrite affinity (K_{NO_2}) of comammox *Nitrospira* on community assembly applying non-equimolar feeding ($\text{NH}_3:\text{NO}_2^-\text{:NO}_3^- = 500:375:500 \mu\text{M}$) and hypoxia conditions (1.0 μM , 1.5 μM and 3.0 μM of O_2). Relative abundances of *Nitrospira* metabolic activities (AO, NO, CMX, NRMX and An-NRMX) and anammox bacteria (AMX), with each correspondent floc images (bottom panels) assuming nitrite affinity (K_{NO_2}) equal to **A)** 1.0 μM of NO_2^- , **B)** 12.5 μM of NO_2^- and **C)** 449.2 μM of NO_2^- . Nitrate affinity of comammox *Nitrospira* was assumed equal to nitrite affinity value. Labels over each bar show Anammox:*Nitrospira* ratio at steady state. The statistical significance between different oxygen concentrations and nitrite affinities are shown in Tables D.11 and D.12, respectively. Black circles on floc images represent inactive individuals.

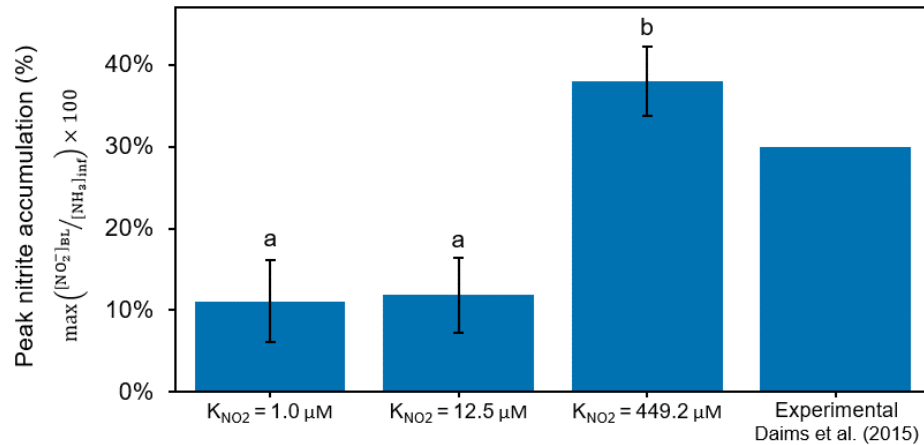


Figure 7.6. Influence of nitrite affinity (K_{NO_2}) of comammox *Nitrospira* on transient accumulation of nitrite (expressed as percentage) at $93.8 \mu\text{M O}_2$. Only ammonia was fed ($1000 \mu\text{M NH}_3$). Error bars show standard deviation of $n = 3$ simulation replicates. Bars that do not share similar letters denote statistical significance, $p < 0.05$.

7.5. Conclusions

Based on the state-of-the-art knowledge of comammox *Nitrospira* and a bioenergetics analysis, the *in-silico* experiments presented in this study predict that metabolic heterogeneity for comammox *Nitrospira* is necessary for its survival under oxygen limiting environments. Spatial transcriptomics would be needed to fully confirm our *in-silico* findings (e.g., parallel-sequential fluorescence in situ hybridization; par-seqFISH (Dar et al., 2021)), but according to our simulation experiments, metabolic heterogeneity is a mechanistic explanation of the early findings on comammox *Nitrospira* – its co-existence with anammox bacteria under hypoxic conditions (van Kessel et al., 2015), the dominance of complete nitrification activity in nitrogen limiting environments, and the transient accumulation of nitrite under aerobic conditions (Daims et al., 2015). When availability of nitrite is lower than ammonia, this work predicts that maximization of anaerobic nitrogen removal by anammox bacteria is possible by suppressing comammox *Nitrospira* performing NO activity.

Additionally, the results presented here suggest that the taxonomy of comammox *Nitrospira* would have a significant impact on the co-existence of comammox *Nitrospira* and anammox bacteria. In this case, *N. inopinata*, with a lower nitrite affinity, would be a better partner of anammox bacteria than *Ca. N. kreftii*. In fact, the first stable partnership between anammox bacteria and comammox *Nitrospira* was achieved with *N. inopinata* (Gottshall et al., 2021).

8.

Conclusions and Recommendations.

The present chapter will conclude this thesis by restating the research aims and objectives, summarising the key research findings in relation to the objectives, and discussing the value and contribution of these findings. It will also evaluate the limitations of this study and suggest new lines of research.

8.1. Restatement of Research Objectives

The work undertaken in this thesis aimed to elucidate the ecological mechanisms that rule the community assembly of nitrifiers addressing the following research objectives:

- To identify the ecological niches in which a specific population of aerobic nitrifiers will dominate based on the kinetic parameters that define the microbial growth and known biochemical information.
- To develop an *in-silico* methodology in order to study the influence of the ecological interactions and the environment on the microbial community assembly.
- To evaluate the influence of cell-cell, cell-environment and cell-space interactions on the community of nitrifiers in aggregates.
- To investigate the survival capacity of comammox bacteria under nitrogen and oxygen limiting conditions considering their potential metabolic heterogeneity.

8.2. Main Findings

Microbial communities are complex ecological systems, and the nitrifying community is not an exception. Despite the apparent simplicity of the nitrification process, the oxidation of ammonia to nitrate via nitrite is catalysed by a vast microbial diversity. Even both bacterial and archaeal domains participate on the oxidation of ammonia to nitrite. The comprehension of the complex ecological network of nitrifiers will permit us the development of better biotechnologies for the removal of nitrogen pollutants of sewage and improve the controllability of those already in use. Moreover, the explanation of domain redundancy in ammonia oxidation, the ecological niches of ammonia-oxidizing bacteria (AOB), ammonia-oxidizing archaea (AOA), complete ammonia oxidizers (CMX) and nitrite-oxidizing bacteria (NOB), and their relative contribution to the global nitrification remain unknown. In general, life strategies (r-, K-, Y-strategy) have been used to define ecological niches of microbial cohorts, being K- and Y-strategies the predicted best options to survive in oligotrophic environments (Andrews & Harris, 1986; Pfeiffer et al., 2001).

8.2.1. Biochemistry defines ecological niches of aerobic nitrifiers

In general, the trends associated with life strategies (r-, K-, Y-strategy) are supported by the meta-analysis presented in Chapter 3, but only in ammonia oxidizers – AOA and CMX present low maximum specific growth rate, high affinity for ammonia and high growth yield (K- and Y-strategists), whereas AOB show higher maximum specific growth rate, lower affinity for ammonia and lower growth yield (r-strategists). However, from the comprehensive analysis of the kinetic parameters of nitrifiers within the same microbial cohort, some inconsistencies were found, which complicate the definition of ecological niches for AOB and AOA. First, an overlap in the range of specific affinities for ammonia obtained for AOB and AOA was found. This means that some AOB species would be capable to compete with AOA in oligotrophic environments, especially from the *Nitrospira* genus. Additionally, similar specific affinities for oxygen between AOB and AOA were found, suggesting that AOB could compete with AOA in hypoxic environments. In fact, the capacity of AOA (such as *Nitrosopumilus maritimus*) to survive in oceanic environments where oxygen is undetectable would be attributed to the capacity to produce oxygen from the NO dismutation (Kraft et al., 2022), instead to their affinity for oxygen. On the other hand, huge physiological and biochemical diversity was observed for NOB (Daims et al., 2016). Notably, the results of this analysis contradict the assumption that ammonia oxidizers have higher affinity for oxygen than NOB (Jubany et al., 2008; Wiesmann, 1994). Although *Nitrobacter* have a lower affinity for oxygen, *Nitrospira* have a similar affinity to AOB and AOA. Additionally, this study shows that the measured kinetic parameters (and potential niche specializations) are mainly defined by the fundamental differences in the biochemistry of the different populations of nitrifiers – complete versus partial ammonia oxidation, archaea versus bacteria, different terminal oxidases, different carbon fixation pathways or periplasmic versus cytoplasmic NXR.

In sum, this meta-analysis highlights the importance of considering the microbial taxonomy (such as genus and species), the biochemistry of populations, and the metabolic versatility of microbes to define the ecological niches of nitrifying populations. Additionally, the lack of defined ecological niches in nitrification might not be only because a lack of environmental variables, but due to a niche overlapping. Distinct nitrifying cohorts seem to co-dominate in the same ecological niche.

8.2.2. Ecological, environmental and spatial controls of microbial community assembly in aggregates

The *in-silico* study presented in Chapter 6 shows how dynamics of microbial communities in aggregates can be explained by three types of interactions: cell-cell interactions (ecological interactions), cell-environment interactions (*e.g.*, nutrient concentrations or shear forces) and cell-space interactions (space competition and spatial distribution of microbial populations), being the last generally overlooked. This study illustrates how space competition controls the colony size and distribution of populations. Intriguingly, the spatial distribution of populations, controlled by the cell-cell and cell-space interactions, have in turn implications on microbial fitness and its survival. The radial distribution of microbial populations (referred as *columned stratification* and associated with competition) increases the chance of less competitive individuals to thrive and co-exist with populations that grow faster. On the other hand, the concentric disposition of communities (referred as *layered stratification* and associated with commensalism) would be the optimal distribution for the metabolic division of labour. On the other hand, this study shows that although ecological interactions between populations in aggregates dictate their distribution, the environment (cell-environment interactions) is controlling their final observed spatial distribution. This suggests that the spatial distribution of populations and therefore, the overall activity of the microbial community can be controlled by the applied conditions, such as the concentration of substrates, shear forces (both evaluated in Chapter 6) or others like pH or antibiotics.

From an ecological perspective, the study of nitrification is of great interest because it combines synergistic and antagonistic interactions. They also generate microbial aggregates, including additional layers of complexity in the understanding of the community assembly of nitrifiers. The findings presented in Chapter 6 illustrate the importance of the coaggregation for nitrifying populations. Both mentioned distributions promote the co-existence of nitrifying populations in any circumstances, even if these are competing for oxygen. In fact, the seasonal nitrous oxide emissions in wastewater treatment plants, due to the nitrification failure, was correlated with the loss of NOB and filamentous bacteria, being responsible for aggregate morphology (Gruber et al., 2021). Additionally, the results of this study would explain why the prolonged repression of NOB to achieve partial nitrification is not possible by reducing oxygen concentration alone (Poot et al., 2016).

8.2.3. Metabolic heterogeneity explains the early discoveries of comammox *Nitrospira*

The discovery of complete ammonia oxidation (comammox) was the latest big breakthrough in nitrification, ruling out the thought that full nitrification is an obligated two-step process. Although great advances have been made on the understanding of comammox process and who catalyses it (NOB belonging to *Nitrospira* genus, so-called comammox *Nitrospira*), there is still an open debate about the oxygen requirements for the chemoautotrophic growth of comammox *Nitrospira*. This thesis predicts that metabolic heterogeneity (*i.e.*, metabolic differences between individuals of the same population) for comammox *Nitrospira* is the key for their adaptability and survival under oxygen-limiting environments, thus providing an answer to the aforementioned debate. Moreover, metabolic heterogeneity explains the early findings on comammox *Nitrospira*. On the one hand, the co-existence of individuals performing ammonia oxidation and nitrite oxidation would generate the transient accumulation of nitrite under the aerobic conditions observed by Daims et al. (2015). On the other hand, metabolic heterogeneity for comammox *Nitrospira* would prompt the stable co-existence with anammox bacteria observed by van Kessel et al. (2015), thanks to the presence of comammox *Nitrospira* performing ammonia oxidation and nitrate-reducing ammonia oxidation. Understanding the underlying mechanisms of the collaboration between comammox *Nitrospira* and anammox bacteria will allow us to apply this promising community for nitrogen removal, significantly reducing the energy consumption, N₂O emissions and sludge production. This *in-silico* study predicts that the optimization of anaerobic nitrogen removal by anammox bacteria might be achieved by (i) decreasing the oxygen concentration, reducing the inhibition of anammox bacteria); (ii) feeding less nitrite than ammonia, ensuring the suppression of nitrite oxidation activity; and (iii) selecting specific *Nitrospira* species as a partner for anammox bacteria (such as *Nitrospira inopinata*, with lower nitrite affinity than *Candidatus Nitrospira kreftii*).

8.2.4. Theoretical and quantitative research in microbial ecology using mathematical modelling

The *in-silico* bottom-up methodology, together with the gradual increment of complexity of the simulated system, permits the comprehension of the genuine influence of the processes and dynamics that rule the microbial community assembly (such as diffusion, ecological interactions, shear forces, nutrient availability, feeding regime or (eco)physiological

properties of microbes). Moreover, the theoretical knowledge generated from the study of the discrete elements and processes can be transferred to more complex systems giving, in turn, outcomes closer to nature's observations. The study of comammox *Nitrospira* is an illustrative example of this. First, the enrichment levels of comammox *Nitrospira* were not predicted considering only ammonia-limiting environments, but they were predicted when microbial aggregation and the diffusion of compounds were considered. Then, the survival of comammox *Nitrospira* under hypoxic conditions was only predicted considering metabolic heterogeneity explaining, in turn, the transient accumulation of nitrite in aerobic conditions with high levels of ammonia. Finally, the levels of accumulated nitrite observed experimentally by Daims et al. (2015) (30% of the added ammonia) were predicted when the physiological characterization of *Nitrospira inopinata* was considered.

Overall, this thesis applies an *in-silico* bottom-up methodology for the theoretical understanding of the ecological mechanisms that shape the community assembly of nitrifiers. In essence, the *in-silico* bottom-up methodology is the combination of mathematical models with a systematic fragmentation of the domain and the critical selection of their key elements and processes. In addition to unveiling the intrinsic dynamics that shape the microbial community in aggregates, this approach allows for the development of new quantitative measurements of ecological dynamics, such as the (global) eco-interaction modulus (ϕ_{EI}) presented in Chapter 6 and applied in Chapter 7, and the ecological analysis using the multivariate Kendall's τ (τ_N) presented in Chapter 7. The eco-interaction modulus might not only be useful for the prediction of spatial distribution of populations in aggregates when two ecological interactions are present, but also for describing the ecological environment of complex ecological systems (*i.e.*, more than two ecological interactions), detecting the dominant substrate that controls the microbial community assembly. Bear in mind that the development of quantitative measurements of ecology is a crucial step to translate these patterns to new ecological theories, laws and rules (on which all explanations and predictions in science are based). Thus, this research could be used as the basis and an example of hypothesis and theory-based research in microbial ecology using mathematical modelling. Additionally, it also states the importance of the integration of top-down and bottom-up studies, where the former give us the information and techniques to define the (putative) patterns of nature and the latter allow us to develop new mechanistic explanations that generate the patterns. The statement of new theories

increases the precision and reliability of our predictions, accelerating the identification of new patterns.

8.3. Proposed Future Research and Current Limitations

The results presented in this work expand our comprehension of the ecological principles that control microbial community assembly using the nitrifying community as case study. This thesis covers the physiological diversity of nitrifiers and their ecological interactions, several environmental factors (such as nutrients availability, shear forces and feeding regimes) and the space competition. Despite the limitations inherent to the parameters that define the microbial growth (maximum specific growth rate and substrate affinity from Monod equation) and cell maintenance (Bodegom, 2007; Hellweger, 2017), the systematic analysis of the parameters from nitrifiers, together with information in the biochemistry, permit us to understand better the ecological niches of this community. For this reason, more meta-analyses about physiological properties (such as the one presented in Chapter 3) should be performed for other microbial communities, not only to create a broader kinetic database for modelling, but also to identify new ecological trends that might help us to identify ecological niches. This thesis also expands our understanding of how interspecies interactions (neutralism, competition and commensalism) and environmental conditions control the community assembly in aggregates. However, there are still ecological interactions to be investigated, such as parasitism, predation, amensalism or co-protection. Investigating these ecological interactions may reveal new ecological insights from other microbial communities, such as fermentative ones. Additionally, theoretical equal-fitness communities (*i.e.*, with same growth kinetics) was assumed in both *in-silico* studies, in which differences in growth kinetics might influence in the community dynamics.

This thesis also shows that the physiological properties of comammox *Nitrospira* can play a role in microbial community assembly, competition and ecological niche. Therefore, another line of research might be to investigate the influence of the physiological properties of nitrifiers to the community assembly of nitrifiers, especially of nitrite-oxidizing bacteria. The consideration of physiological diversity of nitrite-oxidizing bacteria might identify the limits of the repression of nitrite oxidation, being of great interest for the optimization of partial nitrification/anammox process (Pedrouso et al., 2021), and the comprehension of seasonal N₂O emissions observed in wastewater treatment plants (Gruber et al., 2021). Considering the influence of oxygen availability on N₂O emissions by ammonia-oxidizing

bacteria (Goreau et al., 1980; Khalil et al., 2004; Lipschultz et al., 1981; Zhu et al., 2013), and the drop of oxygen inside the aggregate, it might be interesting to include a better description of biotic and abiotic generation of N_2O to the model in order to analyse the dynamics function of the operational conditions and community dynamics. A better understanding of these factors may reveal new strategies to control the seasonal emissions of N_2O in wastewater treatment plants.

A limitation of this work was the lack of robust experimental data regarding the actual influence of ecological dynamics described in Chapter 6, and the experimental corroboration of the metabolic heterogeneity for comammox *Nitrospira* (at least under the environmental conditions tested). Recently, novel promising techniques have been developed for the analysis of aggregate dynamics and the detection of metabolic heterogeneity for comammox *Nitrospira*, such as multiscale spatial segregation (Segregation package), parallel sequential fluorescence in situ hybridization (par-seqFISH), RAINBOW-seq or differential isotope labelling by amino acids (DILAC) (Dar et al., 2021; Dogsa & Mandic-Mulec, 2023; Kamrad et al., 2023; Wang et al., 2023). However, the application of these techniques to comammox *Nitrospira* is challenging due to the small size of cells and their tendency to form aggregates. Moreover, there is still no experimental evidence of the metabolic activities proposed by Kleerebezem and Lucker (2021). The results presented could guide the identification of comammox *Nitrospira* catalysing nitrate-reducing ammonia oxidation (NRMX) and/or the anaerobic nitrite-reducing ammonia oxidation (An-NRMX).

Although this work was focused on the ecological aspect of nitrifiers, there are still other factors with implications on the community assembly in aggregates to be explored, *e.g.*, the synthesis of extracellular polymeric substances (EPS). The EPS matrix creates a structural integrity for microbial aggregates, providing protection to the microbial community from the harsh environments, and expanding the functional attributes of aggregates. Although both nitrifying cohorts (ammonia oxidizers and nitrite-oxidizing bacteria) contribute to the structural integrity of aggregates, the synthesized EPS and the rate of secretion might differ. However, the composition of EPS and their physical properties are not yet fully understood. The incorporation of EPS synthesis to the mathematical model would also improve the description of shear forces and the detachment process that the aggregates undergo. Fragmentation of aggregates and dispersion/invasion of planktonic microbes are other important processes associated to the aggregate formation that have not considered in this thesis.

Appendix A - Chapter 3

Contents

Supplementary Text – Materials and Methods

Supplementary Tables – Tables A.1 – A.12

Supplementary Figures – Figures A.1 – A.9

Supplementary Text - Materials and Methods

Estimation of kinetic parameters. Temperature and pH

To obtain the values of Arrhenius coefficients (θ) (Eq. A.1), linear regression and least squares method is applied to set the best fit of the Arrhenius function to the experimental data. First, the Eq. A.1 is linearized using natural logarithm, considering that θ is the exponential of constant C (e^C).

$$\ln\left(\frac{\mu_{T1}}{\mu_{20}}\right) = \theta \cdot (T - 20) \quad (\text{A.1})$$

Then, a linear regression is applied to obtain an initial value of C and, subsequently, a value of θ . Finally, least squares method is used to set better the equation to the experimental data, using as initial values of θ those obtained from the linear regression. Table A.1 presents the values of θ obtained and also the references of the experimental data used to calculate them. Analogously, the parameters that correlated the pH influence with the μ_{\max} values, (Eq. 3.2) are obtained by least squares method, assigning the initial values of $pK1$ and $pK2$ considering their definition: $\mu_{\max}(pK_1) = \mu_{\max}(pK_2) = 1/2 \cdot \mu_{\max}(pH_{op})$. The kinetic parameters and experimental data used to obtain the equation parameters were taken from literature (see Figure A.1).

Supplementary Tables

Table A.1. Arrhenius coefficient (θ) of nitrifying bacteria and archaea. Effect of temperature on maximum growth rate.

Culture	θ	Temperature (°C)	pH	References
Ammonia-oxidizing bacteria (non-marine)				
Mixed culture	1.114	7.0 – 21.0	7.0 – 7.8	† (1)
<i>Nitrosomonas</i> species	1.098	7.0 – 30.0	7.0 – 7.8	† (2)
<i>Nitrospira</i> species	1.126	3.0 – 21.0	7.5	† (3)
<i>Nitrospira</i> sp. 40K1	1.110	3.0 – 21.0	7.5	(Jiang, 1999)
<i>Nitrospira</i> sp. AF	1.146	3.0 – 31.0	7.5	(Jiang, 1999)
<i>Nitrospira</i> sp. B6	1.114	3.0 – 26.0	7.5	(Jiang, 1999)
<i>Nitrospira</i> sp. L115	1.132	3.0 – 26.0	7.5	(Jiang, 1999)
Ammonia-oxidizing bacteria (marine)				
Mixed culture	1.114	7.0 – 21.0	7.0 – 7.8	† (1)
<i>Nitrosomonas</i> species	1.098	7.0 – 30.0	7.0 – 7.8	† (2)
Ammonia-oxidizing archaea (non-marine)				
Mixed culture	1.126	10.0 – 30.0	6.0 – 7.5	† (4)
<i>Nitrososphaera koreensis</i>	1.150	15.0 – 30.0	6.0 – 8.0	(Jung et al., 2011)
<i>Nitrososphaera vienennsis</i>	1.180	10.0 – 30.0	?	(Tourna et al., 2011)
<i>Nitrososphaera gargensis</i>	1.126	20.0 – 46.0	?	† (4)
Ammonia-oxidizing archaea (marine)				
Mixed culture	1.114	10.0 – 25.0	5.9 – 8.7	† (5)
<i>Nitrosopumilus maritimus</i>	1.120	5.0 – 32.0	7.3	(Qin et al., 2014)
Nitrite-oxidizing bacteria (non-marine)				
Mixed culture	1.087	5.0 – 25.0	7.0 – 7.5	† (6)
<i>Nitrobacter</i> species	1.089	5.0 – 25.0	7.0 – 7.5	† (7)
<i>Nitrospira</i> species	1.088	5.0 – 25.0	7.0 – 7.5	† (8)
<i>Ca. Nitrotoga arctica</i>	1.109	5.0 – 15.0	7.0 – 7.5	† (9)
<i>Nitrobacter agilis</i>	1.104	2.5 – 25.0	7.8	(Leenen et al., 1997)
<i>Nitrospira defluvii</i>	1.110	10.0 – 27.5	7.4	(Wegen et al., 2019)
Nitrite-oxidizing bacteria (marine)				
<i>Nitrococcus mobilis</i>	1.087	5.0 – 25.0	7.0 – 7.5	† (6)
<i>Nitrospina</i> species	1.087	5.0 – 25.0	7.0 – 7.5	† (7)
<i>Nitrospira</i> species	1.088	5.0 – 25.0	7.0 – 7.5	† (8)
<i>Nitrotoga</i> species	1.109	5.0 – 15.0	7.0 – 7.5	† (9)

† Estimated

(1) Average of *Nitrosomonas* spp. (1.116, 1.101, 1.078) and *Nitrospira* spp. (1.110, 1.146, 1.114, 1.132) (Buswell et al., 1953; Helder & De Vries, 1983; Jiang, 1999; Knowles et al., 1965)(2) Average of *Nitrosomonas* spp. (1.116, 1.101, 1.078) (Buswell et al., 1953; Helder & De Vries, 1983; Knowles et al., 1965)(3) Average of *Nitrospira* spp. (1.110, 1.146, 1.114, 1.132) (Jiang, 1999)(4) Average of *N. aquarius* (1.083), *N. vienennsis* (1.180) and *Ca. N. exaquare* (1.114) (Sauder et al., 2017; Sauder et al., 2018; Tourna et al., 2011)(5) Average of *N. maritimus* (1.120), *N. cobalaminigenes* (1.097) and *N. ureiphilus* (1.126) (Qin et al., 2014)(6) Average of *Nitrobacter* spp. (1.104, 1.108, 1.080, 1.064), *Nitrospira* spp. (1.066, 1.110), *Nitrotoga* spp. (1.046, 1.172) and mixed culture of NOB (1.084, 1.036) (Blackburne et al., 2007b; Helder & De Vries, 1983; Kitzinger et al., 2018; Knowles et al., 1965; Leenen et al., 1997; Randall et al., 1984; Stratton & McCarty, 1967; Wegen et al., 2019)(7) Average of *Nitrobacter* spp. (1.104, 1.108, 1.080, 1.064) (Helder & De Vries, 1983; Knowles et al., 1965; Leenen et al., 1997; Randall et al., 1984)(8) Average of *Nitrospira* spp. (1.066, 1.110) (Blackburne et al., 2007b; Wegen et al., 2019)(9) Average of *Nitrotoga* spp. (1.046, 1.172) (Kitzinger et al., 2018; Wegen et al., 2019)

Table A.2. Maximum specific growth rate (μ_{max}) values at 20°C of nitrifying bacteria and archaea.

Culture	μ_{max} (h ⁻¹)	$\theta^{(1)}$	pH	References
Ammonia-oxidizing bacteria (non-marine)				
Mixed culture	0.033 – 0.042	1.114	7.5 – 7.8	(Hao et al., 2002; Henze et al., 2006; Jubany et al., 2008; Vadivelu et al., 2006)
<i>Nitrosomonas europaea</i>	0.014 – 0.035	1.098	7.0 – 7.8	(Belsler & Schmidt, 1980; Keen & Prosser, 1987; Station et al., 1961)
<i>Nitrosomonas oligotropha</i>	0.014 – 0.031	1.098	7.5	(French et al., 2012; Stehr et al., 1995)
<i>Nitrospira</i> sp. 40K1	0.009	1.110	7.5	(Jiang, 1999)
<i>Nitrospira</i> sp. AF	0.004	1.146	7.5	(Jiang, 1999)
<i>Nitrospira</i> sp. B6	0.010	1.114	7.5	(Jiang, 1999)
<i>Nitrospira</i> sp. L115	0.010	1.132	7.5	(Jiang, 1999)
Ammonia-oxidizing bacteria (marine)				
<i>Nitrosomonas marina</i>	0.018	1.098	7.6	(Glover, 1985)
<i>Nitrosococcus oceani</i>	0.014	1.114	8.1	(Glover, 1985)
Ammonia-oxidizing archaea (non-marine)				
Mixed culture	0.008 - 0.009	1.126	7.5	(Jung et al., 2011)
<i>Nitrososphaera koreensis</i>	0.009	1.150	6.0 – 8.0	(Jung et al., 2011)
<i>Nitrososphaera vienennsis</i>	0.002	1.180	7.6	(Kits et al., 2017)
<i>Nitrososphaera gargensis</i>	0.002	1.126	7.6	(Kits et al., 2017)
Ammonia-oxidizing archaea (marine)				
Mixed culture	0.005 – 0.15	1.126	8.0 – 8.2	(Park et al., 2010; Santoro & Casciotti, 2011)
<i>Nitrosopumilus maritimus</i>	0.008 – 0.013	1.120	7.0 – 7.6	(Könneke et al., 2005; Martens-Habbenha et al., 2009; Qin et al., 2017)
<i>Nitrosopumilus piranensis</i>	0.003	1.180	7.1	(Bayer et al., 2015)
<i>Nitrosopumilus adriaticus</i>	0.003	1.180	7.1	(Bayer et al., 2015)
Complete ammonia-oxidizing bacteria (CMX)				
<i>Nitrospira inopinata</i>	0.002	1.076	7.6	(Kits et al., 2017)
Nitrite-oxidizing bacteria (non-marine)				
<i>Nitrobacter vulgaris</i>	0.027 – 0.038	1.089	7.4 – 7.6	(Bock et al., 1990; Nowka et al., 2015)
<i>Nitrospira</i> sp. ND1	0.006	1.088	7.8 – 8.0	(Ushiki et al., 2017)
<i>Nitrospira japonica</i>	0.012	1.088	7.8 – 8.0	(Ushiki et al., 2017)
<i>Ca. Nitrotoga arctica</i>	0.0215	1.109	7.4 – 7.6	(Nowka et al., 2015)
<i>Nitrobacter agilis</i>	0.016 – 0.017	1.104	7.8	(Hunik et al., 1993; Leenen et al., 1997)
<i>Nitrobacter winogradskyi</i>	0.005 – 0.034	1.089	7.3 – 7.8	(Both et al., 1992; Gay et al., 1984; Nowka et al., 2015)
<i>Nitrospira defluvii</i>	0.0081	1.110	7.4 – 7.6	(Nowka et al., 2015)
<i>Nitrospira lenta</i>	0.0095	1.088	7.4 – 7.6	(Nowka et al., 2015)
<i>Nitrospira moscoviensis</i>	0.005 – 0.017	1.088	7.4 – 7.8	(Kindaichi et al., 2006; Nowka et al., 2015)
<i>Nitrobacter hamburgensis</i>	0.005 – 0.088	1.089	7.3 – 7.6	(Both et al., 1992; Nowka et al., 2015)
Nitrite-oxidizing bacteria (marine)				
<i>Nitrococcus mobilis</i>	0.033 – 0.036	1.087	7.6 – 7.8	(Glover, 1985; Watson & Waterbury, 1971)
<i>Nitrotoga</i> sp. AM1	0.0194	1.109	7.8	(Ishii et al., 2017)
<i>Nitrospira marina</i>	0.0153	1.088	7.8	(Kitzinger et al., 2020)
<i>Nitrospina watsonii</i>	0.0142	1.087	8.0	(Spieck et al., 2014)
<i>Nitrospira</i> sp. Ecomares	0.004 – 0.012	1.088	7.5	(Keuter, 2011)
Average values ± Standard deviation (number of samples, n)				
AOB (n = 20)	0.021 ± 0.012	–	–	–
AOA (n = 7)	0.006 ± 0.004	–	–	–
CMX (n = 1)	0.002	–	–	–

(1) Arrhenius coefficient. Table A.1 gathers the valid temperature range to each Arrhenius coefficient and references.

(2) OMZ: Oxygen Minimum Zone

Table A.3. Specific affinity for oxygen ($a^0_{O_2}$) of nitrifying bacteria and archaea.

Culture	$a^0_{O_2}$ (L/g-Bio/h)	T (°C)	pH	References
Ammonia-oxidizing bacteria (non-marine)				
Mixed culture	90.47	25	7.5	(Sánchez et al., 2001)
<i>Nitrosomonas europaea</i>	121.68 – 2222.22	25	7.5	(Laanbroek et al., 1994; Laanbroek & Gerards, 1993; Park et al., 2010)
Ammonia-oxidizing archaea (non-marine)				
<i>Nitrosoarchaeum koreensis</i>	338.03	25	7.5	(Jung et al., 2011)
Ammonia-oxidizing archaea (marine)				
Mixed culture	995.02	25	7.5	(Park et al., 2010)
<i>Nitrosopumilus maritimus</i>	1619.43	25	7.5	(Martens-Habbena et al., 2009)
Nitrite-oxidizing bacteria (non-marine)				
<i>Nitrobacter hamburgensis</i>	23.34 – 63.06	25	7.5	(Laanbroek et al., 1994)
<i>Nitrobacter winogradskyi</i>	79.71 – 116.31	25	7.5	(Laanbroek & Gerards, 1993)
<i>Nitrospira</i> sp. ND1	0.05 – 0.21	25	8.0	(Ushiki et al., 2017)
<i>Nitrospira japonica</i>	0.05 – 0.21	25	8.0	(Ushiki et al., 2017)
Average values ± Standard deviation (number of samples, n)				
AOB (n = 9)	1045.90 ± 834.92	–	–	–
AOA (n = 4)	984.16 ± 640.77	–	–	–
C-type NOB (n = 7)	171.53 ± 260.28	–	–	–
P-type NOB (n = 2)	1016.36 ± 41.75	–	–	–

Factors: 1.9mgBio(dry)/mg of protein; 194fgBio(dry)/cell; 3gBio(wet)/gBio(dry)

Table A.4. Specific affinity for ammonia ($a^0_{NH_3}$) of ammonia oxidizing bacteria and archaea.

Culture	$a^0_{NH_3}$ (L/g-Bio/h)	T (°C)	pH	References
Ammonia-oxidizing bacteria (non-marine)				
Mixed culture	29.24	20	7.7	(Yoshioka et al., 1982)
<i>Nitrosomonas europaea</i>	3.56 – 38.73	25 – 30	7.5 – 7.8	(Laanbroek et al., 1994; Laanbroek & Gerards, 1993; Martens-Habbena et al., 2009; Park et al., 2010)
<i>Nitrospira</i> sp. 40K1	637.96	22	7.8	(Jiang, 1999)
<i>Nitrospira</i> sp. AF	1384.02	22	7.8	(Jiang, 1999)
<i>Nitrospira</i> sp. B6	628.65	22	7.8	(Jiang, 1999)
<i>Nitrospira</i> sp. L115	688.76	22	7.8	(Jiang, 1999)
<i>Nitrosomonas oligotropha</i>	0.0067 – 0.0618	27 – 30	7.5 – 7.8	(Stehr et al., 1995)
Ammonia-oxidizing bacteria (marine)				
<i>Nitrosococcus oceani</i>	0.0077 – 0.595	?	?	(Martens-Habbena et al., 2009; Ward, 1987)
Ammonia-oxidizing archaea (non-marine)				
<i>Nitrosotenuis uzoensis</i>	105.18 – 125.19	30	7.6	(Kits et al., 2017)
<i>Nitrososphaera gargensis</i>	773.81 – 1350.35	30	7.6	(Kits et al., 2017)
<i>Nitrososphaera vienennensis</i>	913.98 – 1169.59	30	7.6	(Kits et al., 2017)
<i>Nitrosoarchaeum koreensis</i>	2796.85	25	7	(Jung et al., 2011)
Ammonia-oxidizing archaea (marine)				
<i>Nitrosopumilus maritimus</i>	31120.71	30	7.5	(Martens-Habbena et al., 2009)
Complete ammonia-oxidizing bacteria (CMX)				
<i>Nitrospira inopinata</i>	2488.04 – 3558.90	30	7.6	(Kits et al., 2017)
<i>Ca. Nitrospira kreftii</i>	5864.14 – 7415.09	25	7.5	(Sakoula et al., 2021)
Average values ± Standard deviation (number of samples, n)				
AOB (n = 17)	240.00 ± 390.75	–	–	–
AOA (n = 10)	4242.89 ± 9461.33	–	–	–
CMX (n = 2)	4287.66 ± 1765.09	–	–	–

Factors: 1.9mgBio(dry)/mg of protein; 194fgBio(dry)/cell; 3gBio(wet)/gBio(dry); 0.15pg of protein/cell (Button, 1998; González-Cabaleiro et al., 2019)

Table A.5. Specific affinity for nitrite (a^{0NO_2}) of nitrite oxidizing bacteria.

Culture	a^{0NO_2} (L/g-Bio/h)	T (°C)	pH	References
Nitrite-oxidizing bacteria (non-marine)				
<i>Nitrobacter winogradskyi</i>	10.56 – 62.72	23 – 30	7.3 – 7.6	(Both et al., 1992; Nowka et al., 2015; Tsai & Tuovinen, 1985)
<i>Nitrobacter hamburgensis</i>	2.17 – 20.64	25 – 28	7.3 – 7.5	(Both et al., 1992; Laanbroek et al., 1994; Nowka et al., 2015)
<i>Nitrobacter agilis</i>	9.88 – 14.73	20 – 30	6.5 – 8.5	(Tsai & Tuovinen, 1985)
<i>Nitrobacter vulgaris</i>	587.18	28	7.5	(Nowka et al., 2015)
<i>Nitrospira defluvii</i>	935.67	28	7.5	(Nowka et al., 2015)
<i>Nitrospira moscoviensis</i>	350.88	37	7.5	(Nowka et al., 2015)
<i>Nitrospira lenta</i>	129.95	28	7.5	(Nowka et al., 2015)
<i>Nitrospira japonica</i>	543.86	25	8.0	(Ushiki et al., 2017)
<i>Nitrospira sp. ND1</i>	1315.79	25	8.0	(Ushiki et al., 2017)
<i>Ca. Nitrotoga arctica</i>	78.64	17	7.5	(Nowka et al., 2015)
Nitrite-oxidizing bacteria (marine)				
<i>Nitrosococcus mobilis</i>	175.44	28	7.8	(Jacob et al., 2017)
<i>Nitrospira sp. Ecomares</i>	69.53	28	7.8	(Jacob et al., 2017)
<i>Nitrotoga sp. AM1</i>	288.85	16	7.8	(Ishii et al., 2017)
<i>Nitrospina watsonii</i>	345.25	28	7.8	(Jacob et al., 2017)
Average values ± Standard deviation (number of samples, n)				
C-type NOB (n = 23)	74.17 ± 168.81	–	–	–
P-type NOB (n = 7)	527.28 ± 451.01	–	–	–
sP-type NOB (n = 5)	145.76 ± 91.49	–	–	–

Factors: 1.9mgBio(dry)/mg of protein; 194fgBio(dry)/cell; 3gBio(wet)/gBio(dry); 0.15pg of protein/cell (Button, 1998; González-Cabaleiro et al., 2019)

Table A.6. Biomass growth yield (Y_{XS}) of ammonia oxidizing bacteria and archaea.

Culture	Y_{XS} (g-Bio/g-NH ₃)	T (°C)	pH	References
Ammonia-oxidizing bacteria (non-marine)				
Mixed culture	0.0329 – 0.0107	21 – 25	7.0 – 8.5	(Jubany et al., 2008; Sharma & Ahler, 1976)
<i>Nitrosospira sp. 40K1</i>	0.0326	22	7.8	(Jiang, 1999)
<i>Nitrosospira sp. AF</i>	0.0127	22	7.8	(Jiang, 1999)
<i>Nitrosospira sp. B6</i>	0.0507	22	7.8	(Jiang, 1999)
<i>Nitrosospira sp. L115</i>	0.0489	22	7.8	(Jiang, 1999)
<i>Nitrosomonas europaea</i>	0.052 – 0.084	30	8.0	(Bruijn et al., 1995; Keen & Prosser, 1987; Kits et al., 2017)
Ammonia-oxidizing bacteria (marine)				
<i>Nitrosococcus oceani</i>	0.081, 0.047	28 – 30	7.5	(Kits et al., 2017; Könneke et al., 2014)
Ammonia-oxidizing archaea (non-marine)				
<i>Nitrososphaera gargensis</i>	0.096 – 0.109	30	7.6	(Kits et al., 2017)
<i>Nitrososphaera vienennsis</i>	0.096 – 0.103	30	7.6	(Kits et al., 2017)
Ammonia-oxidizing archaea (marine)				
<i>Nitrosopumilus maritimus</i>	0.068 – 0.092	28 – 30	7.5 – 7.8	(Könneke et al., 2014; Martens-Habbena et al., 2009; Qin et al., 2017)
<i>Nitrosopumilus piranensis</i>	0.0744	32.5	7.1	(Bayer et al., 2015)
<i>Nitrosopumilus adriaticus</i>	0.081	30	7.1	(Bayer et al., 2015)
Complete ammonia-oxidizing bacteria (CMX)				
<i>Nitrospira inopinata</i>	0.125 – 0.137	30	7.6	(Kits et al., 2017)
Average values ± Standard deviation (number of samples, n)				
AOB (n = 9)	0.054 ± 0.024	–	–	–
AOA (n = 9)	0.088 ± 0.014	–	–	–

Factors: 1.9mgBio(dry)/mg of protein; 194fgBio(dry)/cell; 3gBio(wet)/gBio(dry); 1.416gCOD/gBio; 0.4gBio(D)/L/OD₆₀₀ (Button, 1998; González-Cabaleiro et al., 2019; F. Li et al., 2018)

Table A.7. Biomass growth yield (Y_{XS}) of nitrite oxidizing bacteria.

Culture	Y_{XS} (g-Bio/g-NO ₂)	T (°C)	pH	References
Nitrite-oxidizing bacteria (non-marine)				
<i>Nitrospira japonica</i>	0.043	25	8.0	(Ushiki et al., 2017)
<i>Nitrobacter agilis</i>	0.0126	30	8.0	(Hunik et al., 1994)
<i>Nitrobacter winogradskyi</i>	0.0103	28	7.5	(Nowka et al., 2015)
<i>Nitrospira sp.</i> ND1	0.0258	25	8.0	(Ushiki et al., 2017)
<i>Nitrospira moscoviensis</i>	0.0149 – 0.0264	37	7.5 – 8.6	(Ehrich et al., 1995; Nowka et al., 2015)
<i>Nitrobacter hamburgensis</i>	0.0133 – 0.0266	28 – 30	7.5 – 7.8	(Nowka et al., 2015; Starkenburg, Arp, et al., 2008)
<i>Nitrospira lenta</i>	0.0158	38	7.5	(Nowka et al., 2015)
<i>Nitrospira defluvii</i>	0.0151	28	7.5	(Nowka et al., 2015)
<i>Ca. Nitrotoga arctica</i>	0.0126	17	7.5	(Nowka et al., 2015)
<i>Nitrobacter vulgaris</i>	0.0123	28	7.5	(Nowka et al., 2015)
Nitrite-oxidizing bacteria (marine)				
<i>Nitrospira watsonii</i>	0.0273	28	?	(Spieck et al., 2014)
<i>Nitrospira sp.</i> Ecomares	0.0074 – 0.0372	25	7.0 – 7.5	(Keuter, 2011)
<i>Nitrospira marina</i>	0.005 – 0.0119	28	7.6 – 8.0	(Watson et al., 1986)
Average values ± Standard deviation (number of samples, n)				
C-type NOB (n = 10)	0.022 ± 0.012	–	–	–
P-type NOB (n = 11)	0.021 ± 0.012	–	–	–

⁽¹⁾Theoretical value. Maximum growth yield

⁽²⁾ See Supplementary text – Materials and Methods. OMZ: Oxygen Minimum Zone

Factors: 1.9mgBio(dry)/mg of protein; 194fgBio(dry)/cell; 3gBio(wet)/gBio(dry); 1.416gCOD/gBio (Button, 1998; González-Cabaleiro et al., 2019; F. Li et al., 2018)

Table A.8. Inventory of the terminal oxidases of ammonia and nitrite oxidisers. The presence of terminal oxidase in each nitrifier groups is indicated with their references.

Terminal oxidase	AOB	AOA	NOB		
			Nitrobacter	Nitrospira	Nitrospina
Cytochrome c oxidase aa ₃	[1]	[2]	[3]		
Putative cytochrome <i>bd</i> -like				[4]	
Cytochrome c oxidase cbb ₃	[5] ⁽¹⁾				[4]

[1] References: (Sedlacek et al., 2019; Thandar et al., 2016; Whittaker et al., 2000)

[2] References: (Schäfer & Penefsky, 2008; Walker et al., 2010)

[3] References: (Nomoto et al., 1993; Starkenburg et al., 2006; Tanaka et al., 1983)

[4] References: (Lücker et al., 2010)

[5] References: (Sedlacek et al., 2019)

⁽¹⁾ Isolated only in *Nitrosomonas eutropha* and *Nitrosomonas* cluster 7 strain GH22

Table A.9. Intrinsic half-saturation constant for oxygen (K_{O_2}) of terminal oxidases isolated in nitrifiers.

Terminal oxidase	$E^{(1)}$ (μM)	$M^{(2)}$ (μM)	$L^{(3)}$ (nM)	References
Cytochrome c oxidase aa ₃	0.97 – 5.00	ND ⁽⁴⁾	50 – 62	[1]
Putative cytochrome <i>bd</i> -like	0.27 – 4.00	0.27 – 0.41	8 – 24	[2]
Cytochrome c oxidase cbb ₃	0.08 – 0.98	0.011 – 0.151	4 – 7	[3]

⁽¹⁾ Method to determine K_{O_2} : Oxygen electrode method. Cultures: *P. aeruginosa*, *B. cereus*, *E. coli*, *A. vinelandii*. *B. japonicum* and mitochondrial c. aa₃. ⁽²⁾ Method to determine K_{O_2} : Deoxygenation kinetics of oxymyoglobin. Cultures: *P. aeruginosa*, *A. vinelandii* and *Rhizobium spp.* ⁽³⁾ Method to determine K_{O_2} : Deoxygenation kinetics of oxyleghemoglobin. Cultures: *B. japonicum*, *K. pneumoniae*, *E. coli*, mitochondrial c. aa₃, *A. vinelandii*, *P. aeruginosa* and *Bradyrhizobium spp.* ⁽⁴⁾ ND, not determined

[1] References: (Arai et al., 2014; Cooper et al., 2003; Garcia-Horsman et al., 1991; Preisig et al., 1996)

[2] References: (Arai et al., 2014; Belevich et al., 2007; Belevich et al., 2005; D'Mello et al., 1994; D'Mello et al., 1996; Kita et al., 1984; Kolonay et al., 1994; Mason et al., 2009; Rice & Hempfling, 1978; Smith et al., 1990)

[3] References: (Arai et al., 2014; Bergersen & Turner, 1980; Hirai et al., 2016; Preisig et al., 1996)

Table A.10. References of apparent substrate affinity ($K_{m(app)}$) for O_2 of nitrite-oxidizing bacteria (NOB).

Genera	Growth measurements	Activity measurements
<i>Nitrobacter</i>	(Blackburne et al., 2008; Hunik et al., 1994; Ohgaki & Wantawin, 1989; Wiesmann, 1994)	(Boon & Laudelout, 1960; Laanbroek et al., 1994; Laanbroek & Gerards, 1993)
<i>Nitrospira</i>	(Park et al., 2017)	(Ushiki et al., 2017)
<i>Nitrospina</i>	ND ⁽⁴⁾	(Bristow et al., 2016)

⁽⁴⁾ ND, not determined

Table A.11. Summary and description of the data collected from literature of considered ammonia oxidizers. References are provided in Supplementary Tables.

	C [†]	Growth rate (μ_{max})			Ammonia affinity (a^{NH_3})			Oxygen affinity (a^{O_2})			Growth yield (Y_{XS})						
		n [‡]	SO [†]	M [§]	TI [¶]	n	SO	M	I	n	SO	M	I				
Ammonia-oxidizing bacteria (non-marine)																	
Mixed culture (Mx AOB-FW)	Mx	6	N, W	R, CO, M	S	8	N, W	R, M, D	S	7	W	R, M, B	S	7	N, W	D, B, M, R	S
<i>Nitrosomonas europaea</i>	P	7	N	B, D, P	S	6	N, W	P, D, B	S	11	N, W	R, P, M	S	3	N	D, B, E	S
<i>Nitrosomonas oligotropha</i>	E, P	3	N	P, R	S	2	N	P, R	S	3	N, W	R, B	S	0			
<i>Nitrosospira sp. 40K1</i>	P	1	N	D	S	1	N	D	S	0				1	N	D	S
<i>Nitrosospira sp. AF</i>	P	1	N	D	S	1	N	D	S	0				1	N	D	S
<i>Nitrosospira sp. B6</i>	P	1	W	D	S	1	W	D	S	0				1	W	D	S
<i>Nitrosospira sp. L115</i>	P	1	N	D	S	1	N	D	S	0				1	N	D	S
Ammonia-oxidizing bacteria (marine)																	
Mixed culture (Mx AOB-SW)	Mx	3	N	M	WM	3	N	M	WM	0				0			
<i>Nitrosomonas marina</i>	P	1	N	B	S	0				0				0			
<i>Nitrosococcus oceanii</i>	P	1	N	B	S	4	N	B	S	0				2	N	D, B	S
Ammonia-oxidizing archaea (non-marine)																	
Mixed culture (Mx AOA-FW)	Mx	2	N	P	S	2	N	R	S	1	N	R	S	0			
<i>Nitrososphaera koreensis</i>	E	1	N	R, P	S	1	N	R	S	1	N	R	S	0			
<i>Nitrososphaera viennensis</i>	P	1	N	P	S	3	N	R	S	1	N	R	S	4	N	PC	S
<i>Nitrososphaera gargensis</i>	P	1	N	P	S	2	N	R	S	0				4	N	PC	S
<i>Nitrosotenus uzoensis</i>	E	0				2	N	R	S	0				0			
Ammonia-oxidizing archaea (marine)																	
Mixed culture (Mx AOA-SW)	Mx	4	N	R, P	NM	1	N	R	NM	1	N	R	NM	0			
Mixed culture from OMZ ^(*)	Mx	0				0				2	N	R	NM	0			
<i>Nitrosopumilus maritimus</i>	P	3	N	R	S	2	N	R, B	S	2	N	R	S	3	N	D, E	S
<i>Nitrosopumilus piranensis</i>	E	1	N	E	S	0				0				1	N	E	S
<i>Nitrosopumilus adriaticus</i>	E	1	N	E	S	0				0				1	N	E	S
Complete ammonia-oxidizing bacteria (CMX)																	
<i>Nitrospira inopinata</i>	P	1	N	P	S	1	N	R	S	0				4	N	PC	S
<i>Ca. Nitrospira kreftlii</i>	E	0				1	N	R	S	0				0			

† C = Culture type; Mx – Mixed culture; P – Pure culture; E – Enriched culture

‡ n = Number of parameters

§ SO = Sample origin; N – Natural environment; W – Wastewater treatment plant

¶ M = Experimental method; R – Respirometry; D – Cell density/Cell count; CO – Maximum CO₂ uptake rate; M – Model; B – Biolography; P – Product/substrate rates or log plot; PC – Protein content; E – Estimated ($\Upsilon_{NS} = \Delta XVAS$)

TI = Medium; S – Synthetic medium; NM – Natural medium; WM – Real wastewater

(*) OMZ: Oxygen Minimum Zone

Table A.12. Summary and description of the data collected from literature of considered nitrite oxidizers. References are provided in Supplementary Tables.

	C [†]	Growth rate (µmax)			Nitrite affinity (a ^{NO2})			Oxygen affinity (a ^{O2})			Growth yield (Y _{xs})						
		n [†]	SO [†]	M [‡]	n	SO	M	n	SO	M	n	SO	M				
Nitrite-oxidizing bacteria (non-marine)																	
Mixed culture (Mx NOB-FW)	Mx	5	N, W	M, D	S	5	N, W	R, D, M	S	13	N, W	M, B, R	S	6	N, W	M, D, B	S
<i>Nitrobacter vulgaris</i>	P	2	W	D	S	1	W	R	S	0				1	W	PC	S
<i>Nitrospira sp.</i> ND1	P	1	W	D	S	1	W	P	S	2	W	R	S	2	W	E	S
<i>Nitrospira japonica</i>	P	1	W	D	S	1	W	P	S	2	W	R	S	1	W	E	S
<i>Ca. Nitotoga arctica</i>	P	1	N	D	S	0			S	0				1	N	PC	S
<i>Nitrobacter agilis</i>	P	2	W	M	S	18	N, W	R	S	2	N, W	B, M	S	1	N	M	S
<i>Nitrobacter winogradskyi</i>	P	6	N	D, M	S	10	N, W	M, R	S	2	N, W	R, P	S	2	N, W	PC, M	S
<i>Nitrospira deflavii</i>	P	1	W	D	S	1	W	R	S	0				1	W	PC	S
<i>Nitrospira lentia</i> ^(c)	P	1	W	D	S	0			S	0				1	W	PC	S
<i>Nitrospira moscovensis</i>	P	2	N, W	D, M	S	1	N, W	M, R	S	0				2	N	PC, E	S
<i>Nitrobacter hamburgensis</i>	P	5	N	D	S	5	N	R	S	2	N	R	S	2	N	PC, E	S
Nitrite-oxidizing bacteria (marine)																	
Mixed culture (Mx NOB-SW)	Mx	0				0				1	W	R	S	0			
<i>Nitrococcus mobilis</i>	P	2	N	D	S	2	N	R	S	0				0			
<i>Nitrotoga sp.</i> AM1	E	1	N	D	S	0				0				0			
<i>Nitrospira marina</i>	P	1	N	D	S	0				0				1	N	E	S
<i>Nitrospira gracilis</i>	P	1	N	D	S	0				0				0			
<i>Nitrospira watsonii</i>	E	1	N	D	S	2	N	R	S	0				1	N	E	S
<i>Nitrospinae</i> phyl. from OMZ ^(d)	Mx	2	N	D	NM	2	N	M	NM	2	N	R	NM	0			
<i>Nitrospira sp.</i> Ecomares	P	2	W	D	NM	2	W	R	S	0				2	W	D, E	NM

[†] C = Culture type; Mx – Mixed culture; P – Pure culture; E – Enriched culture

[‡] n = Number of parameters

[§] SO = Sample origin; N – Natural environment; W – Wastewater treatment plant

[¶] M = Experimental method; R – Respirometry; D – Cell density/Cell count; CO – Maximum CO₂ uptake rate; M – Model; B – Bibliography; P – Product substrate rates or log plot; PC – Protein content; E – Estimated (Y_{xs} = ΔX/ΔS)

^{||} I = Medium; S – Synthetic medium; NM – Natural medium; WM – Real wastewater

^(d) OMZ: Oxygen Minimum Zone

Supplementary Figures

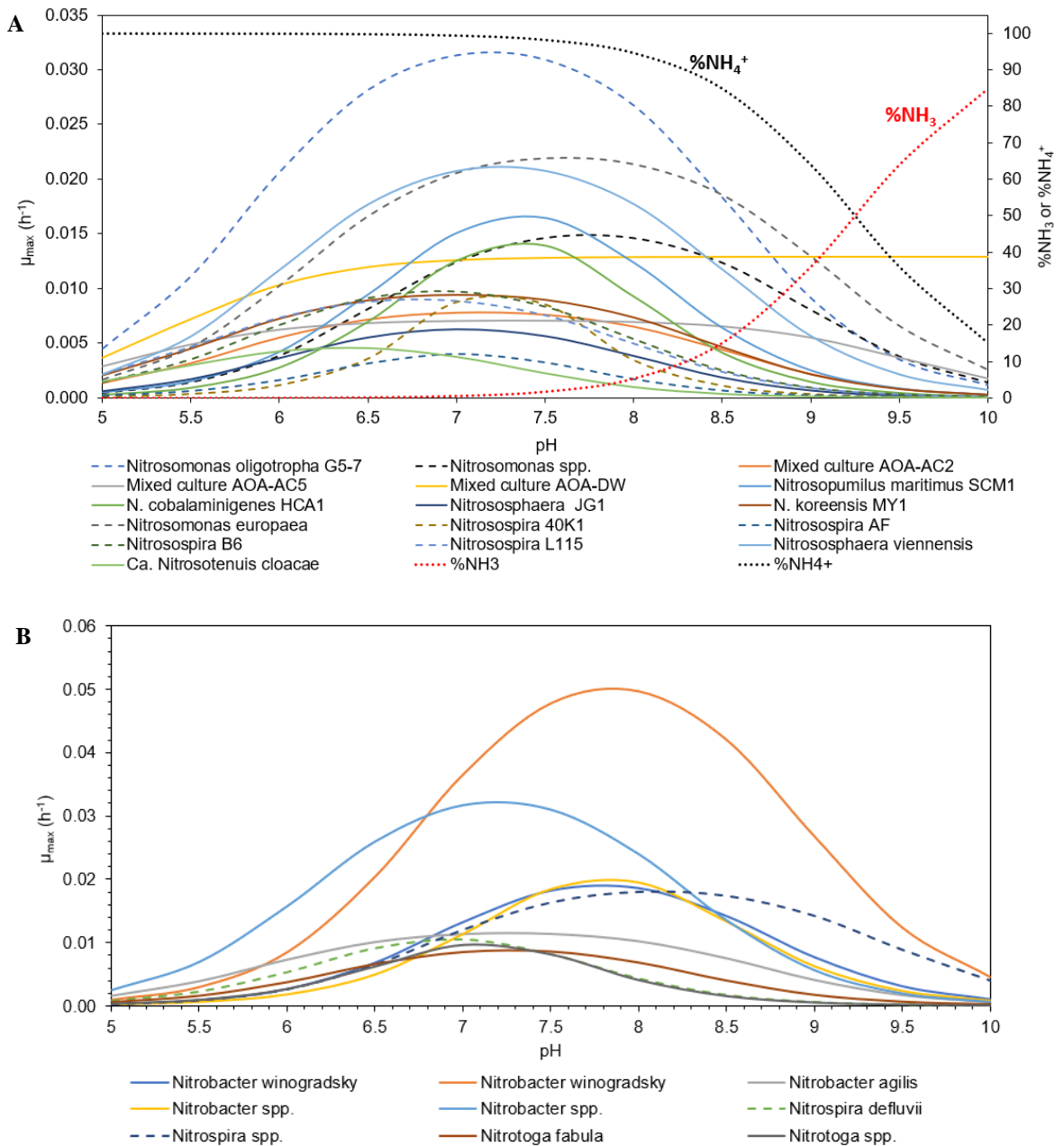


Figure A.1. **A)** Maximum specific growth rate of (μ_{max}) of AOB and AOA as a function of the pH. Dashed lines represent AOA and solid lines represent AOB. Dotted red line represents the percentage of free ammonia (NH₃) and dotted black line represents the percentage of ammonium (NH₄⁺) in function of pH. References: (Anthonisen et al., 1976; Antoniou et al., 1990; French et al., 2012; Jiang, 1999; Jung et al., 2011; Kim et al., 2012; Li et al., 2016; Qin et al., 2014; Tourna et al., 2011). **B)** Maximum specific growth rate of (μ_{max}) of NOB as function of the pH. Dashed lines represent species belonging of genus Nitrospira and solid lines represent species belonging of genus Nitrobacter. References: (Blackburne et al., 2007a, 2007b; Boon & Laudelout, 1960; Hunik et al., 1993; Keen & Prosser, 1987; Kitzing et al., 2018; Wegen et al., 2019; Zhang et al., 2018).

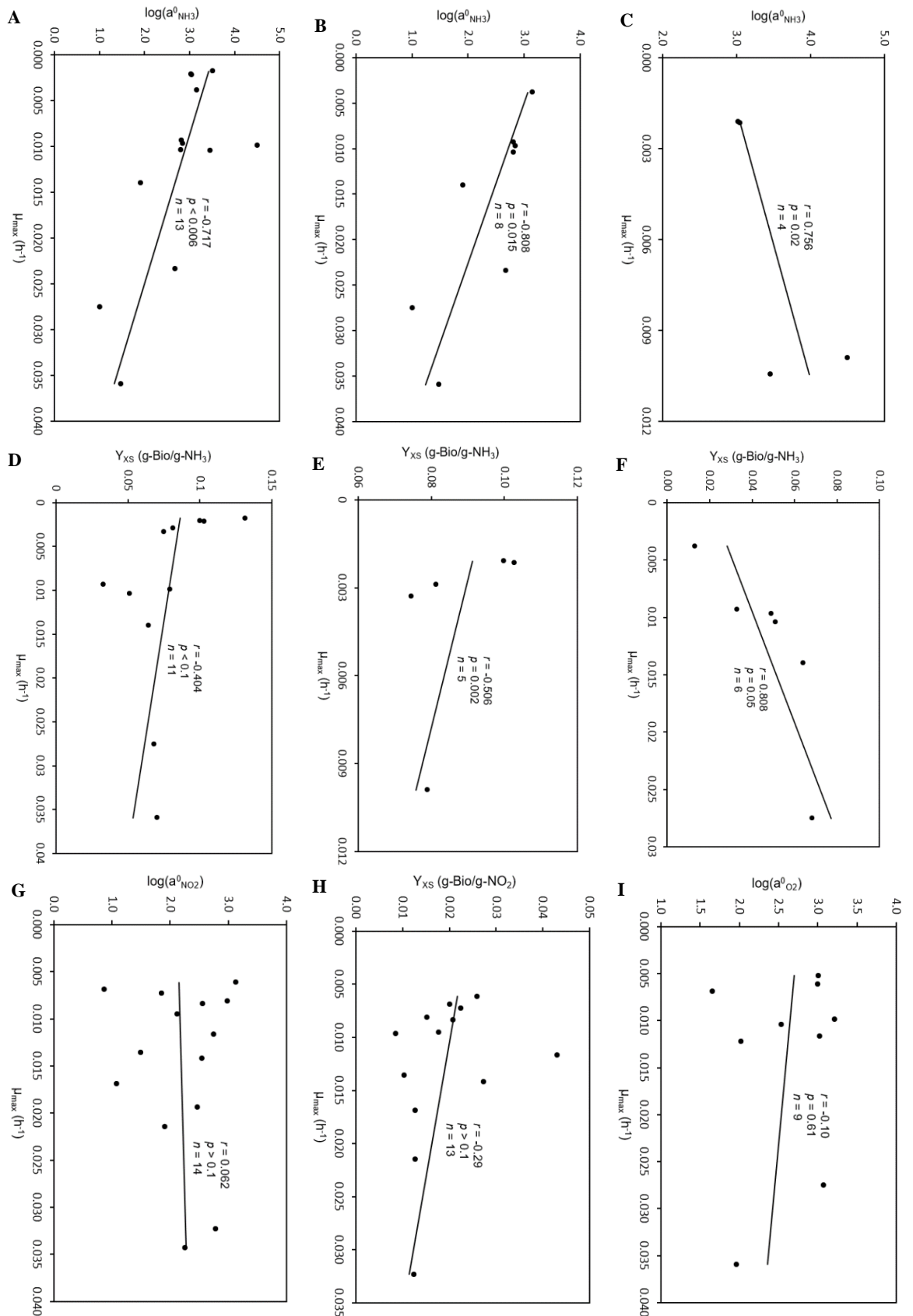


Figure A.2. Regression fits to different kinetic datasets of nitrifiers and their corresponding Pearson correlation coefficient (r) with significance (p value) and sample size (n). **A** μ_{max} versus $a^0_{NH_3}$ of AOB, AOA and CMX **B** μ_{max} versus $a^0_{NH_3}$ of AOB only **C** μ_{max} versus $a^0_{NH_3}$ of AOA only **D** μ_{max} versus Y_{XS} of AOB, AOA and CMX (excluding acidophilic AOB) **E** μ_{max} versus Y_{XS} of AOA only **F** μ_{max} versus Y_{XS} of AOB only **G** μ_{max} versus $a^0_{NO_2}$ of NOB **H** μ_{max} versus Y_{XS} of NOB **I** μ_{max} versus $a^0_{NO_2}$ of AOB, AOA and NOB.

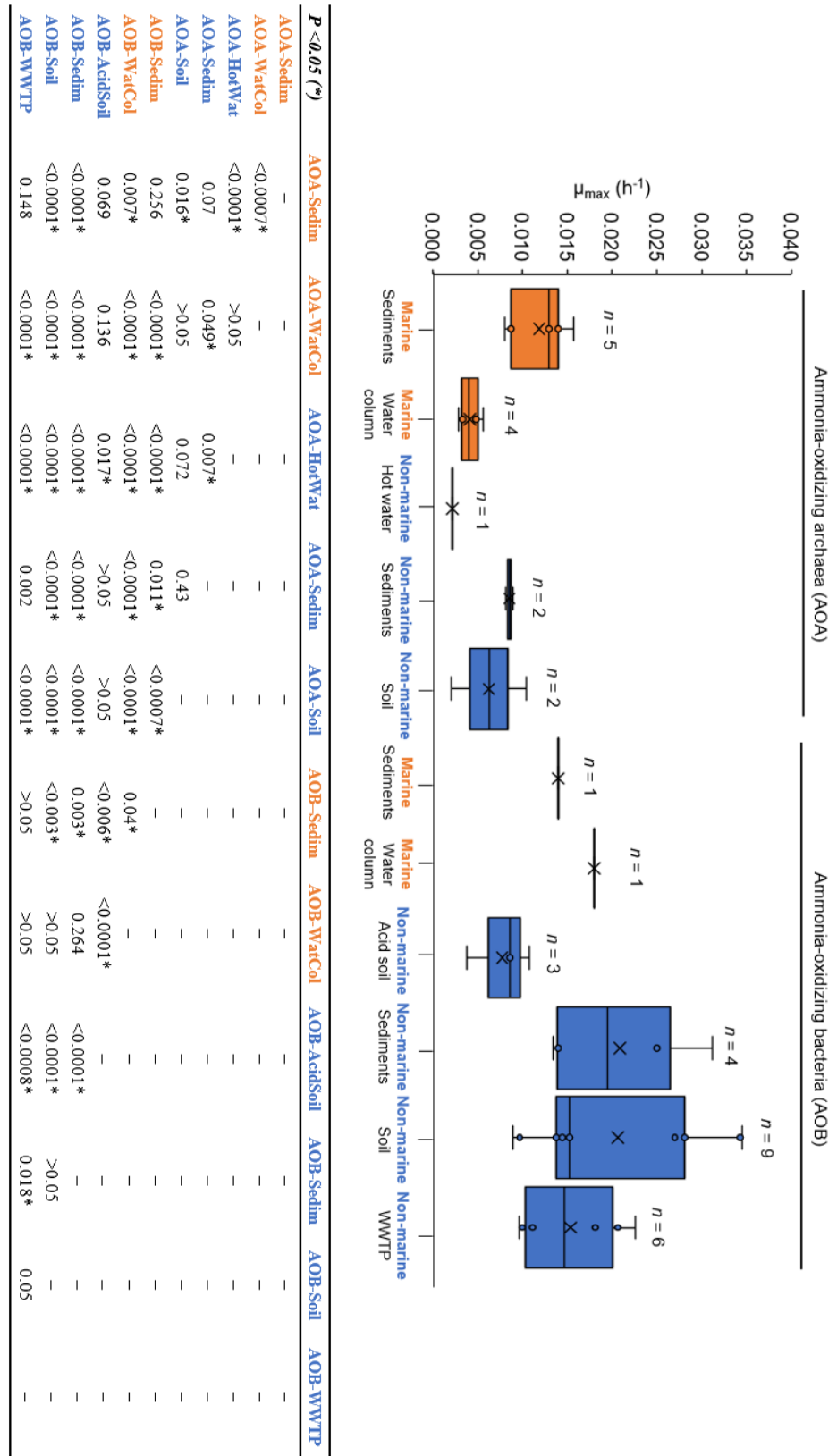


Figure A.3. AOB and AOA maximum growth rates (μ_{max}) from distinct environments. *P*-values (One-way ANOVA) between environments on bottom table. Number of bibliographic data is indicated above each boxplot. Boxplots depict the 75-100% quantile range, with the centre line depicting the median (50% quantile) and crosses depicting the average value. Data of each environment are shown as points. Table legend: Sedim – Sediments; WatCol – Water column; HotWat – Hot water; AcidSoil – Acidic soil; WWTP – Wastewater Treatment Plant.

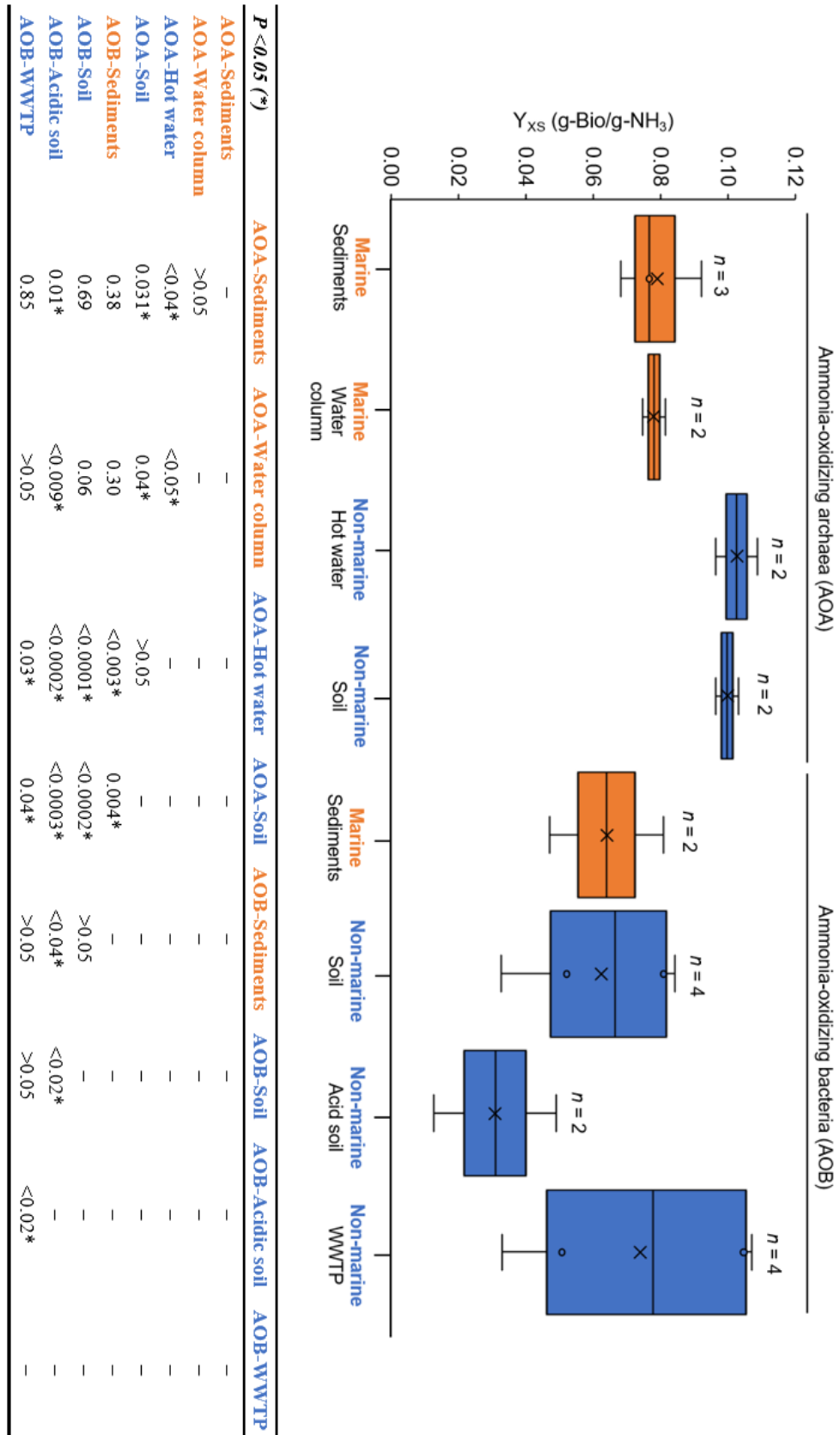


Figure A.4. AOB and AOA growth yields (Y_{XS}) from distinct environments. *P*-values (One-way ANOVA) between environments on bottom table. Number of bibliographic data is indicated above each boxplot. Boxplots depict the 75-100% quantile range, with the centre line depicting the median (50% quantile) and crosses depicting the average value. Data of each environment are shown as points. Table legend: WWTP – Wastewater Treatment Plant.

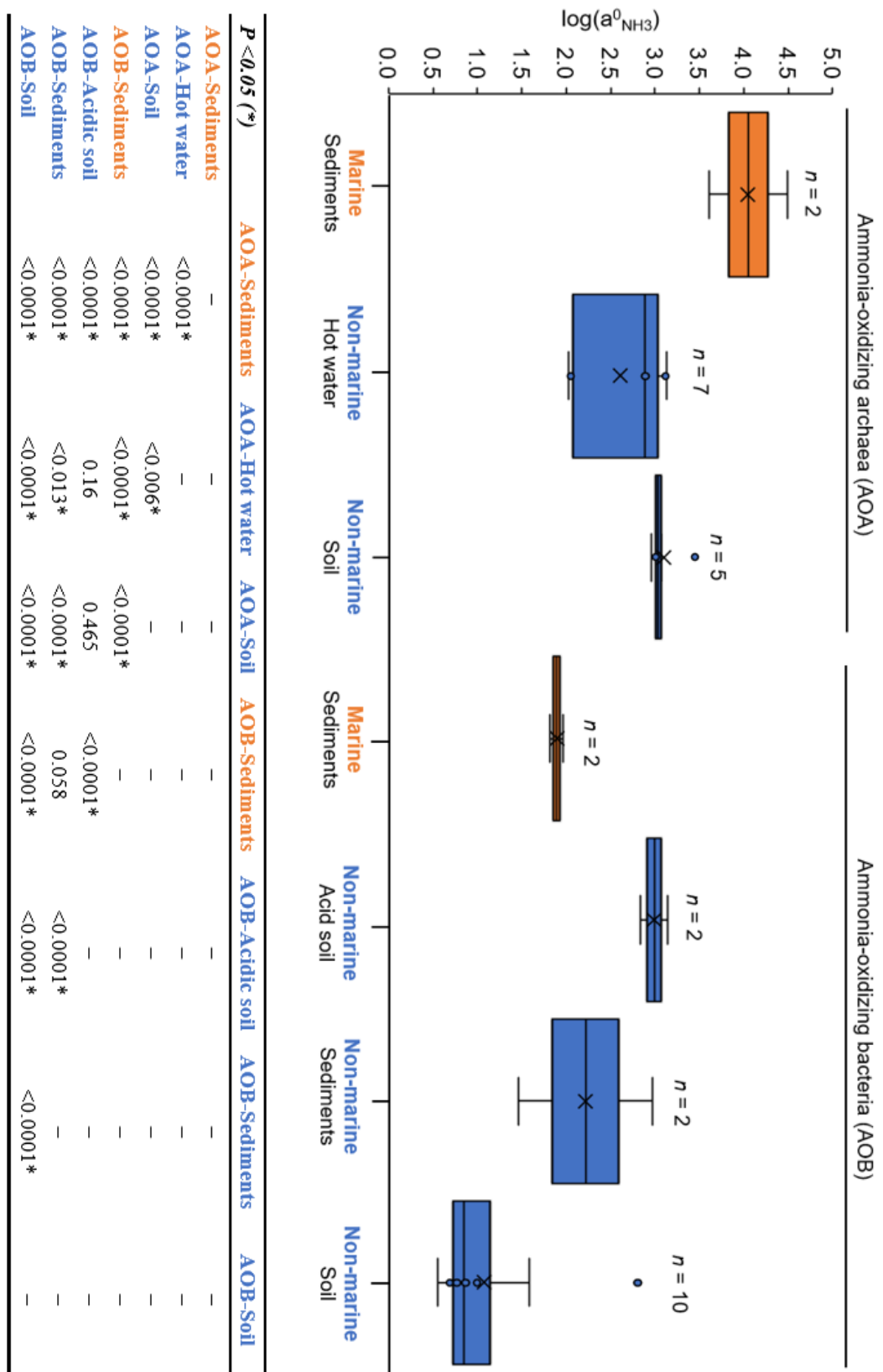


Figure A.5. AOB and AOA specific affinity for ammonia ($a^0_{NH_3}$) from distinct environments. *P*-values (One-way ANOVA) between environments on bottom table. Number of bibliographic data is indicated above each boxplot. Boxplots depict the 75-100% quantile range, with the centre line depicting the median (50% quantile) and crosses depicting the average value. Data of each environment are shown as points. Values of $a^0_{NH_3}$ were \log_{10} transformed before statistical analysis due to the order of magnitude difference in the determined values.

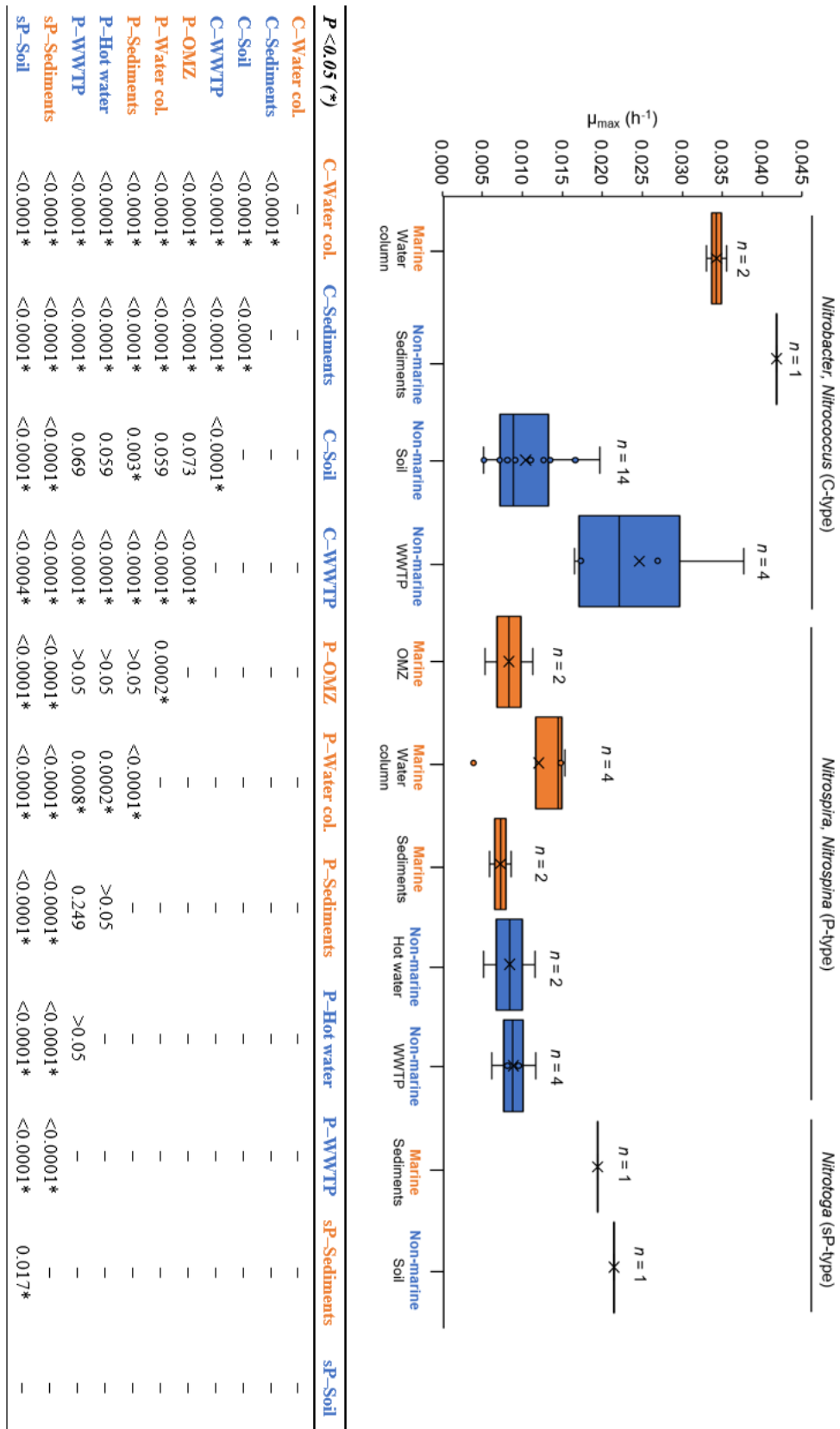


Figure A.6. NOB maximum growth rates (μ_{max}) from distinct environments. P-values (One-way ANOVA) between environments on bottom table. Number of bibliographic data is indicated above each boxplot. Boxplots depict the 75-100% quantile range, with the centre line depicting the median (50% quantile) and crosses depicting the average value. Data of each environment are shown as points. Table legend: OMZ – Oxygen Minimum Zone; Water col. – Water column; WWTP – Wastewater Treatment Plant.

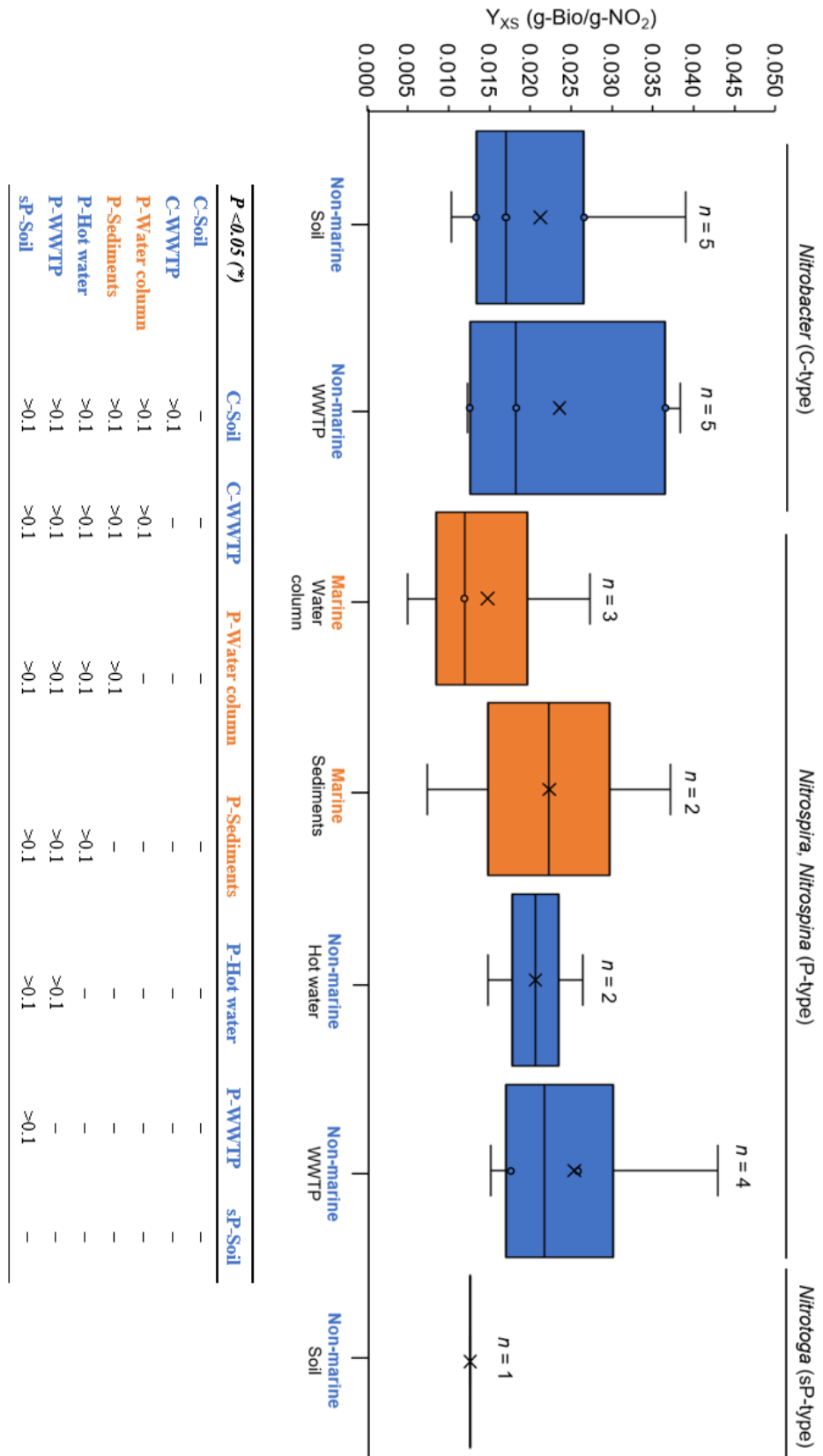


Figure A.7. NOB growth yields (Y_{xs}) from distinct environments. P-values (One-way ANOVA) between environments on bottom table. Number of bibliographic data is indicated above each boxplot. Boxplots depict the 75-100% quantile range, with the centre line depicting the median (50% quantile) and crosses depicting the average value. Data of each environment are shown as points. Table legend: WWTP – Wastewater Treatment Plant.

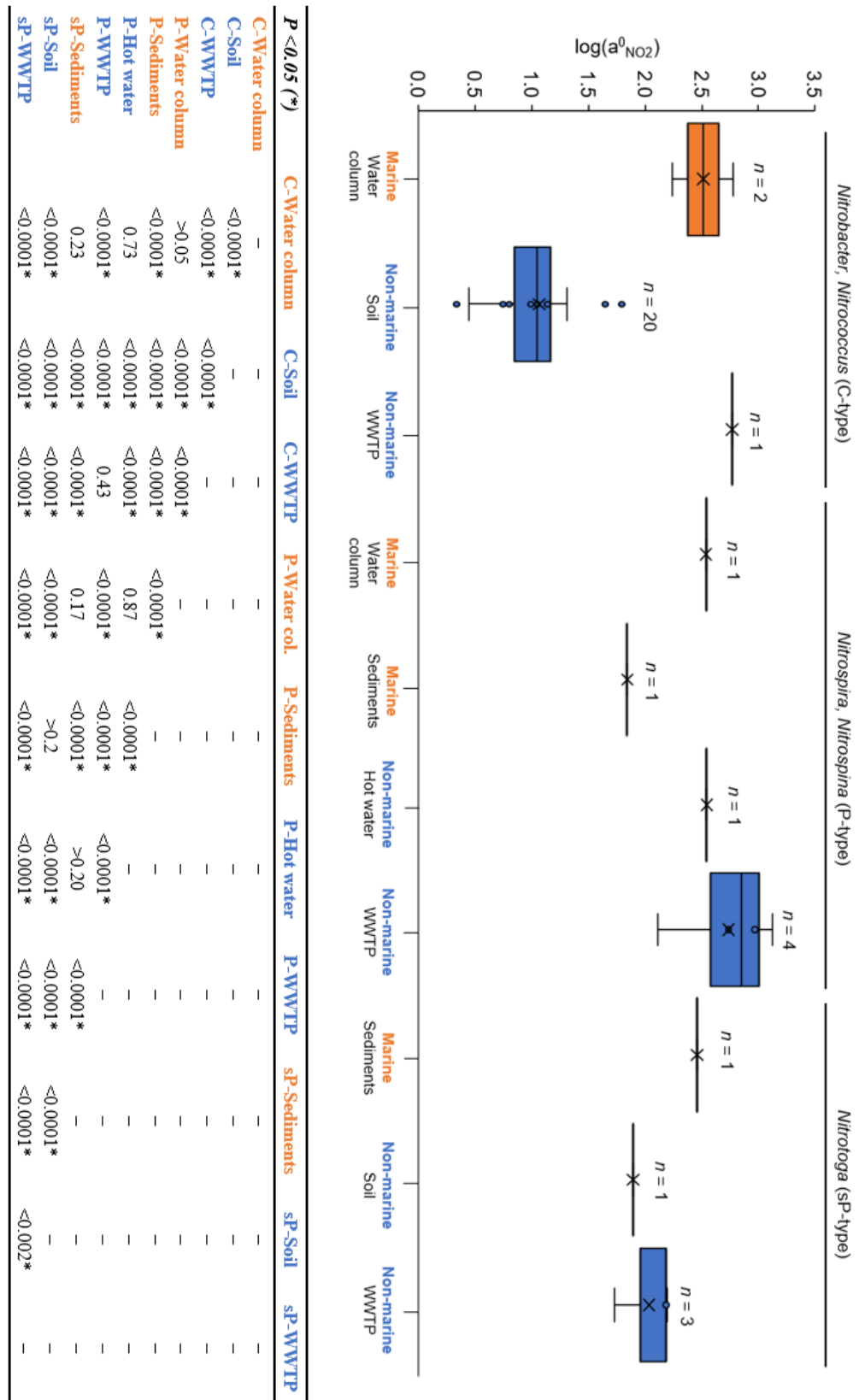


Figure A.8. NOB specific affinity for nitrite ($a^0_{NO_2}$) from distinct environments. P-values (One-way ANOVA) between environments on bottom table. Number of bibliographic data is indicated above each boxplot. Boxplots depict the 75-100% quantile range, with the centre line depicting the median (50% quantile) and crosses depicting the average value. Data of each environment are shown as points. Values of $a^0_{NO_2}$ were log10 transformed before statistical analysis due to the order of magnitude difference in the determined values. Table legend: WWTP – Wastewater Treatment Plant.

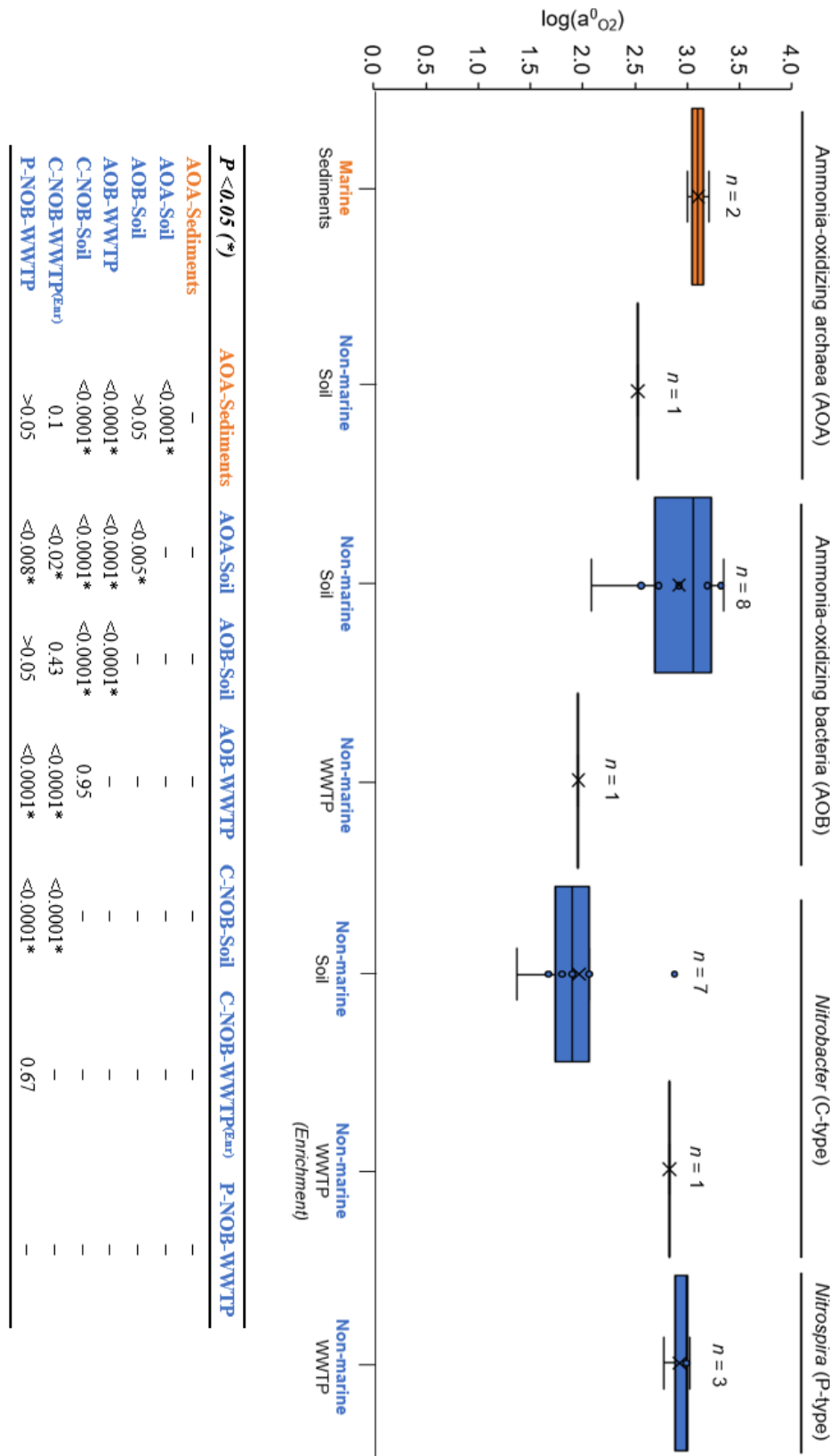


Figure A.9. AOB, AOA and NOB specific affinity for oxygen ($a^0_{O_2}$) from distinct environments. *P*-values (One-way ANOVA) between environments on bottom table. Number of bibliographic data is indicated above each boxplot. Boxplots depict the 75-100% quantile range, with the centre line depicting the median (50% quantile) and crosses depicting the average value. Data of each environment are shown as points. Values of $a^0_{NO_2}$ were \log_{10} transformed before statistical analysis due to the order of magnitude difference in the determined values. Table legend: WWTP – Wastewater Treatment Plant.

Appendix B - Chapter 5

Contents

Quadtree algorithm

Definition of diffusion and no-diffusion regions

Integration algorithm

Rearrangement of diffusion-reaction equation in matrixial form

Deduction of RES equation

Quadtree algorithm

Overlap detection and shoving computation between microbes could be an expensive operation. If a rough overlap algorithm (*i.e.*, comparing each pair of microbes) is applied in an aggregate with 1000 microbes, it would require 1×10^6 operations (*i.e.*, time complexity of $O(n^2)$). To improve shoving computation, the number of checks should be reduced. Two microbes that are at opposite sites on aggregate (or far enough) cannot possibly overlap, so there is no need to check for an overlap between them. Here is where *quadtree* comes into play. Applying quadtree in overlap detection and shoving computation the number of checks is reduced significantly, turning the time complexity from $O(n^2)$ to $O(n \log n)$.

Quadtree is a tree data structure in which an internal node is sectioned in four child nodes, and each of those children could potentially be sectioned into four. Basically, quadtrees are used to split a 2D regional space by recursively subdividing it into four regions. In this case, the number of microbes in each subregion dictates if these regions must be divided or not – if a specific region holds a higher number of microbes than the maximum number (so-called *capacity*), then this region will be divided into four new regions. Figure B.1 shows an example of how quadtree works in a system in which it has a *capacity* of one microbe (*i.e.*, only one microbe per region).

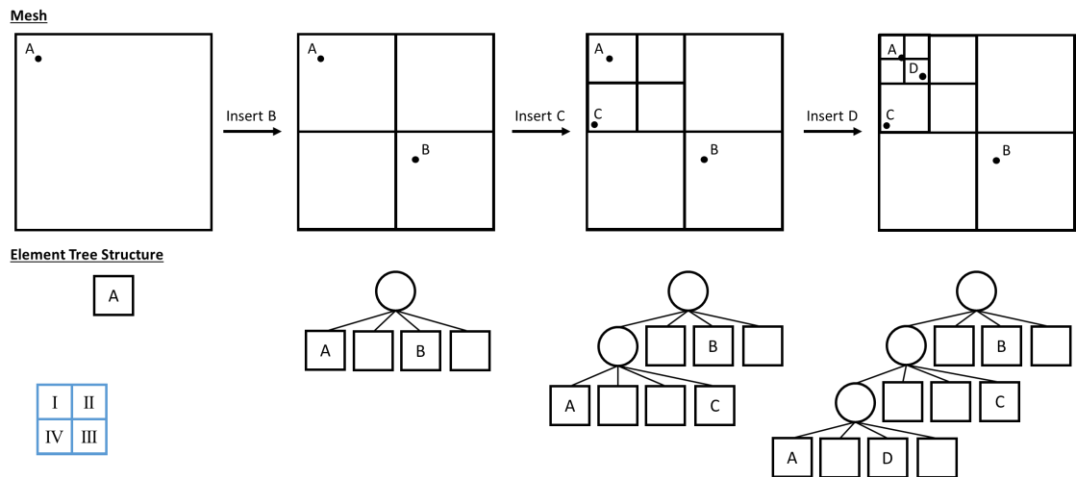


Figure B.1. Quadtree representation (capacity = 1). Each circle represents a microbe in the system. Subregions are labelled clockwise (see blue grid on bottom-left of figure).

Once understood how quadtree is created (mesh and data structure), it is time to figure out how quadtree plays in shoving algorithm. First, it is necessary to create a new quadtree mesh and tree data structure (Figure B.2). Every time that a division occurs, quadtree must be updated for the new microbes and their locations. Afterwards, each microbe is *inserted* on quadtree, that is, it is set in a specific region (or node).

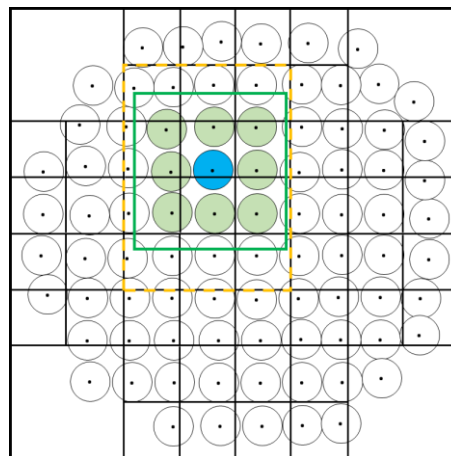


Figure B.2. Selection of neighbours (green circles) of microbe *m* (blue circle). The centre of circle (black dot) indicates the exact position of microbe. In this example, quadtree capacity is 4 (i.e., maximum 4 microbes per region). Green square represents the neighbourhood zone of microbe *m* (blue circle), and dashed orange square shows all regions that intersect with the neighbourhood zone of microbe *m*.

Before executing the overlap detection, the neighbours of all microbes are established. For that, it is firstly created a *neighbourhood zone* that surrounds each microbe (i.e., microbe is on the centre of neighbourhood zone). As the quadtree is not updated after every shoving

step, the *neighbourhood zone* is set to 4 times the maximum radius of microbes. Then, for each microbe, the regions (or subregions) which intersects with its *neighbourhood zone* are selected and, subsequently, it is evaluated whether microbes located in those intersect regions are within the neighbourhood zone or not (Figure B.2).

Finally, overlap assessment and shoving estimation (if needed) are only performed over the neighbour individuals (Eqs. 5.8 – 5.13). Because bacteria are not motile and, therefore, will not move very far from the original position, it is assumed that chosen neighbouring bacteria stay constant. An overview of the shoving algorithm is presented in Figure B.3.

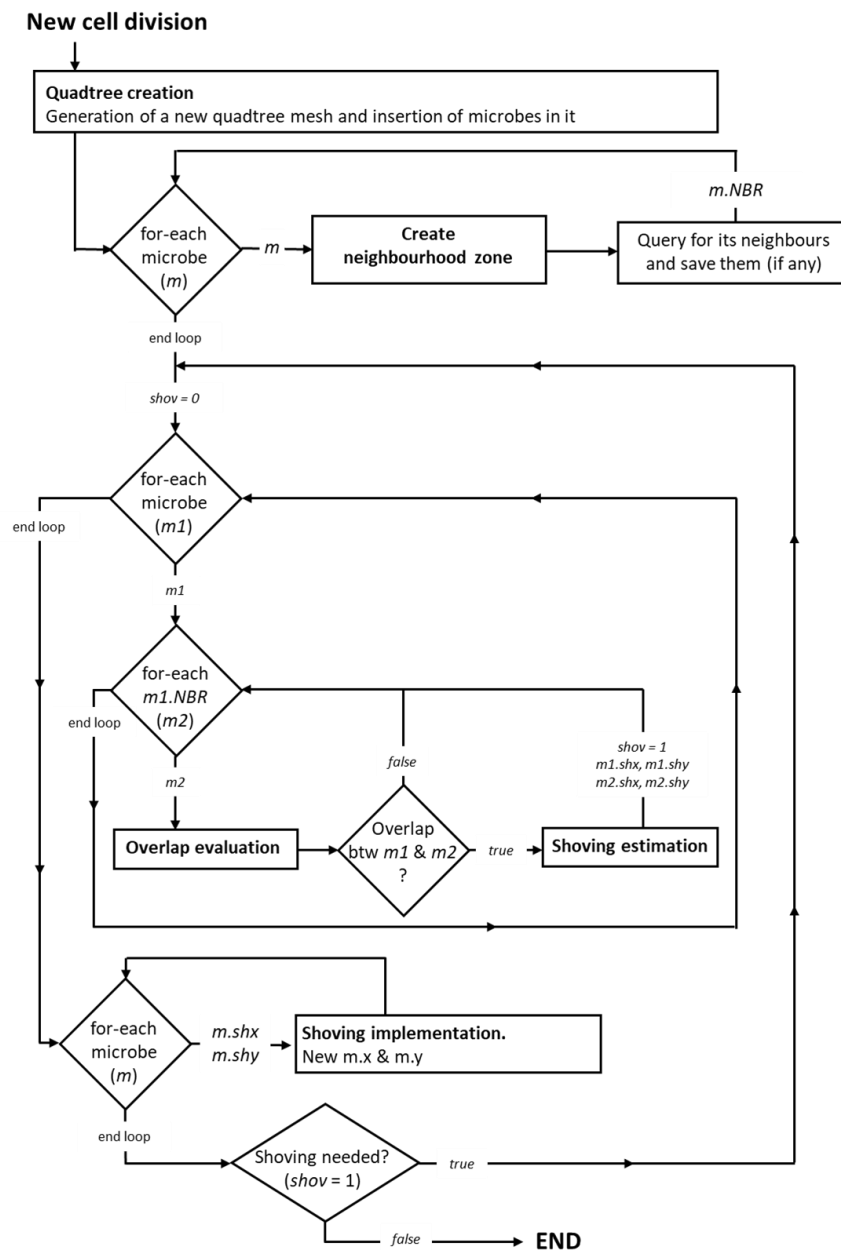


Figure B.3. Scheme of shoving algorithm. Legend: $m.shx$ and $m.shy$ – displacement of microbe m due to shoving of the others; $m.NBR$ – neighbours of microbe m .

Definition of diffusion and no-diffusion regions

The diffusion region, where diffusion-reaction equation is solved, comprises the aggregate region and boundary layer. The aggregate region corresponds to cells in which bacteria are growing. Boundary layer is the region of grid cells in the immediate vicinity of boundary layer.

The distinction of the diffusion region starts with the detection of which nodes are potentially in this region, creating a preliminary diffusion region (Figure B.4A). For that, the minimum and maximum position of microbes on domain in coordinate x and y plus the boundary layer thickness are considered. The computational cost is reduced by using this preliminary diffusion region instead of the entire simulation domain.

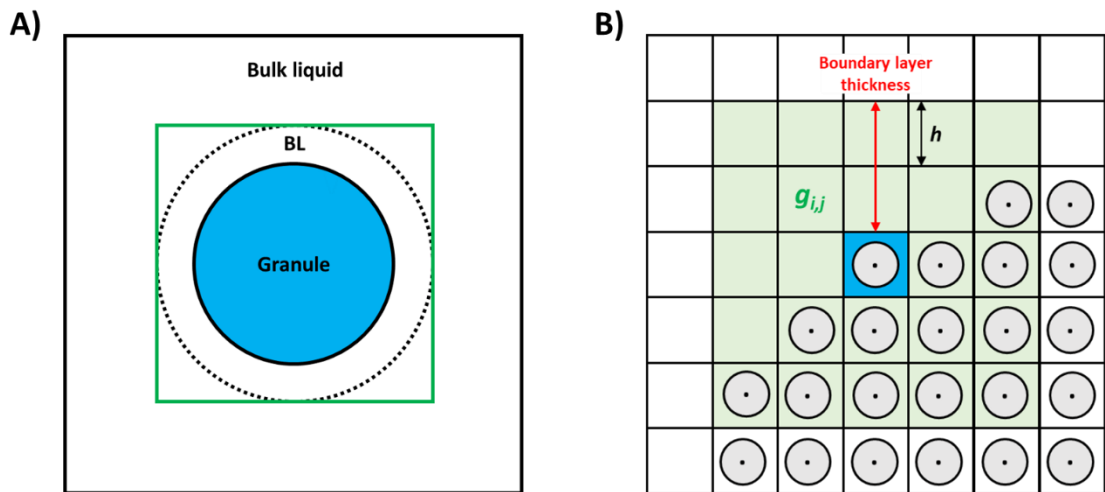


Figure B.4. Detection of diffusion region. **A)** Representation of preliminary diffusion region (green square). Legend: BL – boundary layer. **B)** Neighbouring grid cells (green squares, $g_{i,j}$) of a specific boundary grid cell with microbes (blue square) with potential to be included in diffusion region.

Then, grid cells with bacteria (at least one individual) are determined and included in the diffusion region defining the aggregate region. To recognise which grid cells are belonging to the boundary layer region (and including them in diffusion region), the boundary grid cells with microbes (*i.e.*, the outermost grid cells of aggregate region) must be sought. An efficient way to find them is through the convolution of aggregate region matrix and *edge detection kernel* (Eq. B.1).

$$[K]_{ED} = \begin{pmatrix} -1/8 & -1/8 & -1/8 \\ -1/8 & 1 & -1/8 \\ -1/8 & -1/8 & -1/8 \end{pmatrix} \quad (\text{B.1})$$

Once boundary grid cells with microbes are found, it is time to check whether the neighbouring grid cells ($g_{i,j}$) belong to the boundary layer region and, thus, the diffusion region. By dividing the boundary layer thickness by grid size (h), the extent of the neighbouring grid cells with possibility to belong the boundary layer region is obtained (Figure B.4B).

Finally, the focus region is defined, establishing the region of the simulation domain where diffusion-reaction equation is solved, and the pseudo-steady state is checked. The flowchart of the diffusion region determination is presented in Figure B.5.

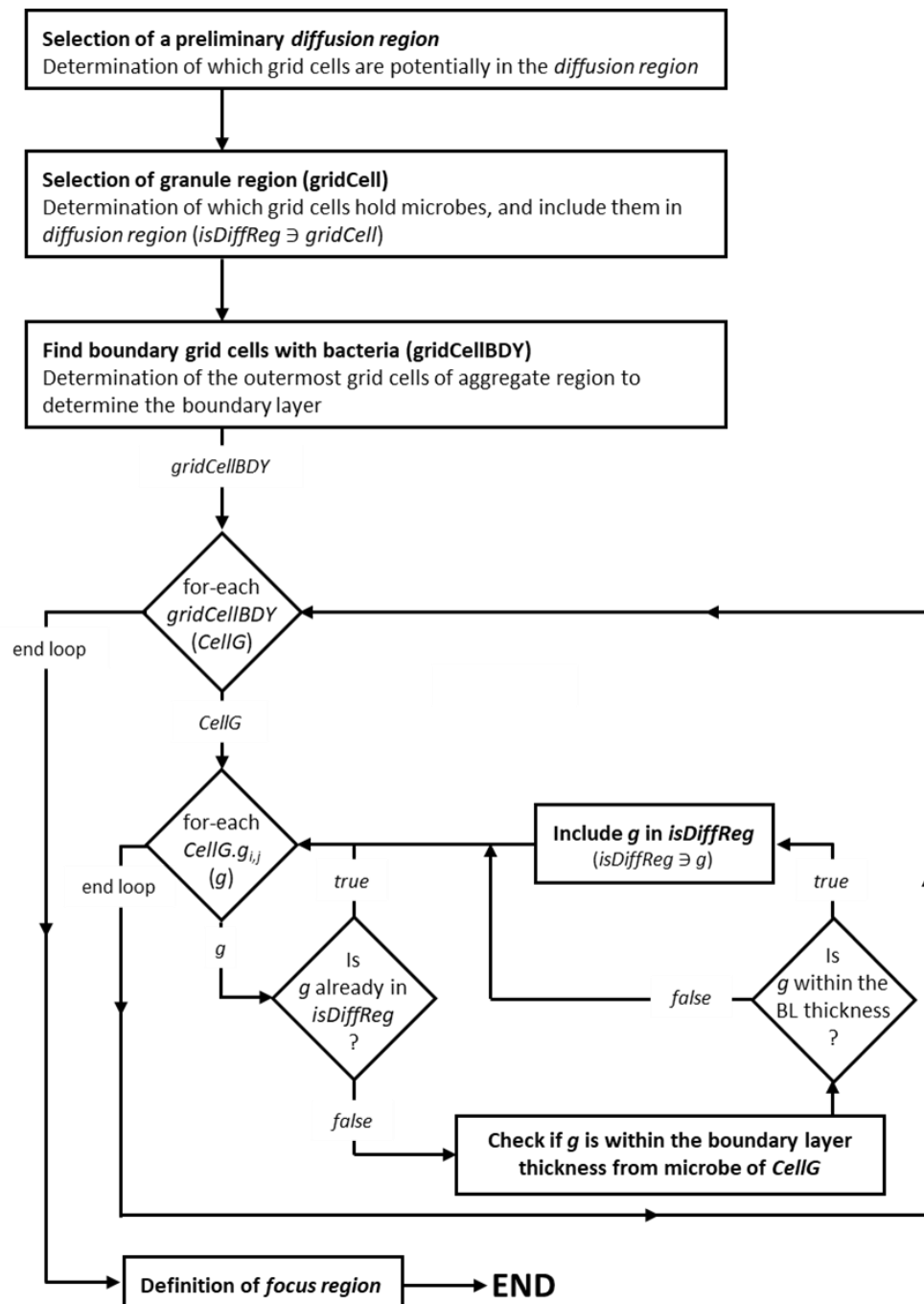


Figure B.5. Algorithm of diffusion region determination.

Integration algorithm

An overall scheme of model integration is presented in Figure B.6.

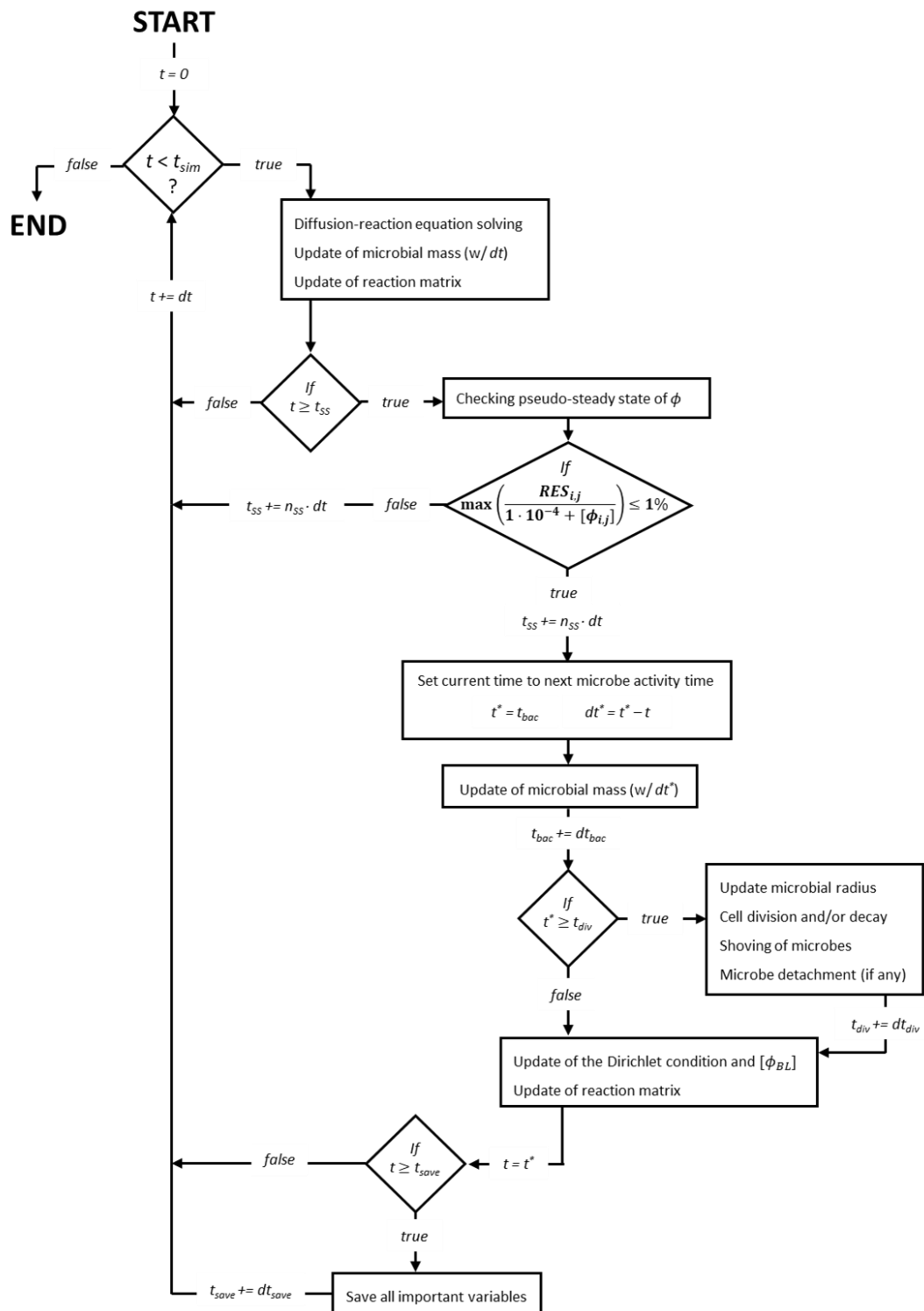


Figure B.6. Algorithm scheme of the integration process.

Rearrangement of diffusion-reaction equation in matrixial form

Let consider the two-dimensional diffusion-reaction equation (Eq. B.2)

$$\frac{\partial}{\partial t} \phi_{i,j}^t = \mathbb{D} \cdot \nabla_{xy}^2 \phi_{i,j}^t + R(\phi_{i,j}^t) \quad (\text{B.2})$$

where $\phi_{i,j}^t$ refers to the concentration of a soluble component in a position of the simulation domain (i, j) and in a time step (t) , and \mathbb{D} refers to the effective coefficient of diffusion. Applying the implicit Crank-Nicholson method to discretize in time the diffusion term, and explicit forward Euler formula for reaction term, Eq. B.3 is obtained.

$$\frac{\phi_{i,j}^{n+1} - \phi_{i,j}^n}{h_t} = \mathbb{D} \cdot \frac{1}{2} [\nabla_{xy}^2 \phi_{i,j}^{n+1} + \nabla_{xy}^2 \phi_{i,j}^n] + R(\phi_{i,j}^n) \quad n \in 1 \dots N_t \quad (\text{B.3})$$

Let use convolution method and the *Laplacian kernel* to compute $\nabla_{xy}^2 \phi_{i,j}^n$ (finite-difference method, Eq. B.4) and define the constant α as Eq. B.5:

$$\nabla^2 \phi_{i,j}^n = \frac{1}{h^2} ([L] * \phi_{i,j}^n) \quad (\text{B.4})$$

$$\alpha := \frac{\mathbb{D} \cdot h_t}{2 \cdot h^2} \quad (\text{B.5})$$

Now, diffusion-reaction equation can be rewritten in matrixial form, obtaining Eq. B.6.

$$[\phi^{n+1}] - [\phi^n] = \alpha [L] * [\phi^{n+1}] + \alpha [L] * [\phi^n] + R([\phi^n]) \cdot h_t$$

$$[\phi^{n+1}] - \alpha [L] * [\phi^{n+1}] = [\phi^n] + \alpha [L] * [\phi^n] + R([\phi^n]) \cdot h_t$$

$$\text{Multiplicative identity} \rightarrow [I_k] * [\phi^{n+1}] - \alpha [L] * [\phi^{n+1}] = [I_k] * [\phi^n] + \alpha [L] * [\phi^n] + R([\phi^n]) \cdot h_t$$

$$\text{Distributivity property} \rightarrow ([I_k] - \alpha [L]) * [\phi^{n+1}] = ([I_k] + \alpha [L]) * [\phi^n] + R([\phi^n]) \cdot h_t$$

$$([I_k] - \alpha [L]) * [\phi^{n+1}] = ([I_k] + \alpha [L]) * [\phi^n] + R([\phi^n]) \cdot h_t \quad (\text{B.6})$$

Deduction of RES equation

The steady-state of soluble components ($\phi_{i,j}$) is defined by Eq. B.7.

$$0 = \mathbb{D} \cdot \nabla_{xy}^2 \phi_{i,j} + R(\phi_{i,j}) \quad (\text{B.7})$$

Applying finite-difference method for space discretization through *Laplacian kernel* $[L]$ and coevolution method, plus considering the boundary conditions (Dirichlet condition), Eq. B.8 is obtained.

$$0 = \mathbb{D} \cdot \frac{1}{h^2} \cdot ([L] * [\phi]^\gamma) + R([\phi]) \quad (\text{B.8})$$

The units of this expression are $[\text{mol} \cdot \text{m}^{-3} \cdot \text{h}^{-1}]$. Because the same expression but with concentration units $[M]$ is needed, every term of Eq. B.8 is multiplied by the characteristic diffusion time (h^2/\mathbb{D}), obtaining the Eq. B.9.

$$0 = [L] * [\phi]^\gamma + (h^2/\mathbb{D}) \cdot R([\phi]) \quad (\text{B.9})$$

Assuming that the system reaches the pseudo-steady state when RES is lower than a tolerance, RES expression is defined as Eq. B.10.

$$RES := [L] * [\phi]^\gamma + (h^2/\mathbb{D}) \cdot R([\phi]) \leq Tol \quad (\text{B.10})$$

Appendix C - Chapter 6

Contents

Supplementary Text – Decision of the selection of eco-interactions

Supplementary Tables – Tables C.1 – C.3

Supplementary Figures – Figures C.1 – C.11

Supplementary Videos – Videos C.1 – C.3

Supplementary Text - Decision of the selection of eco-interactions

Considering *neutralism* [0,0], *competition* [-,-], *commensalism* [0,+], *mutualism* [+,+], *parasitism* [-,+], and *amensalism* [-,0] as the 6 main ecological interactions (Figure 6.1), this study has focused on the three first cases (*neutralism*, *competition* and *commensalism*) and concurrence of *competition* and *commensalism*. The reasons of the decision are stated below:

- *Mutualism* [+,+]. Distinguishing cross-feeding (or *syntrophy*) and co-protection (or *symprostasy*) as two specific ecological interactions belonging to mutualism:
 1. Cross-feeding (*substrate-related mutualism*). This ecological interaction has already been studied by Mitri, S. *et al.*, 2011 and Momeni *et al.*, 2013, evaluating the influence of substrate(s) concentration and the presence of competition between microbial communities. Additionally, *mutualism* is one of the less frequent ecological interactions among culturable bacteria (only 5% of all assessed interactions among 20 soil bacteria across 40 carbon environments corresponded to a mutualistic interaction; study from Kehe *et al.*, 2021 (Kehe *et al.*, 2021). As stated in Palmer and Foster, 2022 (Palmer & Foster, 2022) – “*Negative interaction prevails, and cooperation, where two species both benefits, is typically rare*”.
 2. Co-protection (*inhibitor-related mutualism*). From an ecological perspective, the resource availability has a direct impact on interactions among species (*e.g.*, a limited resource environment intensifies the competition for this resource). For this reason, the influence of substrate concentration has been evaluated in this study. Note that when inhibition of some community member is present in the system (either for presence of inhibitor in the environment, (*co*)*protection*; or produced by

other community member, *amensalism*), the inhibitory influence is strengthened as higher is the concentration of inhibitor. Therefore, co-protection has an inverse substance-related trend to the selected ecological interactions (*neutralism*, *competition* and *commensalism*). For this reason, co-protection is not included in this study.

- *Parasitism* [-,+]. One of the aims of this study is to study the combination of two ecological interactions in which one have a positive impact (as *commensalism*) and the other a negative impact (as *competition*). Due to *parasitism* has already a negative impact in one of the species, this eco-interaction is not included.
- *Amensalism* [-,0]. As (co)protection, *amensalism* has an inverse substance-related trend to the selected ecological interactions (*neutralism*, *competition* and *commensalism*). Moreover, *amensalism* has already a negative impact in one of the species. For these reasons, this eco-interaction is not included.

Supplementary Tables

Table C.1. Summary of kinetic parameters of microbial populations (B1, B2, B3) for all simulation setups.

Process	Process rate (h ⁻¹)	Kinetic parameters
Neutralism		
Growth of B1	$\mu_{max,B1} \cdot \frac{[A]}{K_{A,B1}+[A]} \cdot X_{B1}$	Maximum growth rate (μ_{max}): $\mu_{max,B1} = 1d^{-1}$ $\mu_{max,B2} = 1d^{-1}$ $\mu_{max,B3} = 1d^{-1}$
Growth of B2	$\mu_{max,B2} \cdot \frac{[B]}{K_{B,B2}+[B]} \cdot X_{B2}$	
Growth of B3	$\mu_{max,B3} \cdot \frac{[C]}{K_{C,B3}+[C]} \cdot X_{B3}$	
Competition		
Growth of B1	$\mu_{max,B1} \cdot \frac{[A]}{K_{A,B1}+[A]} \cdot X_{B1}$	Decay coefficient^a (b): $b_{B1} = 0.25d^{-1}$ $b_{B2} = 0.25d^{-1}$ $b_{B3} = 0.25d^{-1}$
Growth of B2	$\mu_{max,B2} \cdot \frac{[A]}{K_{A,B2}+[A]} \cdot X_{B2}$	
Growth of B3	$\mu_{max,B3} \cdot \frac{[A]}{K_{A,B3}+[A]} \cdot X_{B3}$	
Commensalism		
Growth of B1	$\mu_{max,B1} \cdot \frac{[A]}{K_{A,B1}+[A]} \cdot X_{B1}$	Affinity constant for A (K_A): $K_{A,B1} = 0.01mM$ $K_{A,B2} = 0.01mM$ $K_{A,B3} = 0.01mM$
Growth of B2	$\mu_{max,B2} \cdot \frac{[B]}{K_{B,B2}+[B]} \cdot X_{B2}$	
Growth of B3	$\mu_{max,B3} \cdot \frac{[C]}{K_{C,B3}+[C]} \cdot X_{B3}$	
Competition + Commensalism		
Growth of B1	$\mu_{max,B1} \cdot \frac{[A]}{K_{A,B1}+[A]} \cdot \frac{[O_2]}{K_{O_2,B1}+[O_2]} \cdot X_{B1}$	Affinity constant for B (K_B): $K_{B,B1} = 0.01mM$ $K_{B,B2} = 0.01mM$ $K_{B,B3} = 0.01mM$
Growth of B2	$\mu_{max,B2} \cdot \frac{[B]}{K_{B,B2}+[B]} \cdot \frac{[O_2]}{K_{O_2,B2}+[O_2]} \cdot X_{B2}$	
Growth of B3	$\mu_{max,B3} \cdot \frac{[C]}{K_{C,B3}+[C]} \cdot \frac{[O_2]}{K_{O_2,B3}+[O_2]} \cdot X_{B3}$	
Affinity constant for C (K_C): $K_{C,B1} = 0.01mM$ $K_{C,B2} = 0.01mM$ $K_{C,B3} = 0.01mM$		
Affinity constant for O₂ (K_{O_2}): $K_{O_2,B1} = 0.001mM$ $K_{O_2,B2} = 0.001mM$ $K_{O_2,B3} = 0.001mM$		
For all simulation setups		
Decay of B1	$b_{B1} \cdot X_{B1}$	
Decay of B2	$b_{B2} \cdot X_{B2}$	
Decay of B3	$b_{B3} \cdot X_{B3}$	

^a Decay ratio is 25% of maximum growth rate (μ_{max}) (Bodegom, 2007).

Table C.2. Stoichiometric matrix of microbial populations (B1, B2, B3) for all simulation setups.

Process	Compounds ^a							
	A	B	C	D	O ₂	B1	B2	B3
Neutralism (A,B,C)								
Growth of B1	$-1/Y_{B1}^b$	0	0	$1/Y_{B1}$	0	1	0	0
Growth of B2	0	$-1/Y_{B2}^b$	0	$1/Y_{B2}$	0	0	1	0
Growth of B3	0	0	$-1/Y_{B3}^b$	$1/Y_{B3}$	0	0	0	1
Competition (A)								
Growth of B1	$-1/Y_{B1}$	$1/Y_{B1}$	0	0	0	1	0	0
Growth of B2	$-1/Y_{B2}$	$1/Y_{B2}$	0	0	0	0	1	0
Growth of B3	$-1/Y_{B3}$	$1/Y_{B3}$	0	0	0	0	0	1
Commensalism (A,B,C)								
Growth of B1	$-1/Y_{B1}$	$1/Y_{B1}$	0	0	0	1	0	0
Growth of B2	0	$-1/Y_{B2}$	$1/Y_{B2}$	0	0	0	1	0
Growth of B3	0	0	$-1/Y_{B3}$	$1/Y_{B3}$	0	0	0	1
Competition (O₂) + Commensalism (A,B,C)								
Growth of B1	$-1/Y_{B1}$	$1/Y_{B1}$	0	0	$-1/Y_{B1}$	1	0	0
Growth of B2	0	$-1/Y_{B2}$	$1/Y_{B2}$	0	$-1/Y_{B2}$	0	1	0
Growth of B3	0	0	$-1/Y_{B3}$	$1/Y_{B3}$	$-1/Y_{B3}$	0	0	1
For all simulation setups								
Decay of B1	0	0	0	0	0	-1	0	0
Decay of B2	0	0	0	0	0	0	-1	0
Decay of B3	0	0	0	0	0	0	0	-1

^a Units: mol·L⁻¹^b All bacteria have the same growth yield: $Y_{B1} = Y_{B2} = Y_{B3} = 0.01 \text{ (mol X)·(mol S)}^{-1}$

Table C.3. Details of simulation experiments. For each setup, eco-interactions between microbial species, environment of the reactor, and substrate concentrations on bulk liquid ($[A]$, $[B]$, $[C]$ and $[D]$) are specified. Also, it includes in which Figures the results are shown.

Setup	Specifications	Figures
Setup 1: Saturation One eco-interaction	<ul style="list-style-type: none"> Replicates (3-6) of each simulation experiment Substrate concentrations (A, B and C): $[S]_T$: 100mM, 10mM, 1mM^a Ecological interactions and influent characterization: <ul style="list-style-type: none"> <u>Neutralism</u>: feeding of A, B, and C $\rightarrow [A] = [B] = [C] = [S]_T/3$ <u>Competition</u>: feeding of A $\rightarrow [A] = [S]_T$ <u>Commensalism</u>: feeding of A $\rightarrow [A] = [S]_T$ 	<u>All eco-inter.</u> Fig. 6.3 Figs. C.1 & C.2 Videos C.1 & C.2
Setup 2: Anaerobic One eco-interaction	<ul style="list-style-type: none"> Replicates (3-6) of each simulation experiment Substrate concentrations (A, B, C): $[S]_T$: 1mM, 0.5mM, 0.2mM, 0.1mM Ecological interactions and influent characterization: <ul style="list-style-type: none"> <u>Neutralism</u>: feeding of A, B, and C $\rightarrow [A] = [B] = [C] = [S]_T/3$ <u>Competition</u>: feeding of A $\rightarrow [A] = [S]_T$ <u>Commensalism</u>: feeding of A $\rightarrow [A] = [S]_T$ 	<u>Neutralism</u> Fig. 6.4 <u>Competition</u> Figs 6.5 & 6.9 Video C.3 <u>Commensalism</u> Figs. 6.6 & 6.9 Fig. C.4 <u>All eco-inter.</u> Fig. C.3
Setup 3: Aerobic Two eco-interactions	<ul style="list-style-type: none"> Replicates (3-6) of each simulation experiment Substrate concentrations (A, B and C): $[S]_T$: 1mM, 0.5mM, 0.1mM, 0.05mM Oxygen concentrations: $[O_2]$: 10mg·L⁻¹, 6mg·L⁻¹, 3.75mg·L⁻¹, 1.90mg·L⁻¹, 1mg·L⁻¹, 0.5mg·L⁻¹ Ecological interactions and bulk liquid characterization: <ul style="list-style-type: none"> <u>Commensalism + competition</u>: feeding of A and O₂ $\rightarrow [A]_{BL} = [S]_T$ 	<u>Commensalism plus competition</u> Figs 6.7 - 6.9 Figs. C.5 - C.10 Video C.3

^a Consideration until substrates started to become limiting inside aggregate.

Supplementary Figures

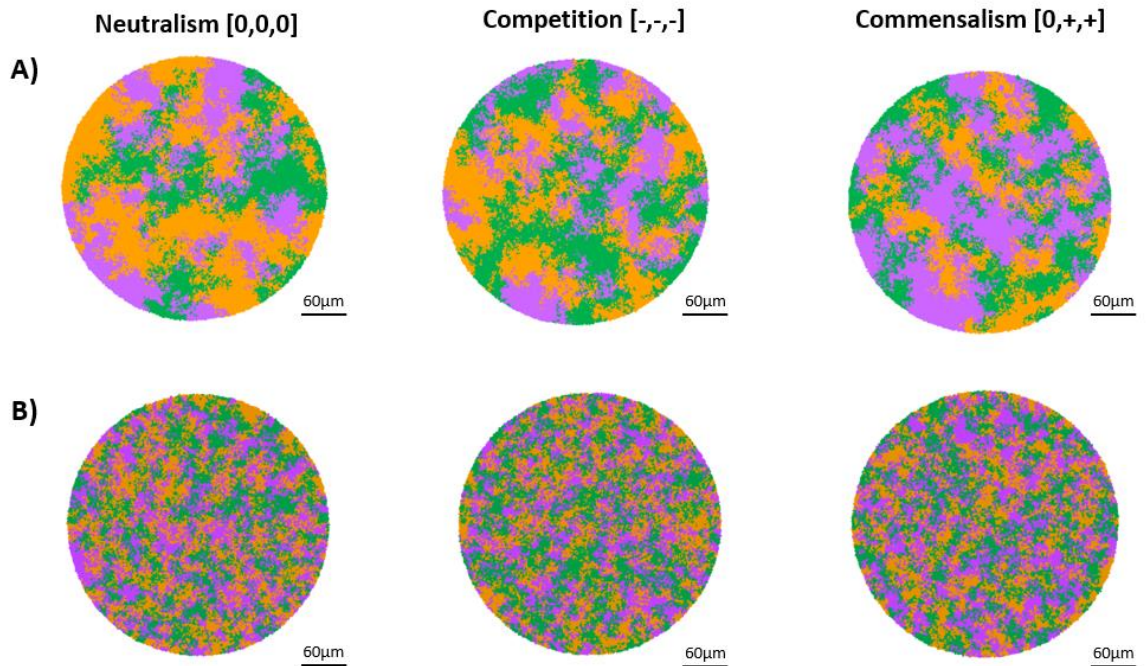


Figure C.1. Influence of inoculum size and substrate gradients on intermixing of microbial populations considering neutralism, competition and commensalism with $[S]_T = 100 \text{ mM}$. **A)** Aggregate pictures captured at 8 d of simulation starting with an inoculum size of $20 \text{ }\mu\text{m}$ (diameter) and considering diffusion resistance of substrates. **B)** Aggregate pictures captured at 4 d of simulation starting with an inoculum size of $160 \text{ }\mu\text{m}$ (replicating the starting point of Mitri et al. (2016)) and removing the substrate gradients (no diffusion resistance). None of the simulations are in steady state yet.

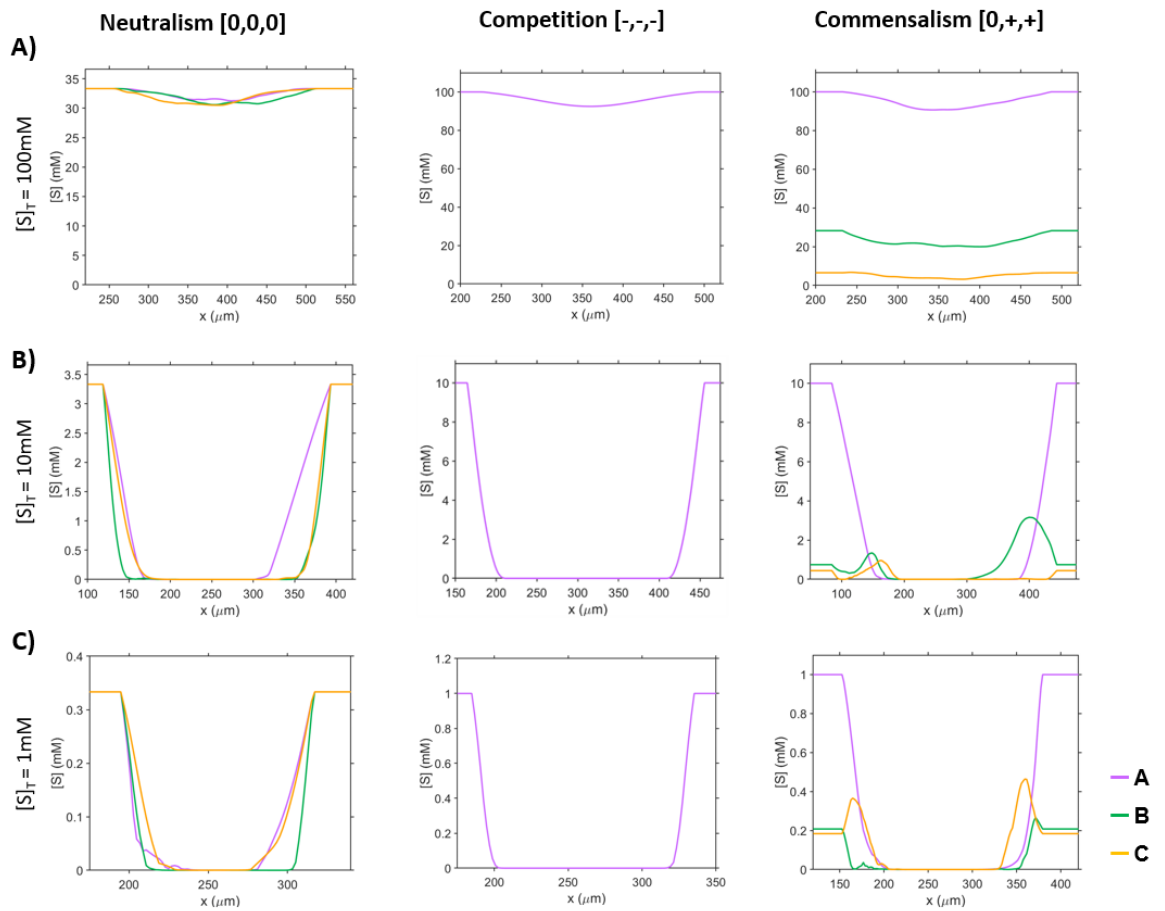


Figure C.2. Substrate profiles on the transverse plane of aggregates considering neutralism, competition or commensalism. **A)** Substrate profiles from simulations at $[S]_T = 100 \text{ mM}$ ($t = 8 \text{ d}$). **B)** Substrate profiles from simulations at $[S]_T = 10 \text{ mM}$ ($t = 10 \text{ d}$). **C)** Substrate profiles from simulations at $[S]_T = 1 \text{ mM}$ ($t = 15 \text{ d}$). Legend: [A] – purple line; [B] – green line; [C] – orange line.

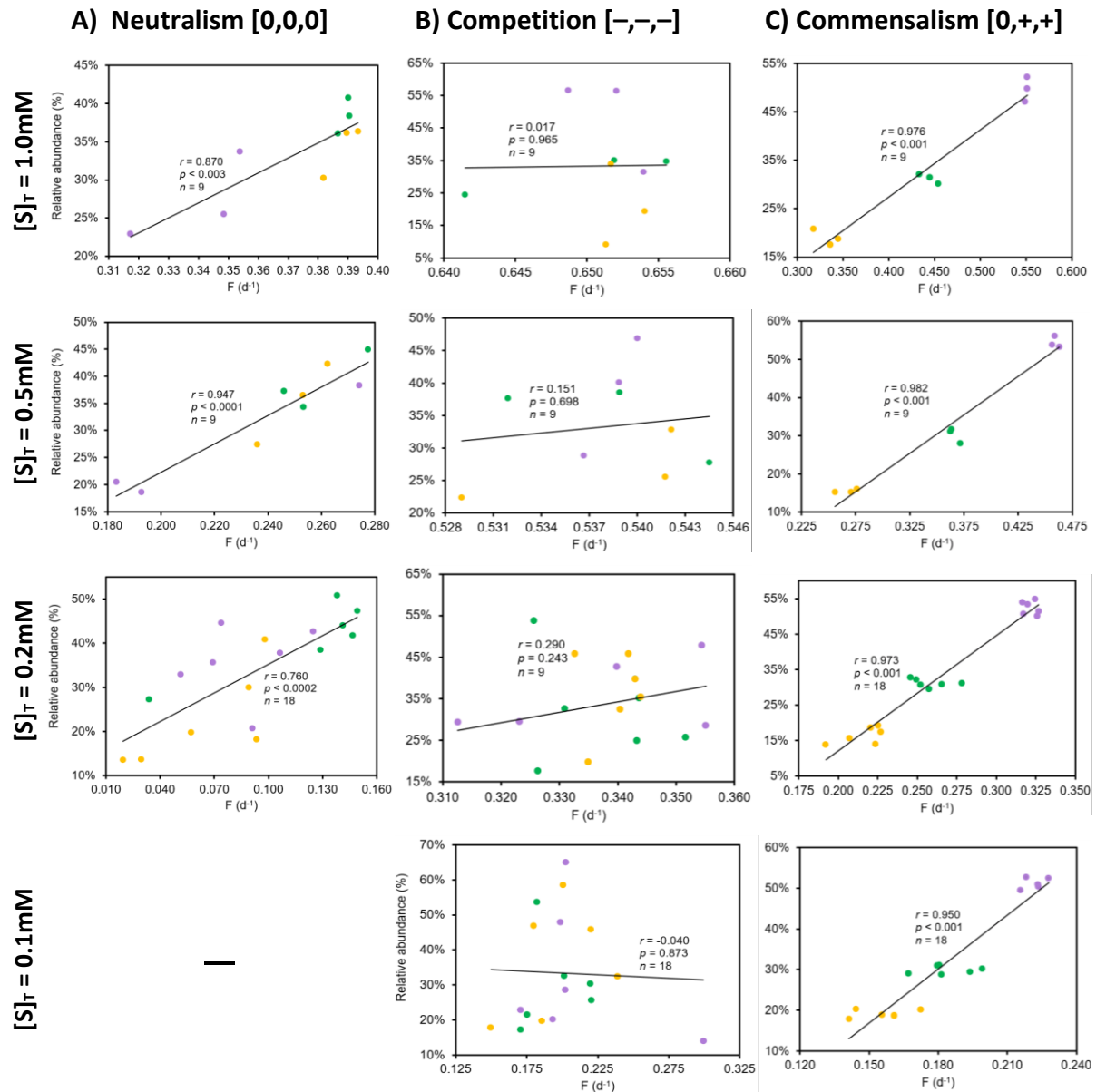


Figure C.3. Regression fits to different relative abundance/microbial fitness data pairs from simulation experiments with their corresponding Pearson's coefficient (r) with their significance value (p -value) and sample size (n). A) Neutralism simulations. B) Competition simulations. C) Commensalism simulations. Legend: B1– purple circles; B2 – green circles; B3 – orange circles.

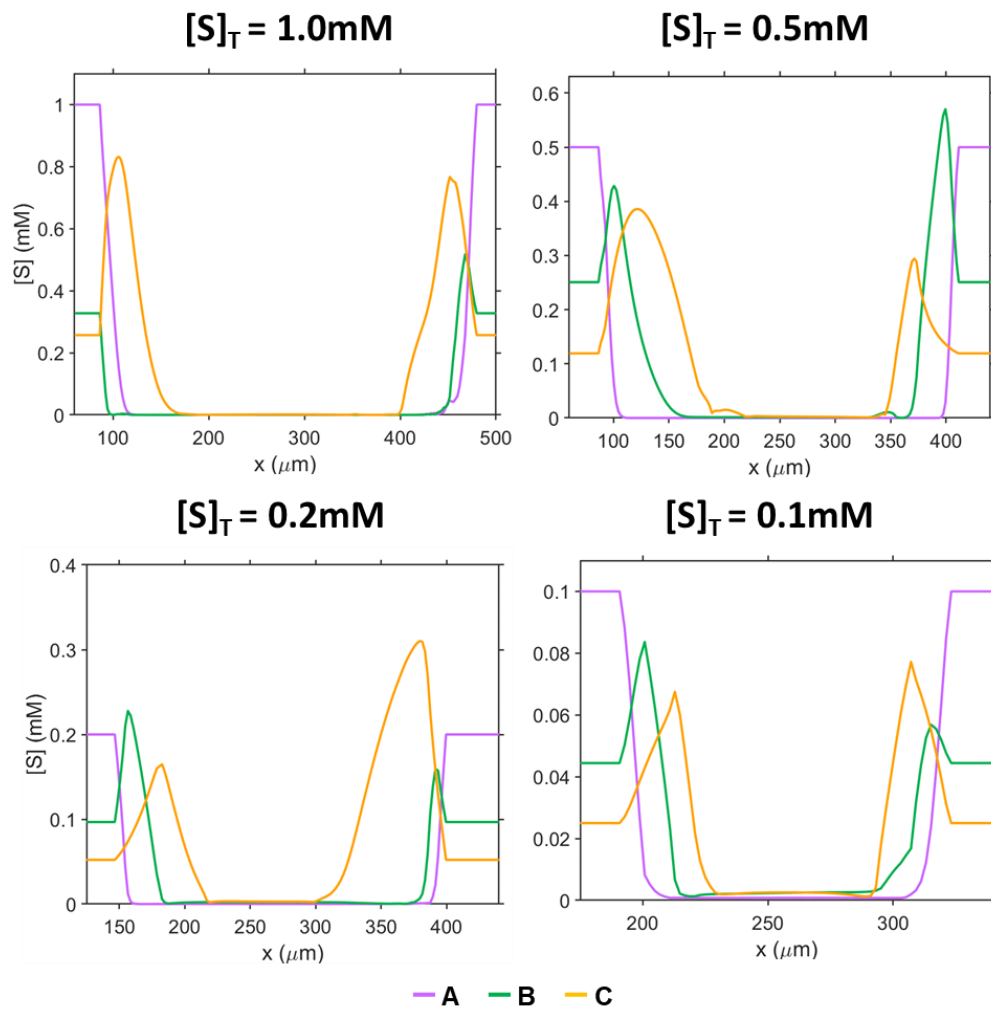


Figure C.4. Substrate profiles on the transverse plane of aggregates considering commensalism. Legend: [A] – purple line; [B] – green line; [C] – orange line.

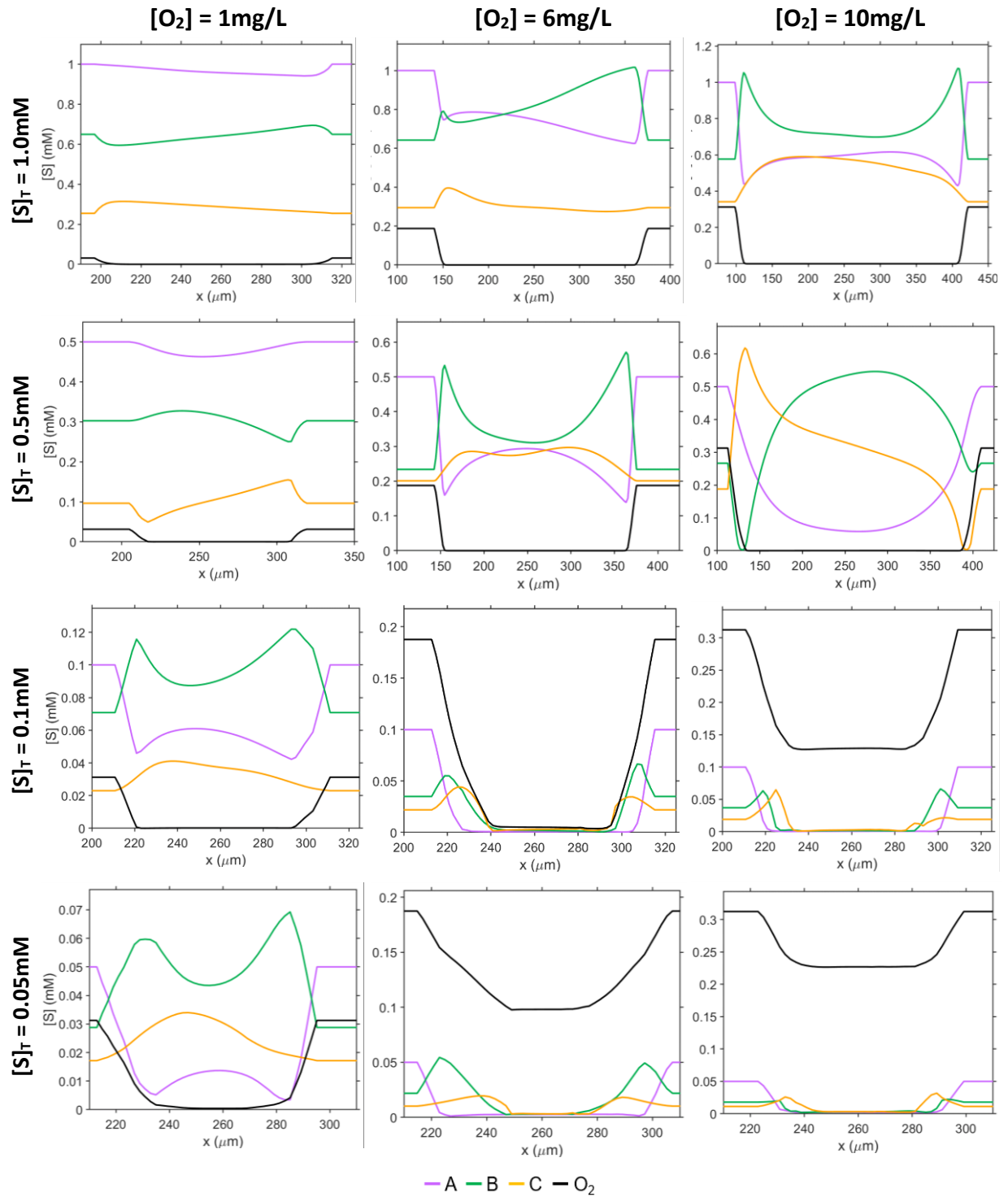
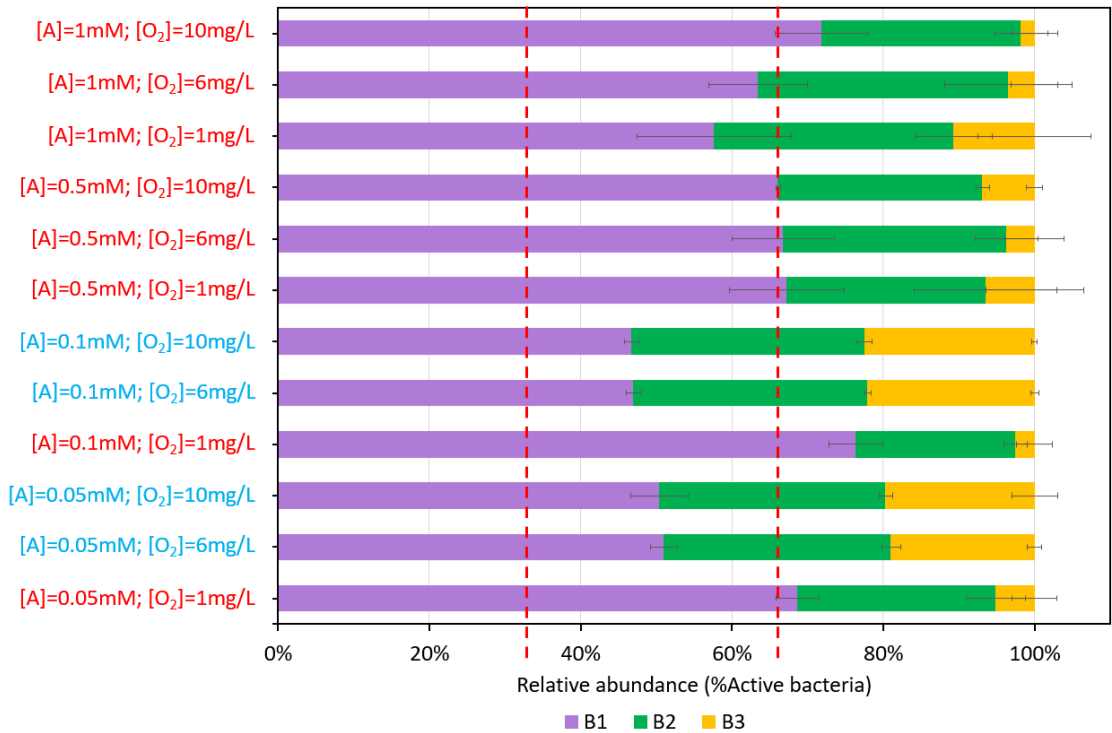


Figure C.5. Substrate profiles on the transverse plane of aggregates considering commensalism and competition. Legend: [A] – purple line; [B] – green line; [C] – orange line; $[O_2]$ – black line.



[A] [O ₂]	1.0 10	1.0 6	1.0 1	0.5 10	0.5 6	0.5 1	0.1 10	0.1 6	0.1 1	0.05 10	0.05 6	0.05 1
1.0 10	-	-	-	-	-	-	-	-	-	-	-	-
1.0 6	ns ns ns	-	-	-	-	-	-	-	-	-	-	-
1.0 1	ns ns ns	ns ns ns	-	-	-	-	-	-	-	-	-	-
0.5 10	ns ns ns	ns ns ns	ns ns ns	-	-	-	-	-	-	-	-	-
0.5 6	ns ns ns	ns ns ns	ns ns ns	ns ns ns	-	-	-	-	-	-	-	-
0.5 1	ns ns ns	ns ns ns	ns ns ns	ns ns ns	ns ns ns	-	-	-	-	-	-	-
0.1 10	* ns **	* ns **	ns ns ns	*** ** **	* ns *	* ns *	-	-	-	-	-	-
0.1 6	* ns **	* ns **	ns ns ns	*** ** **	* ns *	* ns *	ns ns ns	-	-	-	-	-
0.1 1	ns ns ns	ns ns ns	ns ns ns	** ns	ns ns ns	ns ns ns	** ** **	** ** **	-	-	-	-
0.05 10	* ns **	ns ns **	ns ns ns	** *	* ns **	* ns *	ns ns ns	ns ns ns	** ** **	-	-	-
0.05 6	* ns **	ns ns **	ns ns ns	** ** **	ns ns *	* ns *	* ns *	* ns *	** ** **	ns ns ns	-	-
0.05 1	ns ns ns	ns ns ns	ns ns ns	ns ns ns	ns ns ns	ns ns ns	** ns **	** ns **	* ns ns	** ns **	** ns **	-

Figure C.6. Relative abundance of active bacteria from simulation experiments considering commensalism and competition. Dashed red lines indicate 33.33% and 66.66% relative abundances. Colour of asterisks points out what bacteria it refers to. In the table are shown the significant level of the difference between B1, B2 and B3 relative abundances. Significance level legend: ns, not significant; *, $p < 0.05$; **, $p < 0.01$; ***, $p < 0.001$. Colours of y-axis text and table headers indicate the ecological environment (and spatial distribution of microbial populations) of simulation experiments: red – competitive environment (columned stratification); blue – commensal environment (layered stratification).

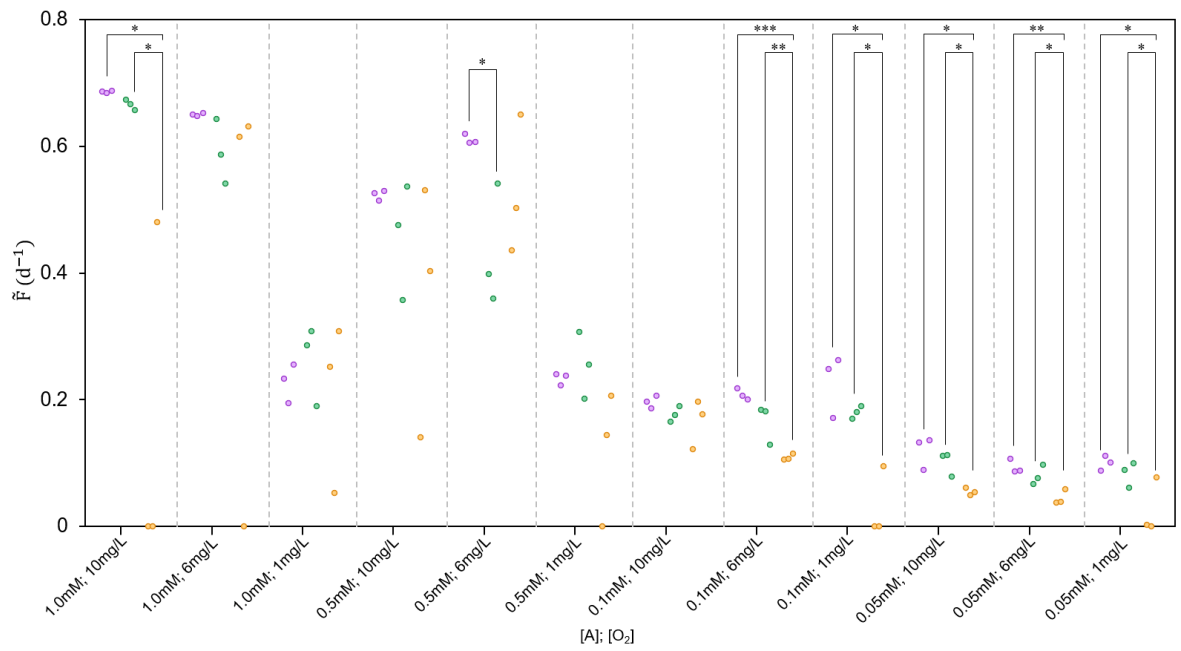


Figure C.7. Microbial fitness (F) from simulation experiments considering commensalism and competition. Asterisks indicate the significance level of the difference between B1, B2 and B3 specific growth rate. Significance level legend: ns, not significant; *, $p < 0.05$; **, $p < 0.01$; ***, $p < 0.001$.

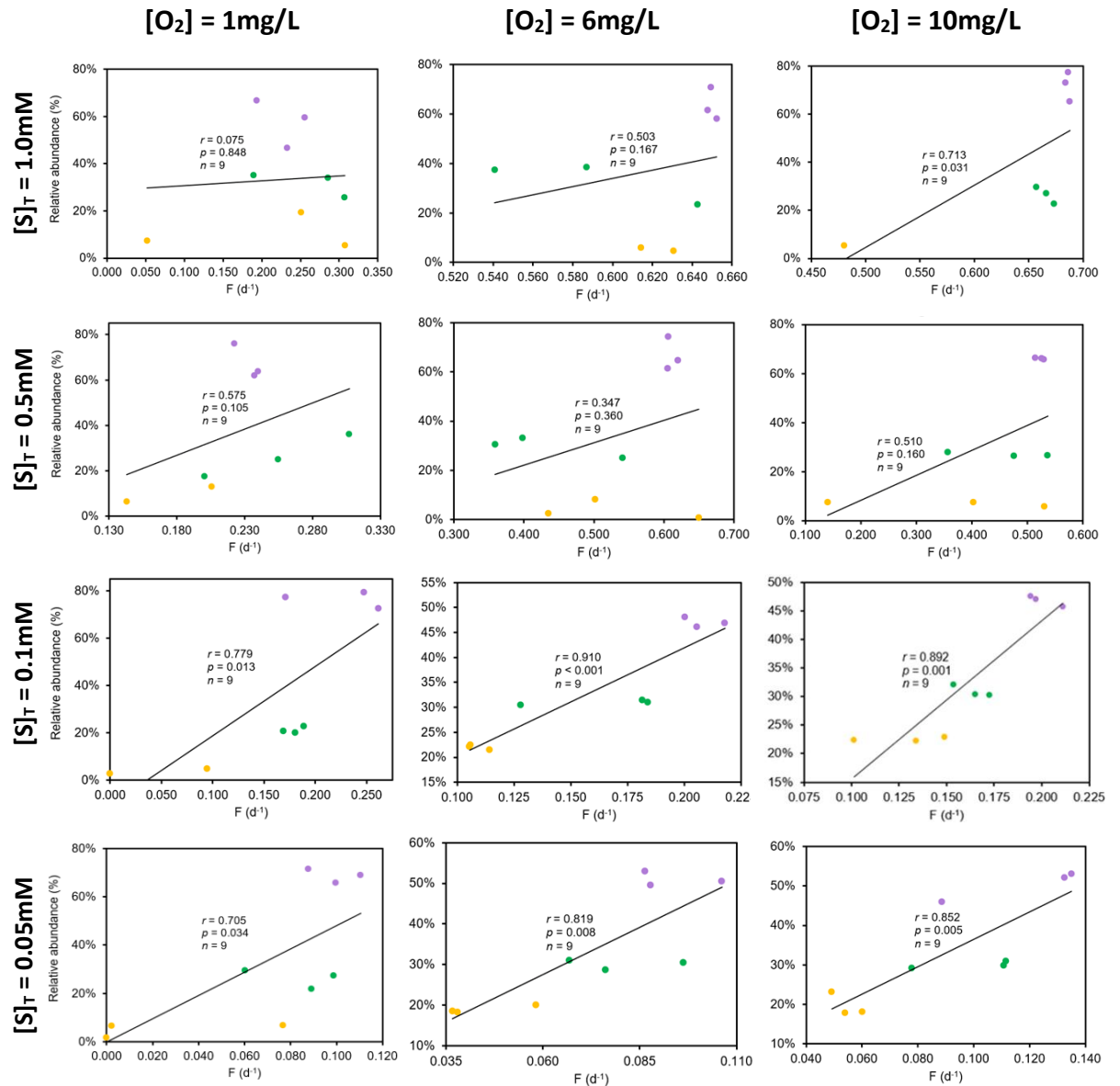


Figure C.8. Regression fits to different relative abundance/microbial fitness data pairs from simulation experiments considering commensalism and competition with their corresponding Pearson's coefficient (r) with their significance value (p -value) and sample size (n). Legend: B1 – purple circles; B2 – green circles; B3 – orange circles.

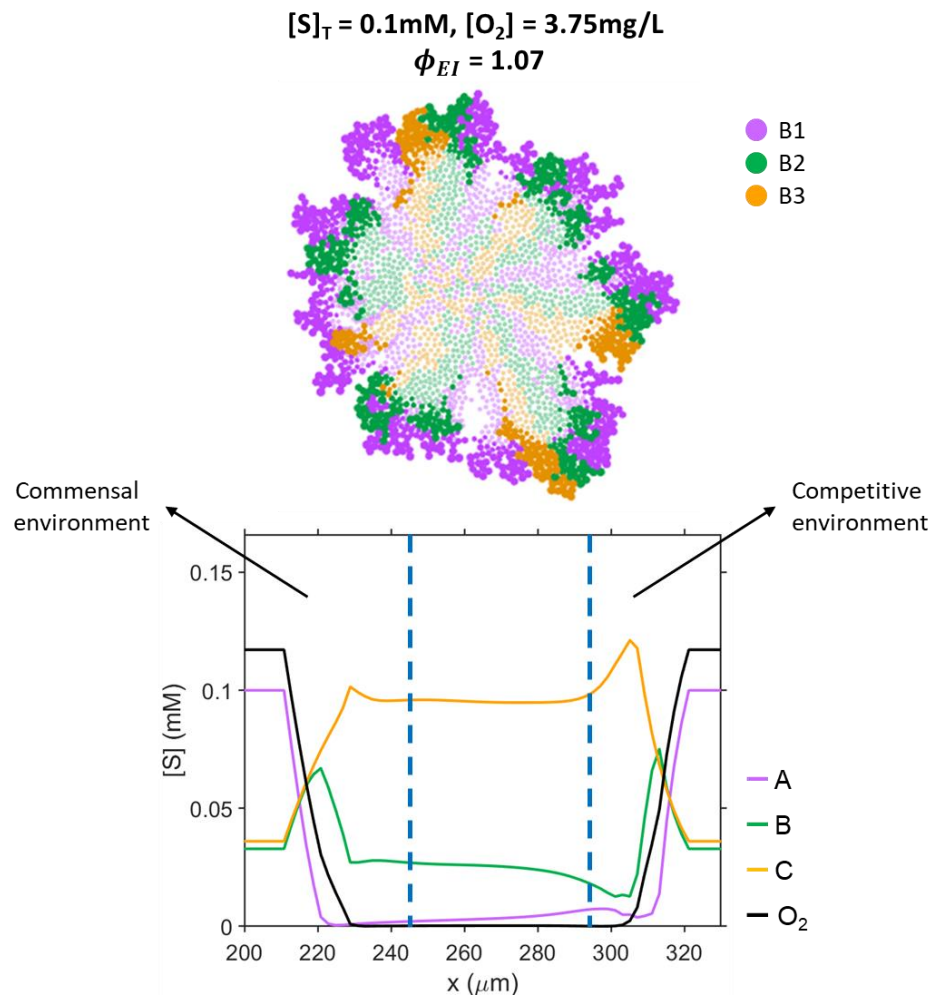


Figure C.9. Ecological environment distribution in a hybrid stratification case considering concurrence of commensalism and competition ($[S]_T = 0.1\text{ mM}$, $[O_2] = 3.75\text{ mg/L}$; $\phi_{EI} = 1.07$). Inactive bacteria are shown in a lighter colour. The substrate profiles are from the transverse plane of aggregate.

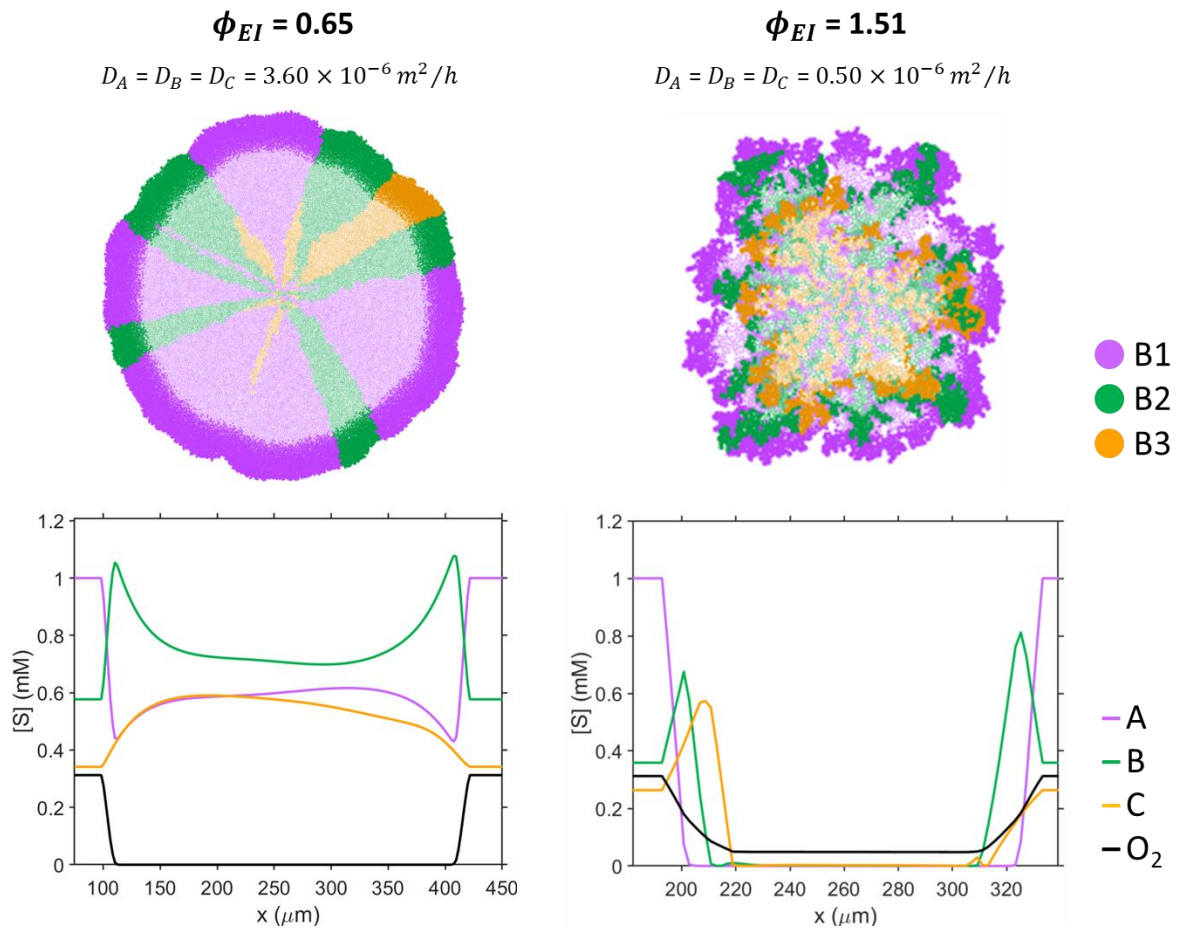


Figure C.10. Influence of substrate diffusivity on spatial distribution of microbial populations (commensalism + competition; $[S]_T = 1.0 \text{ mM}$, $[O_2] = 10.0 \text{ mg/L}$). Inactive bacteria are shown in a lighter colour. The substrate profiles are from the transverse plane of aggregates.

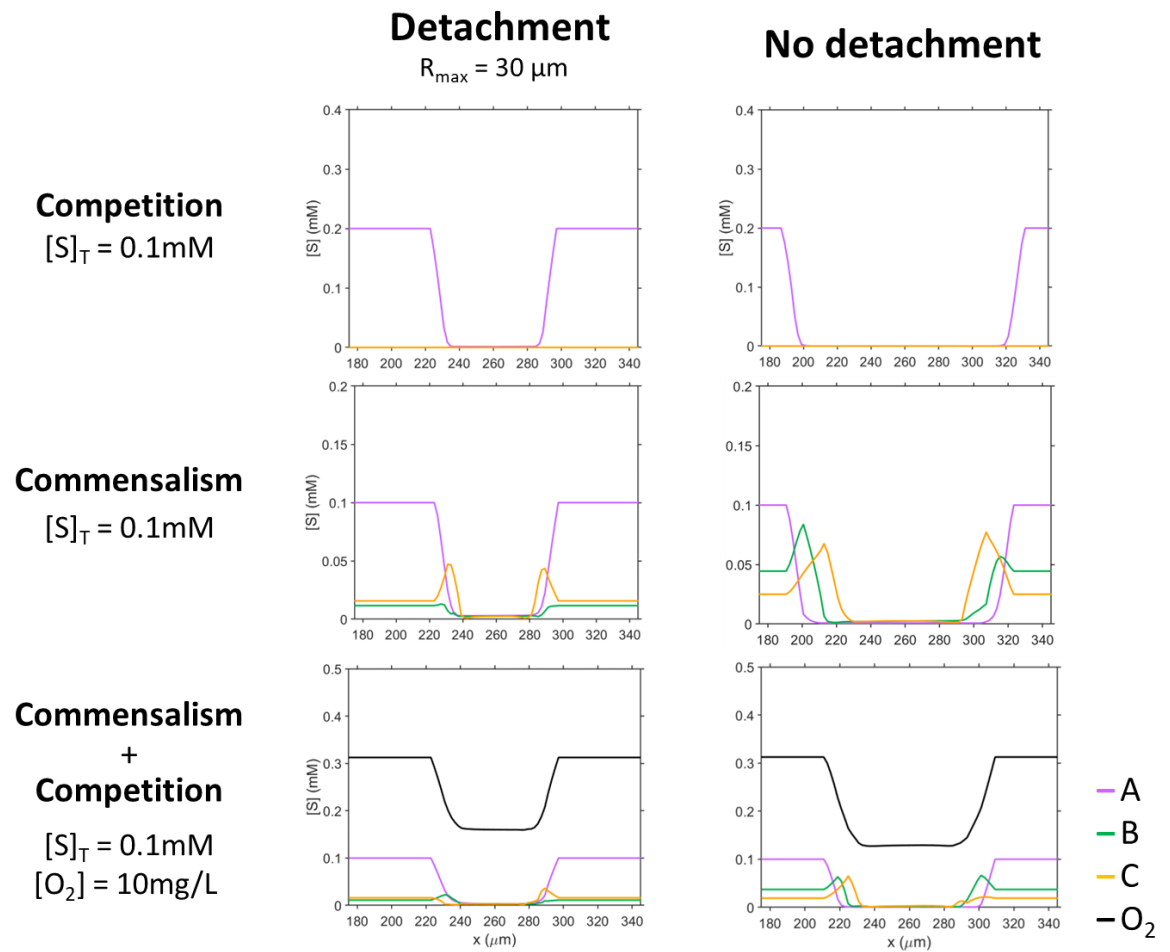


Figure C.11. Substrate profiles on the transverse plane of aggregates considering or not detachment.

Supplementary Videos

Video C.1. Development of aggregates and substrate profiles from simulations considering neutralism, competition and commensalism with $[S]_T = 10 \text{ mM}$ (from 0 d to 10 d).

Video C.2. Development of aggregates and substrate profiles from simulations considering neutralism, competition and commensalism with $[S]_T = 1 \text{ mM}$ (from 0 d to 15 d).

Video C.3. Development of aggregates and substrate profiles from simulations considering or not the influence of shear forces (detachment) (from 0 d to 50 d). The simulation experiments including detachment were started with the same inoculum as those without detachment with the objective to observe the genuine impact of the shear force in the spatial distribution of the microbial populations.

Supplementary videos presented in this section are available on PLOS Computational Biology Journal (Martinez-Rabert et al., 2022) – [Environmental and ecological controls of the spatial distribution of microbial populations in aggregates | PLOS Computational Biology](#).

Appendix D - Chapter 7

Contents

Supplementary Methods – Calculation of growth yield through TEEM2

Supplementary Discussion – Ecological environment and the dominant substrate

Supplementary Tables – Tables D.1 – D.12

Supplementary Figures – Figures D.1 – D.9

Supplementary Methods. Calculation of growth yield through TEEM2

The estimated growth yield values were compared with the growth yield calculated through Thermodynamic Electron Equivalents revised Model (TEEM2) (McCarty, 2007). TEEM2 is a generalized method for the estimation of the growth yield of any microbial functional group based on thermodynamics. The balance between anabolism and catabolism is closed using electron equivalent units (eeq) and specific assumptions related with the necessary energy to growth.

TEEM2 considers the use of half oxidoreductive reactions for electron donor (eD) and electron acceptor (eA). In this case, all comammox *Nitrospira* metabolisms are based on three half reactions of eD ($NH_4^+ \rightarrow NO_2^-$, $NO_2^- \rightarrow NO_3^-$, $NH_4^+ \rightarrow NO_3^-$; Eqs. D.1 – D.3, respectively), and three half reactions of eA ($O_2 \rightarrow H_2O$, $NO_3^- \rightarrow NO_2^-$, $NO_2^- \rightarrow NO$; Eqs. D.4 – D.6, respectively). The methods for developing all half reaction and the Gibbs energy of formation ($\Delta G_f^{o'}$) of each chemical component are provided by Rittmann and McCarty (Rittmann & McCarty, 2020).





For each metabolism of comammox *Nitrospira*, the energy produced in the catabolism (ΔG_r , Eq. D.7) is determined from the half reaction reduction potentials for the eA ($\Delta G_a^{o'}$) and eD ($\Delta G_d^{o'}$). One of the modifications involved in TEEM2 is the consideration that oxygenase reactions generally require the input of energy and reducing power in the form of NADH. This is represented by the difference between $\Delta G_a^{o'}$ of oxygen (-78.72 kJ/eeq) and $\Delta G_d^{o'}$ of the NADH/NAD⁺ half reduction equation (30.88 kJ/eeq), which equals to -109.6 kJ/eeq (McCarty, 2007). In this case, 2/6 of electrons from ammonia are employed in its oxygenase step, which means that the actual energy loss is -36.52 kJ/eeq. Thus, the energy loss in kJ per mole of donor is included in Eq. D.7, where q is the number of times an oxygenase is used in the complete oxidation of the respective eD.

$$\Delta G_r = \Delta G_a^{o'} - \Delta G_d^{o'} - q \cdot \Delta G_{xy} \quad (\text{D.7})$$

Half reactions for electron donor and cell synthesis are combined to produce the synthesis reaction, referred here as Gibbs free energy for synthesis (ΔG_S). In TEEM2, ΔG_S is evaluated by Eq. D.8.

$$\Delta G_S = \frac{\Delta G_{fa} - \Delta G_d}{\epsilon^m} + \frac{\Delta G_{in} - \Delta G_{fa}}{\epsilon^n} + \frac{\Delta G_{pc}}{\epsilon} \quad (\text{D.8})$$

Where ΔG_{fa} is the Gibbs free energy of the half reaction for formaldehyde (46.53 kJ/eeq), ΔG_{in} is the Gibbs free energy of the half reaction of intermediate synthesis (30.9 kJ/eeq), and ΔG_{pc} is the Gibbs free energy for cell synthesis (18.8 kJ/eeq, assuming the cell relative composition of C₅H₇O₂N and ammonia as the source for cell synthesis). m and n are two adjustments that are set as follows: m equals 1 for C1 compounds (as CO₂) and equals n for all others; the exponent n equals +1 if $m = n$ and $(\Delta G_{in} - \Delta G_d) > 0$, otherwise it equals -1. The overall reaction for cell growth is obtained by combining in proper proportion (represented by A , Eq. D.9) the synthesis reaction and energy reaction, considering that only part of the energy reaction will be employed for the synthesis of new biomass (energy-transfer efficiency, ϵ). Finally, the growth yield is determined from A expressed in eeq units (represented by f_S^o , Eq. D.10) or in molar units (represented by $Y_{X/D}$, Eq. D.11).

$$A = -\Delta G_S / (\epsilon \cdot \Delta G_r) \quad (\text{D.9})$$

$$f_S^o = 1/(1 + A) \quad (\text{D.10})$$

$$Y_{X/D} = (\gamma_D/\gamma_X) \cdot f_S^o \quad (\text{D.11})$$

Where γ_D is the degree of reduction of electron donor (6 eeq/mol_{NH3} for AO, NRMX and An-NRMX; 2 eeq/mol_{NO2} for NO; 8 eeq/mol_{NH3} for CMX) and γ_X is the degree of reduction of biomass (20 eeq/mol_X), respectively. The energy-transfer efficiency (ϵ) is a key factor that needs to be assumed or calibrated to solve Eq. D.9 (McCarty, 2007). The reported growth yield values of pure (or enriched) culture of AOB, NOB and CMX were used to calibrate ϵ for aerobic nitrifiers. For this, the Solver tool of Microsoft Excel (selecting GRG Nonlinear method) was employed. The average ϵ value found for aerobic nitrifiers (AOB, NOB and CMX) was 0.258 ± 0.040 ($n = 13$; see Table D.6). This ϵ value was used to estimate the growth yields of comammox *Nitrospira* metabolisms (Table 7.1; Method section of Chapter 7).

Supplementary Discussion. Ecological environment and dominant substrate

In Chapter 6 was shown how the eco-interaction modulus ($\phi_{EI}^{A/B}$, Eq. D.12) is able to predict which is the most limiting substrate in microbial aggregates.

$$\phi_{EI}^{A/B} = \frac{\phi_A}{\phi_B} = \frac{\sqrt{(n_A \cdot q_A)/(D_A \cdot C_A)}}{\sqrt{(n_B \cdot q_B)/(D_B \cdot C_B)}} \quad (D.12)$$

Where n_i is the relative abundance of the microbial population that consume the substrate i , q_i is the specific substrate uptake rate, D_i is the diffusion coefficient and C_i is the concentration of substrate in bulk liquid. If $\phi_{EI}^{A/B}$ is higher than 1.0, substrate A is the most limiting substrate. If $\phi_{EI}^{A/B}$ is lower than 1.0, B is the most limiting substrate.

As stated in Chapter 6 (Section 6.2.2), the limiting substrate would establish the ecological environment and control the microbial community assembly. In this study, it was assumed that the microbial system comammox *Nitrospira/anammox* bacteria is shaped by four limiting substrates: ammonia, nitrite, nitrate and oxygen. In order to predict which substrate is the most limiting, a global eco-interaction modulus (ϕ_{EI}^{A*} , Eq. D.13) is defined based on the $\phi_{EI}^{A/B}$ values of each pair of limiting substrates: $\phi_{EI}^{NH_3/NO_2}$, $\phi_{EI}^{NH_3/NO_3}$, $\phi_{EI}^{NH_3/O_2}$, $\phi_{EI}^{NO_2/NO_3}$, $\phi_{EI}^{NO_2/O_2}$ and $\phi_{EI}^{NO_3/O_2}$.

$$\phi_{EI}^{A*} = \left[\prod_{i \neq A} \phi_{EI}^{A/i} \times \prod_{i \neq A} 1/\phi_{EI}^{i/A} \right]^{1/(S-1)} \quad (D.13)$$

Where S is the number of limiting substrates. As higher is ϕ_{EI}^{A*} , more limiting is substrate A compared to the others, and vice versa. For each limiting substrate:

$$\phi_{EI}^{NH_3*} = \left[\phi_{EI}^{NH_3/NO_2} \times \phi_{EI}^{NH_3/NO_3} \times \phi_{EI}^{NH_3/O_2} \right]^{1/3} \quad (D.14)$$

$$\phi_{EI}^{NO_2*} = \left[\left(1/\phi_{EI}^{NH_3/NO_2} \right) \times \phi_{EI}^{NO_2/NO_3} \times \phi_{EI}^{NO_2/O_2} \right]^{1/3} \quad (D.15)$$

$$\phi_{EI}^{NO_3*} = \left[\left(1/\phi_{EI}^{NH_3/NO_3} \right) \times \left(1/\phi_{EI}^{NO_2/NO_3} \right) \times \phi_{EI}^{NO_3/O_2} \right]^{1/3} \quad (D.16)$$

$$\phi_{EI}^{O_2^*} = \left[\left(1 / \phi_{EI}^{NH_3/O_2} \right) \times \left(1 / \phi_{EI}^{NO_2/O_2} \right) \times \left(1 / \phi_{EI}^{NO_3/O_2} \right) \right]^{1/3} \quad (D.17)$$

The transient change of global eco-interaction modulus for all limiting substrates (ammonia, nitrite, nitrate and oxygen) are shown in Figures D.8 and D.9 (first 50 weeks and full simulation, respectively).

The influence of reducing or withdrawing nitrite in feeding on the NO suppression is clearly shown in the 1st row of Figure D.8. When only ammonia was fed, the dominant substrate of the community assembly was nitrite ($\phi_{EI}^{NO_2^*}$ is the highest), whereas ammonia and oxygen was more dominant than nitrite during the first weeks of simulations in equimolar feeding (favouring the enrichment of NO activity). Under non-equimolar feeding, nitrite and oxygen had similar impact on the community assembly in the first few weeks ($\phi_{EI}^{NO_2^*} \approx \phi_{EI}^{O_2^*}$), representing the threshold of NO suppression via nitrite feeding (with a higher relative concentration of nitrite NO is not suppressed, Figure 7.1B).

On the other hand, the positive correlation observed between oxygen concentration and CMX/AO ratio (Figure D.3B) is also represented by $\phi_{EI}^{NH_3^*}$ and $\phi_{EI}^{O_2^*}$ values, especially in the first weeks of ammonia feeding case. At lower oxygen levels, $\phi_{EI}^{O_2^*}$ is higher than $\phi_{EI}^{NH_3^*}$ values. Then, as higher is the oxygen concentration, $\phi_{EI}^{NH_3^*}$ starts to be higher than $\phi_{EI}^{O_2^*}$ favouring CMX over AO. When equimolar and non-equimolar feeding was applied, ammonia was more dominating than oxygen all the time ($\phi_{EI}^{NH_3^*} > \phi_{EI}^{O_2^*}$), but the difference between $\phi_{EI}^{NH_3^*}$ and $\phi_{EI}^{O_2^*}$ was higher as oxygen concentration was risen, increasing the advantage of CMX over AO activity.

Among the considered limiting substrates, nitrate (with the lowest $\phi_{EI}^{NO_3^*}$ values, except when this was not fed) would be the least dominant substrate, that is, nitrate was the least influential substrate on microbial community assembly.

Supplementary Tables

Table D.1. Key parameter values to calculate ΔG_{cat}^{01} of *Nitrospira* metabolic activities. Values of standard reduction potential at pH 7 (Ψ_i) are from *eQuilibrator 3.0* (Beber et al., 2022). γ_A^* is the number of electrons “accepted” per mole of electron acceptor.

Electron donor/acceptor	Metabolisms	γ_A^* (e ⁻ /mole of eA)	Ψ_i (mV)
UQ/UQH ₂	AO, CMX, NRMX, An-NRMX	–	113
O ₂ /H ₂ O	AO, NO, CMX	4	854
NO ₃ /NO ₂	NO (as eD), NRMX	2	415
NO ₂ /NO	An-NRMX	1	385

Table D.2. List of general parameters used in all simulation experiments.

Parameter	Symbol	Value	Unit	REF
<i>Simulation domain</i>				
Domain size	$L_x \times L_y$	514×514	μm	
Cartesian grid cells	$N_x \times N_y$	257×257	grid cells	
Grid cell size	$\Delta x \times \Delta y$	2×2	μm	
Initial number of flocs	$n_{floc,init}$	12	flocs	
Size of initial aggregates	m_{init}	12	individuals	
<i>Physical parameters: diffusion</i>				
Ammonia (NH_3)	D_{NH_3}	$7.05 \cdot 10^{-6}$	$\text{m}^2 \text{h}^{-1}$	[1]
Nitrite (NO_2^-)	$D_{\text{NO}_2^-}$	$6.88 \cdot 10^{-6}$	$\text{m}^2 \text{h}^{-1}$	[1]
Nitrate (NO_3^-)	$D_{\text{NO}_3^-}$	$6.85 \cdot 10^{-6}$	$\text{m}^2 \text{h}^{-1}$	[1]
Oxygen (O_2)	D_{O_2}	$7.56 \cdot 10^{-6}$	$\text{m}^2 \text{h}^{-1}$	[1]
Carbon dioxide (CO_2)	D_{CO_2}	$6.91 \cdot 10^{-6}$	$\text{m}^2 \text{h}^{-1}$	[1]
Diffusion correction term	σ_{Diff}	0.7	–	[2]
<i>Physical parameters of bacteria</i>				
Density of biomass	ρ_b	500	kg m^{-3}	[3]
Division radius	r_{max}	1	μm	[4]
Inactivation radius	r_{max}	0.464	μm	[4]
Molecular weight ($\text{CH}_{1.8}\text{O}_{0.5}\text{N}_{0.2}$)	MW_b	24.6	g mol^{-1}	[5]
Overlap distance coefficient	$kDist$	1.5	–	
<i>Reactor parameters</i>				
Boundary layer thickness	L_b	5	μm	[6]
Representative volume	V_r	$1.38 \cdot 10^{-3}$	m^3	[7]
Bulk concentration pH	pH	7.0	–	[7]
Temperature	T	20	$^\circ\text{C}$	[7]
Hydraulic retention time	HRT	$140^{(1)}$	h	[7]
<i>Computational parameters</i>				
Steady-state tolerance	tol_{SS}	0.005	$\text{mol L}^{-1} \text{h}^{-1}$	
Diffusion tolerance	tol_{Diff}	$1 \cdot 10^{-8}$	mol m^{-3}	
Maximum bulk concentration change	$\Delta\phi_{bulk,ma.}$	2.0	%	

⁽¹⁾Hydraulic retention time calculated based on the reported reactor size of 7L, cycle times of 12 h and a cycle feed of 600 mL (van Kessel et al., 2015).

• **REF legend:**

- [1]: (Lide, 2006)
- [2]: (van den Berg et al., 2021)
- [3]: (Loferer-Kröbächer et al., 1998; Watson, 1989)
- [4]: (Milo & Philips, 2015)
- [5]: (Roels, 1984)
- [6]: (Suarez et al., 2019)
- [7]: (van Kessel et al., 2015)

Table D.3. Summary of growth kinetics of comammox *Nitrospira* and anammox bacteria. Specific maintenance rate (α) was assumed to be 10% of the maximum growth rate (μ_{\max}) (Bodegom, 2007). $K_{S,N}$ – half saturation constant for substrate N; K_{I,O_2} – inhibition constant for O_2 . Growth kinetic parameters are established assuming non-kinetic competition between metabolic activities of comammox *Nitrospira* and anammox bacteria, consistent with the values reported for anammox bacteria (Straka, 2019; van der Star et al., 2008).

	μ_{\max} (h^{-1})	α (h^{-1})	K_{S,NH_3} (μM)	K_{S,NO_2} (μM)	K_{S,NO_3} (μM)	K_{S,O_2} (μM)	K_{I,O_2} (μM)
AO	0.01	0.001	1.00	–	–	3.13	–
NO	0.01	0.001	–	1.00	–	3.13	–
CMX	0.01	0.001	1.00	–	–	3.13	–
NRMX	0.01	0.001	1.00	–	1.00	3.13	–
An-NRMX	0.01	0.001	1.00	1.00	–	–	–
AMX	0.01	0.001	0.06	1.00	–	–	3.13

Table D.4. Summary of oxygen tolerance of anammox bacteria from literature.

Value (μM)	REF	Comments
Upper oxygen limit (UP)		
0.63	[1]	Anammox activity measured based on ammonium consumption.
1.00	[2]	Anammox activity measured based on ammonium consumption.
3.75	[3]	Anammox activity measured as $^{15}\text{N}^{14}\text{N}$ production in $^{15}\text{NO}_2^-$ ($+^{14}\text{NH}_4^+$) and $^{15}\text{NH}_4^+ + ^{14}\text{NO}_2^-$ incubations. From sea.
13.50	[4]	Anammox activity measured as $^{15}\text{N}^{14}\text{N}$ production in $^{15}\text{NO}_2^-$ ($+^{14}\text{NH}_4^+$) and $^{15}\text{NH}_4^+ + ^{14}\text{NO}_2^-$ incubations. (Sea)
20.00	[5]	Anammox activity measured as $^{15}\text{N}^{14}\text{N}$ production in $^{15}\text{NO}_2^-$ ($+^{14}\text{NH}_4^+$) and $^{15}\text{NH}_4^+ + ^{14}\text{NO}_2^-$ incubations. From sea.
31.25	[6]	Anammox activity measured based on ammonium consumption. (Biofilm)
63.00	[7]	Anammox activity measured based on ammonium consumption. Aggregate biomass was dominated by anammox bacteria (<i>i.e.</i> , scavengers of DO was less than 0.1 %)
Half-maximal activity inhibitory concentration (IC_{50})		
0.89	[8]	Anammox activity measured as $^{15}\text{N}^{14}\text{N}$ production in $^{15}\text{NO}_2^-$ ($+^{14}\text{NH}_4^+$) and $^{15}\text{NH}_4^+ + ^{14}\text{NO}_2^-$ incubations. From sea.
3.40	[5]	Anammox activity measured as $^{15}\text{N}^{14}\text{N}$ production in $^{15}\text{NO}_2^-$ ($+^{14}\text{NH}_4^+$) and $^{15}\text{NH}_4^+ + ^{14}\text{NO}_2^-$ incubations. From sea.
8.00	[4]	Anammox activity measured as $^{15}\text{N}^{14}\text{N}$ production in $^{15}\text{NO}_2^-$ ($+^{14}\text{NH}_4^+$) and $^{15}\text{NH}_4^+ + ^{14}\text{NO}_2^-$ incubations. From sea.
11.10	[5]	Anammox activity measured as $^{15}\text{N}^{14}\text{N}$ production in $^{15}\text{NO}_2^-$ ($+^{14}\text{NH}_4^+$) and $^{15}\text{NH}_4^+ + ^{14}\text{NO}_2^-$ incubations. From sea.
71.88	[9]	Anammox activity measured based on the N_2 production rate. Suspended anammox enrichment culture.
118.75	[9]	Anammox activity measured based on the N_2 production rate. Granular anammox enrichment.
Non-competitive oxygen inhibition constant ($\text{K}_{\text{I},\text{O}_2}$)		
0.313	[2]	Anammox activity measured based on ammonium consumption.
0.092	[10]	Anammox activity measured based on ammonia and nitrite consumption.

• REF legend:

- [1]: (Seuntjens et al., 2018)
- [2]: (Strous et al., 1998)
- [3]: (Egli et al., 2001; Oshiki, Satoh, et al., 2016)
- [4]: (Jensen et al., 2008)
- [5]: (Kalvelage et al., 2011)
- [6]: (Niederdorfer et al., 2021)
- [7]: (Oshiki et al., 2011)
- [8]: (Dalsgaard et al., 2014)
- [9]: (Carvajal-Arroyo et al., 2013)
- [10]: (Straka, 2019)

Table D.5. Metabolic stoichiometries of *Nitrospira* metabolisms and anammox bacteria.

Process ⁽¹⁾	Compounds (M) ⁽²⁾											
	NH ₃	NO ₂	NO ₃	O ₂	CO ₂	N ₂	AO	NO	CMX	NRMX	AnNRMX	AMX
Growth of AO	-1/Y _{xD}	1/Y _{xD}	0	-1.5/Y _{xD}	-1	0	1	0	0	0	0	0
Growth of NO	0	-1/Y _{xD}	1/Y _{xD}	-0.5/Y _{xD}	-1	0	0	1	0	0	0	0
Growth of CMX	-1/Y _{xD}	0	1/Y _{xD}	-2/Y _{xD}	-1	0	0	0	1	0	0	0
Growth of NRMX	-1/Y _{xD}	2/Y _{xD}	-1/Y _{xD}	-1/Y _{xD}	-1	0	0	0	0	1	0	0
Growth of An-NRMX	-1/Y _{xD}	-1/Y _{xD}	0	0	-1	1/Y _{xD}	0	0	0	0	1	0
Growth of AMX	-1/Y _{xD}	-1/Y _{xD}	0	0	-1	1/Y _{xD}	0	0	0	0	0	1
Decay of AO ⁽³⁾	0	0	0	0	1	0	-1	0	0	0	0	0
Decay of NO	0	0	0	0	1	0	0	-1	0	0	0	0
Decay of CMX	0	0	0	0	1	0	0	0	-1	0	0	0
Decay of NRMX	0	0	0	0	1	0	0	0	0	-1	0	0
Decay of An-NRMX	0	0	0	0	1	0	0	0	0	0	-1	0
Decay of AMX	0	0	0	0	1	0	0	0	0	0	0	-1

⁽¹⁾ Although an alternative electron donor for reduction of carbon dioxide to organic biomass precursors (anabolism) is needed, in this study the generation of oxidized electron donor from anabolism was not considered, due to the margin contribution in the nitrogen pool.

⁽²⁾ Stoichiometries of substrate consumption and product synthesis are based on biomass growth yield per mole of electron donor (Y_{xD}): Y_{xNH3} for AO, CMX, An-NRMX, AMX; Y_{xNO2} for NO.

⁽³⁾ Stoichiometries for decay have been simplified at the lowest expression.

Table D.6. Evaluation of ϵ value for aerobic nitrifiers (AOB, NOB, and comammox *Nitrospira*).

	Reported $Y_{X/eD}^{(a)}$	REF	ϵ implied	Calculated $Y_{X/eD}$ ($\epsilon = 0.258$)	
				$Y_{X/eD}^{(a)}$	Error ^(b)
Ammonia-oxidizing bacteria (AOB)					
<i>Nitrosomonas europaea</i>	0.0391	[1]	0.250	0.0413	-0.06
<i>Nitrosomonas europaea</i>	0.0427	[2]	0.263	0.0413	0.03
Nitrite-oxidizing bacteria (NOB)					
<i>Nitrobacter winogradskyi</i>	0.0209	[3]	0.224	0.0262	-0.25
<i>Nitrobacter vulgaris</i>	0.0250	[3]	0.251	0.0262	-0.05
<i>Nitrobacter agilis</i>	0.0257	[4]	0.255	0.0262	-0.02
<i>Nitrobacter hamburgensis</i>	0.0272	[3]	0.265	0.0262	0.04
<i>Ca. Nitrotoga arctica</i>	0.0257	[3]	0.255	0.0262	-0.02
<i>Ca. Nitrospira defluvii</i>	0.0106	[3]	0.152	0.0262	-1.45
<i>Nitrospira marina</i>	0.0243	[5]	0.255	0.0262	-0.02
<i>Nitrospira lenta</i>	0.0303	[3]	0.285	0.0262	0.14
<i>Nitrospira moscoviensis</i>	0.0308	[3]	0.288	0.0262	0.15
<i>Nitrospira moscoviensis</i>	0.0358	[6]	0.320	0.0262	0.27
Complete ammonia-oxidizing bacteria (comammox <i>Nitrospira</i>)					
<i>Nitrospira inopinata</i>	0.0753	[7]	0.294	0.0601	0.20
Average	–	–	0.258	–	–
Std. Dev.	–	–	0.040	–	–
Number	–	–	13	–	–

^(a) Units: mol_{Cx}/mol_{NH₃} for AOB and CMX; mol_{Cx}/mol_{NO₂} for NOB.

^(b) Error is calculated as: $Error = [(Reported Y_{X/eD}) - (Predicted Y_{X/eD})] / (Reported Y_{X/eD})$.

• **REF legend:**

- [1]: (Keen & Prosser, 1987)
- [2]: (Martens-Habbena et al., 2009)
- [3]: (Nowka et al., 2015)
- [4]: (Hunik et al., 1994)
- [5]: (Watson et al., 1986)
- [6]: (Ehrich et al., 1995)
- [7]: (Kits et al., 2017)

Table D.7. Statistical significance (p-value) from comparison of relative abundances of comammox Nitrospira metabolisms and anammox across the different oxygen concentration. A) Ammonia feeding ($NH_3:NO_2:NO_3 = 500:0:0 \mu M$). B) Equimolar feeding ($NH_3:NO_2:NO_3 = 500:500:500 \mu M$). C) Non-equimolar feeding ($NH_3:NO_2:NO_3 = 500:375:500 \mu M$). Symbol legend: ns – not significant; * – $p < 0.05$; ** – $p < 0.01$; * – $p < 0.001$.**

A) [O ₂]	AO	NO	CMX	NRMX	An-NRMX	AMX
1.0μM / 1.5μM	ns	**	ns	ns	ns	**
1.0μM / 3.0μM	ns	***	ns	ns	***	**
1.0μM / 93.8μM	ns	**	*	ns	***	**
1.5μM / 3.0μM	ns	***	ns	ns	***	*
1.5μM / 93.8μM	*	***	**	ns	***	*
3.0μM / 93.8μM	*	***	**	ns	–	–
B) [O ₂]	AO	NO	CMX	NRMX	An-NRMX	AMX
1.0μM / 1.5μM	ns	*	ns	*	ns	*
1.0μM / 3.0μM	**	***	***	ns	*	***
1.0μM / 93.8μM	*	**	**	*	*	***
1.5μM / 3.0μM	*	**	*	ns	*	*
1.5μM / 93.8μM	ns	**	**	ns	*	*
3.0μM / 93.8μM	ns	ns	ns	ns	–	–
C) [O ₂]	AO	NO	CMX	NRMX	An-NRMX	AMX
1.0μM / 1.5μM	ns	**	*	ns	ns	**
1.0μM / 3.0μM	ns	**	*	ns	*	***
1.0μM / 93.8μM	ns	**	**	**	*	***
1.5μM / 3.0μM	ns	***	*	ns	**	***
1.5μM / 93.8μM	ns	***	**	*	**	***
3.0μM / 93.8μM	ns	*	ns	ns	–	–

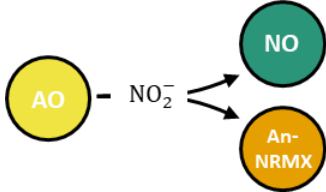
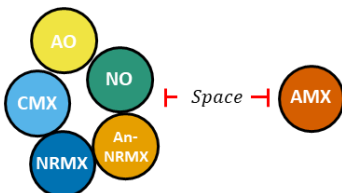
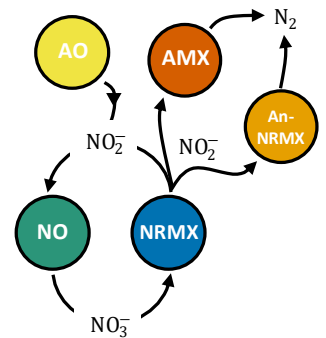
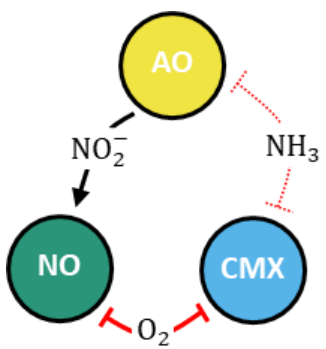
Table D.8. Statistical significance (*p*-value) from comparison of relative abundances of comammox *Nitrospira* metabolisms and anammox across the different N feeding regimes. A) Hypoxic environment with 1.0 μM O_2 . B) Hypoxic environment with 1.5 μM O_2 . C) Hypoxic environment with 3.0 μM O_2 . D) Aerobic environment with 93.8 μM O_2 . Symbol legend: ns – not significant; * – $p < 0.05$; ** – $p < 0.01$; * – $p < 0.001$. Feeding regimes ($\text{NH}_3:\text{NO}_2:\text{NO}_3$): ammonia feeding – 500:0:0 μM ; equimolar feeding – 500:500:500 μM ; non-equimolar feeding – 500:375:500 μM .**

A) Feeding regimes	AO	NO	CMX	NRMX	An-NRMX	AMX
Ammonia feeding / Equimolar feeding	*	**	*	*	ns	***
Ammonia feeding / Non-equimolar feeding	*	ns	*	ns	ns	***
Equimolar feeding / Non-equimolar feeding	*	**	*	**	ns	ns
B) Feeding regimes	AO	NO	CMX	NRMX	An-NRMX	AMX
Ammonia feeding / Equimolar feeding	**	**	**	ns	*	*
Ammonia feeding / Non-equimolar feeding	*	**	**	ns	*	**
Equimolar feeding / Non-equimolar feeding	ns	*	ns	ns	ns	ns
C) Feeding regimes	AO	NO	CMX	NRMX	An-NRMX	AMX
Ammonia feeding / Equimolar feeding	**	***	***	ns	–	–
Ammonia feeding / Non-equimolar feeding	ns	**	ns	ns	–	–
Equimolar feeding / Non-equimolar feeding	ns	ns	ns	ns	–	–
D) $\text{NH}_3:\text{NO}_2:\text{NO}_3$	AO	NO	CMX	NRMX	An-NRMX	AMX
Ammonia feeding / Equimolar feeding	ns	**	**	ns	–	–
Ammonia feeding / Non-equimolar feeding	ns	**	*	ns	–	–
Equimolar feeding / Non-equimolar feeding	ns	*	ns	ns	–	–

Table D.9. Statistical significance (*p*-value) from comparison of *Nitrospira*'s metabolism ratio represented as $\ln(A/B)$ at different nitrogen feeding regimes ($\text{NH}_3:\text{NO}_2:\text{NO}_3$) and oxygen concentrations. A) Metabolic ratios between CMX and division of labour (AO+NO). B) Metabolic ratios between CMX and AO. Symbol legend: ns – not significant; * – $p < 0.05$; ** – $p < 0.01$. Feeding regimes ($\text{NH}_3:\text{NO}_2:\text{NO}_3$): ammonia feeding – 500:0:0 μM ; equimolar feeding – 500:500:500 μM ; non-equimolar feeding – 500:375:500 μM .

A) Feeding regimes	1.0 μM O_2	1.5 μM O_2	3.0 μM O_2	93.8 μM O_2
Ammonia feeding / Equimolar feeding	**	ns	***	**
Ammonia feeding / Non-equimolar feeding	ns	ns	ns	*
Equimolar feeding / Non-equimolar feeding	*	ns	ns	ns
B) Feeding regimes	1.0 μM O_2	1.5 μM O_2	3.0 μM O_2	93.8 μM O_2
Ammonia feeding / Equimolar feeding	ns	ns	ns	ns
Ammonia feeding / Non-equimolar feeding	ns	ns	ns	ns
Equimolar feeding / Non-equimolar feeding	ns	ns	ns	ns

Table D.10. Summary of higher-order interactions (HOI) that influenced the community assembly of comammox *Nitrospira* and anammox bacteria. Continuation of Table D.10 on the next page.

Effect (↑ or ↓)	Feeding ⁽¹⁾	τ_N (p ; n) ⁽²⁾	Representation	
A) Multiple commensal feeding				
↑AO ↑NO ↑An-NRMX	OA _{1.5}	0.2627 (0.0497; 28)		
	UF _{1.5}	0.3368 (0.0137, 27)		
<i>Note: This HOI was not observed between AO, NO and AMX because AMX is a stronger competitor for NO₂ than An-NRMX (↑Y_{X/NO2}).</i>				
B) Space collaboration – Minorities versus majorities				
↑AO ↑NO ↑CMX ↑NRMX	EF _{1.0}	0.5252 (0.0004; 23)		
↑AO ↑NO ↑CMX ↑NRMX ↑An-NRMX	EF _{1.0}	0.3293 (0.0042; 20)		
<i>Note: An-NRMX was also favoured by space collaboration because AMX is a stronger competitor for both NH₃ and NO₂ (↑Y_{X/N}).</i>				
C) Commensal-syntrophic pool				
↑NO ↑NRMX ↑An-NRMX	OA _{1.5}	0.4145 (0.0024; 27)		
		EF _{1.5}		0.4147 (0.0030; 26)
↑AO ↑NO ↑NRMX ↑AMX	OA _{1.5}	0.3079 (0.0397; 23)		
↑AO ↑NO ↑NRMX ↑An-NRMX	OA _{1.5}	0.3021 (0.0435; 26)		
↑AO ↑NO ↑NRMX ↑An-NRMX ↑AMX	OA _{1.5}	0.2243 (0.1439; 22)		
D) Collaborative competition (NO favours division of labour)				
↑AO ↑NO ↓CMX	OA _{1.5}	0.4485 (0.0017; 25)		
	OA _{3.0}	0.5215 (0.0003; 25)		
	OA _{93.8}	0.5636 (<0.0001; 23)		
	EF _{3.0}	0.3573 (0.0123; 25)		
	EF _{93.8}	0.4891 (<0.0001; 22)		
	NF _{1.5}	0.4605 (0.0010; 26)		
	NF _{3.0}	0.3606 (0.0071; 28)		
	NF _{93.8}	0.5760 (<0.0001; 26)		

⁽¹⁾ Feeding: OA – Only ammonia feeding; EF – Equimolar feeding; NF – Non-equimolar feeding. Subscript depicts the concentration of oxygen in μM . ⁽²⁾ τ_N – multivariate Kendall's τ coefficient (see Appendix E); p – significance level (p -value); n – sample size. ⁽³⁾ Red lines depict competition between metabolic activities.

Table D.10. Continuation...

Effect (\uparrow or \downarrow)	Feeding ⁽¹⁾	τ_N (p ; n) ⁽²⁾	Representation	
E) Collaborative competition (NO favours NRMX)				
\uparrow NO \downarrow CMX \uparrow NRMX	OA _{1.5}	0.4043 (0.0056; 24)		
	OA _{3.0}	0.3173 (0.0340; 23)		
	OA _{93.8}	0.4912 (<0.0001 ; 25)		
	EF _{1.5}	0.3983 (0.0064; 24)		
	EF _{3.0}	0.5462 (<0.0001 ; 27)		
	EF _{93.8}	0.5058 (<0.0001 ; 22)		
	NF _{3.0}	0.3647 (0.0055; 29)		
	NF _{93.8}	0.5462 (<0.0001 ; 24)		
	OA _{1.5}	0.3433 (0.0343; 20)		\uparrow AO \uparrow NO \downarrow CMX \uparrow NRMX
	OA _{3.0}	0.3078 (0.0577; 20)		
OA _{93.8}	0.4336 (<0.0001 ; 21)			
EF _{93.8}	0.3142 (0.0062; 20)			
NF _{1.5}	0.2888 (0.0480; 24)			
NF _{93.8}	0.4175 (<0.0001 ; 22)			

Note: The strong competition for O_2 between NO and CMX reduced the capacity of CMX to compete for NH_3 against AO and NRMX.

⁽¹⁾ Feeding: OA – Only ammonia feeding; EF – Equimolar feeding; NF – Non-equimolar feeding. Subscript depicts the concentration of oxygen in μ M. ⁽²⁾ τ_N – multivariate Kendall's τ coefficient (see Appendix E); p – significance level (p -value); n – sample size. ⁽³⁾ Red lines depict competition between metabolic activities.

Table D.11. Statistical significance (p-value) from comparison of relative abundances of comammox *Nitrospira* metabolisms and AMX across the different oxygen concentration. Assuming nitrite affinity of comammox *Nitrospira* equal to A) 1.0 μM of NO_2^- , B) 12.5 μM of NO_2^- and C) 449.2 μM of NO_2^- . Symbol legend: ns – not significant; * – $p < 0.05$; ** – $p < 0.01$; * – $p < 0.001$.**

A) [O ₂]	AO	NO	CMX	NRMX	An-NRMX	AMX
1.0 μM / 1.5 μM	ns	**	*	ns	ns	**
1.0 μM / 3.0 μM	ns	**	*	ns	*	***
1.5 μM / 3.0 μM	ns	***	*	ns	**	***
B) [O ₂]	AO	NO	CMX	NRMX	An-NRMX	AMX
1.0 μM / 1.5 μM	ns	ns	*	*	ns	*
1.0 μM / 3.0 μM	*	**	**	ns	ns	***
1.5 μM / 3.0 μM	*	**	**	ns	ns	***
C) [O ₂]	AO	NO	CMX	NRMX	An-NRMX	AMX
1.0 μM / 1.5 μM	ns	ns	ns	ns	ns	ns
1.0 μM / 3.0 μM	ns	ns	**	ns	ns	*
1.5 μM / 3.0 μM	*	ns	**	ns	ns	*

Table D.12. Statistical significance (p-value) from comparison of relative abundances of comammox *Nitrospira* metabolisms and AMX across the different nitrite affinities of comammox *Nitrospira*. A) Hypoxic environment with 1.0 μM O₂. B) Hypoxic environment with 1.5 μM O₂. C) Hypoxic environment with 3.0 μM O₂. Symbol legend: ns – not significant; * – $p < 0.05$; ** – $p < 0.01$; * – $p < 0.001$.**

A) Nitrite affinity of <i>Nitrospira</i> (K _{NO₂})	AO	NO	CMX	NRMX	An-NRMX	AMX
1.0 μM NO_2^- / 12.5 μM NO_2^-	ns	ns	ns	*	*	**
1.0 μM NO_2^- / 449.2 μM NO_2^-	ns	ns	*	**	*	ns
12.5 μM NO_2^- / 449.2 μM NO_2^-	***	ns	*	**	ns	**
B) Nitrite affinity of <i>Nitrospira</i> (K _{NO₂})	AO	NO	CMX	NRMX	An-NRMX	AMX
1.0 μM NO_2^- / 12.5 μM NO_2^-	*	**	ns	ns	**	***
1.0 μM NO_2^- / 449.2 μM NO_2^-	ns	**	ns	*	**	***
12.5 μM NO_2^- / 449.2 μM NO_2^-	ns	ns	*	*	ns	**
C) Nitrite affinity of <i>Nitrospira</i> (K _{NO₂})	AO	NO	CMX	NRMX	An-NRMX	AMX
1.0 μM NO_2^- / 12.5 μM NO_2^-	ns	*	ns	ns	ns	**
1.0 μM NO_2^- / 449.2 μM NO_2^-	ns	***	ns	ns	ns	**
12.5 μM NO_2^- / 449.2 μM NO_2^-	ns	***	*	*	ns	*

Supplementary Figures

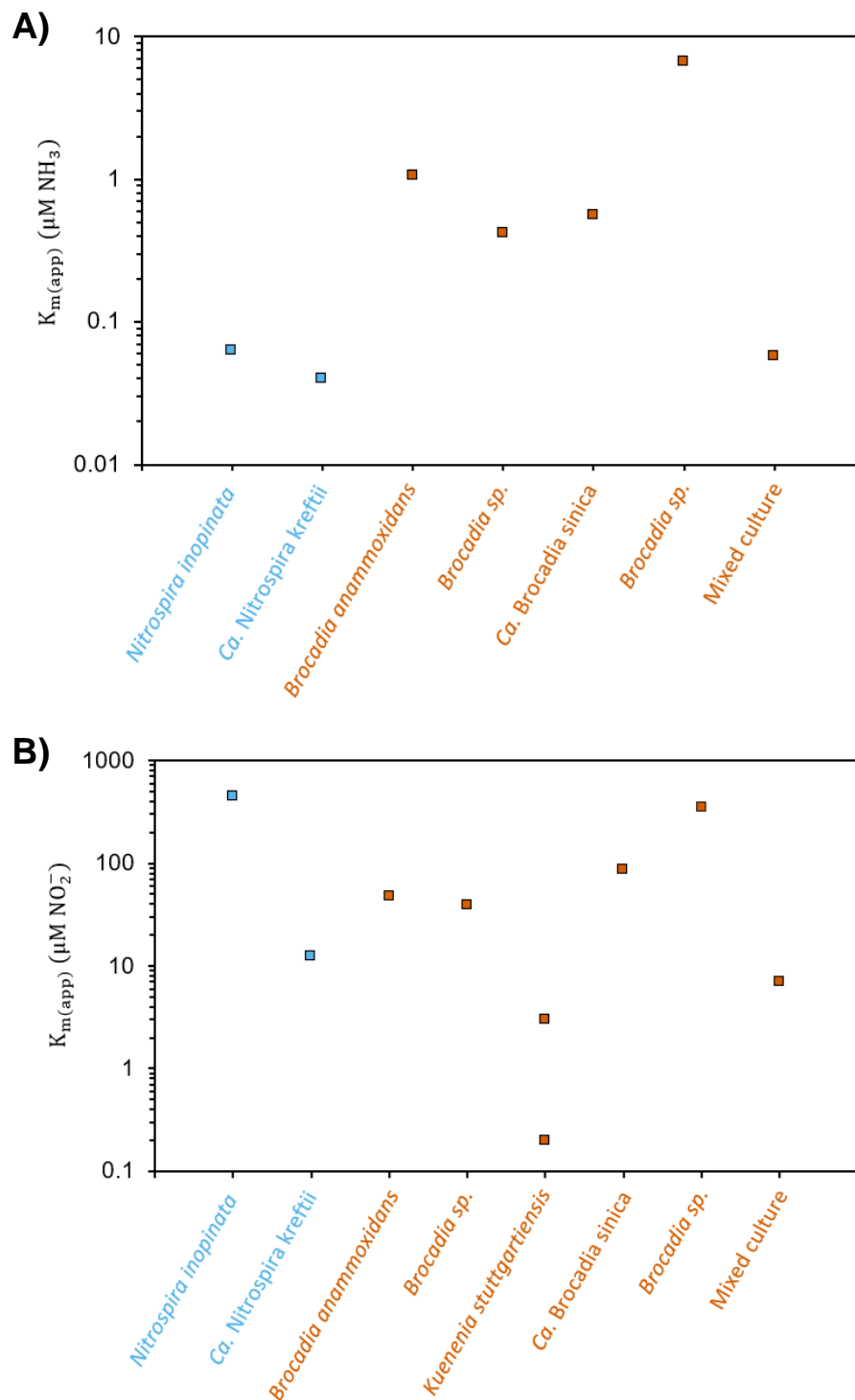


Figure D.1. Apparent substrate affinity ($K_{m(app)}$) for ammonia (panel A) and nitrite (panel B) of comammox *Nitrospira* and anammox bacteria. Colour legend: light blue – comammox *Nitrospira*; orange – anammox bacteria. References of substrate affinities for: comammox *Nitrospira* – (Kits et al., 2017; Sakoula et al., 2021); anammox bacteria – (Ni et al., 2009; Oshiki et al., 2011; Puyol et al., 2013; Straka, 2019; Strous, Kuenen, et al., 1999; van der Star et al., 2008).

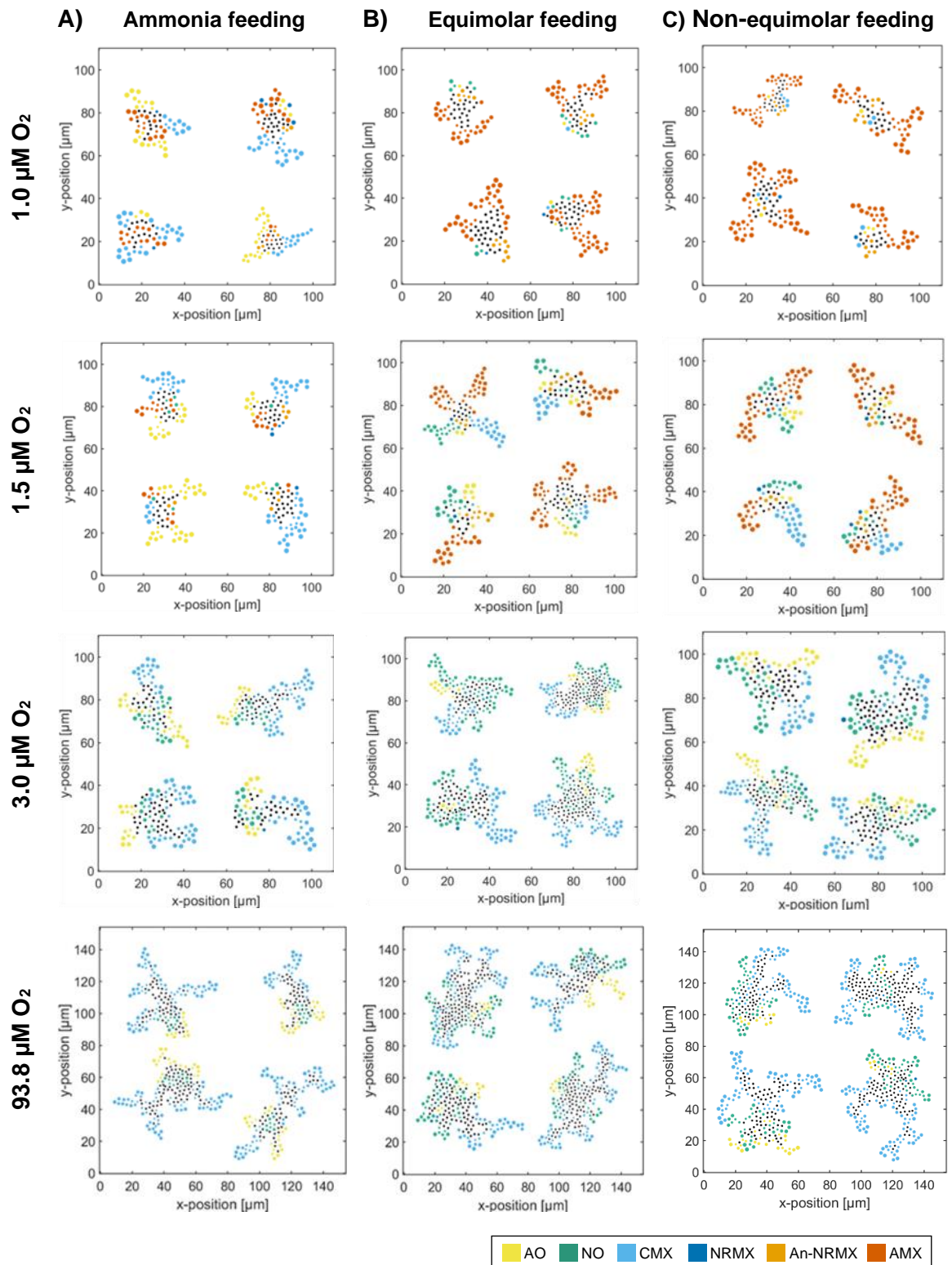


Figure D.2. Additional floc images of comammox *Nitrospira* and anammox bacteria community from simulations at different nitrogen feeding regimes and oxygen concentrations (1.0, 1.5, 3.0, 93.8 μM). Ammonia feeding ($\text{NH}_3:\text{NO}_2:\text{NO}_3 = 500:0:0 \mu\text{M}$). **B)** Equimolar feeding ($\text{NH}_3:\text{NO}_2:\text{NO}_3 = 500:500:500 \mu\text{M}$). **C)** Non-equimolar feeding ($\text{NH}_3:\text{NO}_2:\text{NO}_3 = 500:375:500 \mu\text{M}$). Black circles represent inactive individuals.

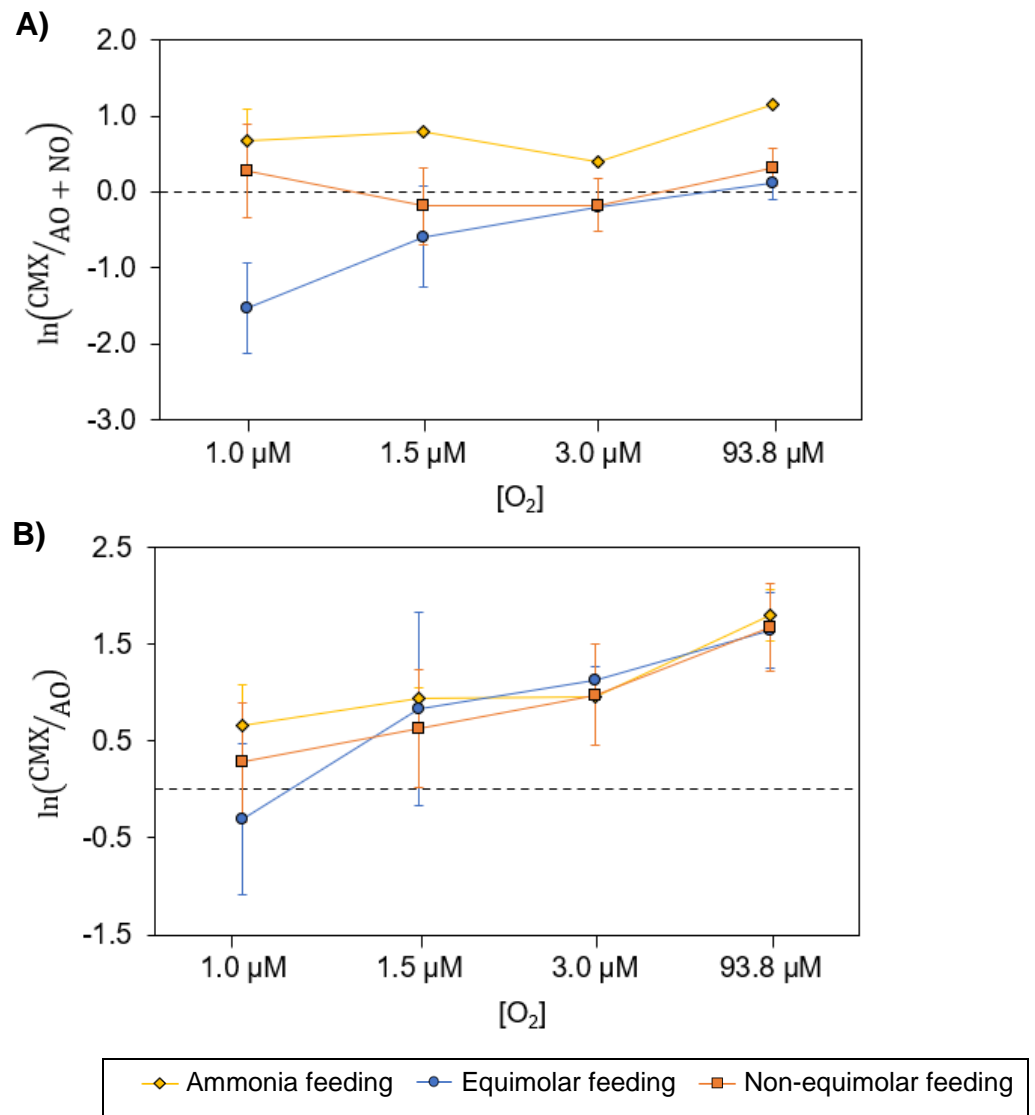


Figure D.3. Metabolic ratios of *Nitrospira* (AO, NO and CMX) represented as $\ln(A/B)$ at different nitrogen feeding regimes ($\text{NH}_3:\text{NO}_2:\text{NO}_3$ ratio) and oxygen concentrations. **A)** Metabolic ratios between CMX and division of labour (AO+NO). **B)** Metabolic ratios between CMX and AO. Error bars show standard deviation of $n = 3$ simulation replicates. Feeding regimes – ammonia feeding: 500:0:0 μM ; equimolar feeding: 500:500:500 μM ; non-equimolar feeding: 500:375:500 μM . The statistical significance between the different nitrogen feeding regimes is shown in Table D.9.

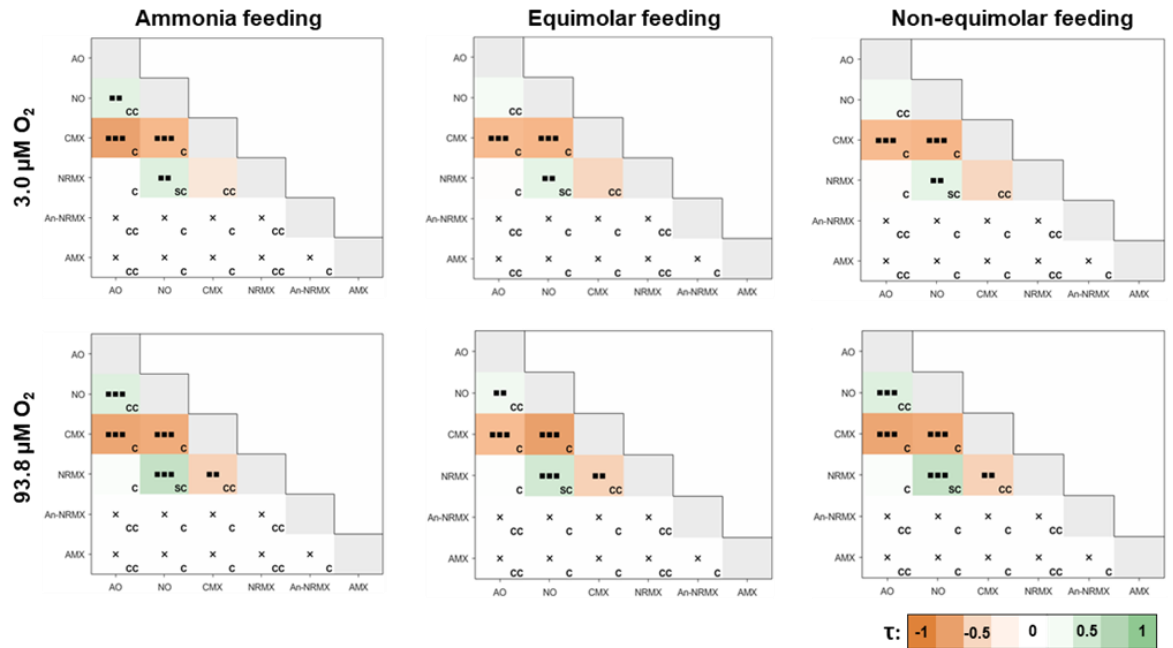


Figure D.4. Ecological analysis at flocculation level under conditions where only comammox *Nitrospira* remained active (3.0 and 93.8 μM of O_2). Ammonia feeding ($\text{NH}_3:\text{NO}_2:\text{NO}_3 = 500:0:0$ μM , left panels), equimolar feeding ($\text{NH}_3:\text{NO}_2:\text{NO}_3 = 500:500:500$ μM , centre panels), and non-equimolar feeding ($\text{NH}_3:\text{NO}_2:\text{NO}_3 = 500:375:500$ μM , right panels). The correlation coefficients of metabolisms are presented on a colour scale. Dotted cells indicate statistically significant correlation (\square : $p < 0.05$; \blacksquare : $p < 0.01$; $\blacksquare\blacksquare$: $p < 0.001$). Cross symbol (x) indicates no co-existence of the metabolic pair at the end of the simulation experiments. Bottom-right labels indicate the ecological interaction of metabolic pair: CC – Commensalism + Competition; SC – Syntrophism + Competition; C – Competition. Sample sizes employed for Kendall's τ calculation are shown in Figure D.5.

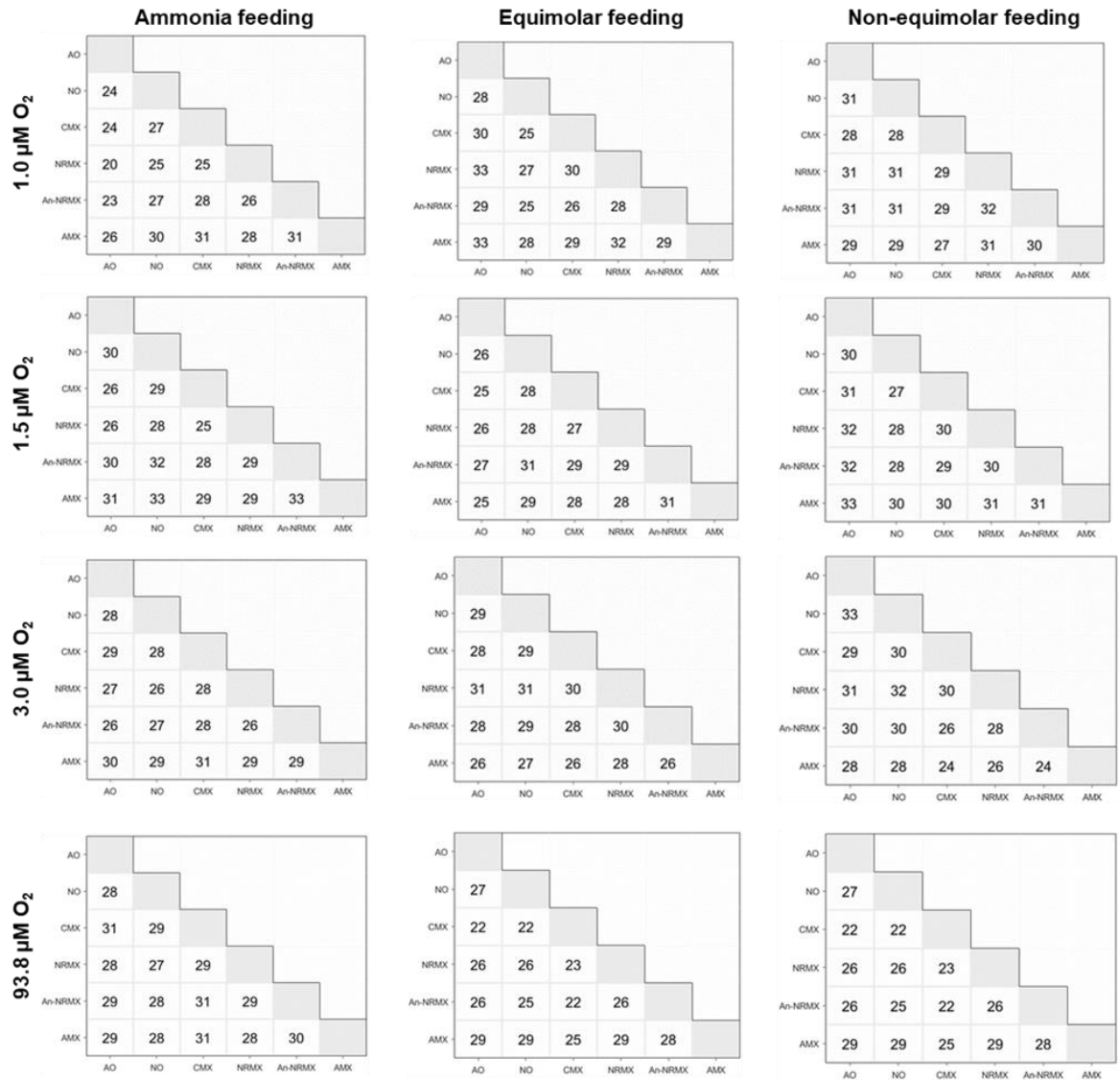


Figure D.5. Sample sizes employed for Kendall's coefficient calculation. Different nitrogen feeding regime was applied: ammonia feeding (left panels, $\text{NH}_3:\text{NO}_2:\text{NO}_3 = 500:0:0 \mu\text{M}$), equimolar feeding (centre panels, $\text{NH}_3:\text{NO}_2:\text{NO}_3 = 500:500:500 \mu\text{M}$), and non-equimolar feeding (right panels, $\text{NH}_3:\text{NO}_2:\text{NO}_3 = 500:375:500 \mu\text{M}$). Total replicates: 36 in all conditions.

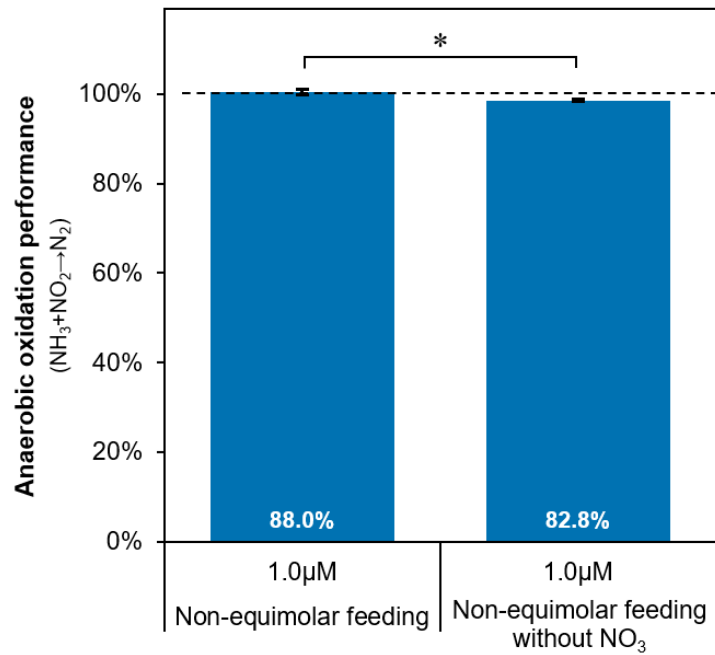


Figure D.6. Influence of nitrate concentration in influent to anaerobic oxidation performance (ammonia and nitrite oxidation to N₂) expressed as percentage. Data labels depict the relative abundance of anaerobic activities (An-NRMX and AMX). Feeding regimes: non-equimolar feeding – 500:375:500 μM; non-equimolar feeding without NO₃ – 500:375:0 μM. Error bars show standard deviation of n = 3 simulation replicates. Asterisks denote p-value significance where *, p < 0.05. For more information about the calculus of the anaerobic oxidation performance (see Methods of Chapter 7 – Parameters for the quantification of nitrogen removal).

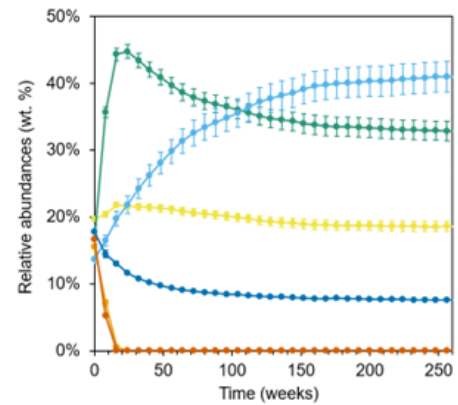
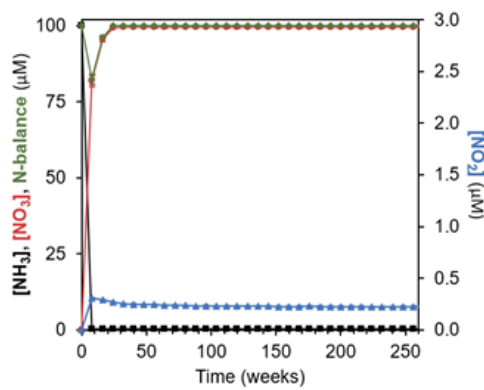
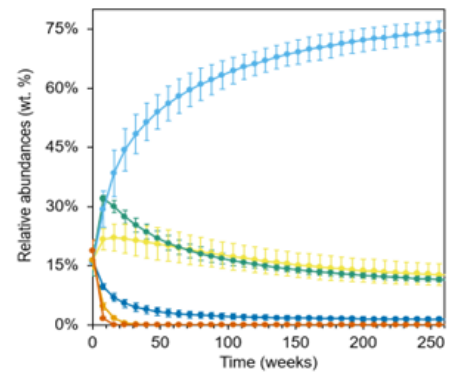
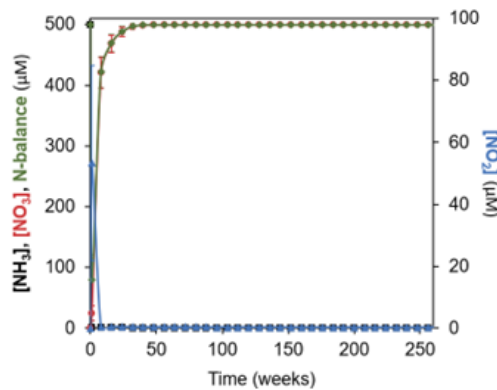
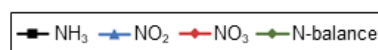
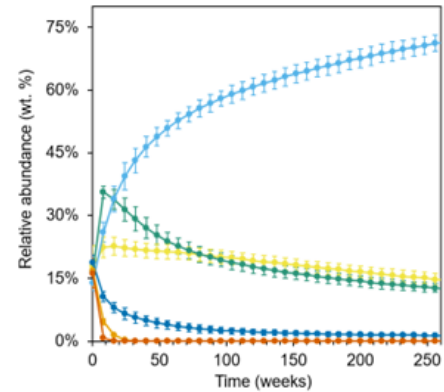
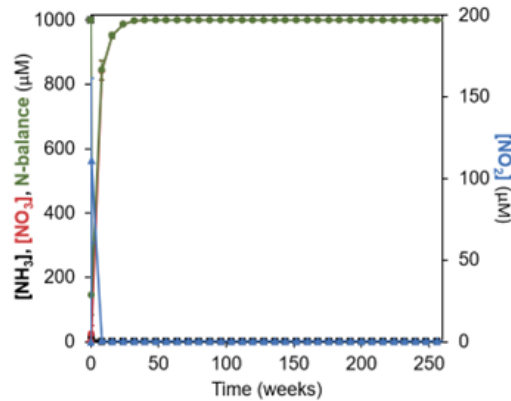
A) Ammonia feeding (100 μM)**B) Ammonia feeding (500 μM)****C) Ammonia feeding (1000 μM)**

Figure D.7. Influence of ammonia concentration to the transient accumulation of nitrite at 93.8 μM of O_2 . Three ammonia concentrations were tested. Full simulation (5.0 years): 100 μM of NH_3 (panels **A**), 500 μM of NH_3 (panels **B**), and 1000 μM of NH_3 (panels **C**). Left panels show the dynamics of nitrogen compounds (NH_3 , NO_2 and NO_3) at the early stages of simulation. Right panels show the evolution of relative abundances of comammox *Nitrospira* and anammox. Error bars show standard deviation of $n = 3$ simulation replicates. If not visible, error bars are smaller than symbols.

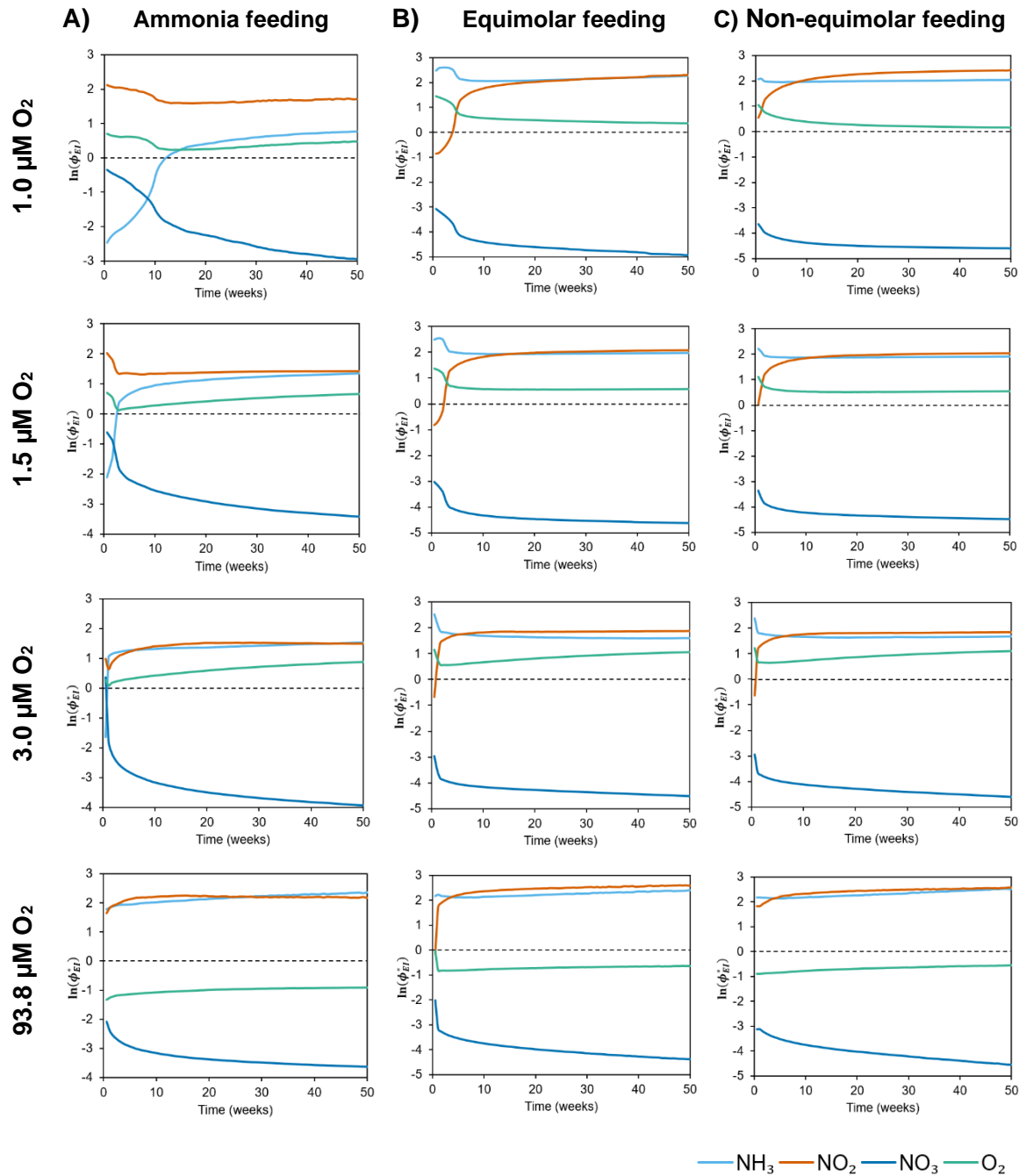


Figure D.8. Analysis of ecological environment and dominant substrates (global eco-interaction modulus, ϕ_{EI}^*). First 50 weeks are shown (full simulation in Fig. D.9). Feeding regimes: only ammonia feeding ($NH_3:NO_2:NO_3 = 500:0:0 \mu M$, left panels), equimolar feeding ($NH_3:NO_2:NO_3 = 500:500:500 \mu M$, centre panels), and non-equimolar feeding ($NH_3:NO_2:NO_3 = 500:375:500 \mu M$, right panels). Error bars show standard deviation of $n = 3$ simulation replicates. If not visible, error bars are smaller than line weight.

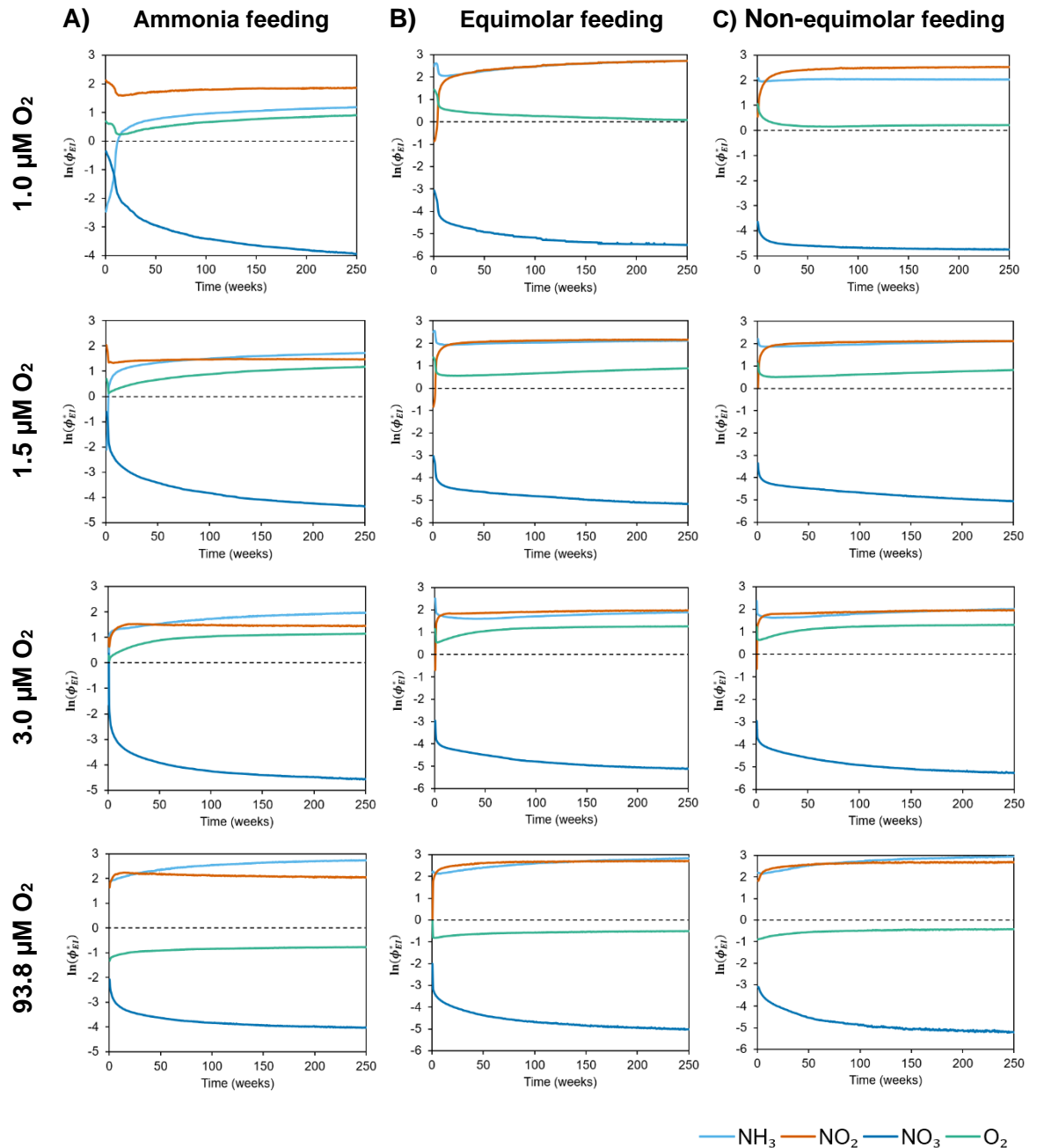


Figure D.9. Analysis of ecological environment and dominant substrates (global eco-interaction modulus, ϕ_{EI}^*). Full simulation (5.0 years). Feeding regimes: only ammonia feeding ($\text{NH}_3:\text{NO}_2:\text{NO}_3 = 500:0:0 \mu\text{M}$, left panels), equimolar feeding ($\text{NH}_3:\text{NO}_2:\text{NO}_3 = 500:500:500 \mu\text{M}$, centre panels), and non-equimolar feeding ($\text{NH}_3:\text{NO}_2:\text{NO}_3 = 500:375:500 \mu\text{M}$, right panels). Error bars show standard deviation of $n = 3$ simulation replicates. If not visible, error bars are smaller than line weight.

Appendix E - Multivariate Kendall's Tau (Tau-N)

Multivariate correlation analysis would play an important role in ecology for the quantification and interpretation of interactions between more than two species (known as higher-order interactions) (Ludington, 2022). Among the existing correlations analyses for two variables, Kendall's τ correlation (Kendall, 1938) is of special interest because (i) is based on either being distribution-free or having a specified distribution but without specific parameters (*i.e.*, a non-parametric measure), (ii) the simplicity of its methodology and (iii) the property of τ to be close to a normality distribution even for low number of observations (n). For two observed variables (X and Y), the Kendall's τ correlation is defined as

$$\tau = \frac{(\text{number of concordant pairs}) - (\text{number of discordant pairs})}{(\text{number of pairs})}$$

Here, a novel multivariate generalization of Kendall's τ coefficient is proposed to describe the association between more than two variables (multiple variables, $N \geq 2$). The proposed method can be used to state which tendency follows a set of multiple joint variables, allowing to describe complex data trends as, for example, the mentioned higher-order interactions. Although in this methodology has been developed from Kendall (1938) work, *concordance/discordance* concept has not been utilized to describe the correlation between the variables. This is because the loss of information that lies in *discordance* concept when more than two observed variables are considered. Instead, this methodology has been built up based on the concept of *paired orthants*. Because of this, the formulation of *conventional* Kendall's τ (*i.e.*, the non-parametric correlation between two variables based on the concept of *concordance/discordance*; Kendall, 1938) has been also revised.

Limitations of the *discordance* concept for multiple variables

The intuitive way to define the *concordance* and *discordance* concepts is this: two random variables (X and Y) are *concordant* when large (small) values of X go with large (small) values of Y , whereas these two are *discordant* when large values of X go with small values of Y or vice versa.

Let $(x_1, y_1), \dots, (x_n, y_n)$ be a set of observations of the joint random variables X and Y , such that all the values of (x_i) and (y_i) are unique. If a reference point is fixed $((x_i^*, y_i^*) \in \mathbb{R}^2)$, it is possible to determine four subsets of \mathbb{R}^2 (quadrants, Q):

$$Q_I(x_i^*, y_i^*) = \{(x_j, y_j) \in \mathbb{R}^2: x_i^* < x_j, y_i^* < y_j\}$$

$$Q_{II}(x_i^*, y_i^*) = \{(x_j, y_j) \in \mathbb{R}^2: x_i^* > x_j, y_i^* < y_j\}$$

$$Q_{III}(x_i^*, y_i^*) = \{(x_j, y_j) \in \mathbb{R}^2: x_i^* > x_j, y_i^* > y_j\}$$

$$Q_{IV}(x_i^*, y_i^*) = \{(x_j, y_j) \in \mathbb{R}^2: x_i^* < x_j, y_i^* > y_j\}$$

Definition 1. Let $(x_i^*, y_i^*, \dots, k_i^*)$ the reference point of a set of observations of K joint random variables $\langle X, Y, \dots, K \rangle$. An orthant in N -dimensions is considered the intersection of mutually orthogonal half-spaces through the reference point. An orthant in 2-dimensions is a quadrant (Q), in 3-dimensions an octant (O), and for more than three a hyperoctant (nH).

Note that in quadrant Q_I (Q_{III}) large (small) values of X go with large (small) values of Y – definition of *concordance*; and in quadrant Q_{II} (Q_{IV}) small (large) values of X go with large (small) values of Y – definition of *discordance* (Figure E.1).

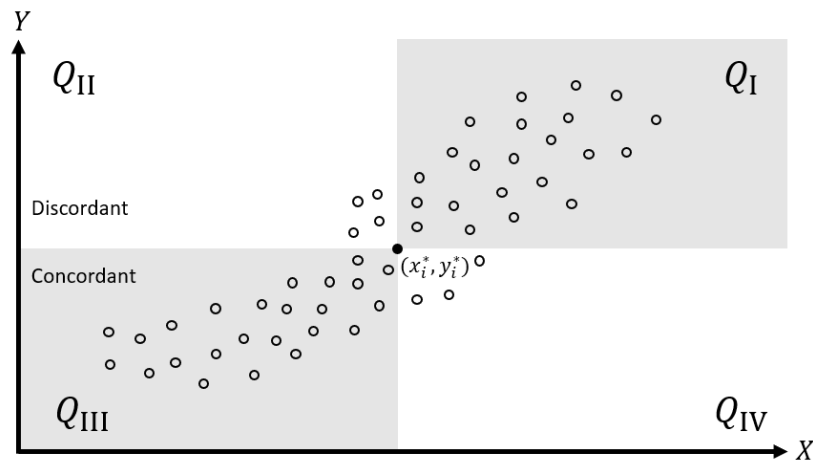


Figure E.1. Visual representation of concordance and discordance for two joint variables (X and Y). All points in the grey area are concordant, and all points in the white area are discordant with respect to (x_i^*, y_i^*) .

Definition 2. Let H and H' two independent set of observations. H is more concordant than H' if, for all $(x, y) \in \mathbb{R}^2$,

$$\Pr\{(x, y) \in [Q_I(x, y) \vee Q_{III}(x, y)] \mid H\} > \Pr\{(x, y) \in [Q_I(x, y) \vee Q_{III}(x, y)] \mid H'\}$$

or H is less discordant than H' if, for all $(x, y) \in \mathbb{R}^2$,

$$\Pr\{(x, y) \in [Q_{II}(x, y) \vee Q_{IV}(x, y)] \mid H\} < \Pr\{(x, y) \in [Q_{II}(x, y) \vee Q_{IV}(x, y)] \mid H'\}.$$

Existing non-parametric rank correlation analysis, such as Kendall's τ (Kendall, 1938) or Spearman's ρ (Spearman, 1904), are based on the evaluation of the probability of *concordance* and *discordance*. For this reason, these are known as *measures of concordance*, satisfying the set of axioms propose by Scarsini (Scarsini, 1984). Considering Scarsini's axioms, the following result is immediate for a pair of random variables:

Proposition 1. *A pair of observations, (x_i, y_i) and (x_j, y_j) , are concordant if have the property $\text{sgn}(x_j - x_i) = \text{sgn}(y_j - y_i)$ and these are discordant if satisfy the condition $\text{sgn}(x_j - x_i) = -\text{sgn}(y_j - y_i)$ (or $\text{sgn}(x_j - x_i) \neq \text{sgn}(y_j - y_i)$). $\text{sgn}(\chi)$ is the signum function of χ (Eq. E.1):*

$$\text{sgn}(\chi) := \begin{cases} -1 & \text{if } \chi < 0, \\ 0 & \text{if } \chi = 0, \\ 1 & \text{if } \chi > 0. \end{cases} \quad (\text{E.1})$$

Now the ordinary statement of *concordance* and *discordance* is defined for three variables (X , Y and Z), the maximum set in which can be clearly represented with the Cartesian coordinate system. Let $(x_1, y_1, z_1), \dots, (x_n, y_n, z_n)$ be a set of observations of the joint random variables X , Y and Z , such that all the values of (x_i) , (y_i) and (z_i) are unique. If a reference point $(x_i^*, y_i^*, z_i^*) \in \mathbb{R}^3$ is fixed, it is possible to determine eight subsets of \mathbb{R}^3 (octants, O):

$$O_I(x_i^*, y_i^*, z_i^*) = \{(x_j, y_j, z_j) \in \mathbb{R}^3: x_i^* < x_j, y_i^* < y_j, z_i^* < z_j\}$$

$$O_{II}(x_i^*, y_i^*, z_i^*) = \{(x_j, y_j, z_j) \in \mathbb{R}^3: x_i^* < x_j, y_i^* < y_j, z_i^* > z_j\}$$

$$O_{III}(x_i^*, y_i^*, z_i^*) = \{(x_j, y_j, z_j) \in \mathbb{R}^3: x_i^* > x_j, y_i^* < y_j, z_i^* > z_j\}$$

$$O_{IV}(x_i^*, y_i^*, z_i^*) = \{(x_j, y_j, z_j) \in \mathbb{R}^3: x_i^* > x_j, y_i^* < y_j, z_i^* < z_j\}$$

$$O_V(x_i^*, y_i^*, z_i^*) = \{(x_j, y_j, z_j) \in \mathbb{R}^3: x_i^* < x_j, y_i^* > y_j, z_i^* < z_j\}$$

$$O_{VI}(x_i^*, y_i^*, z_i^*) = \{(x_j, y_j, z_j) \in \mathbb{R}^3: x_i^* < x_j, y_i^* > y_j, z_i^* > z_j\}$$

$$O_{VII}(x_i^*, y_i^*, z_i^*) = \{(x_j, y_j, z_j) \in \mathbb{R}^3: x_i^* > x_j, y_i^* > y_j, z_i^* > z_j\}$$

$$O_{VIII}(x_i^*, y_i^*, z_i^*) = \{(x_j, y_j, z_j) \in \mathbb{R}^3: x_i^* > x_j, y_i^* > y_j, z_i^* < z_j\}$$

Note that on the octant O_I (O_{VII}) large (small) values of X go with large (small) values of Y and Z – definition of *concordance*; whereas on the octant O_{II} (O_{VIII}) large (small) values of X go with large (small) values of Y and small (large) values of Z , octant O_{III} (O_V) small (large) values of X go with large (small) values of Y and small (large) values of Z , and octant

O_{IV} (O_{VI}) small (large) values of X go with large (small) values of Y and large (small) values of Z – all of them do not follow the *concordance* definition and, therefore, would be interpreted as definitions of *discordance* (Figure E.2)

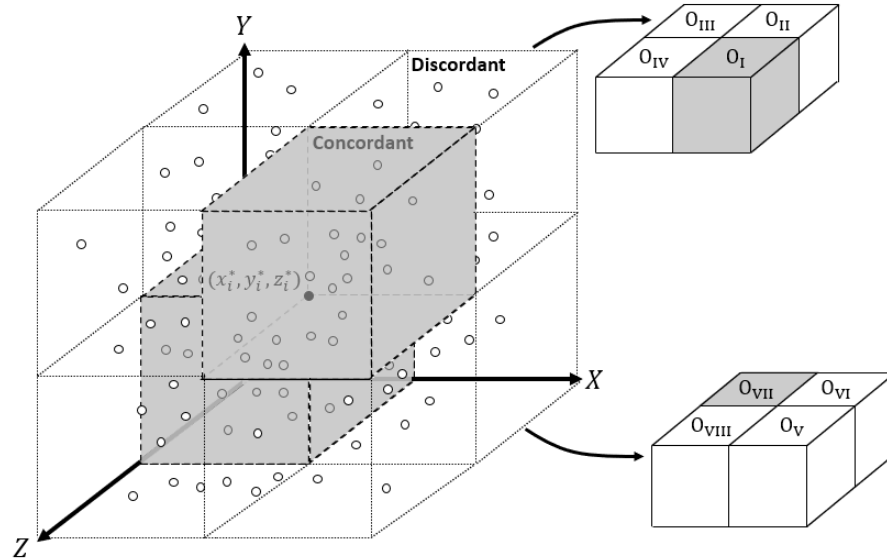


Figure E.2. Representation of concordance and discordance for three joint variables (X, Y, Z). All points in grey region are concordant, and all points in white region are discordant with respect to (x_i^*, y_i^*, z_i^*) .

Then, for any pair of observations (x_i, y_i, \dots, k_i) and (x_j, y_j, \dots, k_j) from a set of K variables $\langle X, Y, Z, \dots, K \rangle$, the following result is direct:

Proposition 2. A pair of observations, each with K variables, (x_i, y_i, \dots, k_i) and (x_j, y_j, \dots, k_j) are concordant if $\text{sgn}(x_j - x_i) = \text{sgn}(y_j - y_i) = \dots = \text{sgn}(k_j - k_i)$. Contrary, they are discordant if (at least) one non-equal is found between the pair of observation (i.e., $\dots = \text{sgn}(z_j - z_i) \neq \text{sgn}(c_j - c_i) = \dots$).

The binary nature of *concordance/discordance* condition (i.e., if dataset is not *concordant* then is *discordant* and vice versa) implies a loss of information in *discordance* definition when more than two observed variables are considered ($H(x, y, \dots, k) \in \mathbb{R}^N$, $N > 2$). For example, in the set of three observed variables ($H(x, y, z) \in \mathbb{R}^3$), these situations

large (small) values of X go with large (small) values of Y and small (large) values of Z ,

small (large) values of X go with large (small) values of Y and small (large) values of Z ,

small (large) values of X go with large (small) values of Y and large (small) values of Z ,

are not the same, although all of them would be considered *discordant* situations. Each situation is differentiable to the others, having its own *data trend*.

Definition of *paired* orthants and individual *data trend* coefficients

The orthants of a N -dimension (\mathbb{R}^N) can be associated to a set of signs ($[\pm]$). Let $(x_i^*, y_i^*, \dots, k_i^*)$ the reference point of a set of observations of the joint random variables $\langle X, Y, \dots, K \rangle$. The associated symbols of each orthant is set based on the difference between the dataset (x_j, y_j, \dots, k_j) and the reference point (*i.e.*, $\Delta k_{ji}^* = k_j - k_i^*$). For example, for a set $H(x, y) \in \mathbb{R}^2$, the associated signs for each quadrant (Q) are:

$$Q_I(x_i^*, y_i^*) = \{(x_j, y_j) \in \mathbb{R}^2: \Delta x_{ji}^* > 0, \Delta y_{ji}^* > 0\} \equiv [+ , +]$$

$$Q_{II}(x_i^*, y_i^*) = \{(x_j, y_j) \in \mathbb{R}^2: \Delta x_{ji}^* < 0, \Delta y_{ji}^* > 0\} \equiv [- , +]$$

$$Q_{III}(x_i^*, y_i^*) = \{(x_j, y_j) \in \mathbb{R}^2: \Delta x_{ji}^* < 0, \Delta y_{ji}^* < 0\} \equiv [- , -]$$

$$Q_{IV}(x_i^*, y_i^*) = \{(x_j, y_j) \in \mathbb{R}^2: \Delta x_{ji}^* > 0, \Delta y_{ji}^* < 0\} \equiv [+ , -]$$

and the associated signs for each octant (O) are:

$$O_I(x_i^*, y_i^*, z_i^*) = \{(x_j, y_j, z_j) \in \mathbb{R}^3: \Delta x_{ji}^* > 0, \Delta y_{ji}^* > 0, \Delta z_{ji}^* > 0\} \equiv [+ , + , +]$$

$$O_{II}(x_i^*, y_i^*, z_i^*) = \{(x_j, y_j, z_j) \in \mathbb{R}^3: \Delta x_{ji}^* > 0, \Delta y_{ji}^* > 0, \Delta z_{ji}^* < 0\} \equiv [+ , + , -]$$

$$O_{III}(x_i^*, y_i^*, z_i^*) = \{(x_j, y_j, z_j) \in \mathbb{R}^3: \Delta x_{ji}^* < 0, \Delta y_{ji}^* > 0, \Delta z_{ji}^* < 0\} \equiv [- , + , -]$$

$$O_{IV}(x_i^*, y_i^*, z_i^*) = \{(x_j, y_j, z_j) \in \mathbb{R}^3: \Delta x_{ji}^* < 0, \Delta y_{ji}^* > 0, \Delta z_{ji}^* > 0\} \equiv [- , + , +]$$

$$O_V(x_i^*, y_i^*, z_i^*) = \{(x_j, y_j, z_j) \in \mathbb{R}^3: \Delta x_{ji}^* > 0, \Delta y_{ji}^* < 0, \Delta z_{ji}^* > 0\} \equiv [+ , - , +]$$

$$O_{VI}(x_i^*, y_i^*, z_i^*) = \{(x_j, y_j, z_j) \in \mathbb{R}^3: \Delta x_{ji}^* > 0, \Delta y_{ji}^* < 0, \Delta z_{ji}^* < 0\} \equiv [+ , - , -]$$

$$O_{VII}(x_i^*, y_i^*, z_i^*) = \{(x_j, y_j, z_j) \in \mathbb{R}^3: \Delta x_{ji}^* < 0, \Delta y_{ji}^* < 0, \Delta z_{ji}^* < 0\} \equiv [- , - , -]$$

$$O_{VIII}(x_i^*, y_i^*, z_i^*) = \{(x_j, y_j, z_j) \in \mathbb{R}^3: \Delta x_{ji}^* < 0, \Delta y_{ji}^* < 0, \Delta z_{ji}^* > 0\} \equiv [- , - , +]$$

The orthants determined for \mathbb{R}^2 (quadrants, Q) and \mathbb{R}^3 (octants, O) can be *paired* based on their associated signs (pairing these through the equality: $Oh_\alpha = \neg Oh_\beta$). For an observation with two joint variables ($H(x, y) \in \mathbb{R}^2$), the definition of *paired quadrants* ($Q_\alpha \otimes Q_\beta$) are:

$$Q_I(x_i^*, y_i^*) = \neg Q_{III}(x_i^*, y_i^*) \equiv [+ , +] = \neg[- , -] \Rightarrow Q_I \otimes Q_{III}$$

$$Q_{II}(x_i^*, y_i^*) = \neg Q_{VI}(x_i^*, y_i^*) \equiv [- , +] = \neg[+ , -] \Rightarrow Q_{II} \otimes Q_{VI}$$

where $Q_I \otimes Q_{III}$ and $Q_{II} \otimes Q_{VI}$ would correspond to the *concordance* and *discordance* definition for a set $H(x, y) \in \mathbb{R}^2$, respectively (Figure E.1).

For an observation with three joint variables ($H(x, y, z) \in \mathbb{R}^3$), the definition of *paired octants* ($O_\alpha \otimes O_\beta$) are:

$$O_I(x_i^*, y_i^*, z_i^*) = \neg Q_{VII}(x_i^*, y_i^*, z_i^*) \equiv [+ , + , +] = \neg[- , - , -] \Rightarrow O_I \otimes O_{VII}$$

$$O_{II}(x_i^*, y_i^*, z_i^*) = \neg Q_{VIII}(x_i^*, y_i^*, z_i^*) \equiv [+ , + , -] = \neg[- , - , +] \Rightarrow O_{II} \otimes O_{VIII}$$

$$O_{III}(x_i^*, y_i^*, z_i^*) = \neg Q_V(x_i^*, y_i^*, z_i^*) \equiv [- , + , -] = \neg[+ , - , +] \Rightarrow O_{III} \otimes O_V$$

$$O_{IV}(x_i^*, y_i^*, z_i^*) = \neg Q_{VI}(x_i^*, y_i^*, z_i^*) \equiv [- , + , +] = \neg[+ , - , -] \Rightarrow O_{IV} \otimes O_{VI},$$

where $O_I \otimes O_{VII}$ would correspond to the *concordance* definition for a set $H(x, y, z) \in \mathbb{R}^3$. Then, for any observation with K joint variables ($H(x, y, \dots, k) \in \mathbb{R}^N$), the following result is immediate:

Proposition 3. *A couple of orthants (Oh_α and Oh_β) of a given reference point ($x_i^*, y_i^*, \dots, k_i^*$) are paired if and only if satisfies the property $Oh_\alpha(x_i^*, y_i^*, \dots, k_i^*) = \neg Oh_\beta(x_i^*, y_i^*, \dots, k_i^*)$. For any number of joint variables (N), the total of paired orthants ($Oh_\alpha \otimes Oh_\beta$) is equivalent to $2^N/2$.*

The set of symbols associated to each *paired orthants* ($[\pm, \pm, \dots, \pm] = \neg[\mp, \mp, \dots, \mp]$) is what defines the *data trend*. A straightforward way to evaluate the correlation between two variables is through probabilities (Kendall, 1938). Then, the *data trend* for a set of observations from $H(x, \dots, k) \in \mathbb{R}^N$ can be stated as the probability of a dataset to reside on the *paired orthants*. For example, the probabilities of a set $H(x, y) \in \mathbb{R}^2$ to reside in one of the *paired quadrants* ($Q_\alpha \otimes Q_\beta$), and the respective *data trends* ($[\pm, \pm] \otimes [\mp, \mp]$) are:

$$\Pi_{Q_{III}}^{Q_I} \equiv \Pi_{[-,-]}^{[+,+]} = \Pr\{(x, y) \in [Q_I(x, y) \vee Q_{III}(x, y)] | H\} \equiv \Pr\{(x, y) \rightarrow [[+, +] \vee [-, -]] | H\}$$

$$\Pi_{Q_{IV}}^{Q_{II}} \equiv \Pi_{[+,-]}^{[-,+]} = \Pr\{(x, y) \in [Q_{II}(x, y) \vee Q_{IV}(x, y)] | H\} \equiv \Pr\{(x, y) \rightarrow [[-, +] \vee [+ , -]] | H\}$$

For a set $H(x, y, z) \in \mathbb{R}^3$, the probabilities to reside on the *paired octants* ($O_\alpha \otimes O_\beta$) and the respective *data trends* ($[\pm, \pm, \pm] \otimes [\mp, \mp, \mp]$) are:

$$\Pi_{O_{VII}}^{O_I} \equiv \Pi_{[-,-,-]}^{[+,+,+]} = \Pr\{(x, y, z) \in [O_I(x, y, z) \vee O_{VII}(x, y, z)] | H\} \equiv \Pr\{(x, y, z) \rightarrow [[+, +, +] \vee [-, -, -]] | H\}$$

$$\Pi_{O_{VIII}}^{O_{II}} \equiv \Pi_{[-,-,+]}^{[+,+,-]} = \Pr\{(x, y, z) \in [O_{II}(x, y, z) \vee O_{VIII}(x, y, z)] | H\} \equiv \Pr\{(x, y, z) \rightarrow [[+, +, -] \vee [-, -, +]] | H\}$$

$$\Pi_{O_V}^{O_{III}} \equiv \Pi_{[-,+,-]}^{[+,-,+]} = \Pr\{(x, y, z) \in [O_{III}(x, y, z) \vee O_V(x, y, z)] | H\} \equiv \Pr\{(x, y, z) \rightarrow [[-, +, -] \vee [+ , -, +]] | H\}$$

$$\Pi_{O_{VI}}^{O_{IV}} \equiv \Pi_{[-,+,-]}^{[-,+,-]} = \Pr\{(x, y, z) \in [O_{IV}(x, y, z) \vee O_{VI}(x, y, z)] | H\} \equiv \Pr\{(x, y, z) \rightarrow [[-, +, +] \vee [+ , -, -]] | H\}$$

Then, any individual *data trend* coefficient ($\delta_{[\pm]}^{[\mp]}$) can be defined as

$$\delta_{[\mp]}^{[\pm]} = \Pi_{[\mp]}^{[\pm]} \equiv \frac{(\# \text{ of pairs in } Oh_\alpha \otimes Oh_\beta)}{\binom{n}{2}} = \frac{(\# \text{ of pairs following } [\pm]) + (\# \text{ of pairs following } [\mp])}{\binom{n}{2}}$$

where $\binom{n}{2} = \frac{n \cdot (n-1)}{2}$ is the binomial coefficient for the number of ways to choose two items from n observations. The $\delta_{[\mp]}^{[\pm]}$ value lies between 0 and 1 inclusive, taking 1 if and only if all the probability mass lies on one of the *paired orthants* ($Oh_\alpha \otimes Oh_\beta$), that is, the dataset follows certain *data trend* entirely ($[\pm] \otimes [\mp]$). The value of 0 states the null probability of following the respective *data trend* ($[\pm] \otimes [\mp]$) of the coefficient $\delta_{[\mp]}^{[\pm]}$. If observed variables are independent, then all $\delta_{[\mp]}^{[\pm]}$ coefficients are equal to $2/2^N$ (where N is the number of joint variables). The value of $2/2^N$ is referred here as the *reliable point* (r_p).

Recalling the definition of the associated signs ($\Delta k_{ji} = k_j - k_i^*$) and *data trends* ($[\pm] \otimes [\mp]$), the explicit expression of the individual *data trend* coefficients for $H(x, y) \in \mathbb{R}^2$ ($\delta_{[\mp]}^{[\pm]}$) are:

$$\delta_{[-,-]}^{[+,+]} = \frac{2}{n \cdot (n-1)} \cdot \sum_{j>i} ([\Delta x_{ji} > 0 \wedge \Delta y_{ji} > 0] \vee [\Delta x_{ji} < 0 \wedge \Delta y_{ji} < 0])$$

$$\delta_{[+,-]}^{[-,+]} = \frac{2}{n \cdot (n-1)} \cdot \sum_{j>i} ([\Delta x_{ji} < 0 \wedge \Delta y_{ji} > 0] \vee [\Delta x_{ji} > 0 \wedge \Delta y_{ji} < 0]),$$

and for $H(x, y, z) \in \mathbb{R}^3$, the explicit expression of $\delta_{[\mp]}^{[\pm]}$ coefficients are:

$$\delta_{[-,-,-]}^{[+,+,+]} = \frac{2}{n \cdot (n-1)} \cdot \sum_{j>i} ([\Delta x_{ji} > 0 \wedge \Delta y_{ji} > 0 \wedge \Delta z_{ji} > 0] \vee [\Delta x_{ji} < 0 \wedge \Delta y_{ji} < 0 \wedge \Delta z_{ji} < 0])$$

$$\delta_{[-,-,+]}^{[+,-,+]} = \frac{2}{n \cdot (n-1)} \cdot \sum_{j>i} ([\Delta x_{ji} > 0 \wedge \Delta y_{ji} > 0 \wedge \Delta z_{ji} < 0] \vee [\Delta x_{ji} < 0 \wedge \Delta y_{ji} < 0 \wedge \Delta z_{ji} > 0])$$

$$\delta_{[-,+,-]}^{[+,-,-]} = \frac{2}{n \cdot (n-1)} \cdot \sum_{j>i} ([\Delta x_{ji} < 0 \wedge \Delta y_{ji} > 0 \wedge \Delta z_{ji} < 0] \vee [\Delta x_{ji} > 0 \wedge \Delta y_{ji} < 0 \wedge \Delta z_{ji} > 0])$$

$$\delta_{[+,-,-]}^{[-,+,-]} = \frac{2}{n \cdot (n-1)} \cdot \sum_{j>i} ([\Delta x_{ji} < 0 \wedge \Delta y_{ji} > 0 \wedge \Delta z_{ji} > 0] \vee [\Delta x_{ji} > 0 \wedge \Delta y_{ji} < 0 \wedge \Delta z_{ji} < 0])$$

Then, for any observation with K joint variables ($H(x, y, \dots, k) \in \mathbb{R}^N$), the explicit expressions for any $\delta_{[\mp]}^{[\pm]}$ coefficient is:

$$\delta_{[\mp]}^{[\pm]} = \frac{2}{n \cdot (n-1)} \cdot \sum_{j>i} ([\Delta x_{ji} \geq 0 \wedge \Delta y_{ji} \geq 0 \wedge \dots \wedge \Delta k_{ji} \geq 0] \vee [\Delta x_{ji} \leq 0 \wedge \Delta y_{ji} \leq 0 \wedge \dots \wedge \Delta k_{ji} \leq 0])$$

where a reduced form of this expression would be:

$$\delta_{[\mp, \mp, \dots, \mp]}^{[\pm, \pm, \dots, \pm]} = \frac{2}{n \cdot (n-1)} \cdot \sum_{j>i} \left(\bigwedge [\Delta c_{ji} \geq 0] \vee \bigwedge [\Delta c_{ji} \leq 0] \right), \Delta c_{ji} = \langle \Delta x_{ji}, \Delta y_{ji}, \dots, \Delta k_{ji} \rangle \quad (\text{E.2})$$

The multivariate Kendall's τ . Definition of global *data trend* coefficients

The $\delta_{[\mp]}^{[\pm]}$ coefficients presented above correspond to the individual probability of each possible *data trend*. However, it would be more convenient to express these in terms of global probability (global *data trend* coefficients, $\tau_{[\mp]}^{[\pm]}$). For two observed variables, only one $\tau_{[\mp]}^{[\pm]}$ coefficient is sufficient to describe all possible *data trends*, corresponding to the *conventional* Kendall's τ coefficient (Kendall, 1938):

$$\tau = \delta_{[-,-]}^{[+,+]} - \delta_{[-,+]}^{[+,-]} \quad (\text{E.3})$$

When more than two observed variables are considered (X, Y, \dots, K), a total of $2^N/2$ (corresponding to the number of *paired orthants*) $\tau_{[\mp]}^{[\pm]}$ coefficients are necessary to describe all possible *data trends* $\langle \tau_{[\mp]}^{[\pm]}_i, \tau_{[\mp]}^{[\pm]}_j, \dots, \tau_{[\mp]}^{[\pm]}_d \rangle$. In order to estimate any $\tau_{[\mp]}^{[\pm]}$ coefficient (*e.g.*, $\tau_{[\mp]}^{[\pm]}_i$), first it is computed the differences between the individual *data trend* coefficient $\delta_{[\mp]}^{[\pm]}_i$ and the others individual coefficients $\langle \delta_{[\mp]}^{[\pm]}_j, \dots, \delta_{[\mp]}^{[\pm]}_d \rangle$. Then, a modified geometric mean (able to consider both positive and negative values) is applied to the calculated differences (de la Cruz & Kreft, 2018):

$$\left\{ \prod_{i=1}^{nc} (1 + a_i) \right\}^{(1/nc)} - 1$$

Where a_i is the difference between the individual *data trend* coefficients, and nc the number of comparisons between the individual *data trends* coefficients ($2^N/2 - 1$).

Considering a set of observation with three joint variables ($H(x, y, z) \in \mathbb{R}^3$), the global probabilities of their *data trends* ($\tau_{[\mp, \mp, \mp]}^{[\pm, \pm, \pm]}$) are evaluated by:

$$\begin{aligned} \tau_{[-,-,-]}^{[+,+,+]} &= \sqrt[3]{\left\{ 1 + \left(\delta_{[-,-,-]}^{[+,+,+]} - \delta_{[-,-,+]}^{[+,+,+]} \right) \right\} \cdot \left\{ 1 + \left(\delta_{[-,-,-]}^{[+,+,+]} - \delta_{[-,+,-]}^{[+,+,+]} \right) \right\} \cdot \left\{ 1 + \left(\delta_{[-,-,-]}^{[+,+,+]} - \delta_{[+,-,-]}^{[+,+,+]} \right) \right\}} - 1 \\ \tau_{[-,-,+]}^{[+,+,-]} &= \sqrt[3]{\left\{ 1 + \left(\delta_{[-,-,+]}^{[+,+,-]} - \delta_{[-,-,-]}^{[+,+,-]} \right) \right\} \cdot \left\{ 1 + \left(\delta_{[-,-,+]}^{[+,+,-]} - \delta_{[-,+,-]}^{[+,+,-]} \right) \right\} \cdot \left\{ 1 + \left(\delta_{[-,-,+]}^{[+,+,-]} - \delta_{[+,-,-]}^{[+,+,-]} \right) \right\}} - 1 \\ \tau_{[-,+,-]}^{[+,-,-]} &= \sqrt[3]{\left\{ 1 + \left(\delta_{[-,+,-]}^{[+,-,-]} - \delta_{[-,-,-]}^{[+,-,-]} \right) \right\} \cdot \left\{ 1 + \left(\delta_{[-,+,-]}^{[+,-,-]} - \delta_{[-,+,-]}^{[+,-,-]} \right) \right\} \cdot \left\{ 1 + \left(\delta_{[-,+,-]}^{[+,-,-]} - \delta_{[+,-,-]}^{[+,-,-]} \right) \right\}} - 1 \\ \tau_{[+,-,-]}^{[+,-,+]} &= \sqrt[3]{\left\{ 1 + \left(\delta_{[+,-,-]}^{[+,-,+]} - \delta_{[-,-,-]}^{[+,-,+]} \right) \right\} \cdot \left\{ 1 + \left(\delta_{[+,-,-]}^{[+,-,+]} - \delta_{[-,+,-]}^{[+,-,+]} \right) \right\} \cdot \left\{ 1 + \left(\delta_{[+,-,-]}^{[+,-,+]} - \delta_{[+,-,-]}^{[+,-,+]} \right) \right\}} - 1 \end{aligned}$$

For any number of joint variables $(H(x, y, \dots, k) \in \mathbb{R}^N)$, the general expression for $\tau_{[\mp]}^{[\pm]}$ coefficients correspond to:

$$\tau_{[\mp]}^{[\pm]} = \left[\prod_{j \neq i} \left\{ 1 + \left(\delta_{[\mp]}^{[\pm]} - \delta_{[\mp]}^{[\pm]} \right) \right\} \right]^{\left(\frac{2^N}{2} - 1 \right)^{-1}} - 1 \quad (\text{E.4})$$

The $\tau_{[\mp]}^{[\pm]}$ coefficient lies between -1 and 1 inclusive, taking 1 if and only if all the probability mass lies on the specific *data trend* $([\pm] \odot [\mp])$. The value of -1 states the null probability of the dataset to follow this specific *trend*, following another *data trend* entirely. If observed variables are independent, then all $\tau_{[\mp]}^{[\pm]}$ coefficients are equal to 0 . All $\delta_{[\mp]}^{[\pm]}$ coefficients above the r_p will have a positive $\tau_{[\mp]}^{[\pm]}$ coefficient, whereas those $\delta_{[\mp]}^{[\pm]}$ coefficients below the r_p will have a negative $\tau_{[\mp]}^{[\pm]}$ coefficient. The $\delta_{[\mp]}^{[\pm]}$ coefficients equal to r_p will have a $\tau_{[\mp]}^{[\pm]}$ equal 0 .

Sampling distribution and statistical hypothesis for $\tau_{[\mp]}^{[\pm]}$ coefficients

To measure the significance of an observed *data trend*, it is necessary to know whether the value could have arisen by chance from a universe in which all the possible rankings of n objects occur an equal number of times. It is, therefore, necessary to consider the distribution of *trends* in such universe. The distribution of τ tends to normality for large number of observations and surprisingly close to normality even for low number of observations. The fact that τ tends to normality even for low number of observations was proved by Kendall (1938).

Then, the distribution of $\tau_{[\mp]}^{[\pm]}$ (in which all existing *data trends* would also occur with the same frequency) also converges towards a normal distribution with a mean of 0 and a variance equal to:

$$\sigma_\tau^2 = \frac{2(2n + 5)}{9n(n - 1)}$$

Where n is the number of observations. Therefore, the null hypothesis test can be performed by transforming $\tau_{[\mp]}^{[\pm]}$ into statistic Z_τ as:

$$Z_\tau = \frac{\tau_{[\mp]}^{[\pm]}}{\sigma_\tau} = \frac{\tau_{[\mp]}^{[\pm]}}{\sqrt{\frac{2(2n+5)}{9n(n-1)}}} \quad (\text{E.5})$$

Thus, to test whether a set of variables significantly follows a certain trend, one computes Z_τ and finds the cumulative probability for a standard normal distribution at $-|Z_\tau|$.

Algorithm

Now, the algorithm for the direct estimation of all $\tau_{[\pm]}^{[\pm]}$ coefficients ($i = 1, \dots, 2^N/2$, being N the number of joint variables) is described in the following steps.

Step 1. Obtention of all *data trends* ($[\pm] \oslash [\mp]$) associated to *paired orthant* ($Oh_\alpha \oslash Oh_\beta$).

First the permutation with repetition of the positive (+) and negative (-) signs is performed, and then the permutation results are *pared* based on $[\pm] = \neg[\mp]$.

Step 2. Calculation of all individual *data trend* coefficient ($\delta_{[\mp]}^{[\pm]}$) with the Eq. E.2. The direct computation of the summation $\sum_{j>i}(\dots)$ involves two nested iterations:

```
f = 0;
for j = 2:n
    for i = 1:j-1
        diff = dataset(j,:) - dataset(i,:);
        f = f + or(eq(sym_up, gt(diff, 0)), eq(sym_down, gt(diff, 0)));
    end
end
```

Where n is the number of observations, sym_up is the set of $[\pm]$, sym_down is the set of $[\mp]$, $\text{gt}(A, B)$ determines if ‘A is greater than B’, and $\text{eq}(A, B)$ determines if ‘A and B are equal’.

Step 3. Calculation of global *data trend* coefficients ($\tau_{[\mp]}^{[\pm]}$) with Eq. E.3 for $N = 2$, and Eq. E.4 for $N > 2$.

Step 4. Statistical analysis with the Eq. E.5 and the normal cumulative distribution function.

MATLAB has an in-build function to find the cumulative probability for a standard normal distribution: `normcdf()`. To obtain the p -value for a 2-sided test, the number from the normal cumulative distribution function is multiplied by two.

$$p = 2 * \text{normcdf}(-|Z_\tau|).$$

The source code to produce the results presented below is available on a public GitHub repository at <https://github.com/soundslikealloy/multivarcorr>.

Examples

Examples of applying multivariate Kendall’s τ analysis (τ -N) to different sets of joint variables have been included: two and three variables on Table E.1 ($H(S1, S2) \in \mathbb{R}^2$ and

$H(S1, S2, S3) \in \mathbb{R}^3$, respectively), four variables on Table E.2 ($H(S1, S2, S3, S4) \in \mathbb{R}^4$), five joint variables on Table E.3 ($H(S1, S2, S3, S4, S5) \in \mathbb{R}^5$), and six joint variables on Table E.4 ($H(S1, S2, S3, S4, S5, S6) \in \mathbb{R}^6$).

Table E.1. Examples of data trend measurement (τ_N) for $H(S1, S2) \in \mathbb{R}^2$ and $H(S1, S2, S3) \in \mathbb{R}^3$.

$N (r_p)$	Series ($n = 12$)	$\delta [0, 1]$	$\tau_N [-1, 1]$	p
2 (0.5000)	S1: 1, 3, 5, 7, 9, 11, 13, 15, 17, 19, 21, 23 S2: 1, 3, 5, 7, 9, 11, 13, 15, 17, 19, 21, 23	$\delta_{[-,-]}^{[+,+]} = 1.0000$ $\delta_{[+,-]}^{[-,+]} = 0.0000$	$\tau = 1.0000$	<0.0001
	S1: 1, 3, 9, 7, 15, 13, 21, 23, 5, 11, 17, 19 S2: 23, 21, 15, 17, 9, 11, 3, 1, 19, 13, 7, 5	$\delta_{[-,-]}^{[+,+]} = 0.0000$ $\delta_{[+,-]}^{[-,+]} = 1.0000$	$\tau = -1.0000$	<0.0001
	S1: 1, 3, 5, 7, 9, 11, 13, 15, 17, 19, 21, 23 S2: 1, 5, 9, 11, 6, 13, 17, 12, 22, 20, 25, 23	$\delta_{[-,-]}^{[+,+]} = 0.9091$ $\delta_{[+,-]}^{[-,+]} = 0.0909$	$\tau = 0.8182$	0.0002
	S1: 5, 8, 9, 16, 12, 1, 14, 3, 15, 21, 13, 1 S2: 7, 15, 3, 20, 24, 23, 24, 20, 21, 5, 23, 15 *100% random distribution	$\delta_{[-,-]}^{[+,+]} = 0.4918$ $\delta_{[+,-]}^{[-,+]} = 0.5082$	$\tau = -0.0164$	0.9409
3 (0.2500)	S1: 1, 3, 5, 7, 9, 11, 13, 15, 17, 19, 21, 23 S2: 1, 3, 5, 7, 9, 11, 13, 15, 17, 19, 21, 23 S3: 1, 3, 5, 7, 9, 11, 13, 15, 17, 19, 21, 23	$\delta_{[-,-,-]}^{[+,+,+]} = 1.0000$ $\delta_{[-,-,+]}^{[-,+,+]} = 0.0000$ $\delta_{[-,+,-]}^{[+,-,+]} = 0.0000$ $\delta_{[+,-,-]}^{[-,-,+]} = 0.0000$	$\tau_{[-,-,-]}^{[+,+,+]} = 1.0000$ $\tau_{[-,-,+]}^{[-,+,+]} = -1.0000$ $\tau_{[-,+,-]}^{[+,-,+]} = -1.0000$ $\tau_{[+,-,-]}^{[-,-,+]} = -1.0000$	<0.0001 <0.0001 <0.0001 <0.0001
	S1: 1, 3, 5, 7, 9, 11, 13, 15, 17, 19, 21, 23 S2: 23, 21, 19, 17, 15, 13, 11, 9, 7, 5, 3, 1 S3: 1, 3, 5, 7, 9, 11, 13, 15, 17, 19, 21, 23	$\delta_{[-,-,-]}^{[+,+,+]} = 0.000$ $\delta_{[-,-,+]}^{[-,+,+]} = 0.000$ $\delta_{[-,+,-]}^{[+,-,+]} = 1.000$ $\delta_{[+,-,-]}^{[-,-,+]} = 0.0000$	$\tau_{[-,-,-]}^{[+,+,+]} = -1.0000$ $\tau_{[-,-,+]}^{[-,+,+]} = -1.0000$ $\tau_{[-,+,-]}^{[+,-,+]} = 1.0000$ $\tau_{[+,-,-]}^{[-,-,+]} = -1.0000$	<0.0001 <0.0001 <0.0001 <0.0001
	S1: 1, 3, 5, 7, 9, 11, 13, 15, 17, 19, 21, 23 S2: 23, 21, 19, 17, 15, 13, 11, 9, 7, 5, 3, 1 S3: 23, 21, 19, 17, 15, 13, 11, 9, 7, 5, 3, 1	$\delta_{[-,-,-]}^{[+,+,+]} = 0.0000$ $\delta_{[-,-,+]}^{[-,+,+]} = 1.0000$ $\delta_{[-,+,-]}^{[+,-,+]} = 0.0000$ $\delta_{[+,-,-]}^{[-,-,+]} = 0.0000$	$\tau_{[-,-,-]}^{[+,+,+]} = -1.0000$ $\tau_{[-,-,+]}^{[-,+,+]} = 1.0000$ $\tau_{[-,+,-]}^{[+,-,+]} = -1.0000$ $\tau_{[+,-,-]}^{[-,-,+]} = -1.0000$	<0.0001 <0.0001 <0.0001 <0.0001
	S1: 23, 12, 19, 12, 9, 5, 3, 1, 20, 7, 12, 17 S2: 2, 13, 5, 10, 15, 4, 20, 23, 3, 17, 11, 8 S3: 22, 11, 19, 15, 4, 8, 3, 1, 21, 6, 13, 17	$\delta_{[-,-,-]}^{[+,+,+]} = 0.1111$ $\delta_{[-,-,+]}^{[-,+,+]} = 0.0000$ $\delta_{[-,+,-]}^{[+,-,+]} = 0.8889$ $\delta_{[+,-,-]}^{[-,-,+]} = 0.0000$	$\tau_{[-,-,-]}^{[+,+,+]} = -0.3502$ $\tau_{[-,-,+]}^{[-,+,+]} = -0.5378$ $\tau_{[-,+,-]}^{[+,-,+]} = 0.8511$ $\tau_{[+,-,-]}^{[-,-,+]} = -0.5378$	0.1610 0.0192 0.0002 0.0192
	S1: 19, 8, 6, 16, 7, 9, 13, 4, 14, 10, 11, 22 S2: 1, 4, 4, 7, 13, 5, 20, 12, 17, 23, 23, 19 S3: 16, 22, 1, 2, 22, 23, 11, 9, 2, 20, 10, 5 *100% random distribution	$\delta_{[-,-,-]}^{[+,+,+]} = 0.2419$ $\delta_{[-,-,+]}^{[-,+,+]} = 0.2742$ $\delta_{[-,+,-]}^{[+,-,+]} = 0.1613$ $\delta_{[+,-,-]}^{[-,-,+]} = 0.3226$	$\tau_{[-,-,-]}^{[+,+,+]} = -0.0130$ $\tau_{[-,-,+]}^{[-,+,+]} = 0.0302$ $\tau_{[-,+,-]}^{[+,-,+]} = -0.1189$ $\tau_{[+,-,-]}^{[-,-,+]} = 0.0958$	0.9530 0.8915 0.5905 0.6647

Table E.2. Examples of data trend measurement (τ_N) for $H(S1, S2, S3, S4) \in \mathbb{R}^4$.

$N (r_p)$	Series ($n = 12$)	$\delta [0, 1]$	$\tau_N [-1, 1]$	p
4 (0.1250)	S1: 23, 21, 19, 17, 15, 13, 11, 9, 7, 5, 3, 1 S2: 23, 21, 19, 17, 15, 13, 11, 9, 7, 5, 3, 1 S3: 1, 3, 5, 7, 9, 11, 13, 15, 17, 19, 21, 23 S4: 23, 21, 19, 17, 15, 13, 11, 9, 7, 5, 3, 1	$\delta_{[-,-,-,-]}^{[+,+,+,+]} = 0.0000$	$\tau_{[-,-,-,-]}^{[+,+,+,+]} = -1.0000$	<0.0001
		$\delta_{[+,-,-,-]}^{[-,+,+,+]} = 0.0000$	$\tau_{[+,-,-,-]}^{[-,+,+,+]} = -1.0000$	<0.0001
		$\delta_{[-,+,-,-]}^{[+,-,+,+]} = 0.0000$	$\tau_{[-,+,-,-]}^{[+,-,+,+]} = -1.0000$	<0.0001
		$\delta_{[+,-,+,-]}^{[-,-,+,+]} = 0.0000$	$\tau_{[+,-,+,-]}^{[-,-,+,+]} = -1.0000$	<0.0001
		$\delta_{[-,+,-,+]}^{[+,-,-,+]} = 1.0000$	$\tau_{[-,+,-,+]}^{[+,-,-,+]} = 1.0000$	<0.0001
		$\delta_{[+,-,-,+]}^{[-,+,-,+]} = 0.0000$	$\tau_{[+,-,-,+]}^{[-,+,-,+]} = -1.0000$	<0.0001
		$\delta_{[-,-,-,+]}^{[+,-,-,+]} = 0.0000$	$\tau_{[-,-,-,+]}^{[+,-,-,+]} = -1.0000$	<0.0001
		$\delta_{[+,-,-,+]}^{[-,-,-,+]} = 0.0000$	$\tau_{[+,-,-,+]}^{[-,-,-,+]} = -1.0000$	<0.0001
	S1: 12, 3, 6, 11, 10, 9, 21, 22, 4, 7, 23, 4 S2: 15, 13, 1, 9, 19, 5, 9, 11, 8, 23, 18, 9 S3: 10, 1, 2, 14, 18, 11, 12, 16, 7, 5, 13, 6 S4: 6, 10, 17, 4, 18, 5, 22, 13, 15, 14, 2, 11 *100% random distribution	$\delta_{[-,-,-,-]}^{[+,+,+,+]} = 0.1905$	$\tau_{[-,-,-,-]}^{[+,+,+,+]} = 0.0712$	0.7473
		$\delta_{[+,-,-,-]}^{[-,+,+,+]} = 0.0635$	$\tau_{[+,-,-,-]}^{[-,+,+,+]} = -0.0745$	0.7361
		$\delta_{[-,+,-,-]}^{[+,-,+,+]} = 0.1429$	$\tau_{[-,+,-,-]}^{[+,-,+,+]} = 0.0163$	0.9413
		$\delta_{[+,-,+,-]}^{[-,-,+,+]} = 0.0635$	$\tau_{[+,-,+,-]}^{[-,-,+,+]} = -0.0745$	0.7361
		$\delta_{[-,+,-,+]}^{[+,-,-,+]} = 0.0476$	$\tau_{[-,+,-,+]}^{[+,-,-,+]} = -0.0925$	0.6755
		$\delta_{[+,-,-,+]}^{[-,+,-,+]} = 0.1429$	$\tau_{[+,-,-,+]}^{[-,+,-,+]} = 0.0163$	0.9413
		$\delta_{[-,-,-,+]}^{[+,-,-,+]} = 0.0476$	$\tau_{[-,-,-,+]}^{[+,-,-,+]} = -0.0925$	0.6755
		$\delta_{[+,-,-,+]}^{[-,-,-,+]} = 0.3016$	$\tau_{[+,-,-,+]}^{[-,-,-,+]} = 0.2006$	0.3639
	S1: 1, 3, 5, 7, 9, 11, 13, 15, 17, 19, 21, 23 S2: 23, 21, 22, 17, 16, 13, 15, 9, 4, 5, 3, 2 S3: 1, 6, 5, 7, 9, 25, 13, 2, 17, 22, 11, 23 S4: 20, 23, 19, 17, 15, 9, 11, 10, 7, 6, 3, 5	$\delta_{[-,-,-,-]}^{[+,+,+,+]} = 0.0000$	$\tau_{[-,-,-,-]}^{[+,+,+,+]} = -0.2034$	0.3573
		$\delta_{[+,-,-,-]}^{[-,+,+,+]} = 0.1818$	$\tau_{[+,-,-,-]}^{[-,+,+,+]} = 0.0197$	0.9291
		$\delta_{[-,+,-,-]}^{[+,-,+,+]} = 0.0303$	$\tau_{[-,+,-,-]}^{[+,-,+,+]} = -0.1657$	0.4533
		$\delta_{[+,-,+,-]}^{[-,-,+,+]} = 0.0152$	$\tau_{[+,-,+,-]}^{[-,-,+,+]} = -0.1845$	0.4037
		$\delta_{[-,+,-,+]}^{[+,-,-,+]} = 0.0152$	$\tau_{[-,+,-,+]}^{[+,-,-,+]} = -0.1845$	0.4037
		$\delta_{[+,-,-,+]}^{[-,+,-,+]} = 0.7273$	$\tau_{[+,-,-,+]}^{[-,+,-,+]} = 0.6872$	0.0019
		$\delta_{[-,-,-,+]}^{[+,-,-,+]} = 0.0152$	$\tau_{[-,-,-,+]}^{[+,-,-,+]} = -0.1845$	0.4037
		$\delta_{[+,-,-,+]}^{[-,-,-,+]} = 0.0152$	$\tau_{[+,-,-,+]}^{[-,-,-,+]} = -0.1845$	0.4037

Table E.3. Examples of data trend measurement (τ_N) for $H(S1, S2, S3, S4, S5) \in \mathbb{R}^5$.

$N(r_p)$	Series ($n = 12$)	$\delta [0, 1]$	$\tau_N [-1, 1]$	p
5 (0.0625)	S1: 22, 14, 12, 7, 21, 11, 9, 23, 17, 6, 18, 20 S2: 9, 2, 18, 10, 16, 21, 7, 4, 17, 22, 19, 14 S3: 16, 21, 15, 5, 18, 13, 20, 7, 17, 2, 19, 9 S4: 6, 16, 15, 8, 5, 17, 10, 12, 3, 11, 4, 18 S5: 8, 2, 22, 19, 15, 11, 3, 23, 14, 7, 16, 21 *100% random distribution	$\delta_{[-,-,-,-,-]}^{[+,+,+,+,+]} = 0.0455$	$\tau_{[-,-,-,-,-]}^{[+,+,+,+,+]} = -0.0194$	0.9299
		$\delta_{[+,-,-,-,-]}^{[-,+,+,+,+]} = 0.0000$	$\tau_{[+,-,-,-,-]}^{[-,+,+,+,+]} = -0.0679$	0.7587
		$\delta_{[-,+,-,-,-]}^{[+,-,+,+,+]} = 0.0909$	$\tau_{[-,+,-,-,-]}^{[+,-,+,+,+]} = 0.0291$	0.8952
		$\delta_{[+,-,-,-,-]}^{[-,-,+,+,+]} = 0.0000$	$\tau_{[+,-,-,-,-]}^{[-,-,+,+,+]} = -0.0679$	0.7587
		$\delta_{[-,-,+,-,-]}^{[+,-,-,+,+]} = 0.0606$	$\tau_{[-,-,+,-,-]}^{[+,-,-,+,+]} = -0.0033$	0.9882
		$\delta_{[+,-,-,-,-]}^{[-,+,-,+,+]} = 0.1212$	$\tau_{[+,-,-,-,-]}^{[-,+,-,+,+]} = 0.0616$	0.7806
		$\delta_{[-,-,+,-,-]}^{[+,-,-,+,+]} = 0.1212$	$\tau_{[-,-,+,-,-]}^{[+,-,-,+,+]} = 0.0616$	0.7806
		$\delta_{[+,-,-,-,-]}^{[-,-,-,+,+]} = 0.0758$	$\tau_{[+,-,-,-,-]}^{[-,-,-,+,+]} = 0.0129$	0.9534
		$\delta_{[-,-,+,-,-]}^{[+,-,-,+,+]} = 0.0000$	$\tau_{[-,-,+,-,-]}^{[+,-,-,+,+]} = -0.0679$	0.7587
		$\delta_{[+,-,-,-,-]}^{[-,+,-,+,+]} = 0.0758$	$\tau_{[+,-,-,-,-]}^{[-,+,-,+,+]} = 0.0129$	0.9534
		$\delta_{[-,-,+,-,-]}^{[+,-,-,+,+]} = 0.1364$	$\tau_{[-,-,+,-,-]}^{[+,-,-,+,+]} = 0.0778$	0.7248
		$\delta_{[+,-,-,-,-]}^{[-,-,-,+,+]} = 0.0000$	$\tau_{[+,-,-,-,-]}^{[-,-,-,+,+]} = -0.0679$	0.7587
		$\delta_{[-,-,+,-,-]}^{[+,-,-,+,+]} = 0.1364$	$\tau_{[-,-,+,-,-]}^{[+,-,-,+,+]} = 0.0778$	0.7248
		$\delta_{[+,-,-,-,-]}^{[-,+,-,+,+]} = 0.0758$	$\tau_{[+,-,-,-,-]}^{[-,+,-,+,+]} = 0.0129$	0.9534
		$\delta_{[-,-,+,-,-]}^{[+,-,-,+,+]} = 0.0455$	$\tau_{[-,-,+,-,-]}^{[+,-,-,+,+]} = -0.0194$	0.9299
		$\delta_{[+,-,-,-,-]}^{[-,-,-,+,+]} = 0.0152$	$\tau_{[+,-,-,-,-]}^{[-,-,-,+,+]} = -0.0517$	0.8149
		$\delta_{[-,-,+,-,-]}^{[+,-,-,+,+]} = 0.0156$	$\tau_{[-,-,+,-,-]}^{[+,-,-,+,+]} = -0.0732$	0.7406
		$\delta_{[+,-,-,-,-]}^{[-,+,+,+,+]} = 0.0313$	$\tau_{[+,-,-,-,-]}^{[-,+,+,+,+]} = -0.0559$	0.8004
		$\delta_{[-,+,-,-,-]}^{[+,-,+,+,+]} = 0.0938$	$\tau_{[-,+,-,-,-]}^{[+,-,+,+,+]} = 0.0130$	0.9529
		$\delta_{[+,-,-,-,-]}^{[-,-,+,+,+]} = 0.6563$	$\tau_{[+,-,-,-,-]}^{[-,-,+,+,+]} = 0.6331$	0.0042
$\delta_{[-,-,+,-,-]}^{[+,-,-,+,+]} = 0.0000$	$\tau_{[-,-,+,-,-]}^{[+,-,-,+,+]} = -0.0905$	0.6823		
$\delta_{[+,-,-,-,-]}^{[-,+,-,+,+]} = 0.0313$	$\tau_{[+,-,-,-,-]}^{[-,+,-,+,+]} = -0.0559$	0.8004		
S1: 23, 15, 19, 5, 12, 13, 8, 9, 2, 5, 3, 1	$\delta_{[-,-,+,-,-]}^{[+,-,-,+,+]} = 0.0000$	$\tau_{[-,-,+,-,-]}^{[+,-,-,+,+]} = -0.0905$	0.6823	
S2: 21, 25, 19, 15, 17, 9, 11, 10, 7, 2, 3, 5	$\delta_{[+,-,-,-,-]}^{[-,-,-,+,+]} = 0.0782$	$\tau_{[+,-,-,-,-]}^{[-,-,-,+,+]} = 0.0042$	0.9850	
S3: 10, 3, 5, 2, 9, 11, 10, 15, 17, 25, 21, 23	$\delta_{[-,-,+,-,-]}^{[+,-,-,+,+]} = 0.0000$	$\tau_{[-,-,+,-,-]}^{[+,-,-,+,+]} = -0.0905$	0.6823	
S4: 1, 5, 3, 7, 9, 11, 10, 15, 17, 20, 21, 23	$\delta_{[+,-,-,-,-]}^{[-,+,-,+,+]} = 0.0000$	$\tau_{[+,-,-,-,-]}^{[-,+,-,+,+]} = -0.0905$	0.6823	
S5: 4, 3, 5, 7, 10, 11, 13, 19, 17, 16, 21, 23	$\delta_{[-,-,+,-,-]}^{[+,-,-,+,+]} = 0.0313$	$\tau_{[-,-,+,-,-]}^{[+,-,-,+,+]} = -0.0559$	0.8004	
$\delta_{[+,-,-,-,-]}^{[-,-,-,+,+]} = 0.0000$	$\tau_{[+,-,-,-,-]}^{[-,-,-,+,+]} = -0.0905$	0.6823		
$\delta_{[-,-,+,-,-]}^{[+,-,-,+,+]} = 0.0000$	$\tau_{[-,-,+,-,-]}^{[+,-,-,+,+]} = -0.0905$	0.6823		
$\delta_{[+,-,-,-,-]}^{[-,+,-,+,+]} = 0.0313$	$\tau_{[+,-,-,-,-]}^{[-,+,-,+,+]} = -0.0559$	0.8004		
$\delta_{[-,-,+,-,-]}^{[+,-,-,+,+]} = 0.0313$	$\tau_{[-,-,+,-,-]}^{[+,-,-,+,+]} = -0.0559$	0.8004		
$\delta_{[+,-,-,-,-]}^{[-,-,-,+,+]} = 0.0000$	$\tau_{[+,-,-,-,-]}^{[-,-,-,+,+]} = -0.0905$	0.6823		
$\delta_{[-,-,+,-,-]}^{[+,-,-,+,+]} = 0.0000$	$\tau_{[-,-,+,-,-]}^{[+,-,-,+,+]} = -0.0905$	0.6823		

Table E.4. Examples of data trend measurement (τ_N) for $H(S1, S2, S3, S4, S5, S6) \in \mathbb{R}^6$.

$N(r_p)$	Series ($n = 12$)	$\delta [0, 1]$	$\tau_N [-1, 1]$	p
6 (0.0313)	S1: 10, 19, 7, 9, 1, 17, 6, 23, 3, 8, 13, 11 S2: 9, 5, 17, 15, 23, 7, 3, 1, 21, 19, 11, 13 S3: 9, 5, 17, 15, 23, 10, 3, 1, 18, 19, 11, 18 S4: 9, 5, 12, 15, 23, 7, 8, 1, 22, 19, 11, 13 S5: 9, 10, 17, 15, 20, 7, 3, 1, 21, 19, 11, 13 S6: 15, 19, 7, 9, 1, 17, 21, 23, 3, 5, 13, 20	$\delta_{[-,-,-,-,-,-]}^{[+,+,+,+,+,+]} = 0.0154$	$\tau_{[-,-,-,-,-,-]}^{[+,+,+,+,+,+]} = -0.0290$	0.8957
		$\delta_{[+,-,-,-,-,-]}^{[-,+,+,+,+,+]} = 0.0462$	$\tau_{[+,-,-,-,-,-]}^{[-,+,+,+,+,+]} = 0.0035$	0.9874
		$\delta_{[-,+,-,-,-,-]}^{[+,-,+,+,+,+]} = 0.0000$	$\tau_{[-,+,-,-,-,-]}^{[+,-,+,+,+,+]} = -0.0452$	0.8379
		$\delta_{[+,-,+,-,-,-]}^{[-,+,-,+,+,+]} = 0.0000$	$\tau_{[+,-,+,-,-,-]}^{[-,+,-,+,+,+]} = -0.0452$	0.8379
		$\delta_{[-,+,-,+,-,-]}^{[+,-,+,-,+,+]} = 0.0000$	$\tau_{[-,+,-,+,-,-]}^{[+,-,+,-,+,+]} = -0.0452$	0.8379
		$\delta_{[+,-,+,-,+,-]}^{[-,+,-,+,-,+,+]} = 0.0000$	$\tau_{[+,-,+,-,+,-]}^{[-,+,-,+,-,+,+]} = -0.0452$	0.8379
		$\delta_{[-,+,-,+,-,+]}^{[+,-,+,-,+,-,+,+]} = 0.0000$	$\tau_{[-,+,-,+,-,+]}^{[+,-,+,-,+,-,+,+]} = -0.0452$	0.8379
		$\delta_{[+,-,+,-,+,-]}^{[-,+,-,+,-,+,-,+,+]} = 0.0000$	$\tau_{[+,-,+,-,+,-]}^{[-,+,-,+,-,+,-,+,+]} = -0.0452$	0.8379
		$\delta_{[-,+,-,+,-,+]}^{[+,-,+,-,+,-,+,-,+,+]} = 0.0000$	$\tau_{[-,+,-,+,-,+]}^{[+,-,+,-,+,-,+,-,+,+]} = -0.0452$	0.8379
		$\delta_{[+,-,+,-,+,-]}^{[-,+,-,+,-,+,-,+,-,+,+]} = 0.0000$	$\tau_{[+,-,+,-,+,-]}^{[-,+,-,+,-,+,-,+,-,+,+]} = -0.0452$	0.8379
		$\delta_{[-,+,-,+,-,+]}^{[+,-,+,-,+,-,+,-,+,-,+,+]} = 0.0000$	$\tau_{[-,+,-,+,-,+]}^{[+,-,+,-,+,-,+,-,+,-,+,+]} = -0.0452$	0.8379
		$\delta_{[+,-,+,-,+,-]}^{[-,+,-,+,-,+,-,+,-,+,-,+,+]} = 0.0000$	$\tau_{[+,-,+,-,+,-]}^{[-,+,-,+,-,+,-,+,-,+,-,+,+]} = -0.0452$	0.8379
		$\delta_{[-,+,-,+,-,+]}^{[+,-,+,-,+,-,+,-,+,-,+,-,+,+]} = 0.0000$	$\tau_{[-,+,-,+,-,+]}^{[+,-,+,-,+,-,+,-,+,-,+,-,+,+]} = -0.0452$	0.8379
		$\delta_{[+,-,+,-,+,-]}^{[-,+,-,+,-,+,-,+,-,+,-,+,-,+,+]} = 0.0000$	$\tau_{[+,-,+,-,+,-]}^{[-,+,-,+,-,+,-,+,-,+,-,+,-,+,+]} = -0.0452$	0.8379
		$\delta_{[-,+,-,+,-,+]}^{[+,-,+,-,+,-,+,-,+,-,+,-,+,-,+,+]} = 0.0000$	$\tau_{[-,+,-,+,-,+]}^{[+,-,+,-,+,-,+,-,+,-,+,-,+,-,+,+]} = -0.0452$	0.8379
		$\delta_{[+,-,+,-,+,-]}^{[-,+,-,+,-,+,-,+,-,+,-,+,-,+,-,+,+]} = 0.0000$	$\tau_{[+,-,+,-,+,-]}^{[-,+,-,+,-,+,-,+,-,+,-,+,-,+,-,+,+]} = -0.0452$	0.8379
		$\delta_{[-,+,-,+,-,+]}^{[+,-,+,-,+,-,+,-,+,-,+,-,+,-,+,-,+,+]} = 0.0000$	$\tau_{[-,+,-,+,-,+]}^{[+,-,+,-,+,-,+,-,+,-,+,-,+,-,+,-,+,+]} = -0.0452$	0.8379
		$\delta_{[+,-,+,-,+,-]}^{[-,+,-,+,-,+,-,+,-,+,-,+,-,+,-,+,-,+,+]} = 0.0000$	$\tau_{[+,-,+,-,+,-]}^{[-,+,-,+,-,+,-,+,-,+,-,+,-,+,-,+,-,+,+]} = -0.0452$	0.8379
		$\delta_{[-,+,-,+,-,+]}^{[+,-,+,-,+,-,+,-,+,-,+,-,+,-,+,-,+,-,+,+]} = 0.0000$	$\tau_{[-,+,-,+,-,+]}^{[+,-,+,-,+,-,+,-,+,-,+,-,+,-,+,-,+,-,+,+]} = -0.0452$	0.8379
		$\delta_{[+,-,+,-,+,-]}^{[-,+,-,+,-,+,-,+,-,+,-,+,-,+,-,+,-,+,-,+,+]} = 0.0000$	$\tau_{[+,-,+,-,+,-]}^{[-,+,-,+,-,+,-,+,-,+,-,+,-,+,-,+,-,+,-,+,+]} = -0.0452$	0.8379
		$\delta_{[-,+,-,+,-,+]}^{[+,-,+,-,+,-,+,-,+,-,+,-,+,-,+,-,+,-,+,-,+,+]} = 0.0154$	$\tau_{[-,+,-,+,-,+]}^{[+,-,+,-,+,-,+,-,+,-,+,-,+,-,+,-,+,-,+,-,+,+]} = -0.0290$	0.8957
		$\delta_{[+,-,+,-,+,-]}^{[-,+,-,+,-,+,-,+,-,+,-,+,-,+,-,+,-,+,-,+,-,+,+]} = 0.0000$	$\tau_{[+,-,+,-,+,-]}^{[-,+,-,+,-,+,-,+,-,+,-,+,-,+,-,+,-,+,-,+,-,+,+]} = -0.0452$	0.8379
		$\delta_{[-,+,-,+,-,+]}^{[+,-,+,-,+,-,+,-,+,-,+,-,+,-,+,-,+,-,+,-,+,-,+,+]} = 0.0000$	$\tau_{[-,+,-,+,-,+]}^{[+,-,+,-,+,-,+,-,+,-,+,-,+,-,+,-,+,-,+,-,+,-,+,+]} = -0.0452$	0.8379
		$\delta_{[+,-,+,-,+,-]}^{[-,+,-,+,-,+,-,+,-,+,-,+,-,+,-,+,-,+,-,+,-,+,-,+,+]} = 0.0000$	$\tau_{[+,-,+,-,+,-]}^{[-,+,-,+,-,+,-,+,-,+,-,+,-,+,-,+,-,+,-,+,-,+,-,+,+]} = -0.0452$	0.8379
		$\delta_{[-,+,-,+,-,+]}^{[+,-,+,-,+,-,+,-,+,-,+,-,+,-,+,-,+,-,+,-,+,-,+,-,+,+]} = 0.0154$	$\tau_{[-,+,-,+,-,+]}^{[+,-,+,-,+,-,+,-,+,-,+,-,+,-,+,-,+,-,+,-,+,-,+,-,+,+]} = -0.0290$	0.8957
		$\delta_{[+,-,+,-,+,-]}^{[-,+,-,+,-,+,-,+,-,+,-,+,-,+,-,+,-,+,-,+,-,+,-,+,-,+,+]} = 0.0308$	$\tau_{[+,-,+,-,+,-]}^{[-,+,-,+,-,+,-,+,-,+,-,+,-,+,-,+,-,+,-,+,-,+,-,+,-,+,+]} = -0.0127$	0.9541
		$\delta_{[-,+,-,+,-,+]}^{[+,-,+,-,+,-,+,-,+,-,+,-,+,-,+,-,+,-,+,-,+,-,+,-,+,-,+,+]} = 0.0000$	$\tau_{[-,+,-,+,-,+]}^{[+,-,+,-,+,-,+,-,+,-,+,-,+,-,+,-,+,-,+,-,+,-,+,-,+,-,+,+]} = -0.0452$	0.8379
		$\delta_{[+,-,+,-,+,-]}^{[-,+,-,+,-,+,-,+,-,+,-,+,-,+,-,+,-,+,-,+,-,+,-,+,-,+,-,+,+]} = 0.0000$	$\tau_{[+,-,+,-,+,-]}^{[-,+,-,+,-,+,-,+,-,+,-,+,-,+,-,+,-,+,-,+,-,+,-,+,-,+,-,+,+]} = -0.0452$	0.8379
		$\delta_{[-,+,-,+,-,+]}^{[+,-,+,-,+,-,+,-,+,-,+,-,+,-,+,-,+,-,+,-,+,-,+,-,+,-,+,-,+,+]} = 0.0462$	$\tau_{[-,+,-,+,-,+]}^{[+,-,+,-,+,-,+,-,+,-,+,-,+,-,+,-,+,-,+,-,+,-,+,-,+,-,+,-,+,+]} = 0.0035$	0.9874
		$\delta_{[+,-,+,-,+,-]}^{[-,+,-,+,-,+,-,+,-,+,-,+,-,+,-,+,-,+,-,+,-,+,-,+,-,+,-,+,-,+,+]} = 0.0000$	$\tau_{[+,-,+,-,+,-]}^{[-,+,-,+,-,+,-,+,-,+,-,+,-,+,-,+,-,+,-,+,-,+,-,+,-,+,-,+,-,+,+]} = -0.0452$	0.8379
$\delta_{[-,+,-,+,-,+]}^{[+,-,+,-,+,-,+,-,+,-,+,-,+,-,+,-,+,-,+,-,+,-,+,-,+,-,+,-,+,-,+,+]} = 0.0000$	$\tau_{[-,+,-,+,-,+]}^{[+,-,+,-,+,-,+,-,+,-,+,-,+,-,+,-,+,-,+,-,+,-,+,-,+,-,+,-,+,-,+,+]} = -0.0452$	0.8379		
$\delta_{[+,-,+,-,+,-]}^{[-,+,-,+,-,+,-,+,-,+,-,+,-,+,-,+,-,+,-,+,-,+,-,+,-,+,-,+,-,+,-,+,+]} = 0.0000$	$\tau_{[+,-,+,-,+,-]}^{[-,+,-,+,-,+,-,+,-,+,-,+,-,+,-,+,-,+,-,+,-,+,-,+,-,+,-,+,-,+,-,+,+]} = -0.0452$	0.8379		
$\delta_{[-,+,-,+,-,+]}^{[+,-,+,-,+,-,+,-,+,-,+,-,+,-,+,-,+,-,+,-,+,-,+,-,+,-,+,-,+,-,+,-,+,+]} = 0.6615$	$\tau_{[-,+,-,+,-,+]}^{[+,-,+,-,+,-,+,-,+,-,+,-,+,-,+,-,+,-,+,-,+,-,+,-,+,-,+,-,+,-,+,-,+,+]} = 0.6504$	0.0032		
$\delta_{[+,-,+,-,+,-]}^{[-,+,-,+,-,+,-,+,-,+,-,+,-,+,-,+,-,+,-,+,-,+,-,+,-,+,-,+,-,+,-,+,-,+,+]} = 0.1231$	$\tau_{[+,-,+,-,+,-]}^{[-,+,-,+,-,+,-,+,-,+,-,+,-,+,-,+,-,+,-,+,-,+,-,+,-,+,-,+,-,+,-,+,-,+,+]} = 0.0845$	0.7022		

References

- Aakra, Å., Utåker, J. B., Pommerening-Röser, A., Koops, H. P., & Nes, I. F. (2001). Detailed phylogeny of ammonia-oxidizing bacteria determined by rDNA sequences and DNA homology values. *International Journal of Systematic and Evolutionary Microbiology*, 51(6), 2021-2030. <https://doi.org/10.1099/00207713-51-6-2021>
- Abby, S. S., et al. (2018). Candidatus Nitrosocaldus cavascurensis, an ammonia oxidizing, extremely thermophilic archaeon with a highly mobile genome [Original Research]. *Frontiers in Microbiology*, 9. <https://doi.org/10.3389/fmicb.2018.00028>
- Abeliovich, A., & Vonshak, A. (1992). Anaerobic metabolism of Nitrosomonas europaea. *Archives of Microbiology*, 158(4), 267-270. <https://doi.org/10.1007/BF00245243>
- Ackermann, M. (2015). A functional perspective on phenotypic heterogeneity in microorganisms. *Nature Reviews Microbiology*, 13(8), 497-508. <https://doi.org/10.1038/nrmicro3491>
- Allesina, S., & Tang, S. (2012). Stability criteria for complex ecosystems. *Nature*, 483(7388), 205-208. <https://doi.org/10.1038/nature10832>
- Almstrand, R., et al. (2014). Three-dimensional stratification of bacterial biofilm populations in a moving bed biofilm reactor for nitrification-anammox. *International Journal of Molecular Sciences*, 15(2), 2191-2206. <https://doi.org/10.3390/ijms15022191>
- Alonso-Sáez, L., et al. (2012). Role for urea in nitrification by polar marine archaea. *PNAS*, 109(44), 17989-17994. <https://doi.org/10.1073/pnas.1201914109>
- Alphenaar, P. A., Pérez, M. C., & Lettinga, G. (1993). The influence of substrate transport limitation on porosity and methanogenic activity of anaerobic sludge granules. *Applied Microbiology and Biotechnology*, 39(2), 276-280. <https://doi.org/10.1007/BF00228619>
- Alves, R. J. E., Minh, B. Q., Urich, T., Von Haeseler, A., & Schleper, C. (2018). Unifying the global phylogeny and environmental distribution of ammonia-oxidising archaea based on amoA genes. *Nature Communications*, 9(1), 1-17. <https://doi.org/10.1038/s41467-018-03861-1>
- Andersen, K. B., & Von Meyenburg, K. (1980). Are growth rates of Escherichia coli in batch cultures limited by respiration? *Journal of Bacteriology*, 144(1), 114-123. <https://doi.org/10.1128/jb.144.1.114-123.1980>
- Andrews, J. H., & Harris, R. F. (1986). r- and K-selection and microbial ecology. *Advances in Microbial Ecology*, 99 - 147. https://doi.org/10.1007/978-1-4757-0611-6_3
- Anthonisen, A. C., Loehr, R. C., Prakasam, T. B. S., & Srinath, E. G. (1976). Inhibition of nitrification by ammonia and nitrous acid. *Journal of the Water Pollution Control Federation*, 48(5), 835-852.
- Antoniou, P., Hamilton, J., Koopman, B., Jain, R., Holloway, B., Lyberatos, G., & Svoronos, S. A. (1990). Effect of temperature and pH on the effective maximum specific growth rate of nitrifying bacteria. *Water Research*, 24(1), 97-101. [https://doi.org/10.1016/0043-1354\(90\)90070-M](https://doi.org/10.1016/0043-1354(90)90070-M)
- Arai, H., Kawakami, T., Osamura, T., Hirai, T., Sakai, Y., & Ishii, M. (2014). Enzymatic characterization and in vivo function of five terminal oxidases in Pseudomonas aeruginosa. *Journal of Bacteriology*, 196(24), 4206-4215. <https://doi.org/10.1128/JB.02176-14>

- Arp, D. J., Sayavedra-Soto, L. A., & Hommes, N. G. (2002). Molecular biology and biochemistry of ammonia oxidation by *Nitrosomonas europaea*. *Archives of Microbiology*, 178(4), 250-255. <https://doi.org/10.1007/s00203-002-0452-0>
- Arthur, W., & Mitchell, P. (1989). A Revised scheme for the classification of population interactions. *Oikos*, 56(1), 141-143. <https://doi.org/10.2307/3566099>
- Bairey, E., Kelsic, E. D., & Kishony, R. (2016). High-order species interactions shape ecosystem diversity. *Nature Communications*, 7(1), 12285. <https://doi.org/10.1038/ncomms12285>
- Baolan, H., et al. (2014). pH-dominated niche segregation of ammonia-oxidising microorganisms in Chinese agricultural soils. *FEMS Microbiology Ecology*, 90(1), 290-299. <https://doi.org/10.1111/1574-6941.12391>
- Barber, J. N., et al. (2022). Species interactions constrain adaptation and preserve ecological stability in an experimental microbial community. *The ISME Journal*. <https://doi.org/10.1038/s41396-022-01191-1>
- Battye, W., Aneja, V. P., & Schlesinger, W. H. (2017). Is nitrogen the next carbon? *Earth's Future*, 5(9), 894-904. <https://doi.org/10.1002/2017EF000592>
- Bauer, E., Zimmermann, J., Baldini, F., Thiele, I., & Kaleta, C. (2017). BacArena: Individual-based metabolic modeling of heterogeneous microbes in complex communities. *PLOS Computational Biology*, 13(5), e1005544. <https://doi.org/10.1371/journal.pcbi.1005544>
- Bayer, B., et al. (2015). Physiological and genomic characterization of two novel marine thaumarchaeal strains indicates niche differentiation. *The ISME Journal*, 10(5), 1051-1063. <https://doi.org/10.1038/ismej.2015.200>
- Beber, M. E., Gollub, M. G., Mozaffari, D., Shebek, K. M., Flamholz, Avi I., Milo, R., & Noor, E. (2022). eQuilibrator 3.0: a database solution for thermodynamic constant estimation. *Nucleic Acids Research*, 50(D1), D603-D609. <https://doi.org/10.1093/nar/gkab1106>
- Belevich, I., Borisov, V. B., Bloch, D. A., Konstantinov, A. A., & Verkhovsky, M. I. (2007). Cytochrome bd from *Azotobacter vinelandii*: evidence for high-affinity oxygen binding. *Biochemistry*, 46(39), 11177-11184. <https://doi.org/10.1021/bi700862u>
- Belevich, I., Borisov, V. B., Konstantinov, A. A., & Verkhovsky, M. I. (2005). Oxygenated complex of cytochrome bd from *Escherichia coli*: stability and photolability. *FEBS Letters*, 579(21), 4567-4570. <https://doi.org/10.1016/j.febslet.2005.07.011>
- Bellocchi, G., Rivington, M., Donatelli, M., & Matthews, K. (2010). Validation of biophysical models: issues and methodologies. A review. *Agronomy for Sustainable Development*, 30(1), 109-130. <https://doi.org/10.1051/agro/2009001>
- Belser, L. W., & Schmidt, E. L. (1980). Growth and oxidation kinetics of three genera of ammonia oxidizing. *FEMS Microbiology Letters*, 7(3), 213-216. <https://doi.org/10.1111/j.1574-6941.1980.tb01628.x>
- Beman, J. M., Bertics, V., Braunschweiler, T., & Wilson, J. (2012). Quantification of ammonia oxidation rates and the distribution of ammonia-oxidizing archaea and bacteria in marine sediment depth profiles from Catalina Island, California [Original Research]. *Frontiers in Microbiology*, 3. <https://doi.org/10.3389/fmicb.2012.00263>
- Berg, C., Vandieken, V., Thamdrup, B., & Jürgens, K. (2015). Significance of archaeal nitrification in hypoxic waters of the Baltic Sea. *The ISME Journal*, 9(6), 1319-1332. <https://doi.org/10.1038/ismej.2014.218>
- Berg, I. A. (2011). Ecological aspects of the distribution of different autotrophic CO₂ fixation pathways. *Applied and Environmental Microbiology*, 77(6), 1925-1936. <https://doi.org/10.1128/AEM.02473-10>
- Bergersen, F. J., & Turner, G. L. (1980). Properties of terminal oxidase systems of bacteroids from root nodules of soybean and cowpea and of N₂-fixing bacteria grown in

- continuous culture. *Journal of General Microbiology*, 118(1), 235-252. <https://doi.org/10.1099/00221287-118-1-235>
- Berks, B. C., Ferguson, S. J., Moir, J. W. B., & Richardson, D. J. (1995). Enzymes and associated electron transport systems that catalyse the respiratory reduction of nitrogen oxides and oxyanions. *Biochimica et Biophysica Acta - Bioenergetics*, 1232(3), 97-173. [https://doi.org/10.1016/0005-2728\(95\)00092-5](https://doi.org/10.1016/0005-2728(95)00092-5)
- Blackburne, R., Vadivelu, V. M., Yuan, Z., & Keller, J. (2007a). Determination of growth rate and yield of nitrifying bacteria by measuring carbon dioxide uptake rate. *Water Environment Research*, 79(12), 2437-2445. <https://doi.org/10.2175/106143007x212139>
- Blackburne, R., Vadivelu, V. M., Yuan, Z., & Keller, J. (2007b). Kinetic characterisation of an enriched *Nitrospira* culture with comparison to *Nitrobacter*. *Water Research*, 41(14), 3033-3042. <https://doi.org/10.1016/j.watres.2007.01.043>
- Blackburne, R., Yuan, Z., & Keller, J. (2008). Partial nitrification to nitrite using low dissolved oxygen concentration as the main selection factor. *Biodegradation*, 19, 303-312. <https://doi.org/10.1007/s10532-007-9136-4>
- Bock, E. (1976). Growth of *Nitrobacter* in the presence of organic matter - II. Chemoorganotrophic growth of *Nitrobacter agilis*. *Archives of Microbiology*, 108(3), 305-312. <https://doi.org/10.1007/BF00454857>
- Bock, E., Koops, H.-p., Rudert, M., & Abteilung, M. (1990). A new facultatively nitrite oxidizing bacterium, *Nitrobacter vulgaris* sp. nov. *Archives of Microbiology*, 153, 105-110. <https://doi.org/10.1007/BF00247805>
- Bock, E., Schmidt, I., Stüven, R., & Zart, D. (1995). Nitrogen loss caused by denitrifying *Nitrosomonas* cells using ammonium or hydrogen as electron donors and nitrite as electron acceptor. *Archives of Microbiology*, 163(1), 16-20. <https://doi.org/10.1007/BF00262198>
- Boddicker, A. M., & Mosier, A. C. (2018). Genomic profiling of four cultivated *Candidatus Nitrotoga* spp. predicts broad metabolic potential and environmental distribution. *The ISME Journal*, 12, 2864-2882. <https://doi.org/10.1038/s41396-018-0240-8>
- Bodegom, P. V. (2007). Microbial maintenance: a critical review on its quantification. *Microbial Ecology*, 53, 513-523. <https://doi.org/10.1007/s00248-006-9049-5>
- Boon, B., & Laudelout, H. (1960). Kinetics of the nitrite oxidation by *Nitrobacter winogradskyi*. *Biochemical Journal*, 85(3), 440 - 447. <https://doi.org/10.1042/bj0850440>
- Borer, B., Ataman, M., Hatzimanikatis, V., & Or, D. (2019). Modeling metabolic networks of individual bacterial agents in heterogeneous and dynamic soil habitats (IndiMeSH). *PLOS Computational Biology*, 15(6), e1007127. <https://doi.org/10.1371/journal.pcbi.1007127>
- Borer, B., Ciccarese, D., Johnson, D., & Or, D. (2020). Spatial organization in microbial range expansion emerges from trophic dependencies and successful lineages. *Communications Biology*, 3(1), 685. <https://doi.org/10.1038/s42003-020-01409-y>
- Both, G. J., Gerards, S., & Laanbroek, H. J. (1992). Kinetics of nitrite oxidation in two *Nitrobacter* species grown in nitrite-limited chemostats. *Archives of Microbiology*, 157, 436-441. <https://doi.org/10.1007/BF00249101>
- Breugelmans, P., Barken, K. B., Tolker-Nielsen, T., Hofkens, J., Dejonghe, W., & Springael, D. (2008). Architecture and spatial organization in a triple-species bacterial biofilm synergistically degrading the phenylurea herbicide linuron. *FEMS Microbiology Ecology*, 64(2), 271-282. <https://doi.org/10.1111/j.1574-6941.2008.00470.x>
- Briggs, W., Henson, V., & McCormick, S. (2000). *A multigrid tutorial* (2nd Edition ed.).

- Bristow, L. A., et al. (2016). Ammonium and nitrite oxidation at nanomolar oxygen concentrations in oxygen minimum zone waters. *PNAS*, *113*(38). <https://doi.org/10.1073/pnas.1600359113>
- Bronstein, J. L. (1994). Our current understanding of mutualism. *The Quarterly Review of Biology*, *69*(1), 31-51. <https://doi.org/10.1086/418432>
- Bruggeman, F. J., Planqué, R., Molenaar, D., & Teusink, B. (2020). Searching for principles of microbial physiology. *FEMS Microbiology Reviews*, *44*(6), 821-844. <https://doi.org/10.1093/femsre/fuaa034>
- Bruijn, P. D., Graaf, A. A. V. D., Jetten, M. S. M., Robertson, L. A., & Kuenen, J. G. (1995). Growth of *Nitrosomonas europaea* on hydroxylamine. *FEMS Microbiology Letters*, *125*(2-3), 179-184. <https://doi.org/10.1111/j.1574-6968.1995.tb07355.x>
- Buswell, A. M., Shiota, T., Lawrence, N., & Meter, I. V. A. N. (1953). Laboratory studies on the kinetics of the growth of *Nitrosomonas* with relation to the nitrification phase of the BOD test. *Applied Microbiology*, *2*(3), 21-25. <https://doi.org/10.1128/am.2.1.21-25.1954>
- Button, D. K. (1985). Kinetics of nutrient-limited transport and microbial growth. *Microbiological Reviews*, *49*(3), 270-297. <https://doi.org/10.1128/mr.49.3.270-297.1985>
- Button, D. K. (1991). Biochemical basis for whole-cell uptake kinetics: specific affinity, oligotrophic capacity, and the meaning of the Michaelis constant. *Applied and Environmental Microbiology*, *57*(7), 6. <https://doi.org/10.1128/aem.57.7.2033-2038.1991>
- Button, D. K. (1998). Nutrient uptake by microorganisms according to kinetic parameters from theory as related to cytoarchitecture. *Microbiology and Molecular Biology Reviews*, *62*(3), 636-645. <https://doi.org/10.1128/MMBR.62.3.636-645.1998>
- Cai, Y.-M. (2020). Non-surface Attached Bacterial Aggregates: A Ubiquitous Third Lifestyle [Review]. *Frontiers in Microbiology*, *11*(3106). <https://doi.org/10.3389/fmicb.2020.557035>
- Caranto, J. D., & Lancaster, K. M. (2017). Nitric oxide is an obligate bacterial nitrification intermediate produced by hydroxylamine oxidoreductase. *PNAS*, *114*(31), 8217-8222. <https://doi.org/10.1073/pnas.1812827115>
- Caranto, J. D., Vilbert, A. C., & Lancaster, K. M. (2016). *Nitrosomonas europaea* cytochrome P460 is a direct link between nitrification and nitrous oxide emission. *PNAS*, *113*(51), 14704-14709. <https://doi.org/10.1073/pnas.1611051113>
- Carlson, R., & Srienc, F. (2004). Fundamental *Escherichia coli* biochemical pathways for biomass and energy production: identification of reactions. *Biotechnology and Bioengineering*, *85*(1), 1-19. <https://doi.org/10.1002/bit.10812>
- Carvajal-Arroyo, J. M., Sun, W., Sierra-Alvarez, R., & Field, J. A. (2013). Inhibition of anaerobic ammonium oxidizing (anammox) enrichment cultures by substrates, metabolites and common wastewater constituents. *Chemosphere*, *91*(1), 22-27. <https://doi.org/10.1016/j.chemosphere.2012.11.025>
- Chain, P., et al. (2003). Complete genome sequence of the ammonia-oxidizing bacterium and obligate chemolithoautotroph *Nitrosomonas europaea*. *Journal of Bacteriology*, *185*(9), 2759-2773. <https://doi.org/10.1128/JB.185.9.2759>
- Chao, Y., Mao, Y., Yu, K., & Zhang, T. (2016). Novel nitrifiers and comammox in a full-scale hybrid biofilm and activated sludge reactor revealed by metagenomic approach. *Applied Microbiology and Biotechnology*, *100*, 8225-8237. <https://doi.org/10.1007/s00253-016-7655-9>
- Charney, J. G., Fjörtoft, R., & Neumann, J. V. (1950). Numerical integration of the barotropic vorticity equation. *Tellus*, *2*(4), 237-254. <https://doi.org/10.3402/tellusa.v2i4.8607>

- Chen, G., Ekama, G. A., van Loosdrecht, M. C. M., & Brdjanovic, D. (2020). *Biological wastewater treatment: principles, modeling and design*. IWA Publishing. <https://doi.org/10.2166/9781789060362>
- Chen, J., Nie, Y., Liu, W., Wang, Z., Shen, W., & Taylor, A. E. (2017). Ammonia-oxidizing archaea are more resistant than denitrifiers to seasonal precipitation changes in an acidic subtropical forest soil. *Frontiers in Microbiology*, 8(July), 1-12. <https://doi.org/10.3389/fmicb.2017.01384>
- Chen, Y., Lin, C.-J., Lan, H., Fu, S., & Zhan, H. (2010). Evaluation of kinetic parameters and mass transfer of glucose-fed granules under hypoxic conditions. *Biotechnology and Bioprocess Engineering*, 15(6), 931-936. <https://doi.org/10.1007/s12257-010-0060-9>
- Christensen, B. B., Haagensen, J. A. J., Heydorn, A., & Molin, S. (2002). Metabolic commensalism and competition in a two-species microbial consortium. *Applied and Environmental Microbiology*, 68(5), 2495-2502. <https://doi.org/10.1128/AEM.68.5.2495-2502.2002>
- Ciccarese, D., Micali, G., Borer, B., Ruan, C., Or, D., & Johnson, D. R. (2022). Rare and localized events stabilize microbial community composition and patterns of spatial self-organization in a fluctuating environment. *The ISME Journal*, 16(5), 1453-1463. <https://doi.org/10.1038/s41396-022-01189-9>
- Claros, J., Jimenez, E., Aguado, D., Ferrer, J., Seco, A., & Serralta, J. (2013). Effect of pH and HNO₂ concentration on the activity of ammonia-oxidizing bacteria in a partial nitrification reactor. *Water Science & Technology*, 67(11), 2587-2594. <https://doi.org/10.2166/wst.2013.132>
- Cole, A. C., Semmens, M. J., & LaPara, T. M. (2004). Stratification of activity and bacterial community structure in biofilms grown on membranes transferring oxygen. *Applied and Environmental Microbiology*, 70(4), 1982-1989. <https://doi.org/10.1128/AEM.70.4.1982-1989.2004>
- Cooper, C. E., et al. (2003). Nitric oxide and peroxyxynitrite cause irreversible increases in the K_m for oxygen of mitochondrial cytochrome oxidase: In vitro and in vivo studies. *Biochimica et Biophysica Acta - Bioenergetics*, 1607(1), 27-34. <https://doi.org/10.1016/j.bbabi.2003.08.003>
- Costa, E., Pérez, J., & Kreft, J. U. (2006). Why is metabolic labour divided in nitrification? *Trends in Microbiology*, 14(5), 213-219. <https://doi.org/10.1016/j.tim.2006.03.006>
- Costerton, J. W., Geesey, G. G., & Cheng, K. J. (1978). How bacteria stick. *Sci Am*, 238(1), 86-95. <https://doi.org/10.1038/scientificamerican0178-86>
- Cui, H., Zhang, L., Zhang, Q., Li, X., & Peng, Y. (2023). Enrichment of comammox bacteria in anammox-dominated low-strength wastewater treatment system within microaerobic conditions: cooperative effect driving enhanced nitrogen removal. *Chemical Engineering Journal*, 453, 139851. <https://doi.org/10.1016/j.cej.2022.139851>
- Cusick, J. A., Wellman, C. L., & Demas, G. E. (2021). The call of the wild: using non-model systems to investigate microbiome-behaviour relationships. *Journal of Experimental Biology*, 224(10). <https://doi.org/10.1242/jeb.224485>
- D'Mello, R., Hill, S., & Poole, R. K. (1994). Determination of the oxygen affinities of terminal oxidases in *Azotobacter vinelandii* using the deoxygenation of oxyleghaemoglobin and oxymyoglobin: cytochrome bd is a low-affinity oxidase. *Microbiology*, 140(6), 1395-1402. <https://doi.org/10.1099/00221287-140-6-1395>
- D'Mello, R., Hill, S., & Poole, R. K. (1996). The cytochrome bd quinol oxidase in *Escherichia coli* has an extremely high oxygen affinity and two oxygen-binding haems: Implications for regulation of activity in vivo by oxygen inhibition. *Microbiology*, 142(4), 755-763. <https://doi.org/10.1099/00221287-142-4-755>

- Daebeler, A., et al. (2018). Cultivation and genomic analysis of “Candidatus Nitrosocaldus islandicus,” an obligately thermophilic, ammonia-oxidizing Thaumarchaeon from a hot spring biofilm in Graendalur Valley, Iceland [Original Research]. *Frontiers in Microbiology*, 9. <https://doi.org/10.3389/fmicb.2018.00193>
- Daims, H., et al. (2015). Complete nitrification by Nitrospira bacteria. *Nature*, 528(7583), 504-509. <https://doi.org/10.1038/nature16461>
- Daims, H., Lückner, S., & Wagner, M. (2016). A new perspective on microbes formerly known as nitrite-oxidizing bacteria. *Trends in Microbiology*, 24(9), 699-712. <https://doi.org/10.1016/j.tim.2016.05.004>
- Dal Co, A., van Vliet, S., Kiviet, D. J., Schlegel, S., & Ackermann, M. (2020). Short-range interactions govern the dynamics and functions of microbial communities. *Nature Ecology & Evolution*, 4(3), 366-375. <https://doi.org/10.1038/s41559-019-1080-2>
- Dalsgaard, T., et al. (2014). Oxygen at nanomolar levels reversibly suppresses process rates and gene expression in anammox and denitrification in the oxygen minimum zone of northern Chile. *mBio*, 5(6), e01966-01914. <https://doi.org/10.1128/mBio.01966-14>
- Dar, D., Dar, N., Cai, L., & Newman, D. K. (2021). Spatial transcriptomics of planktonic and sessile bacterial populations at single-cell resolution. *Science*, 373(6556). <https://doi.org/10.1126/science.abi4882>
- de la Cruz, R., & Kreft, J.-U. (2018). Geometric mean extension for data sets with zeros. arXiv:1806.06403. Retrieved June 01, 2018, from <https://ui.adsabs.harvard.edu/abs/2018arXiv180606403D>
- Diamond, S., Lavy, A., Crits-Christoph, A., Matheus Carnevali, P. B., Sharrar, A., Williams, K. H., & Banfield, J. F. (2022). Soils and sediments host Thermoplasmata archaea encoding novel copper membrane monooxygenases (CuMMOs). *The ISME Journal*, 16(5), 1348-1362. <https://doi.org/10.1038/s41396-021-01177-5>
- Dochain, D., & Vanrolleghem, P. (2015). Dynamical modelling & estimation in wastewater treatment processes. *Water Intelligence Online*. <https://doi.org/10.2166/9781780403045>
- Dogsa, I., & Mandic-Mulec, I. (2023). Multiscale spatial segregation analysis in digital images of biofilms. *Biofilm*, 100157. <https://doi.org/10.1016/j.bioflm.2023.100157>
- Drewnowski, J., Remiszewska-Skwarek, A., Duda, S., & Łagód, G. (2019). Aeration process in bioreactors as the main energy consumer in a wastewater treatment plant. Review of solutions and methods of process optimization. *Processes*, 7(5), 311. <https://doi.org/10.3390/pr7050311>
- Dueholm, M. K. D., et al. (2022). MiDAS 4: A global catalogue of full-length 16S rRNA gene sequences and taxonomy for studies of bacterial communities in wastewater treatment plants. *Nature Communications*, 13(1), 1908. <https://doi.org/10.1038/s41467-022-29438-7>
- Dukovski, I., et al. (2021). A metabolic modeling platform for the computation of microbial ecosystems in time and space (COMETS). *Nature Protocols*, 16(11), 5030-5082. <https://doi.org/10.1038/s41596-021-00593-3>
- Dworkin, M., & Gutnick, D. (2012). Sergei Winogradsky: a founder of modern microbiology and the first microbial ecologist. *FEMS Microbiology Reviews*, 36(2), 364-379. <https://doi.org/10.1111/j.1574-6976.2011.00299.x>
- Egli, K., Fanger, U., Alvarez, P. J. J., Siegrist, H., van der Meer, J. R., & Zehnder, A. J. B. (2001). Enrichment and characterization of an anammox bacterium from a rotating biological contactor treating ammonium-rich leachate. *Archives of Microbiology*, 175(3), 198-207. <https://doi.org/10.1007/s002030100255>
- Ehrich, S., Behrens, D., Lebedeva, E., Ludwig, W., & Bock, E. (1995). A new obligately chemolithoautotrophic, nitrite-oxidizing bacterium, *Nitrospira moscoviensis* sp. nov.

- and its phylogenetic relationship. *Archives of Microbiology*, 164(1), 16-23. <https://doi.org/10.1007/BF02568729>
- Embree, M., Liu, J. K., Al-Bassam, M. M., & Zengler, K. (2015). Networks of energetic and metabolic interactions define dynamics in microbial communities. *PNAS*, 112(50), 15450-15455. <https://doi.org/10.1073/pnas.1506034112>
- Eric, W. K. T., & Kwan, K.-M. (1999). Replication and theory development in organizational science: a critical realist perspective. *The Academy of Management Review*, 24(4), 759-780. <https://doi.org/10.2307/259353>
- Ettwig, K. F., Speth, D. R., Reimann, J., Wu, M. L., Jetten, M. S. M., & Keltjens, J. T. (2012). Bacterial oxygen production in the dark [Hypothesis and Theory]. *Frontiers in Microbiology*, 3. <https://doi.org/10.3389/fmicb.2012.00273>
- Evans, C. R., Kempes, C. P., Price-Whelan, A., & Dietrich, L. E. P. (2020). Metabolic heterogeneity and cross-feeding in bacterial multicellular systems. *Trends in Microbiology*, 28(9), 732-743. <https://doi.org/10.1016/j.tim.2020.03.008>
- Falkowski, P. G., Fenchel, T., & Delong, E. F. (2008). The Microbial Engines That Drive Earth's Biogeochemical Cycles. *Science*, 320(5879), 1034-1039. <https://doi.org/10.1126/science.1153213>
- Flemming, H.-C., Wingender, J., Szewzyk, U., Steinberg, P., Rice, S. A., & Kjelleberg, S. (2016). Biofilms: an emergent form of bacterial life. *Nature Reviews Microbiology*, 14(9), 563-575. <https://doi.org/10.1038/nrmicro.2016.94>
- Freing, A., Wallace, D. W., & Bange, H. W. (2012). Global oceanic production of nitrous oxide. *Philosophical transaction of the royal society*, 367(1593), 1245-1255. <https://doi.org/10.1098/rstb.2011.0360>
- French, E., Kozłowski, J. A., Mukherjee, M., Bullerjahn, G., & Bollmann, A. (2012). Ecophysiological characterization of ammonia-oxidizing archaea and bacteria from freshwater. *Applied and Environmental Microbiology*, 78(16), 5773-5780. <https://doi.org/10.1128/AEM.00432-12>
- Füssel, J., et al. (2017). Adaptability as the key to success for the ubiquitous marine nitrite oxidizer *Nitrococcus*. *Science advances*, 3, 2-11. <https://doi.org/10.1126/sciadv.1700807>
- Garcia-Horsman, J. A., Barquera, B., & Escamilla, J. E. (1991). Two different aa3-type cytochromes can be purified from the bacterium *Bacillus cereus*. *European Journal of Biochemistry*, 199(3), 761-768. <https://doi.org/10.1111/j.1432-1033.1991.tb16181.x>
- Gay, G., Corman, A., & Biologic, L. D. (1984). Comparative study of the growth of two strains of *Nitrobacter* in batch and continuous culture. *Microbial Ecology*, 10, 99-105. <https://doi.org/10.1007/BF02011417>
- Giehl, R. F. H., & von Wirén, N. (2014). Root nutrient foraging. *Plant physiology*, 166(2), 509-517. <https://doi.org/10.1104/pp.114.245225>
- Giuffrè, A., Borisov, V. B., Arese, M., Sarti, P., & Forte, E. (2014). Cytochrome bd oxidase and bacterial tolerance to oxidative and nitrosative stress. *Biochimica et Biophysica Acta - Bioenergetics*, 1837(7), 1178-1187. <https://doi.org/10.1016/j.bbabi.2014.01.016>
- Glover, H. E. (1985). The relationship between inorganic nitrogen oxidation and organic carbon production in batch and chemostat cultures of marine nitrifying bacteria. *Archives of Microbiology*, 142, 45-50. <https://doi.org/10.1007/BF00409235>
- González-Cabaleiro, R., Curtis, T. P., & Ofiteiru, I. D. (2019). Bioenergetics analysis of ammonia-oxidizing bacteria and the estimation of their maximum growth yield. *Water Research*, 154, 238-245. <https://doi.org/10.1016/j.watres.2019.01.054>
- González-Cabaleiro, R., Martínez-Rabert, E., Argiz, L., van Kessel, M. A. H. J., & Smith, C. J. (2021). A framework based on fundamental biochemical principles to engineer

- microbial community dynamics. *Current Opinion in Biotechnology*, 67, 111-118. <https://doi.org/10.1016/j.copbio.2021.01.001>
- González-Cabaleiro, R., Ofiteiru, I. D., Lema, J. M., & Rodríguez, J. (2015). Microbial catabolic activities are naturally selected by metabolic energy harvest rate. *The ISME Journal*, 9(12), 2630-2641. <https://doi.org/10.1038/ismej.2015.69>
- Goreau, T. J., Kaplan, W. A., Wofsy, S. C., McElroy, M. B., Valois, F. W., & Watson, S. W. (1980). Production of NO₂ and N₂O by nitrifying bacteria at reduced concentrations of oxygen. *Applied and Environmental Microbiology*, 40(3), 526-532. <https://doi.org/10.1128/aem.40.3.526-532.1980>
- Gorochoowski, T. E., et al. (2012). BSim: an agent-based tool for modeling bacterial populations in systems and synthetic biology. *PLoS ONE*, 7(8), e42790. <https://doi.org/10.1371/journal.pone.0042790>
- Gottshall, E. Y., et al. (2021). Sustained nitrogen loss in a symbiotic association of comammox Nitrospira and anammox bacteria. *Water Research*, 202. <https://doi.org/10.1016/j.watres.2021.117426>
- Grilli, J., Barabás, G., Michalska-Smith, M. J., & Allesina, S. (2017). Higher-order interactions stabilize dynamics in competitive network models. *Nature*, 548(7666), 210-213. <https://doi.org/10.1038/nature23273>
- Gruber, W., Niederdorfer, R., Ringwald, J., Morgenroth, E., Bürgmann, H., & Joss, A. (2021). Linking seasonal N₂O emissions and nitrification failures to microbial dynamics in a SBR wastewater treatment plant. *Water Research X*, 11, 100098. <https://doi.org/10.1016/j.wroa.2021.100098>
- Gwak, J. H., et al. (2019). Archaeal nitrification is constrained by copper complexation with organic matter in municipal wastewater treatment plants. *The ISME Journal*. <https://doi.org/10.1038/s41396-019-0538-1>
- Hallatschek, O., Hersen, P., Ramanathan, S., & Nelson, D. R. (2007). Genetic drift at expanding frontiers promotes gene segregation. *PNAS*, 104(50), 19926-19930. <https://doi.org/10.1073/pnas.0710150104>
- Han, K., & Levenspiel, O. (1988). Extended monod kinetics for substrate, product, and cell inhibition. *Biotechnology and Bioengineering*, 32(4), 430-447. <https://doi.org/10.1002/bit.260320404>
- Hao, X., Heijnen, J. J., & Loosdrecht, M. C. M. V. (2002). Model-based evaluation of temperature and inflow variations on a partial nitrification – ANAMMOX biofilm process. *Water Research*, 36(19), 4839-4849. [https://doi.org/10.1016/S0043-1354\(02\)00219-1](https://doi.org/10.1016/S0043-1354(02)00219-1)
- Harder, W., & Dijkhuizen, L. (1983). Physiological responses to nutrient limitation. *Annual Review of Microbiology*, 37, 1-23. <https://doi.org/10.1146/annurev.mi.37.100183.000245>
- Harper, W. F., Takeuchi, Y., Riya, S., Hosomi, M., & Terada, A. (2015). Novel abiotic reactions increase nitrous oxide production during partial nitrification: modeling and experiments. *Chemical Engineering Journal*, 281, 1017-1023. <https://doi.org/10.1016/j.cej.2015.06.109>
- Hatzenpichler, R. (2012). Diversity, physiology, and niche differentiation of ammonia-oxidizing archaea. *Applied and Environmental Microbiology*, 78(21), 7501-7510. <https://doi.org/10.1128/AEM.01960-12>
- Haynes, W. M. (2016). *CRC Handbook of Chemistry and Physics*. CRC press. <https://doi.org/10.1201/9781315380476>
- Heijnen, J. J., & van Dijken, J. P. (1992). In search of a thermodynamic description of biomass yields for chemotrophic growth of microorganisms. *Biotechnology and Bioengineering*, 39(8), 833-858. <https://doi.org/10.1002/bit.260390806>

- Heil, J., Vereecken, H., & Brüggemann, N. (2016). A review of chemical reactions of nitrification intermediates and their role in nitrogen cycling and nitrogen trace gas formation in soil. *European Journal of Soil Science*, 67(1), 23-39. <https://doi.org/10.1111/ejss.12306>
- Helder, W., & De Vries, R. T. P. (1983). Estuarine nitrite maxima and nitrifying bacteria (Ems-Dollard estuary). *Netherlands Journal of Sea Research*, 17(1), 1-18. [https://doi.org/10.1016/0077-7579\(83\)90002-9](https://doi.org/10.1016/0077-7579(83)90002-9)
- Hellinga, C., van Loosdrecht, M. C. M., & Heijnen, J. J. (1999). Model based design of a novel process for nitrogen removal from concentrated flows. *Mathematical and Computer Modelling of Dynamical Systems*, 5(4), 351-371. <https://doi.org/10.1076/mcmd.5.4.351.3678>
- Hellweger, F. L. (2017). 75 years since Monod: it is time to increase the complexity of our predictive ecosystem models (opinion). *Ecological Modelling*, 346, 77-87. <https://doi.org/10.1016/j.ecolmodel.2016.12.001>
- Hellweger, F. L., Clegg, R. J., Clark, J. R., Plugge, C. M., & Kreft, J. U. (2016). Advancing microbial sciences by individual-based modelling. *Nature Reviews Microbiology*, 14(7), 461-471. <https://doi.org/10.1038/nrmicro.2016.62>
- Henze, M., Gujer, W., Mino, T., & Van Loosdrecht, M. C. M. (2006). *Activated sludge models ASM1, ASM2, ASM2 and ASM3*. <https://doi.org/10.2166/9781780402369>
- Hink, L., Nicol, G. W., & Prosser, J. I. (2017). Archaea produce lower yields of N₂O than bacteria during aerobic ammonia oxidation in soil. *Environmental Microbiology*, 19(12), 4829-4837. <https://doi.org/10.1111/1462-2920.13282>
- Hirai, T., Osamura, T., Ishii, M., & Arai, H. (2016). Expression of multiple cbb3 cytochrome c oxidase isoforms by combinations of multiple isosubunits in *Pseudomonas aeruginosa*. *PNAS*, 113(45), 12815-12819. <https://doi.org/10.1073/pnas.1613308113>
- Ho, A., Di Lonardo, D. P., & Bodelier, P. L. E. (2017). Revisiting life strategy concepts in environmental microbial ecology. *FEMS Microbiology Ecology*, 93(3), 1-14. <https://doi.org/10.1093/femsec/fix006>
- Hodgskiss, L. H., et al. (2023). Unexpected complexity of the ammonia monooxygenase in archaea. *The ISME Journal*. <https://doi.org/10.1038/s41396-023-01367-3>
- Hoff, J., Daniel, B., Stukenberg, D., Thuronyi, B. W., Waldminghaus, T., & Fritz, G. (2020). *Vibrio natriegens*: an ultrafast-growing marine bacterium as emerging synthetic biology chassis. *Environmental Microbiology*. <https://doi.org/10.1111/1462-2920.15128>
- Hosseinzadeh, P., et al. (2016). A purple cupredoxin from *Nitrosopumilus maritimus* containing a mononuclear type 1 copper center with an open binding site. *Journal of the American Chemical Society*, 138(20), 6324-6327. <https://doi.org/10.1021/jacs.5b13128>
- Hugenholtz, P., Goebel, B. M., & Pace, N. R. (1998). Impact of culture-independent studies on the emerging phylogenetic view of bacterial diversity. *Journal of Bacteriology*, 180(24), 6793-6793. <https://doi.org/10.1128/JB.180.24.6793-6793.1998>
- Hunik, J. H., Bos, C. G., Hoogen, M. P. V. D., De Gooijer, C. D., & Tramper, J. (1994). Co-immobilized *Nitrosomonas europaea* and *Nitrobacter agilis* cells: validation of a dynamic model for simultaneous substrate conversion and growth in K-carrageenan gel beads. *Biotechnology and Bioengineering*, 43, 1153-1163. <https://doi.org/10.1002/bit.260431121>
- Hunik, J. H., Meijer, H. J. G., & Tramper, J. (1993). Kinetics of *Nitrobacter agilis* at extreme substrate, product and salt concentrations. *Applied Microbiology and Biotechnology*, 40(2-3), 442-448. <https://doi.org/10.1007/BF00170408>
- Ishii, K., Fujitani, H., Soh, K., Nakagawa, T., Takahashi, R., & Tsuneda, S. (2017). Enrichment and physiological characterization of a cold-adapted nitrite-oxidizing

- Nitrotoga sp. from an eelgrass sediment. *Applied and Environmental Microbiology*, 83(14), 1-14. <https://doi.org/10.1128/AEM.00549-17>
- Jacob, J., Nowka, B., Merten, V., Sanders, T., Spieck, E., & Dähnke, K. (2017). Oxidation kinetics and inverse isotope effect of marine nitrite-oxidizing isolates. *Aquatic Microbial Ecology*, 80, 289-300. <https://doi.org/10.3354/ame01859>
- Jensen, M., Kuypers, M., Lavik, G., & Thamdrup, B. (2008). Rates and regulation of anaerobic ammonium oxidation and denitrification in the Black Sea. *Limnology and Oceanography*, 53, 23-36. <https://doi.org/10.2307/40006147>
- Jiang, Q. (1999). Comparison of Nitrosospira strains isolated from terrestrial environments. *FEMS Microbiology Ecology*, 30(2), 171-186. [https://doi.org/10.1016/s0168-6496\(99\)00054-9](https://doi.org/10.1016/s0168-6496(99)00054-9)
- Jubany, I., Carrera, J., Lafuente, J., & Baeza, J. A. (2008). Start-up of a nitrification system with automatic control to treat highly concentrated ammonium wastewater: experimental results and modeling. *Chemical Engineering Journal*, 144(3), 407-419. <https://doi.org/10.1016/j.cej.2008.02.010>
- Jung, M.-Y., et al. (2011). Enrichment and characterization of an autotrophic ammonia-oxidizing archaeon of mesophilic Crenarchaeal group I.1a from an agricultural soil. *Applied and Environmental Microbiology*, 77(24), 8635-8647. <https://doi.org/10.1128/AEM.05787-11>
- Jung, M.-Y., et al. (2022). Ammonia-oxidizing archaea possess a wide range of cellular ammonia affinities. *The ISME Journal*, 16(1), 272-283. <https://doi.org/10.1038/s41396-021-01064-z>
- Kalvelage, T., et al. (2011). Oxygen sensitivity of anammox and coupled N-cycle processes in oxygen minimum zones. *PLoS ONE*, 6(12), e29299. <https://doi.org/10.1371/journal.pone.0029299>
- Kamrad, S., et al. (2023). Metabolic heterogeneity and cross-feeding within isogenic yeast populations captured by DILAC. *Nature Microbiology*, 8(3), 441-454. <https://doi.org/10.1038/s41564-022-01304-8>
- Kappler, O., Janssen, P. H., Kreft, J. U., & Schink, B. (1997). Effects of alternative methyl group accepters on the growth energetics of the O-demethylating anaerobe *Holophaga foetida*. *Microbiology*, 143(4), 1105-1114. <https://doi.org/10.1099/00221287-143-4-1105>
- Karimian, E., & Motamedian, E. (2020). ACBM: an integrated agent and constraint based modeling framework for simulation of microbial communities [Article]. *Scientific Reports*, 10(1), Article 8695. <https://doi.org/10.1038/s41598-020-65659-w>
- Kartal, B., & Keltjens, J. T. (2016). Anammox biochemistry: a tale of heme c proteins. *Trends in Biochemical Sciences*, 41(12), 998-1011. <https://doi.org/10.1016/j.tibs.2016.08.015>
- Keen, G. A., & Prosser, J. I. (1987). Steady state and transient growth of autotrophic nitrifying bacteria. *Archives of Microbiology*, 147, 73-79. <https://doi.org/10.1007/BF00492908>
- Kehe, J., Ortiz, A., Kulesa, A., Gore, J., Blainey, P. C., & Friedman, J. (2021). Positive interactions are common among culturable bacteria. *Science advances*, 7(45), eabi7159. <https://doi.org/10.1126/sciadv.abi7159>
- Kendall, M. G. (1938). A new measure of rank correlation. *Biometrika*, 30(1-2), 81-93. <https://doi.org/10.1093/biomet/30.1-2.81>
- Kerou, M., Offre, P., Valledor, L., Abby, S. S., Melcher, M., & Nagler, M. (2016). Proteomics and comparative genomics of *Nitrososphaera viennensis* reveal the core genome and adaptations of archaeal ammonia oxidizers. *PNAS*, 113(18), 7937-7946. <https://doi.org/10.1073/pnas.1601212113>

- Keuter, S. (2011). Characterization of nitrifying bacteria in marine recirculation aquaculture systems with regard to process optimization. *P.h.D work*, 1-114.
- Khalil, K., Mary, B., & Renault, P. (2004). Nitrous oxide production by nitrification and denitrification in soil aggregates as affected by O₂ concentration. *Soil Biology and Biochemistry*, 36(4), 687-699. <https://doi.org/10.1016/j.soilbio.2004.01.004>
- Kim, D.-J., Lee, D.-I., Cha, G.-C., & Keller, J. (2008). Analysis of free ammonia inhibition of nitrite oxidizing bacteria using a dissolved oxygen respirometer. *Environmental Engineering Research*, 13(3), 125-130. <https://doi.org/10.4491/eer.2008.13.3.125>
- Kim, J. G., et al. (2012). Cultivation of a highly enriched ammonia-oxidizing archaeon of thaumarchaeotal group I.1b from an agricultural soil. *Environmental Microbiology*, 14(6), 1528-1543. <https://doi.org/10.1111/j.1462-2920.2012.02740.x>
- Kindaichi, T., Kawano, Y., Ito, T., Satoh, H., & Okabe, S. (2006). Population dynamics and in situ kinetics of nitrifying bacteria in autotrophic nitrifying biofilms as determined by real-time quantitative PCR. *Biotechnology and Bioengineering*, 94, 1111-1121. <https://doi.org/10.1002/bit.20926>
- Kissel, J. C., McCarty, P. L., & Street, R. L. (1984). Numerical simulation of mixed-culture biofilm. *Journal of Environmental Engineering*, 110(2), 393-411. [https://doi.org/10.1061/\(ASCE\)0733-9372\(1984\)110:2\(393\)](https://doi.org/10.1061/(ASCE)0733-9372(1984)110:2(393))
- Kita, K., Konishi, K., & Anraku, Y. (1984). Terminal oxidases of Escherichia coli aerobic respiratory chain. *Journal of Biological Chemistry*, 259(5), 3368-3374. [https://doi.org/10.1016/S0021-9258\(17\)43305-9](https://doi.org/10.1016/S0021-9258(17)43305-9)
- Kits, K. D., et al. (2019). Low yield and abiotic origin of N₂O formed by the complete nitrifier *Nitrospira inopinata*. *Nature Communications*, 10(1), 1-12. <https://doi.org/10.1038/s41467-019-09790-x>
- Kits, K. D., et al. (2017). Kinetic analysis of a complete nitrifier reveals an oligotrophic lifestyle. *Nature Publishing Group*, 549(7671), 269-272. <https://doi.org/10.1038/nature23679>
- Kitzinger, K., et al. (2018). Characterization of the first “Candidatus nitrotoga” isolate reveals metabolic versatility and separate evolution of widespread nitrite-oxidizing bacteria. *mBio*, 9(4), 1-16. <https://doi.org/10.1128/mBio.01186-18>
- Kitzinger, K., et al. (2020). Single cell analyses reveal contrasting life strategies of the two main nitrifiers in the ocean. *Nature Communications*, 11(1), 1-12. <https://doi.org/10.1038/s41467-020-14542-3>
- Kleerebezem, R., & Lücker, S. (2021). Cyclic conversions in the nitrogen cycle. *Frontiers in Microbiology*, 12. <https://doi.org/10.3389/fmicb.2021.622504>
- Kleerebezem, R., Stouten, G., Koehorst, J., Langenhoff, A., Schaap, P., & Smidt, H. (2021). Experimental infrastructure requirements for quantitative research on microbial communities. *Current Opinion in Biotechnology*, 67, 158-165. <https://doi.org/10.1016/j.copbio.2021.01.017>
- Kleerebezem, R., & Van Loosdrecht, M. C. M. (2010). A generalized method for thermodynamic state analysis of environmental systems. *Critical Reviews in Environmental Science and Technology*, 40(1), 1-54. <https://doi.org/10.1080/10643380802000974>
- Knowles, B. Y. G., Downing, A. L., Barrett, M. J., Downing, A. L., & Barrett, M. J. (1965). Determination of kinetic constants for nitrifying bacteria in mixed culture, with the aid of an electronic computer. *Microbiology*, 38(2). <https://doi.org/10.1099/00221287-38-2-263>
- Koch, H., Lücker, S., Albertsen, M., Kitzinger, K., Herbold, C., & Spieck, E. (2015). Expanded metabolic versatility of ubiquitous nitrite-oxidizing bacteria from the genus *Nitrospira*. *PNAS*, 112(36), 11371-11376. <https://doi.org/10.1073/pnas.1506533112>

- Kolonay, J. F., Moshiri, F., Gennis, R. B., Kaysser, T. M., & Maier, R. J. (1994). Purification and characterization of the cytochrome bd complex from *Azotobacter vinelandii*: Comparison to the complex from *Escherichia coli*. *Journal of Bacteriology*, *176*(13), 4177-4181. <https://doi.org/10.1128/jb.176.13.4177-4181.1994>
- Könneke, M., Bernhard, A. E., De La Torre, J. R., Walker, C. B., Waterbury, J. B., & Stahl, D. A. (2005). Isolation of an autotrophic ammonia-oxidizing marine archaeon. *Nature*, *437*(7058), 543-546. <https://doi.org/10.1038/nature03911>
- Könneke, M., Schubert, D. M., Brown, P. C., Hügler, M., Standfest, S., & Schwander, T. (2014). Ammonia-oxidizing archaea use the most energy-efficient aerobic pathway for CO₂ fixation. *PNAS*, *111*(22). <https://doi.org/10.1073/pnas.1402028111>
- Kozłowski, J. A., Stieglmeier, M., Schleper, C., Klotz, M. G., & Stein, L. Y. (2016). Pathways and key intermediates required for obligate aerobic ammonia-dependent chemolithotrophy in bacteria and Thaumarchaeota. *The ISME Journal*, *10*(8), 1836-1845. <https://doi.org/10.1038/ismej.2016.2>
- Kraft, B., Jehmlich, N., Larsen, M., Bristow, L. A., Könneke, M., Thamdrup, B., & Canfield, D. E. (2022). Oxygen and nitrogen production by an ammonia-oxidizing archaeon. *Science*, *375*(6576), 97-100. <https://doi.org/10.1126/science.abe6733>
- Kreft, J.-U. (2004a). Biofilms promote altruism. *Microbiology (Reading)*, *150*(Pt 8), 2751-2760. <https://doi.org/10.1099/mic.0.26829-0>
- Kreft, J.-u. (2004b). Biofilms promote altruism. (2004), 2751-2760. <https://doi.org/10.1099/mic.0.26829-0>
- Kreft, J.-U., Booth, G., & Wimpenny, J. W. T. (1998). BacSim, a simulator for individual-based modelling of bacterial colony growth. *Microbiology*, *144*(12), 3275-3287. <https://doi.org/10.1099/00221287-144-12-3275>
- Kreft, J.-U., Griffin, B. M., & Gonzalez-Cabaleiro, R. (2020). Evolutionary causes and consequences of metabolic division of labour: why anaerobes do and aerobes don't. *Current Opinion in Biotechnology*, *62*, 80-87. <https://doi.org/10.1016/j.copbio.2019.08.008>
- Kreft, J.-U., Picioreanu, C., Wimpenny, J. W. T., & Van Loosdrecht, M. C. M. (2001). Individual-based modelling of biofilms. *Microbiology*, *147*(11), 2897-2912. <https://doi.org/10.1099/00221287-147-11-2897>
- Kuenen, J. G. (2020). Anammox and beyond. *Environmental Microbiology*, *22*(2), 525-536. <https://doi.org/10.1111/1462-2920.14904>
- Kuypers, M. M. M., Marchant, H. K., & Kartal, B. (2018). The microbial nitrogen-cycling network. *Nature Reviews Microbiology*, *16*(5), 263-276. <https://doi.org/10.1038/nrmicro.2018.9>
- Laanbroek, H. J., Bodelier, P. L. E., & Gerards, S. (1994). Oxygen consumption kinetics of *Nitrosomonas europaea* and *Nitrobacter hamburgensis* grown in mixed continuous cultures at different oxygen concentrations. *Archives of Microbiology*, *161*, 156-162. <https://doi.org/10.1007/BF00276477>
- Laanbroek, H. J., & Gerards, S. (1993). Competition for limiting amounts of oxygen between grown in mixed continuous cultures. *Archives of Microbiology*, *159*, 453-459. <https://doi.org/10.1007/BF00288593>
- Lachmann, S. C., Mettler-Altmann, T., Wacker, A., & Spijkerman, E. (2019). Nitrate or ammonium: influences of nitrogen source on the physiology of a green alga. *Ecology and Evolution*, *9*(3), 1070-1082. <https://doi.org/10.1002/ece3.4790>
- Lackner, S., Gilbert, E. M., Vlaeminck, S. E., Joss, A., Horn, H., & van Loosdrecht, M. C. M. (2014). Full-scale partial nitrification/anammox experiences. An application survey. *Water Research*, *55*(0), 292-303. <https://doi.org/10.1016/j.watres.2014.02.032>

- Lagostina, L., et al. (2015). Ammonia-oxidizing Bacteria of the Nitrosospira cluster 1 dominate over ammonia-oxidizing Archaea in oligotrophic surface sediments near the South Atlantic Gyre. *Environmental Microbiology Reports*, 7(3), 404-413. <https://doi.org/10.1111/1758-2229.12264>
- Lancaster, K. M., Caranto, J. D., Majer, S. H., & Smith, M. A. (2018). Alternative bioenergy: updates to and challenges in nitrification metalloenzymology. *Joule*, 2(3), 421-441. <https://doi.org/10.1016/j.joule.2018.01.018>
- Lardon, L. A., Merkey, B. V., Martins, S., Dötsch, A., Picioreanu, C., Kreft, J.-U., & Smets, B. F. (2011). iDynoMiCS: next-generation individual-based modelling of biofilms. *Environmental Microbiology*, 13(9), 2416-2434. <https://doi.org/10.1111/j.1462-2920.2011.02414.x>
- Larsen, B. B., Miller, E. C., Rhodes, M. K., & Wiens, J. J. (2017). Inordinate Fondness Multiplied and Redistributed: the Number of Species on Earth and the New Pie of Life. *The Quarterly Review of Biology*, 92(3), 229-265. <https://doi.org/10.1086/693564>
- Law, Y., Ye, L., Pan, Y., & Yuan, Z. (2012). Nitrous oxide emissions from wastewater treatment processes. *Philosophical transaction of the royal society*, 1265-1277. <https://doi.org/10.1098/rstb.2011.0317>
- Lawson, C. E., et al. (2021). Autotrophic and mixotrophic metabolism of an anammox bacterium revealed by in vivo ¹³C and ²H metabolic network mapping. *The ISME Journal*, 15(3), 673-687. <https://doi.org/10.1038/s41396-020-00805-w>
- Leenen, E. J. T. M., Boxtel, A. M. G. A. V., Englund, G., & Tramper, J. (1997). Reduced temperature sensitivity of immobilized *Nitrobacter agilis* cells caused by diffusion limitation. *Enzyme and Microbial Technology*, 20(8), 573-580. [https://doi.org/10.1016/S0141-0229\(96\)00214-1](https://doi.org/10.1016/S0141-0229(96)00214-1)
- Lehtovirta-Morley, L. E. (2018). Ammonia oxidation: ecology, physiology, biochemistry and why they must all come together. *FEMS Microbiology Letters*, 365(9). <https://doi.org/10.1093/femsle/fny058>
- Lele, U. N., & Watve, M. G. (2014). Bacterial growth rate and growth yield: Is there a relationship? *Proceedings of the Indian National Science Academy*, 80(3), 537-546. <https://doi.org/10.16943/ptinsa/2014/v80i3/55129>
- Lennon, J. T., & Locey, K. J. (2020). More support for Earth's massive microbiome. *Biol Direct*, 15(1), 5. <https://doi.org/10.1186/s13062-020-00261-8>
- Li, B., et al. (2019). NUFEB: a massively parallel simulator for individual-based modelling of microbial communities. *PLOS Computational Biology*, 15(12), e1007125. <https://doi.org/10.1371/journal.pcbi.1007125>
- Li, F., et al. (2018). Genome - scale metabolic model analysis indicates low energy production efficiency in marine ammonia - oxidizing archaea. *AMB Express*, 2, 0-11. <https://doi.org/10.1186/s13568-018-0635-y>
- Li, P.-N., et al. (2018). Nutrient transport suggests an evolutionary basis for charged archaeal surface layer proteins. *The ISME Journal*, 2389-2402. <https://doi.org/10.1038/s41396-018-0191-0>
- Li, S., Duan, H., Zhang, Y., Huang, X., Yuan, Z., Liu, Y., & Zheng, M. (2020). Adaptation of nitrifying community in activated sludge to free ammonia inhibition and inactivation. *Science of the Total Environment*, 728, 138713. <https://doi.org/10.1016/j.scitotenv.2020.138713>
- Li, Y., Ding, K., Wen, X., Zhang, B., Shen, B., & Yang, Y. (2016). A novel ammonia-oxidizing archaeon from wastewater treatment plant: its enrichment, physiological and genomic characteristics. *Nature Publishing Group*(March), 1-11. <https://doi.org/10.1038/srep23747>
- Lide, D. R. (2006). *CRC Handbook of Chemistry and Physics* (87th ed.).

- Lipschultz, F., Zafiriou, O. C., Wofsy, S. C., McElroy, M. B., Valois, F. W., & Watson, S. W. (1981). Production of NO and N₂O by soil nitrifying bacteria. *Nature*, 294(5842), 641-643. <https://doi.org/10.1038/294641a0>
- Liu, R., et al. (2016). Nitrification is a primary driver of nitrous oxide production in laboratory microcosms from different land-use soils. *Frontiers in Microbiology*, 7(September), 1-10. <https://doi.org/10.3389/fmicb.2016.01373>
- Liu, S., et al. (2017). Potential correlated environmental factors leading to the niche segregation of ammonia-oxidizing archaea and ammonia-oxidizing bacteria: a review. *Applied Environmental Biotechnology*, 2(1), 11-19. <https://doi.org/10.26789/AEB.2017.01.002>
- Liu, W., Røder, H. L., Madsen, J. S., Bjarsholt, T., Sørensen, S. J., & Burmølle, M. (2016). Interspecific bacterial interactions are reflected in multispecies biofilm spatial organization. *Frontiers in Microbiology*, 7. <https://doi.org/10.3389/fmicb.2016.01366>
- Liu, Y., & Tay, J.-H. (2002). The essential role of hydrodynamic shear force in the formation of biofilm and granular sludge. *Water Research*, 36(7), 1653-1665. [https://doi.org/10.1016/S0043-1354\(01\)00379-7](https://doi.org/10.1016/S0043-1354(01)00379-7)
- Liu, Y. Q., Liu, Y., & Tay, J. H. (2005). Relationship between size and mass transfer resistance in aerobic granules. *Letters in Applied Microbiology*, 40(5), 312-315. <https://doi.org/10.1111/j.1472-765X.2005.01695.x>
- Loferer-Krößbacher, M., Klima, J., & Psenner, R. (1998). Determination of bacterial cell dry mass by transmission electron microscopy and densitometric image analysis. *Applied and Environmental Microbiology*, 64(2), 688-694. <https://doi.org/10.1128/AEM.64.2.688-694.1998>
- Lu, Y., Xia, X., Cheung, S., Jing, H., & Liu, H. (2019). Differential distribution and determinants of ammonia oxidizing archaea sublineages in the oxygen minimum zone of Costa Rica. *Microorganisms*, 7(10). <https://doi.org/10.3390/microorganisms7100453>
- Lücker, S., Nowka, B., Rattei, T., Spieck, E., & Daims, H. (2013). The genome of *Nitrospina gracilis* illuminates the metabolism and evolution of the major marine nitrite oxidizer. *Frontiers in Microbiology*, 4(February), 1-19. <https://doi.org/10.3389/fmicb.2013.00027>
- Lücker, S., Wagner, M., Maixner, F., Pelletier, E., Koch, H., & Vacherie, B. (2010). A *Nitrospira* metagenome illuminates the physiology and evolution of globally important nitrite-oxidizing bacteria. *PNAS*, 107(30), 13479-13484. <https://doi.org/10.1073/pnas.1003860107>
- Ludington, W. B. (2022). Higher-order microbiome interactions and how to find them. *Trends in Microbiology*. <https://doi.org/10.1016/j.tim.2022.03.011>
- Luo, S., Peng, Y., Liu, Y., & Peng, Y. (2022). Research progress and prospects of complete ammonia oxidizing bacteria in wastewater treatment. *Frontiers of Environmental Science & Engineering*, 16(9), 123. <https://doi.org/10.1007/s11783-022-1555-2>
- Ma, B., Yang, L., Wang, Q., Yuan, Z., Wang, Y., & Peng, Y. (2017). Inactivation and adaptation of ammonia-oxidizing bacteria and nitrite-oxidizing bacteria when exposed to free nitrous acid. *Bioresource Technology*, 245, 1266-1270. <https://doi.org/10.1016/j.biortech.2017.08.074>
- Mangiapià, M., & Scott, K. (2016). From CO₂ to cell: energetic expense of creating biomass using the Calvin–Benson–Bassham and reductive citric acid cycles based on genome data. *FEMS Microbiology Ecology*, 363(7), 1-9. <https://doi.org/10.1093/femsle/fnw054>
- Marco, D. (2011). *Metagenomics: current innovations and future trends*. Caister Academic Press.

- Martens-Habbena, W., Torre, R. D., Stahl, D. A., Berube, P. M., & Urakawa, H. (2009). Ammonia oxidation kinetics determine niche separation of nitrifying archaea and bacteria. *Nature*, *461*(October). <https://doi.org/10.1038/nature08465>
- Martinez-Rabert, E., van Amstel, C., Smith, C., Sloan, W. T., & Gonzalez-Cabaleiro, R. (2022). Environmental and ecological controls of the spatial distribution of microbial populations in aggregates. *PLOS Computational Biology*, *18*(12), e1010807. <https://doi.org/10.1371/journal.pcbi.1010807>
- Mason, M. G., Shepherd, M., Nicholls, P., Dobbin, P. S., Dodsworth, K. S., Poole, R. K., & Cooper, C. E. (2009). Cytochrome bd confers nitric oxide resistance to *Escherichia coli*. *Nature Chemical Biology*, *5*(2), 94-96. <https://doi.org/10.1038/nchembio.135>
- McCarty, P. L. (2007). Thermodynamic electron equivalents model for bacterial yield prediction: modifications and comparative evaluations. *Biotechnology and Bioengineering*, *97*(2), 377-388. <https://doi.org/10.1002/bit.21250>
- Mee, M. T., Collins, J. J., Church, G. M., & Wang, H. H. (2014). Syntrophic exchange in synthetic microbial communities. *PNAS*, *111*(20), E2149-E2156. <https://doi.org/10.1073/pnas.1405641111>
- Melcer, H. (2004). Methods for wastewater characterization in activated sludge modelling. *IWA Publishing books*.
- Milo, R., & Philips, R. (2015). *Cell biology by the numbers* (G. Science, Ed. 1st ed. ed.). <https://doi.org/10.1201/9780429258770>
- Mitri, S., Clarke, E., & Foster, K. R. (2016). Resource limitation drives spatial organization in microbial groups. *The ISME Journal*, *10*(6), 1471-1482. <https://doi.org/10.1038/ismej.2015.208>
- Mitri, S., Xavier, J. B., & Foster, K. R. (2011). Social evolution in multispecies biofilms. *PNAS*, *108*(supplement_2), 10839-10846. <https://doi.org/10.1073/pnas.1100292108>
- Momeni, B., Brileya, K. A., Fields, M. W., & Shou, W. (2013). Strong inter-population cooperation leads to partner intermixing in microbial communities. *Elife*, *2*, e00230. <https://doi.org/10.7554/eLife.00230>
- Momeni, B., Waite, A. J., & Shou, W. (2013). Spatial self-organization favors heterotypic cooperation over cheating. *Elife*, *2*, e00960. <https://doi.org/10.7554/eLife.00960>
- Morin, M. A., Morrison, A. J., Harms, M. J., & Dutton, R. J. (2022). Higher-order interactions shape microbial interactions as microbial community complexity increases. *Scientific Reports*, *12*(1), 22640. <https://doi.org/10.1038/s41598-022-25303-1>
- Mosier, A. C., & Francis, C. A. (2008). Relative abundance and diversity of ammonia-oxidizing archaea and bacteria in the San Francisco Bay estuary. *Environmental Microbiology*, *10*(11), 3002-3016. <https://doi.org/10.1111/j.1462-2920.2008.01764.x>
- Mulder, A., van de Graaf, A. A., Robertson, L. A., & Kuenen, J. G. (1995). Anaerobic ammonium oxidation discovered in a denitrifying fluidized bed reactor. *FEMS Microbiology Ecology*, *16*(3), 177-183. [https://doi.org/10.1016/0168-6496\(94\)00081-7](https://doi.org/10.1016/0168-6496(94)00081-7)
- Müller, R. H., & Babel, W. (1993). Oxidative capacity determines the growth rate with *Acetobacter methanolicus*. *Acta Biotechnologica*, *13*(1), 3-11. <https://doi.org/10.1002/abio.370130102>
- Nadell, C. D., Foster, K. R., & Xavier, J. B. (2010). Emergence of spatial structure in cell groups and the evolution of cooperation. *PLOS Computational Biology*, *6*(3), e1000716. <https://doi.org/10.1371/journal.pcbi.1000716>
- Naylor, J., et al. (2017). Simbiotics: a multiscale integrative platform for 3D modeling of bacterial populations. *ACS Synthetic Biology*, *6*(7), 1194-1210. <https://doi.org/10.1021/acssynbio.6b00315>

- Ni, B.-J., Chen, Y.-P., Liu, S.-Y., Fang, F., Xie, W.-M., & Yu, H.-Q. (2009). Modeling a granule-based anaerobic ammonium oxidizing (anammox) process. *Biotechnology and Bioengineering*, *103*(3), 490-499. <https://doi.org/10.1002/bit.22279>
- Niederdorfer, R., et al. (2021). Distinct growth stages controlled by the interplay of deterministic and stochastic processes in functional anammox biofilms. *Water Research*, *200*, 117225. <https://doi.org/10.1016/j.watres.2021.117225>
- Nielsen, A. T., Tolker-Nielsen, T., Barken, K. B., & Molin, S. (2000). Role of commensal relationships on the spatial structure of a surface-attached microbial consortium. *Environmental Microbiology*, *2*(1), 59-68. <https://doi.org/10.1046/j.1462-2920.2000.00084.x>
- Nomoto, T., Fukumori, Y., & Yamanakat, T. (1993). Membrane-bound cytochrome c is an alternative electron donor for cytochrome aa₃ in *Nitrobacter winogradskyi*. *Journal of Bacteriology*, *175*(14), 4400-4404. <https://doi.org/10.1128/jb.175.14.4400-4404.1993>
- Nowak, M. A., & Sigmund, K. (2004). Evolutionary dynamics of biological games. *Science*, *303*(5659), 793-799. <https://doi.org/10.1126/science.1093411>
- Nowka, B., Daims, H., & Spieck, E. (2015). Comparison of oxidation kinetics of nitrite-oxidizing bacteria: nitrite availability as a key factor in niche differentiation. *Applied and Environmental Microbiology*, *81*(2), 745-753. <https://doi.org/10.1128/AEM.02734-14>
- O'Toole, G., Kaplan, H. B., & Kolter, R. (2000). Biofilm formation as microbial development. *Annu Rev Microbiol*, *54*, 49-79. <https://doi.org/10.1146/annurev.micro.54.1.49>
- Ohgaki, S., & Wantawin, C. (1989). *Nitrification*. <https://doi.org/10.1016/B978-0-444-88030-7.50012-3>
- Oren, A., & Garrity, G. M. (2021). Valid publication of the names of forty-two phyla of prokaryotes. *International Journal of Systematic and Evolutionary Microbiology*, *71*(10). <https://doi.org/10.1099/ijsem.0.005056>
- Oshiki, M., Ali, M., Shinyako-Hata, K., Satoh, H., & Okabe, S. (2016). Hydroxylamine-dependent anaerobic ammonium oxidation (anammox) by "Candidatus Brocadia sinica". *Environmental Microbiology*, *18*(9), 3133-3143. <https://doi.org/10.1111/1462-2920.13355>
- Oshiki, M., Satoh, H., & Okabe, S. (2016). Ecology and physiology of anaerobic ammonium oxidizing bacteria. *Environmental Microbiology*, *18*(9), 2784-2796. <https://doi.org/10.1111/1462-2920.13134>
- Oshiki, M., Shimokawa, M., Fujii, N., Satoh, H., & Okabe, S. (2011). Physiological characteristics of the anaerobic ammonium-oxidizing bacterium 'Candidatus Brocadia sinica'. *Microbiology*, *157*(6), 1706-1713. <https://doi.org/10.1099/mic.0.048595-0>
- Otuzalti, M. M., & Perendeci, N. A. (2018). Modeling of real scale waste activated sludge anaerobic digestion process by Anaerobic Digestion Model 1 (ADM1). *International Journal of Green Energy*, *15*(7), 454-464. <https://doi.org/10.1080/15435075.2018.1479265>
- Palatinszky, M., et al. (2015). Cyanate as an energy source for nitrifiers. *Nature*, *524*(7563), 105-108. <https://doi.org/10.1038/nature14856>
- Palmer, J. D., & Foster, K. R. (2022). Bacterial species rarely work together. *Science*, *376*(6593), 581-582. <https://doi.org/10.1126/science.abn5093>
- Palomo, A., Smets, B. F., Pedersen, A. G., Fowler, S. J., & Dechesne, A. (2018). Comparative genomics sheds light on niche differentiation and the evolutionary history of comammox *Nitrospira*. *The ISME Journal*, *12*, 1779-1793. <https://doi.org/10.1038/s41396-018-0083-3>

- Park, B.-j., Park, S.-j., Yoon, D.-n., Schouten, S., & Damste, J. S. S. (2010). Cultivation of autotrophic ammonia-oxidizing archaea from marine sediments in coculture with sulfur-oxidizing bacteria. *Applied and Environmental Microbiology*, 76. <https://doi.org/10.1128/AEM.01478-10>
- Park, H. D., Wells, G. F., Bae, H., Griddle, C. S., & Francis, C. A. (2006). Occurrence of ammonia-oxidizing archaea in wastewater treatment plant bioreactors. *Applied and Environmental Microbiology*, 72(8), 5643-5647. <https://doi.org/10.1128/AEM.00402-06>
- Park, M.-r., Park, H., & Chandran, K. (2017). Molecular and kinetic characterization of planktonic Nitrospira spp. selectively enriched from activated sludge. *Environmental Science & Technology*, 51(5), 2720–2728. <https://doi.org/10.1021/acs.est.6b05184>
- Pedrouso, A., Vázquez-Padín, J. R., Crutchik, D., & Campos, J. L. (2021). Application of anammox-based processes in urban WWTPs: are we on the right track? *Processes*, 9(8), 1334. <https://doi.org/10.3390/pr9081334>
- Peeters, S. H., & van Niftrik, L. (2019). Trending topics and open questions in anaerobic ammonium oxidation. *Current Opinion in Chemical Biology*, 49, 45-52. <https://doi.org/10.1016/j.cbpa.2018.09.022>
- Peng, X., Jayakumar, A., & Ward, B. (2013). Community composition of ammonia-oxidizing archaea from surface and anoxic depths of oceanic oxygen minimum zones [Original Research]. *Frontiers in Microbiology*, 4. <https://doi.org/10.3389/fmicb.2013.00177>
- Pfeiffer, T., & Schuster, S. (2005). Game-theoretical approaches to studying the evolution of biochemical systems. *Trends in Biochemical Sciences*, 30(1), 20-25. <https://doi.org/10.1016/j.tibs.2004.11.006>
- Pfeiffer, T., Schuster, S., & Bonhoeffer, S. (2001). Cooperation and competition in the evolution of ATP-producing pathways. *Science*, 293, 504-507. <https://doi.org/10.1126/science.293.5534.1436>
- Pjevac, P., Lückner, S., & Daims, H. (2017). AmoA-targeted polymerase chain reaction primers for the specific detection and quantification of comammox Nitrospira in the environment. *Frontiers in Microbiology*, 8, 1-11. <https://doi.org/10.3389/fmicb.2017.01508>
- Pocheville, A. (2015). The ecological niche: history and recent controversies. In T. Heams, P. Huneman, G. Lecointre, & M. Silberstein (Eds.), *Handbook of Evolutionary Thinking in the Sciences* (pp. 547-586). Springer Netherlands. https://doi.org/10.1007/978-94-017-9014-7_26
- Poot, V., Hoekstra, M., Geleijnse, M. A. A., van Loosdrecht, M. C. M., & Perez, J. (2016). Effects of the residual ammonium concentration on NOB repression during partial nitrification with granular sludge. *Water Research*, 106, 518-530. <https://doi.org/10.1016/j.watres.2016.10.028>
- Preisig, O., Zufferey, R., Thöny-Meyer, L., Appleby, C. A., & Hennecke, H. (1996). A high-affinity cbb3-type cytochrome oxidase terminates the symbiosis-specific respiratory chain of Bradyrhizobium japonicum. *Journal of Bacteriology*, 178(6), 1532-1538. <https://doi.org/10.1128/jb.178.6.1532-1538.1996>
- Prosser, J. I. (2020). Putting science back into microbial ecology: a question of approach. *Philosophical Transactions of the Royal Society B: Biological Sciences*, 375(1798), 20190240. <https://doi.org/10.1098/rstb.2019.0240>
- Puyol, D., Carvajal-Arroyo, J. M., Garcia, B., Sierra-Alvarez, R., & Field, J. A. (2014). Kinetics and thermodynamics of anaerobic ammonium oxidation process using Brocadia spp. dominated mixed cultures. *Water Science & Technology*, 69(8), 1682-1688. <https://doi.org/10.2166/wst.2014.074>

- Puyol, D., Garcia, B., & Field, J. A. (2013). Bioresource technology kinetic characterization of *Brocadia* spp. dominated anammox cultures. *Bioresource Technology*, *139*, 94-100. <https://doi.org/10.1016/j.biortech.2013.04.001>
- Qin, W., Amin, S. A., Martens-habbena, W., Walker, C. B., Urakawa, H., & Devol, A. H. (2014). Marine ammonia-oxidizing archaeal isolates display obligate mixotrophy and wide ecotypic variation. *PNAS*, *111*(34). <https://doi.org/10.1073/pnas.1324115111>
- Qin, W., Meinhardt, K. A., Moffett, J. W., Devol, A. H., Armbrust, E. V., Ingalls, A. E., & Stahl, D. A. (2017). Influence of oxygen availability on the activities of ammonia-oxidizing archaea. *Environmental Microbiology Reports*(February). <https://doi.org/10.1111/1758-2229.12525>
- Randall, A. C. W., Buth, D., Randall, C. W., & Buth, D. (1984). Nitrite build-up in activated sludge resulting from temperature effects. *Journal (Water Pollution Control Federation)*, *56*(9), 1045-1049.
- Ren, Z.-Q., et al. (2022). A review on characterizing the metabolite property of anammox sludge by spectroscopy. *Science of the Total Environment*, *817*, 153065. <https://doi.org/10.1016/j.scitotenv.2022.153065>
- Rice, C. W., & Hempfling, W. P. (1978). Oxygen-limited continuous culture and respiratory energy conservation in *Escherichia coli*. *Journal of Bacteriology*, *134*(1), 115-124. <https://doi.org/10.1128/jb.134.1.115-124.1978>
- Rittmann, B. E., & McCarty, P. L. (2020). *Environmental biotechnology: principles and applications* (Second edition. ed.). McGraw-Hill Education. <https://www.accessengineeringlibrary.com/content/book/9781260441604>
- Rodríguez Amor, D., & Dal Bello, M. (2019). Bottom-up approaches to synthetic cooperation in microbial communities. *Life (Basel)*, *9*(1). <https://doi.org/10.3390/life9010022>
- Roels, J. A. (1984). Energetics and kinetics in biotechnology. *The Quarterly Review of Biology*, *59*(2), 179-179. <https://doi.org/10.1086/413814>
- Roots, P., et al. (2019). Comammox *Nitrospira* are the dominant ammonia oxidizers in a mainstream low dissolved oxygen nitrification reactor. *Water Research*, *157*, 396-405. <https://doi.org/10.1016/j.watres.2019.03.060>
- Rosenthal, A. Z., Qi, Y., Hormoz, S., Park, J., Li, S. H.-J., & Elowitz, M. B. (2018). Metabolic interactions between dynamic bacterial subpopulations. *Elife*, *7*, e33099. <https://doi.org/10.7554/eLife.33099>
- Rudge, T. J., Steiner, P. J., Phillips, A., & Haseloff, J. (2012). Computational modeling of synthetic microbial biofilms. *ACS Synthetic Biology*, *1*(8), 345-352. <https://doi.org/10.1021/sb300031n>
- Sakoula, D., Koch, H., Frank, J., Jetten, M. S. M., van Kessel, M. A. H. J., & Lücker, S. (2021). Enrichment and physiological characterization of a novel comammox *Nitrospira* indicates ammonium inhibition of complete nitrification. *The ISME Journal*, *15*(4), 1010-1024. <https://doi.org/10.1038/s41396-020-00827-4>
- Samet, H. (1988). An overview of quadrees, octrees, and related hierarchical data structures. In R. A. Earnshaw, *Theoretical Foundations of Computer Graphics and CAD* Berlin, Heidelberg.
- Sánchez, O., C. Martí, M., Aspé, E., & Roeckel, M. (2001). Nitrification rates in a saline medium at different dissolved oxygen concentrations. *Biotechnology Letters*, *23*, 1597-1602. <https://doi.org/10.1023/A:1011977629398>
- Santoro, A. E., & Casciotti, K. L. (2011). Enrichment and characterization of ammonia-oxidizing archaea from the open ocean: phylogeny, physiology and stable isotope fractionation. *The ISME Journal*, *5*(11), 1796-1808. <https://doi.org/10.1038/ismej.2011.58>

- Santoro, A. E., Francis, C. A., De Siewes, N. R., & Boehm, A. B. (2008). Shifts in the relative abundance of ammonia-oxidizing bacteria and archaea across physicochemical gradients in a subterranean estuary. *Environmental Microbiology*, 10(4), 1068-1079. <https://doi.org/10.1111/j.1462-2920.2007.01547.x>
- Sato, Y., Arai, H., Igarashi, Y., & Ishii, M. (2014). Adaptation of *Hydrogenobacter thermophilus* toward oxidative stress triggered by high expression of alkyl hydroperoxide reductase. *Bioscience, Biotechnology and Biochemistry*, 78(9), 1619-1622. <https://doi.org/10.1080/09168451.2014.921559>
- Sauder, L. A., Albertsen, M., Engel, K., Schwarz, J., Nielsen, P. H., Wagner, M., & Neufeld, J. D. (2017). Cultivation and characterization of *Candidatus Nitrosocosmicus exaquare*, an ammonia-oxidizing archaeon from a municipal wastewater treatment system. *Nature Publishing Group*, 1-16. <https://doi.org/10.1038/ismej.2016.192>
- Sauder, L. A., Engel, K., Lo, C.-c., & Chain, P. (2018). "*Candidatus Nitrosotenuis aquarius*", an ammonia-oxidizing archaeon from a freshwater aquarium biofilter. *Applied and Environmental Microbiology*, 84(19), 1-17. <https://doi.org/10.1128/AEM.01430-18>
- Scarsini, M. (1984). On measures of concordance. *Stochastica*, 8(3), 201-218.
- Schäfer, G., & Penefsky, H. (2008). *Bioenergetics. Energy conservation and conversion* (Vol. 53). Springer. <https://doi.org/10.1017/CBO9781107415324.004>
- Schalk, J., de Vries, S., Kuenen, J. G., & Jetten, M. S. M. (2000). Involvement of a novel hydroxylamine oxidoreductase in anaerobic ammonium oxidation. *Biochemistry*, 39(18), 5405-5412. <https://doi.org/10.1021/bi992721k>
- Schluter, J., Nadell, C. D., Bassler, B. L., & Foster, K. R. (2015). Adhesion as a weapon in microbial competition. *The ISME Journal*, 9(1), 139-149. <https://doi.org/10.1038/ismej.2014.174>
- Schmidt, I., & Bock, E. (1997). Anaerobic ammonia oxidation with nitrogen dioxide by *Nitrosomonas eutropha*. *Archives of Microbiology*, 167(2-3), 106-111. <https://doi.org/10.1007/s002030050422>
- Schmidt, I., & Bock, E. (1998). Anaerobic ammonia oxidation by cell-free extracts of *Nitrosomonas eutropha*. *Antonie van Leeuwenhoek*, 73(3), 271-278. <https://doi.org/10.1023/A:1001572121053>
- Schouten, S., et al. (2004). Stable carbon isotopic fractionations associated with inorganic carbon fixation by anaerobic ammonium-oxidizing bacteria. *Applied and Environmental Microbiology*, 70(6), 3785-3788. <https://doi.org/10.1128/aem.70.6.3785-3788.2004>
- Schramm, A., Heuvel, J., Ottengraf, S., & Planck, M. (1999). Microscale distribution of populations and activities of *Nitrospira* and *Nitrospira* spp. along a macroscale gradient in a nitrifying bioreactor: quantification by in situ hybridization and the use of microsensors. *Applied and Environmental Microbiology*, 65(8), 3690-3696. <https://doi.org/10.1128/AEM.65.8.3690-3696.1999>
- Schramm, A., Larsen, L. H., Revsbech, N. P., Ramsing, N. B., Amann, R., & Schleifer, K. H. (1996). Structure and function of a nitrifying biofilm as determined by in situ hybridization and the use of microelectrodes. *Applied and Environmental Microbiology*, 62(12), 4641-4647. <https://doi.org/10.1128/aem.62.12.4641-4647.1996>
- Sedlacek, C. J., et al. (2019). A physiological and genomic comparison of *Nitrosomonas* cluster 6a and 7 ammonia-oxidizing bacteria. *Microbial Ecology*, 78(4), 985-994. <https://doi.org/10.1007/s00248-019-01378-8>
- Seeliger, S., Janssen, P. H., & Schink, B. (2002). Energetics and kinetics of lactate fermentation to acetate and propionate via methylmalonyl-CoA or acrylyl-CoA. *FEMS Microbiology Letters*, 211(1), 65-70. [https://doi.org/10.1016/S0378-1097\(02\)00651-1](https://doi.org/10.1016/S0378-1097(02)00651-1)

- Sekiguchi, Y., Kamagata, Y., Nakamura, K., Ohashi, A., & Harada, H. (1999). Fluorescence in situ hybridization using 16S rRNA-targeted oligonucleotides reveals localization of methanogens and selected uncultured bacteria in mesophilic and thermophilic sludge granules. *Applied and Environmental Microbiology*, 65(3), 1280-1288. <https://doi.org/10.1128/aem.65.3.1280-1288.1999>
- Seuntjens, D., et al. (2018). High-resolution mapping and modeling of anammox recovery from recurrent oxygen exposure. *Water Research*, 144, 522-531. <https://doi.org/10.1016/j.watres.2018.07.024>
- Shao, Y.-H., & Wu, J.-H. (2021). Comammox *Nitrospira* species dominate in an efficient partial nitrification–anammox bioreactor for treating ammonium at low loadings. *Environmental Science & Technology*, 55(3), 2087-2098. <https://doi.org/10.1021/acs.est.0c05777>
- Sharma, B., & Ahler, R. C. (1976). Nitrification and nitrogen removal. *Water Research*, 11(1), 897-925. [https://doi.org/10.1016/0043-1354\(77\)90078-1](https://doi.org/10.1016/0043-1354(77)90078-1)
- Sharma, S., & Steuer, R. (2019). Modelling microbial communities using biochemical resource allocation analysis. *Journal of The Royal Society Interface*, 16(160), 20190474. <https://doi.org/10.1098/rsif.2019.0474>
- Shen, C., Lemmen, K., Alexander, J., & Pennekamp, F. (2023). Connecting higher-order interactions with ecological stability in experimental aquatic food webs. *Ecology and Evolution*, 13(9), e10502. <https://doi.org/https://doi.org/10.1002/ece3.10502>
- Sliekers, A. O., Derwort, N., Gomez, J. L. C., Strous, M., Kuenen, J. G., & Jetten, M. S. M. (2002). Completely autotrophic nitrogen removal over nitrite in one single reactor. *Water Research*, 36(10), 2475-2482. [https://doi.org/10.1016/S0043-1354\(01\)00476-6](https://doi.org/10.1016/S0043-1354(01)00476-6)
- Smith, A., Hill, S., & Anthony, C. (1990). The purification, characterization and role of the d-type cytochrome oxidase of *Klebsiella pneumoniae* during nitrogen fixation. *Journal of General Microbiology*, 136(1), 171-180. <https://doi.org/10.1099/00221287-136-1-171>
- Sollai, M., Villanueva, L., Hopmans, E. C., Reichart, G. J., & Sinninghe Damsté, J. S. (2019). A combined lipidomic and 16S rRNA gene amplicon sequencing approach reveals archaeal sources of intact polar lipids in the stratified Black Sea water column. *Geobiology*, 17(1), 91-109. <https://doi.org/10.1111/gbi.12316>
- Spearman, C. (1904). The proof and measurement of association between two things. *The American Journal of Psychology*, 15(1), 72-101. <https://doi.org/10.2307/1412159>
- Spieck, E., Aamand, J., Bartosch, S., & Bock, E. (1996). Immunocytochemical detection and location of the membrane-bound nitrite oxidoreductase in cells of *Nitrobacter* and *Nitrospira*. *FEMS Microbiology Letters*, 139(1), 71-76. [https://doi.org/10.1016/0378-1097\(96\)00123-1](https://doi.org/10.1016/0378-1097(96)00123-1)
- Spieck, E., Ehrich, S., & Aamand, J. (1998). Isolation and immunocytochemical location of the nitrite-oxidizing system in *Nitrospira moscoviensis*. *Archives of Microbiology*, 169, 225-230. <https://doi.org/10.1007/s002030050565>
- Spieck, E., Keuter, S., Wenzel, T., Bock, E., & Ludwig, W. (2014). Characterization of a new marine nitrite oxidizing bacterium, *Nitrospina watsonii* sp. nov., a member of the newly proposed phylum “Nitrospinae”. *Systematic and Applied Microbiology*, 37(3), 170-176. <https://doi.org/10.1016/j.syapm.2013.12.005>
- Starkenburg, S. R., Arp, D. J., & Bottomley, P. J. (2008). D-Lactate metabolism and the obligate requirement for CO₂ during growth on nitrite by the facultative lithoautotroph *Nitrobacter hamburgensis*. *Microbiology*, 154, 2473-2481. <https://doi.org/10.1099/mic.0.2008/018085-0>

- Starkenburger, S. R., et al. (2006). Genome sequence of the chemolithoautotrophic nitrite-oxidizing bacterium *Nitrobacter winogradskyi* Nb-255. *Microbiology*, 72(3), 2050-2063. <https://doi.org/10.1128/AEM.72.3.2050>
- Starkenburger, S. R., et al. (2008). Complete genome sequence of *Nitrobacter hamburgensis* X14 and comparative genomic analysis of species within the genus *Nitrobacter*. *Applied and Environmental Microbiology*, 74(9), 2852-2863. <https://doi.org/10.1128/AEM.02311-07>
- Station, R. E., Skinner, F. A., & Walker, N. (1961). Growth of *Nitrosomonas europaea* in batch and continuous culture. *Archiv für Mikrobiologie*, 38, 339-349. <https://doi.org/10.1007/BF00408008>
- Stehr, G., Biittcher, B., Dittberner, P., Rath, G., & Koops, H.-p. (1995). The ammonia-oxidizing nitrifying population of the River Elbe estuary. *FEMS Microbiology Ecology*, 17, 177-186. [https://doi.org/10.1016/0168-6496\(95\)00022-3](https://doi.org/10.1016/0168-6496(95)00022-3)
- Stein, L. Y., & Klotz, M. G. (2016). The nitrogen cycle. *Current Biology*, 26(3), R94-R98. <https://doi.org/10.1016/j.cub.2015.12.021>
- Stewart, F. J., Ulloa, O., & DeLong, E. F. (2012). Microbial metatranscriptomics in a permanent marine oxygen minimum zone. *Environmental Microbiology*, 14(1), 23-40. <https://doi.org/10.1111/j.1462-2920.2010.02400.x>
- Stieglmeier, M., Mooshammer, M., Kitzler, B., Wanek, W., Zechmeister-Boltenstern, S., Richter, A., & Schleper, C. (2014). Aerobic nitrous oxide production through N-nitrosating hybrid formation in ammonia-oxidizing archaea. *The ISME Journal*, 8(5), 1135-1146. <https://doi.org/10.1038/ismej.2013.220>
- Straka, L. L. (2019). Affinity informs environmental cooperation between ammonia-oxidizing archaea (AOA) and anaerobic ammonia-oxidizing (anammox) bacteria. *The ISME Journal*, 13(8), 1997-2004. <https://doi.org/10.1038/s41396-019-0408-x>
- Stratton, F. E., & McCarty, P. L. (1967). Prediction of nitrification effects on the dissolved oxygen balance of streams. *Current Research*, 1(5), 405-410. <https://doi.org/10.1021/es60005a003>
- Strous, M., et al. (1999). Missing lithotroph identified as new planctomycete. *Nature*, 400(6743), 446-449. <https://doi.org/10.1038/22749>
- Strous, M., Heijnen, J. J., Kuenen, J. G., & Jetten, M. S. M. (1998). The sequencing batch reactor as a powerful tool for the study of slowly growing anaerobic ammonium-oxidizing microorganisms. *Applied Microbiology and Biotechnology*, 50(5), 589-596. <https://doi.org/10.1007/s002530051340>
- Strous, M., Kuenen, J. G., & Jetten, M. S. M. (1999). Key physiology of anaerobic ammonium oxidation. *Applied and Environmental Microbiology*, 65(7), 3248-3250. <https://doi.org/10.1128/aem.65.7.3248-3250.1999>
- Suarez, C., Piculell, M., Modin, O., Langenheder, S., Persson, F., & Hermansson, M. (2019). Thickness determines microbial community structure and function in nitrifying biofilms via deterministic assembly. *Scientific Reports*, 9(1), 5110. <https://doi.org/10.1038/s41598-019-41542-1>
- Tanaka, Y., Fukumori, Y., & Yamanaka, T. (1983). Purification of cytochrome a1c1 from *Nitrobacter agilis* and characterization of nitrite oxidation system of the bacterium. *Archives of Microbiology*, 135, 265-271. <https://doi.org/10.1007/BF00413479>
- Tay, J.-H., Ivanov, V., Pan, S., & Tay, S. T.-L. (2002). Specific layers in aerobically grown microbial granules. *Letters in Applied Microbiology*, 34(4), 254-257. <https://doi.org/10.1046/j.1472-765x.2002.01099.x>
- Tempest, D. W., & Neijssel, O. M. (1978). *Eco-physiological aspects of microbial growth in aerobic nutrient-limited* (Vol. 2). https://doi.org/10.1007/978-1-4615-8222-9_3
- Thandar, S. M., Ushiki, N., Fujitani, H., Sekiguchi, Y., & Tsuneda, S. (2016). Ecophysiology and comparative genomics of *Nitrosomonas mobilis* ms1 isolated from autotrophic

- nitrifying granules of wastewater treatment bioreactor. *Frontiers in Microbiology*, 7(NOV), 1-14. <https://doi.org/10.3389/fmicb.2016.01869>
- Thiele, E. W. (1939). Relation between catalytic activity and size of particle. *Industrial & Engineering Chemistry*, 31(7), 916-920. <https://doi.org/10.1021/ie50355a027>
- Thomas, J. W. (1995). *Numerical partial differential equations: finite difference methods*. <https://doi.org/10.1007/978-1-4899-7278-1>
- Tian, H., et al. (2020). A comprehensive quantification of global nitrous oxide sources and sinks. *Nature*, 586(7828), 248-256. <https://doi.org/10.1038/s41586-020-2780-0>
- Tourna, M., et al. (2011). Nitrososphaera viennensis, an ammonia oxidizing archaeon from soil. *PNAS*, 108(20), 8420-8425. <https://doi.org/10.1073/pnas.1013488108>
- Treusch, A. H., Leininger, S., Kletzin, A., Schuster, S. C., Klenk, H.-P., & Schleper, C. (2005). Novel genes for nitrite reductase and Amo-related proteins indicate a role of uncultivated mesophilic crenarchaeota in nitrogen cycling. *Environmental Microbiology*, 7(12), 1985-1995. <https://doi.org/10.1111/j.1462-2920.2005.00906.x>
- Tsai, Y.-l., & Tuovinen, O. H. (1985). Oxygen uptake activity by Nitrobacter spp. in the presence of metal ions and sulfoxyanions. *FEMS Microbiology Letters*, 28(1), 11-14. <https://doi.org/10.1111/j.1574-6968.1985.tb00754.x>
- Ushiki, N., Jinno, M., Fujitani, H., Suenaga, T., Terada, A., & Tsuneda, S. (2017). Nitrite oxidation kinetics of two Nitrospira strains: the quest for competition and ecological niche differentiation. *Journal of Bioscience and Bioengineering*, 123(5), 581-589. <https://doi.org/10.1016/j.jbiosc.2016.12.016>
- Vadivelu, V. M., Yuan, Z., Fux, C., & Keller, J. (2006). Stoichiometric and kinetic characterisation of Nitrobacter in mixed culture by decoupling the growth and energy generation processes. *Biotechnology and Bioengineering*, 94(6), 1176-1188. <https://doi.org/10.1002/bit.20956>
- Vajrala, N., Martens-Habben, W., Sayavedra-Soto, L. A., Schauer, A., Bottomley, P. J., Stahl, D. A., & Arp, D. J. (2013). Hydroxylamine as an intermediate in ammonia oxidation by globally abundant marine archaea. *PNAS*, 110(3), 1006-1011. <https://doi.org/10.1073/pnas.1214272110>
- van den Berg, L., Kirkland, C. M., Seymour, J. D., Codd, S. L., van Loosdrecht, M. C. M., & de Kreuk, M. K. (2020). Heterogeneous diffusion in aerobic granular sludge. *Biotechnology and Bioengineering*, 117(12), 3809-3819. <https://doi.org/10.1002/bit.27522>
- van den Berg, L., Toja Ortega, S., van Loosdrecht, M. C. M., & de Kreuk, M. K. (2022). Diffusion of soluble organic substrates in aerobic granular sludge: effect of molecular weight. *Water Research X*, 16, 100148. <https://doi.org/10.1016/j.wroa.2022.100148>
- van den Berg, L., van Loosdrecht, M. C. M., & de Kreuk, M. K. (2021). How to measure diffusion coefficients in biofilms: a critical analysis. *Biotechnology and Bioengineering*, 118(3), 1273-1285. <https://doi.org/10.1002/bit.27650>
- van den Berg, N. I., et al. (2022). Ecological modelling approaches for predicting emergent properties in microbial communities. *Nature Ecology & Evolution*, 6(7), 855-865. <https://doi.org/10.1038/s41559-022-01746-7>
- van der Star, W. R. L., Miclea, A. I., van Dongen, U. G. J. M., Muyzer, G., Picioreanu, C., & van Loosdrecht, M. C. M. (2008). The membrane bioreactor: a novel tool to grow anammox bacteria as free cells. *Biotechnology and Bioengineering*, 101(2), 286-294. <https://doi.org/10.1002/bit.21891>
- van Dongen, U., Jetten, M. S. M., & van Loosdrecht, M. C. M. (2001). The SHARON®-Anammox® process for treatment of ammonium rich wastewater. *Water Science and Technology*, 44(1), 153-160. <https://doi.org/10.2166/wst.2001.0037>
- van Kessel, M. A. H. J., et al. (2015). Complete nitrification by a single microorganism. *Nature*, 528(7583), 555-559. <https://doi.org/10.1038/nature16459>

- Velicer, G. J., & Lenski, R. E. (1999). Evolutionary trade-offs under conditions of resource abundance and scarcity: Experiments with bacteria. *Ecology*, *80*(4), 1168-1179. [https://doi.org/10.1890/0012-9658\(1999\)080\[1168:ETOUCO\]2.0.CO;2](https://doi.org/10.1890/0012-9658(1999)080[1168:ETOUCO]2.0.CO;2)
- Walker, C. B., et al. (2010). Nitrosopumilus maritimus genome reveals unique mechanisms for nitrification and autotrophy in globally distributed marine crenarchaea. *PNAS*, *107*(19), 8818-8823. <https://doi.org/10.1073/pnas.0913533107>
- Wan, X. S., et al. (2023). Pathways of N₂O production by marine ammonia-oxidizing archaea determined from dual-isotope labeling. *PNAS*, *120*(11), e2220697120. <https://doi.org/10.1073/pnas.2220697120>
- Wang, T., Shen, P., He, Y., Zhang, Y., & Liu, J. (2023). Spatial transcriptome uncovers rich coordination of metabolism in E. coli K12 biofilm. *Nature Chemical Biology*, *19*(8), 940-950. <https://doi.org/10.1038/s41589-023-01282-w>
- Wang, Y., et al. (2017). Comammox in drinking water systems. *Water Research*, *116*, 332-341. <https://doi.org/10.1016/j.watres.2017.03.042>
- Wang, Y., Xu, L., Wang, S., Ye, F., & Zhu, G. (2019). Global distribution of anaerobic ammonia oxidation (anammox) bacteria – field surveys in wetland, dryland, groundwater aquifer and snow. *Frontiers in Microbiology*, *10*(November), 1-12. <https://doi.org/10.3389/fmicb.2019.02583>
- Ward, B. B. (1987). Kinetic studies on ammonia and methane oxidation by Nitrosoccus oceanus. *Archives of Microbiology*, *147*, 126-133. <https://doi.org/10.1007/BF00415273>
- Watson, S. (1989). Nitrifying bacteria. *Bergey's manual of systematic bacteriology*, *3*, 1808-1834.
- Watson, S. W., Book, E., Valois, F. W., Waterbury, J. B., & Schlosser, U. (1986). Nitrospira marina gen. nov. sp. nov.: a chemolithotrophic nitrite-oxidizing bacterium. *Archives of Microbiology*, *144*(1), 1-7. <https://doi.org/10.1007/BF00454947>
- Watson, S. W., & Waterbury, J. B. (1971). Characteristics of two marine nitrite oxidizing bacteria, Nitrospina gracilis nov. gen. nov. sp. and Nitrococcus mobilis nov. gen. nov. sp. *Archives of Microbiology*, *77*, 203-230. <https://doi.org/10.1007/BF00408114>
- Weber, M. F., Poxleitner, G., Hebisch, E., Frey, E., & Opitz, M. (2014). Chemical warfare and survival strategies in bacterial range expansions. *Journal of The Royal Society Interface*, *11*(96), 20140172. <https://doi.org/10.1098/rsif.2014.0172>
- Wegen, S., Nowka, B., & Spieck, E. (2019). Low temperature and neutral pH define "Candidatus Nitrotoga sp." as a competitive nitrite oxidizer in coculture with Nitrospira defluvii. *Applied and Environmental Microbiology*, *85*(9), 1-10. <https://doi.org/10.1128/AEM.02569-18>
- Welch, B. L. (1947). The generalization of Student's problem when several different population variances are involved. *Biometrika*, *34*(1-2), 28-35. <https://doi.org/10.1093/biomet/34.1-2.28>
- Wett, B., & Rauch, W. (2003). The role of inorganic carbon limitation in biological nitrogen removal of extremely ammonia concentrated wastewater. *Water Research*, *37*(5), 1100-1110. [https://doi.org/10.1016/S0043-1354\(02\)00440-2](https://doi.org/10.1016/S0043-1354(02)00440-2)
- Whitman, W. B., Coleman, D. C., & Wiebe, W. J. (1998). Prokaryotes: The unseen majority. *PNAS*, *95*(12), 6578-6583. <https://doi.org/10.1073/pnas.95.12.6578>
- Whittaker, M., Bergmann, D., Arciero, D., & Hooper, A. B. (2000). Electron transfer during the oxidation of ammonia by the chemolithotrophic bacterium Nitrosomonas europaea. *Biochimica et Biophysica Acta - Bioenergetics*, *1459*(2-3), 346-355. [https://doi.org/10.1016/S0005-2728\(00\)00171-7](https://doi.org/10.1016/S0005-2728(00)00171-7)
- Wiesmann, U. (1994). Biological nitrogen removal from wastewater. *Bioethics/Wastewater*, *51*. <https://doi.org/10.1007/BFb0008736>

- Wrage-Mönnig, N., Horn, M. A., Well, R., Müller, C., Velthof, G., & Oenema, O. (2018). The role of nitrifier denitrification in the production of nitrous oxide revisited. *Soil Biology and Biochemistry*, 123, A3-A16. <https://doi.org/10.1016/j.soilbio.2018.03.020>
- Wrage, N., Velthof, G. L., Beusichem, M. L. V., & Oenema, O. (2001). Role of nitrifier denitrification in the production of nitrous oxide. *Soil Biology and Biochemistry*, 33, 1723-1732. [https://doi.org/10.1016/S0038-0717\(01\)00096-7](https://doi.org/10.1016/S0038-0717(01)00096-7)
- Wu, G., Zhang, T., Gu, M., Chen, Z., & Yin, Q. (2020). Review of characteristics of anammox bacteria and strategies for anammox start-up for sustainable wastewater resource management. *Water Science and Technology*, 82(9), 1742-1757. <https://doi.org/10.2166/wst.2020.443>
- Wyffels, S., Hulle, S. W. H. V., Boeckx, P., Volcke, E. I. P., Cleemput, O. V., Vanrolleghem, P. A., & Verstraete, W. (2004). Modeling and simulation of oxygen-limited partial nitrification in a membrane-assisted bioreactor (MBR). *Biotechnology and Bioengineering*, 86(5), 531 - 542. <https://doi.org/10.1002/bit.20008>
- Xavier, J. B., de Kreuk, M. K., Picioreanu, C., & van Loosdrecht, M. C. M. (2007). Multi-scale Individual-based Model of microbial and bioconversion dynamics in aerobic granular sludge. *Environmental Science & Technology*, 41(18), 6410-6417. <https://doi.org/10.1021/es070264m>
- Xavier, J. B., Picioreanu, C., & van Loosdrecht, M. C. (2004). Assessment of three-dimensional biofilm models through direct comparison with confocal microscopy imaging. *Water Science & Technology*, 49(11-12), 177-185. <https://doi.org/10.2166/wst.2004.0834>
- Xia, F., Wang, J.-G., Zhu, T., Zou, B., Rhee, S.-K., & Quan, Z.-X. (2018). Ubiquity and diversity of complete ammonia oxidizers (comammox). *Applied and Environmental Microbiology*, 84(24), e01390-01318. <https://doi.org/10.1128/AEM.01390-18>
- Yang, Y., Daims, H., Liu, Y., Herbold, C. W., Pjevac, P., & Lin, J.-g. (2020). Activity and metabolic versatility of complete ammonia oxidizers in full-scale wastewater treatment systems. *American society for Microbiology*, 11(2), 1-15. <https://doi.org/10.1128/mBio.03175-19>
- Yin, Z., Bi, X., & Xu, C. (2018). Ammonia-oxidizing archaea (AOA) play with ammonia-oxidizing bacteria (AOB) in nitrogen removal from wastewater. *Archaea*, 2018, 1-9. <https://doi.org/10.1155/2018/8429145>
- Yoshioka, T., Terai, H., & Saijo, Y. (1982). Growth kinetic studies of nitrifying bacteria by the immunofluorescent counting method. *Journal of General and Applied Microbiology*, 28, 169-180. <https://doi.org/10.2323/jgam.28.169>
- Yuan, Z., & Vanbriesen, J. M. (2002). Yield prediction and stoichiometry of multi-step biodegradation reactions involving oxygenation [Article]. *Biotechnology and Bioengineering*, 80(1), 100-113. <https://doi.org/10.1002/bit.10355>
- Zacharia, V. M., Ra, Y., Sue, C., Alcalá, E., Reaso, J. N., Ruzin, S. E., & Traxler, M. F. (2021). Genetic network architecture and environmental cues drive spatial organization of phenotypic division of labor in *Streptomyces coelicolor*. *mBio*, 12(3). <https://doi.org/10.1128/mBio.00794-21>
- Zelezniak, A., Andrejev, S., Ponomarova, O., R. Mende, D., & Raosaheb Patil, K. (2015). Metabolic dependencies drive species co-occurrence in diverse microbial communities. *PNAS*, 112(51), E7156-E7156. <https://doi.org/10.1073/pnas.1522642113>
- Zhang, Y., Zhang, Y., Gao, J., Shen, Q., Bai, Z., Zhuang, X., & Zhuang, G. (2018). Optimization of the medium for the growth of *Nitrobacter winogradskyi* by statistical method. *Letters in Applied Microbiology*, 67(3), 306-313. <https://doi.org/10.1111/lam.13036>

- Zhao, J., et al. (2022). Selective enrichment of comammox *Nitrospira* in a moving bed biofilm reactor with sufficient oxygen supply. *Environmental Science & Technology*, 56(18), 13338–13346. <https://doi.org/10.1021/acs.est.2c03299>
- Zhu, X., Burger, M., Doane, T. A., & Horwath, W. R. (2013). Ammonia oxidation pathways and nitrifier denitrification are significant sources of N₂O and NO under low oxygen availability. *PNAS*, 110(16), 6328-6333. <https://doi.org/10.1073/pnas.1219993110>